# Susitna-Watana Hydroelectric Project (FERC No. 14241)

# Glacier and Runoff Changes Study

# Final Study Report

Prepared for

Alaska Energy Authority

SUSITNA-WATANA HYDRO

*Clean, reliable energy for the next 100 years.*

Prepared by

Division of Geological & Geophysical Surveys
Alaska Department of Natural Resources

October 2015

## Authors and Affiliations

Gabriel Wolken[1], Andrew Bliss[2], Regine Hock[2], Erin Whorton[1], Juliana Braun[2], Anna Liljedahl[3,4], Jing Zhang[5], Emily Youcha[3], Jörg Schulla[6], Alessio Gusmeroli[4], Caroline Aubry-Wake[2], A. Cody Beedlow[2], and Andrew Hoffman[2]

[1]Alaska Division of Geological & Geophysical Surveys, 3354 College Road, Fairbanks, Alaska 99709

[2]Geophysical Institute, University of Alaska Fairbanks, 903 Koyukuk Dr., Fairbanks, Alaska 99775

[3]Water and Environmental Research Center, University of Alaska Fairbanks, 306 Tanana Loop, Fairbanks, Alaska 99775

[4]International Arctic Research Center, University of Alaska Fairbanks, 930 N Koyukuk Dr, Fairbanks, AK 99775

[5]Department of Physics, Department of Energy & Environmental Systems, North Carolina A&T State University, Greensboro, NC 27411

[6]Regensdorferstrasse 162, CH 8049 Zürich

### Acknowledgements:

We thanks Alaska Energy Authority for funding this study. We are grateful to the following for assistance with this study: J. Young; A. Gould; R.P. Daanen; M. Balazs; W. Harrison; Geo-Watersheds Scientific; Pathfinder Aviation; Last Frontier Aviation; and Alaska Department of Transportation & Public Facilities, Cantwell Station.

TABLE OF CONTENTS

# LIST OF TABLES

# LIST OF FIGURES

# LIST OF ACRONYMS, ABBREVIATIONS, AND DEFINITIONS

| Abbreviation | Definition |
|---|---|
| A2, A1B and B2 | Emission Scenarios |
| ablation | All processes that reduce the mass of the glacier. Glacier mass reduction occurs through the loss of snow and ice by melting, sublimation and calving. |
| AEA | Alaska Energy Authority |
| AET | Actual Evapotranspiration |
| albedo | A measure of the reflectivity of a surface, expressed as the fraction of the incoming solar radiation reflected by the surface. |
| a.s.l. | Above sea level (as in elevation) |
| BLM | Bureau of Land Management |
| C | Celsius |
| CCSM | Community Climate System Model |
| CMIP | Coupled Model Intercomparison Project |
| CORDEX | Coordinated Regional Climate Downscaling Experiment |
| D | Dimensional |
| DEM | Digital Elevation Model |
| DTM | Digital Terrain Model |
| ECHAM5, GFDL21, MIROC, HAD and CCCMA | General Circulation Models |
| ELA | Equilibrium Line Altitude |
| ET | Evapotranspiration |
| evapotranspiration | The water loss from the surface to the atmosphere via evaporation and transpiration. The sum of evaporation and transpiration. |
| FERC | Federal Energy Regulatory Commission |
| firn | The compacted snow on a glacier that remains after at least one year's ablation season, but has not yet metamorphosed into glacier ice. |
| GCM | General Circulation Model or Global Climate Model |
| GINA | Geographic Information Network of Alaska |
| GRACE | Gravity Recovery and Climate Experiment |
| Gt | Gigaton |
| HOBO | A brand of data logger/sensors by the company Onset |
| IfSAR | Interferometric Synthetic Aperture Radar (a.k.a. InSAR) |
| IPCC | Intergovernmental Panel on Climate Change |
| ISR | Initial Study Report |
| jökulhlaup | A sudden outburst flood of water originating from a glacier melted during a volcanic eruption. Also used when water filling an ice-dammed lake bursts out of the damned portion of the lake resulting in flooding. |
| K | Kelvin |
| km | Kilometer |
| LIA | Little Ice Age |

| Abbreviation | Definition |
|---|---|
| m | Meter |
| mm | Millimeter |
| moulin | A deep pothole or shaft that allows supraglacial meltwater to enter a glacier. |
| NARCCAP | North American Regional Climate Change Assessment Program |
| NCAR | National Center for Atmospheric Research |
| NCDC | National Climatic Data Center |
| NCEP | National Centers for Environmental Prediction |
| NGA | National Geospatial-Intelligence Agency |
| NLCD2001 | National Land Cover Database 2001 |
| NMFS | National Marine Fisheries Service |
| NOAA | National Oceanic and Atmospheric Administration |
| NRCS | Natural Resources Conservation Service |
| NSE | Nash-Sutcliffe Efficiency |
| nunatak | An island of bedrock which projects above the glacier, icefield or ice sheet's surface and is completely surrounded by the ice. |
| NWS | National Weather Service |
| PDO | Pacific Decadal Oscillation |
| periglacial | Describes cold, non-glacial landforms, climates, geomorphic processes or environments. |
| permafrost | Ground that has remained continuously below 0°C for at least two consecutive years. |
| PET | Potential Evapotranspiration |
| PRISM | Parameter-elevation Regressions on Independent Slopes Model |
| RCP6.0 | Representative Concentration Pathway scenario 6.0 |
| RSP | Revised Study Plan |
| SDMI | Alaska Statewide Digital Mapping Initiative |
| SNAP | Scenarios Network for Alaska and Arctic Planning |
| SNOTEL | Snow Telemetry |
| SPD | Study Plan Determination |
| talik | An unfrozen section of ground found above, below, or within a layer of discontinuous permafrost or beneath a body of water in continuous permafrost due to a local anomaly in the thermal, hydrological, hydrogeological or hydrochemical conditions. |
| UBC | University of British Columbia |
| US | United States |
| USGS | United States Geological Survey |
| V-A | Volume-Area |
| V-L | Volume-Length |
| W | Watt |
| w.e. | Water equivalent |
| WaSiM | Water Balance Simulation Model |
| WRF | Weather Research and Forecasting Model |

# EXECUTIVE SUMMARY

| Glacier and Runoff Changes Study | |
|---|---|
| Purpose | Glaciers, permafrost, and the hydrologic cycle are expected to change in response to anticipated future atmospheric warming by the end of this century, thus, impacting water yields to the proposed Susitna-Watana hydroelectric reservoir. This study quantifies future changes in glacier wastage, surface and groundwater, permafrost, and evapotranspiration and their combined effect on runoff into the proposed reservoir. |
| Status | This report summarizes findings about potential future changes in runoff associated with anticipated changes in climate. |
| Highlighted Results and Achievements | This study combines field measurements and computational modeling to provide estimates 21st century river discharge into the proposed reservoir of the Susitna-Watana Hydroelectric Project. A physically-based hydrological model, Water Flow and Balance Simulation Model (WaSiM), is forced with climate inputs from a CCSM CMIP5 RCP6.0 scenario downscaled to a 20km-5km nested grid using the Weather Research and Forecasting (WRF) Model. Climate model projections indicate that from 2010-2029 to 2080-2099 the basin-wide mean-annual temperature will rise 2.5º C and total precipitation will rise 2%, with a 13% decrease in snowfall and a 20% increase in rainfall. Hydrological simulations over the 21st century indicate that glaciers will retreat, evapotranspiration will increase, and permafrost will thaw. Mean specific runoff at the proposed dam site will increase slightly (1.5%) from 1976-1995 to 2016-2035, followed by a notable reduction (7.3%) from 2016-2035 to 2080-2099. By the end of the 21st century, peak spring runoff occurs ~1 month earlier than it did at the beginning of the century, and late summer runoff reduces to about half its original volume during this same interval. |

# 1. INTRODUCTION

On December 14 2012, Alaska Energy Authority (AEA) filed with the Federal Energy Regulatory Commission (FERC or Commission) its Revised Study Plan (RSP), which included 58 individual study plans (AEA 2012). Included within the RSP was the Glacier and Runoff Changes Study, Section 7.7. RSP Section 7.7 focuses on understanding how changes to the Upper Susitna basin hydrology due to glacial retreat and climate change can affect Project operations and environmental resources.

On February 1 2013, FERC staff issued its study plan determination (February 1 SPD) for 44 of the 58 studies, approving 31 studies as filed and 13 with modifications. RSP Section 7.7 was one of the 13 approved with modifications. In the February 1 SPD, FERC recognized the following:

*AEA proposes to analyze the potential effects of climate change on glacier wastage and retreat and the corresponding effects on streamflow entering the proposed reservoir, and evaluate the effects of glacial surges on sediment delivery to the reservoir.*
*Specifically, AEA proposes to:*

1. *review existing literature relevant to glacier retreat in southcentral Alaska and the upper Susitna watershed and summarize the current understanding of potential future changes in runoff associated with glacier wastage and retreat;*
2. *develop a hydrologic modeling framework that utilizes a glacier melt and runoff model (Hock 1999) and a Water Balance Simulation Model (WaSiM) to predict changes in glacier wastage and retreat on runoff in the Susitna basin;*
3. *simulate the inflow of water to the proposed reservoir and predict changes to available inflow using downscaled climate projections up to the year 2100; and*
4. *analyze the potential changes to sediment delivery from the upper Susitna watershed into the reservoir from glacial surges.*

FERC staff recommended the following in the February 1 SPD.

- *We find that the analysis of the potential changes to sediment delivery from the upper Susitna watershed into the reservoir from glacial surges as proposed by AEA is necessary, and therefore, are recommending approval of this portion of AEA's proposed study (item 4 as described above in the applicant's proposed study).*
- *We are not recommending approval of the remainder of AEA's proposed study (items 1-3 as described above in the applicant's proposed study). We have no objection to AEA conducting this portion of the study.*
- *We do not recommend extending the geographic range of the climate change assessment or adding an analysis of the natural resource impacts, as recommended by the NMFS and others.*

On February 21 2013, the National Marine Fisheries Service (NMFS) filed a notice of study dispute pursuant to section 5.14(a) of the Commission's regulations regarding FERC's failure to require AEA to implement the three study components related to glacier runoff and climate change that AEA proposed in the RSP (item 1). A Dispute Resolution Panel Meeting and Technical

Conference was held on April 3 2013 to discuss NMFS' modification requests. On April 26 2013 FERC provided its Study Dispute Determination, requiring the following modification;

*We recommend that AEA review existing literature relevant to glacial retreat and summarize the understanding of potential future changes in runoff associated with glacier wastage and retreat, as described in RSP section 7.7.4.1.*

On May 28 2013, NMFS and the Center for Water Advocacy (Center) filed requests for rehearing of the formal study dispute determination issued on April 26 2013. NMFS and the Center sought rehearing of the Director's finding that studies proposed by the potential applicant, AEA, and NMFS related to global climate change are unnecessary to conduct the Commission's environmental analysis and therefore will not be required to be conducted by AEA. On July 18 2013, FERC rejected the Center's request for rehearing and denied NMFS' request for rehearing.

AEA has adopted the RSP as the Final Study Plan with no modifications.

An initial study report of the results of the literature review was submitted, thus completing the FERC-approved study.

This manuscript supplements the initial study report of Glacier and Runoff Changes (7.7).

## 2. STUDY OBJECTIVES

The primary goal of this study is to analyze the potential impacts of glacier wastage and retreat on the Susitna-Watana Hydroelectric Project (Project). Specifically, how will glacier wastage and retreat, along with associated future changes in climate, affect the flow of water into the proposed reservoir? Currently >120 glaciers flow down the southern flanks of the Alaska Range near 13,832-foot Mount Hayes to form the three forks of the Upper Susitna River (Figure 2-1).

Glaciers in this area provide a significant portion of the total runoff within the Upper Susitna drainage, and it is well documented that these glaciers are currently retreating (see section 3.1.1). Changes to the runoff represented by the continued melting of glaciers is projected to occur, and may affect the Project. Therefore, it is important to understand how changes to the upper Susitna basin hydrology, due to glacier wastage and retreat and climate change can affect Project operations and environmental resources.

The objective of this study is to model the effects of future glacier wastage and retreat on runoff. The study combines field measurements, projections of future climate, and hydrological modeling to provide estimates of future runoff into the proposed 95 $km^2$ and 70 km-long reservoir of the Susitna-Watana Hydroelectric Project.

# 3. BACKGROUND

## 3.1. Glaciers

Glaciers are significant contributors to seasonal river discharge in many parts of the world, serving as frozen reservoirs of water that supplement runoff during warm and dry periods in which there is low flow. Glaciers in northern high-latitude regions have been experiencing increasingly negative cumulative mass balances since the early 1990s (Wolken *et al.* 2013). This trend is anticipated to continue as a consequence of global climate warming, as predicted unambiguously by all current climate models, and is expected to cause accelerated glacier wastage and retreat, thus reducing the storage capacity of snow and ice. As a result, river discharge volumes and timing in seasonal river runoff will change, and glaciers' ability to buffer this flow against seasonal precipitation extremes will be reduced or lost.

### 3.1.1. Glacier Changes in Alaska

Glaciers in Alaska (including northwest Canada) cover ~86,700 $km^2$ corresponding to 12% of all glacierized areas in the world outside the vast Greenland and Antarctic ice sheets (Pfeffer *et al.* 2014). Roughly 14% of the area is drained through 50 tidewater glaciers. The mass balance of a glacier is a widely used index of how glaciers respond to climate variability and change, and is defined as the change in the mass of a glacier over a stated period of time (Cogley *et al.* 2011). Alaskan glaciers have shown a coherent signal in glacier mass loss during the last several decades with acceleration of mass loss during the last two decades. Alaskan glaciers currently exhibit one of the highest glacier wastage rates on Earth (Gardner *et al.* 2013). Current annual thinning rates reach several meters per year for some glaciers that terminate near sea level (VanLooy *et al.* 2006; Larsen *et al.* 2007; Larsen *et al.* 2015). During 1995 to 2001, annual volume loss from Alaskan glaciers equaled 0.27±0.1 mm/yr sea-level equivalent (Arendt *et al.* 2002) and added ~100 $km^3$ $yr^{-1}$ to the freshwater discharge budget for the Gulf of Alaska watershed (Arendt *et al.* 2002). This runoff volume corresponds to about 50% of the annual discharge of the Yukon River (Raymond *et al.* 2007).

A revised estimate using US Geological Survey maps and satellite derived digital elevation models indicate mass losses of 42±9 Gt/yr during 1962 to 2006 (Berthier *et al.* 2010). Gardner *et al.* (2013) estimates a mass loss of 50± 17 Gt $yr^{-1}$ for the period 2003-2009 based on evaluation of several published estimates from the Gravity Recovery and Climate Experiment (GRACE). However, GRACE estimates of mass loss vary widely in Alaska due to a combination of factors (i.e. different spatial and temporal resolutions; Table 3.1.1-1); more research is needed to resolve the discrepancies.

Average thinning rates vary widely across Alaska, but a pattern of recent acceleration is found uniformly. The mass changes are consistent with global atmospheric warming trends. Low-elevation climate station data in Alaska and northwestern Canada indicate that, during the period 1950 – 2002, winter and summer temperatures increased by about 2.08 ± 0.88 and 1.08 ± 0.48 °C, respectively, and precipitation may have increased in most parts (Arendt *et al.* 2009). However, climate-glacier interactions are complex and the precise causes of the observed glacier changes need further investigation.

Alaskan glaciers are expected to continue losing mass in the future (Radić and Hock 2011). 100-year projections of the Alaskan's glacier contribution to sea level rise indicate that Alaska is one of the largest regional contributors with multi-model volume losses varying from 18% to 45% by 2100 in response to temperature and precipitation projections of 14 general circulation models (GCMs) and the Representative Concentration Pathways (RCP) 4.5 and RCP8.5 emission scenarios (Radić *et al.* 2013; Figure 3.1-1).

## 3.1.2. Runoff from Glaciers

### *3.1.2.1. Characteristics of Glacier Discharge*

Glaciers significantly modify streamflow both in quantity and timing, even with low percentages of catchment ice cover (e.g., Meier and Tangborn 1961; Fountain and Tangborn 1985; Chen and Ohmura 1990; Hopkinson and Young 1998; see Hock *et al.* 2005 for review). Glaciers are stores of water, amassing and releasing water on a wide range of time scales, thus, modulating basin hydrology. Distinct characteristics of glacier runoff include (Röthlisberger and Lang 1987; Hock *et al.* 2005):

- *Annual runoff*: Annual runoff from glacierized basins is modulated by the glaciers' mass balances, i.e. the changes in glacier mass over time. Runoff is reduced in years of positive mass balance, as water is withdrawn from the hydrological cycle and put in temporary storage. In contrast, runoff is enhanced during years of negative glacier mass balance since water kept in storage is released, producing more total runoff than in years of positive balance under otherwise similar conditions (Figure 3.1.2.1-1);
- *Diurnal cycles*: Glacier runoff is characterized by pronounced melt-induced diurnal cyclicity. Daily peak flows may increase by several hundred percent of daily minimum flows during days without rainfall;
- *Seasonal variations*: Glacier runoff shows distinct seasonal variations with very low winter runoff and a pronounced and seasonally delayed summer peak compared to non-glacierized basins (Escher-Vetter and Reinwarth 1994). While runoff from the glacier is minimal during the winter season of snow accumulation, runoff is large during the melt season, when melt of winter snow, firn and ice enhance down-glacier river flows;
- *Interannual variability*: Glacier cover dampens year-to-year variability in streamflow; a minimum is reached at 10-40% of glacierization with increasing variability with both lower and higher degrees of ice cover (Lang 1986). This so-called 'glacier compensation' effect occurs because in hot and dry years, glacier melt offsets reduced precipitation inputs;
- *Runoff correlation*: Runoff from highly glacierized basins often correlates with air temperature, while glacier-free basins tend to show positive correlations between runoff and precipitation;
- *Outburst floods*: Glaciers may also cause sudden floods, often referred to as jökulhlaups, posing a potential hazard for downstream populations and infrastructure. These outburst floods may be due to subglacial volcanic eruptions or sudden drainage of sub-glacial, moraine and ice-dammed lakes (e.g., Lliboutry *et al.* 1977; Bjornsson 2003).

In addition to contributing directly to runoff through ice wastage, glacier cover within a drainage basin decreases direct evaporation and plant transpiration, the combination of which can result in

considerably higher water yields for basins with glaciers compared to unglacierized watersheds (Hood and Scott 2008). Furthermore, the proportion of streamflow derived from glacier runoff has pronounced effects on physical (Kyle and Brabets 2001), biogeochemical (Hodson *et al.* 2008; Hood and Berner 2009; Bhatia *et al.* 2013) and biological (Milner *et al.* 2000; Robinson *et al.* 2001) properties of streams. Consequently, changes in watershed glacier cover also have the potential to alter riverine material fluxes. For example, area-weighted watershed fluxes of soluble-reactive phosphorus decrease sharply with declining ice cover (Hood and Scott 2008). Recent studies also suggest that dissolved organic material contained in glacial runoff has a microbial source and is highly labile to marine heterotrophs (Hodson *et al.* 2008; Hood *et al.* 2009).

#### *3.1.2.2. Effects of atmospheric warming on glacier runoff*

The response of glacier runoff to climate changes is complex and will depend on the time-scale considered. Although the mass change response is immediate, some runoff response-variables will change sign at a later stage when enhanced melt rates have caused glacier volume to decrease significantly (Hock *et al.* 2005).

As climate changes and causes glacier mass balances to become progressively more negative, total glacier runoff will initially increase due to enhanced glacier melt rates (Jansson *et al.* 2003; Figure 3.1.2.2-1). In highly glacierized catchments runoff due to glacier mass loss may contribute a substantial fraction of annual water yields. Enhanced melt rates are caused primarily by atmospheric warming but are further accelerated by positive feedback mechanisms. For example, enlargement of bare ice areas due to faster removal of winter snow or loss of firn area will cause reduced albedo, thus increasing the amount of absorbed shortwave radiation and melt (Figure 3.1.2.2-2).

The glacier will respond to prolonged glacier net mass loss by dynamically adjusting its size and shape generally through retreat and thinning. While the mass loss in response to climate forcing is immediate, the geometric adjustment is delayed by the glacier's characteristic response time (Johannesson *et al.* 1989). The initial increase in runoff will be followed by a reduction in runoff as the glacier dwindles and eventually disappears (Figure 3.1.2.2-1). Hence, the ability of the glacier to augment streamflow in periods of otherwise low flow will be diminished and eventually lost. With high percentage of ice cover, the initial increase in runoff can be substantial and result in a higher frequency of flood events that might not be triggered by rainfall events. The timing of the turning point between runoff increase and decrease will depend on the competing effects of increased glacier thinning rates due to increased melt and decreased total melt water due to depletion of the glacier storage, which in turn is governed by both glacier and climate change characteristics. Anticipating the timing of the peak in runoff and the rate of decline in runoff following that peak are key questions in long-term water resource planning (e.g. hydropower development). The replacement of ice by coastal temperate forest and alpine vegetation may lead to further reduced water yields and a major change in catchment-wide nutrient cycling (Wolken *et al.* 2011).

Warming air temperatures prolong the melt season by causing earlier melt onset and later freeze-up (Sharp and Wolken 2011), thus modifying the timing of the seasonal glacier runoff peak. In addition, the pronounced daily cyclicity typical of glacier discharge will, at least in an initial phase, be amplified due to increased daily melt water production and feedback mechanisms. This

increases the risk for floods substantially, especially when strong melt-induced flows coincide with heavy rain events. Feedbacks include more efficient water transport through the glacier as snow and firn layers that typically have large water retention capacity are removed more quickly, and melt waters are evacuated via efficient tunnel systems through the glacier ice (Figure 3.1.2.2-2; Braun *et al.* 2000; Willis *et al.* 2002).

#### *3.1.2.3. Modeling Glacier Runoff*

Glacier runoff has been modeled using stochastic, conceptual and physically based models (see Hock *et al.* 2005 for review). Stochastic models were widely used in the 1960s and 1970s for seasonal and short-term runoff forecasts often tailored to the needs of hydropower facilities. The models compute runoff directly as a function of meteorological variables based on multiple regression techniques (Lang 1968; Jensen and Lang 1973; Ostrem 1973). In contrast, conceptual and physical-based models attempt to compute the individual processes leading to glacier runoff.

Here, the modeling of glacier runoff and its response to climate change involves three principal steps (Hock *et al.* 2005): modeling of (a) glacier mass balance, i.e. the changes in the glacier's mass over the hydrological year; (b) the geometric adjustments of the glacier in response to glacier mass changes; and (c) the routing of melt and rain water through the glacier, i.e. transformation of water inputs into a discharge hydrograph down glacier. Glaciers are often only crudely represented in hydrological models. While many existing watershed models include routines for snow and ice melt, the geometric adjustments and glacier specific discharge routing are often ignored entirely or treated in very rudimentary ways, inhibiting accurate modeling of the modulating effects of glaciers on watershed runoff.

##### *3.1.2.3.1. Glacier Mass Balance*

Mass balance models generally fall into two categories: (a) temperature-index models based on air temperature as the primary index of melt energy (Hock 2003); and (b) physically based energy balance models computing all relevant components of the energy balance (Hock 2005). Although the latter more adequately describe the physics of the processes involved, considerably larger data requirements often inhibit their use. Nevertheless, despite their simplicity temperature-index models have been shown to perform surprisingly well in hydrological modeling on catchment scales. However, they are less suitable to model the diurnal cyclicity of glacier runoff or the accurate representation of the spatial variation in melt rates across a basin.

To improve the physical representation of processes while retaining low data requirements, a complete hierarchy of melt models have been developed with a gradual transition from simple degree-day approaches to energy-balance-type expressions by increasing the number of input variables into model formulations. For example, the UBC-runoff-model (Quick and Pipes 1977) and the HYMET-runoff-model (Tangborn 1984) employ the daily temperature range in addition to air temperature as climatic input for their melt routines, a measure of cloud-cover and, hence solar radiation. Hock (1999) varied the degree-day factor as a function of potential direct solar radiation, thus significantly improving the modeling of both the spatial melt variations and the diurnal melt and glacier discharge amplitudes. This model is also included in WaSiM. Pellicciotti *et al.* (2005) elaborated on this approach by including parameterized shortwave radiation fluxes. Temperature-index models are widely used, promoted by ease of application and low data input

requirements. However model parameters are often not transferable between catchments (MacDougall *et al.* 2011), and it remains unclear how model parameters will change under a different climate, a limitation that needs further research.

#### *3.1.2.3.2. Geometric Adjustments*

Glacier retreats to higher altitudes exert a negative, i.e. stabilizing, feedback on glacier mass change because loss of area at predominantly lower elevations will make the average thinning less pronounced than it would have been without retreat under the same climate conditions. Glacier thinning, in contrast, exerts a positive, i.e. self-amplifying, feedback; with decreasing surface elevation, the glacier is exposed to higher air temperatures, resulting in more negative mass balances. The net effect of these two opposing feedbacks will depend on a number of factors related to climate, glacier geometry and characteristics such as debris coverage (Bodvarsson 1955; Harrison *et al.* 2001; Huss *et al.* 2012). It is crucial to model the geometry changes resulting from climate change to be able to account for the mass-balance feedback and to model the turning point beyond which glacier runoff decreases (Figure 3.1.2.2-1).

Ideally the dynamical adjustment is calculated using physically-based numerical ice flow models. Such models solve a momentum balance equation, either the Stokes equations or an approximation thereof, however, detailed data requirement restrict their use in hydrological modeling. The most common approach to account for the glacier's dynamical adjustments as its mass changes is volume-area (V-A) or volume-length (V-L) scaling (Bahr *et al.* 1997; see section 7.1.1.1). The annual volume change computed from the mass-balance model is subtracted from total glacier volume, and scaling is applied to derive a new area from the updated glacier volume. In case of volume loss, elevation bands or grid cells at lower elevations are then removed from the glacier domain.

Huss *et al.* (2010) suggested an approach of intermediate complexity, distributing the annual volume loss across the glacier surface based on observed typical elevation change patterns, which indicate generally low thinning rates at high elevations and strongly accelerated thinning rates at low elevations. An empirical function relating glacier surface elevation change to normalized elevation range is applied each year to adjust the elevation of each glacier grid cell. Each grid cell with a modeled elevation drop exceeding the current ice thickness is removed from the glacier, thereby also modeling glacier retreat. This approach has successfully been tested on smaller retreating glaciers, but does not provide a mechanism for glacier advance.

#### *3.1.2.3.3. Discharge Routing*

Detailed modeling of the physical processes involved in the transfer of water through a glacier is highly complex. Such models need to account for the time-transgressive growth and decay of conduits and passages through and under the deformable ice, and account for occurrence of crevasses, moulins and other entry points where water can enter the glacier system. Only few such glacier models exist (e.g. Arnold *et al.* 1998; Flowers and Clarke 2002), and generally are used as research tools rather than for routing water through glaciers in watershed models.

Instead, most hydrological models (if they include specific water routing through glaciers at all) adopt the widely used concept in hydrological internal flow routing of linear reservoirs (Chow *et al.* 1988). The glacier is divided into one or several parallel or serial reservoirs, each of which can

be thought of a container of water where outflow is proportional to the stored water volume, which in turn depends on input from melt and rain water. Each reservoir is assigned a unique storage constant that represents the time shift between the centroid of the inflow and that of the outflow thus delaying the reservoir's outflow. A number of variants of this approach have been suggested (Figure 3.1.2.3.3-1), often assigning different storage constants based on the surface types of the glacier. For example, higher storage coefficients are applied for the snow and firn zones than for bare ice, reflecting their profoundly higher water retention capacity. Storage constant are often treated as model parameters obtained from model calibration. Despite its simplicity and pronounced changes in a glacier's internal drainage system throughout the melt season, the approach performs remarkably well (Hock and Noetzli 1997; Escher-Vetter 2000).

### *3.1.2.4. Previous Glacier Runoff Studies*

A large number of studies around the world have highlighted the role of glaciers in the hydrological cycle and indicated significant hydrological changes in response to climate change, including changes in total water amounts and seasonality as described above (e.g., Braun *et al.* 2000; Casassa *et al.* 2009; Rees and Collins 2006; Hagg *et al.* 2006; Horton *et al.* 2006; Yao *et al.* 2007; Huss *et al.* 2008; Immerzeel *et al.* 2008; Koboltschnig *et al.* 2008; Stahl *et al.* 2010; Kobierska *et al.* 2013). Results vary with regard to the importance of glacier runoff relative to total runoff in glacierized catchments (Weber *et al.* 2010; Huss 2011). This can at least partially be explained by varying physical factors such as climate regimes, catchment size, degree of glacierization or glacier mass change rates. However, some of these differences are due to the different ways to define glacier runoff. Definitions of glacier runoff fall into two principal categories (Radić and Hock 2014): (1) those that only consider the net mass loss component of a glacier due to glacier wastage, i.e. runoff is zero if the glacier is in balance or gains mass; and (2) those that consider all meltwater originating from a glacier no matter the magnitude or sign of the mass budget. Glacier runoff generally is much larger if the latter definition is adopted than the former. Hence, the relative importance of glacier runoff to total runoff will differ between these two approaches.

Observations from gauge records in glacierized basins show both increases in runoff, for example, along the coast in southern Alaska (Neal *et al.* 2002), northwestern British Columbia (Fleming and Clarke 2003) or on the Tibetan Plateau (Yao *et al.* 2007), and negative trends in summer streamflow, for example in the southern Canadian Cordillera (Stahl and Moore 2006). The long-term effect of runoff reduction, resulting from a decrease in glacierized area, was also detected by Chen and Ohmura (1990), who analyzed multi-decadal discharge records in the Swiss Alps. Comeau *et al.* (2009) analyzed annual runoff in a large catchment in western Canada and found that reductions in glacier volume, due to receding glaciers, contributed 3% to total runoff during 1975-1998.

Various studies have modeled the impacts of future climate change on runoff in glacierized basins. To provide information in connection with a hydropower scheme, Adalgeirsdottir *et al.* (2006) modeled an increase in annual glacier runoff from ice caps in Iceland of up to 60% until about 2100, followed by a rapid reduction in runoff thereafter. Rees and Collins (2006) applied a hydro-glaciological model to hypothetical catchments with varying fractional ice area in the Himalayas and predicted gradual runoff increase over the next ~50 years, followed by a more abrupt runoff decline to lower than contemporary values over the next few decades. Stahl *et al.* (2008) investigated the sensitivity of streamflow in response to changes in climate and glacier cover for

the Bridge River basin in British Columbia, coupling a hydrological model with a glacier response model. Under the assumption of current climate, the model projected decreases in glacier area by 20% over the next 50 to 100 years causing a similar percentage decrease in summer streamflow.

Recent investigations in the monsoon-affected regions High Asian Mountains indicate that glacier melt may be of lesser importance than previously assumed since monsoon rains and glacier melt will continue to sustain the increasing water demands expected in these areas (Kaser *et al.* 2010; Immerzeel *et al.* 2013). In contrast a number of studies have investigated the hydrological consequences of continued glacier wastage in the tropical Andes in response to climate change in individual watersheds where glacier melt often is the only source of water during the dry season. Juen *et al.* (2007) and Vuille *et al.* (2008) used historical hydrological records and found a decrease in glacier runoff as glaciers shrank and strongly enhanced seasonality. Baraer *et al.* (2012) found that annual discharge in the investigated watersheds in Peru's Cordillera Blanca will be lower than present by 2-30%, with considerably more pronounced effects during the dry season. Several recent studies have highlighted the potential of glacier retreat in modulating runoff regimes, and indicated serious adverse effects on water availability if glacier recession continued (e.g. Pouyaud *et al.* 2005, Juen *et al.* 2007; Mark and Seltzer 2003; Mark and McKenzie 2007; Suarez *et al.* 2008; Kaser *et al.* 2010).

Even in non-arid regions the glacier contribution to river runoff can be substantial. Huss (2011) assessed the contribution of glaciers to runoff from large-scale drainage basins in Europe with areas up to 800,000 $km^2$ over the period 1908-2008 based on modeled monthly mass budget estimates for all glaciers in the European Alps. The glacier runoff defined as the water due to glacier net mass change was computed for each month and compared to monthly river runoff measured at gauges along the entire river lengths. Although ice cover of the investigated basins did not exceed 1% of the total area, the maximum monthly glacier contributions during summer ranged from 4% to 25% between catchments, emphasizing that seasonal glacier contributions can be significant even in basins with little ice cover.

#### *3.1.2.4.1. Alaska*

Few studies have quantified the effect of glaciers on Alaskan rivers. Neal *et al.* (2002) note an increase in runoff in some gauge records for glacier streams along the coast in southern Alaska. Several studies documented the impact of glacier water on the biogeochemical properties of Alaska streams (e.g. Hood and Scott 2008; Hood and Berner 2009). Neal *et al.* (2010) adopted a water balance approach to estimate the contribution of glacier runoff to freshwater discharge into the Gulf of Alaska; a 420,230 $km^2$ watershed covered 18% by glaciers. Glacier runoff (defined as all water including melt and rain water from the glacier area) contributed 47% of the total runoff (870 $km^3\ a^{-1}$), while 10% came from glacier net mass loss alone.

#### *3.1.2.4.2. Upper Susitna Basin*

Between 1981 and 1983, a joint effort between the University of Alaska Fairbanks and R&M Consultants, Inc. on behalf of the Alaska Power Authority (now Alaska Energy Authority) was made to analyze the runoff contributions produced from glaciers in the Susitna River Basin. The project goal was to determine the timing and amount of glacier runoff in order to aid development of water forecast models for the proposed Susitna hydroelectric dam. This study focused on the

four major glaciers located on the southern side of the Eastern Alaska Range at the Susitna River and MacLaren River headwaters. These glaciers are: West Fork Glacier; Susitna Glacier and its Northwest and Turkey Tributaries; East Fork Glacier; and MacLaren Glacier. The glaciers in the Talkeetna Mountains or Eureka Glacier were not included in this study.

The mass balance of the glaciers was determined by the glaciological method, i.e. measuring accumulation and ablation at stakes and in snow pits. The amount of snow and ice that had accumulated and melted was measured at each stake at specific times in the hydrologic year. This method is used to monitor the change in the glacier surface relative to a datum registered to the stake drilled into the glacier. During this study, three stakes were placed on each of the major glaciers at different elevations by mountaineers who used topographic maps to determine site elevations (Figure 3.1.2.4.2-1). One mass balance stake was placed in the ablation zone near 1000 m, one stake was placed at the equilibrium line of the glaciers near 1500 m, and another stake was set in the accumulation zone near 2000 m. Since the mass balance stake distribution was one stake per 50 $km^2$, the mass balance monitoring efforts were considered to be at the reconnaissance level (Clarke *et al.* 1985a). The stakes were typically measured during the spring in April or May, during the summer in late August or early September. The sparse stake measurements of snow depth were supplemented by probing to the late-summer surface.

Mean snow density was used to convert the mass balance stake measurements to water equivalent balances. The mean snow density was calculated by measuring snow density as a function of depth from samples taken in snow pits dug near representative stakes and from cores of the entire snowpack. In May 1981, the winter snowpack and balance (1980 to 1981) was estimated from snow stratigraphy by identifying the late-summer surface while probing snow depth and from the snow pit measurements (Clarke *et al.* 1985b). Snow temperatures versus depth were assessed in snow pits; by May, the snow was isothermal at 0°C (Harrison *et al.* 1983). The mean snow density used in spring and late-summer mass balance calculations was 400 $kg/m^3$, 500 $kg/m^3$ for mid-summer calculations, and 200 $kg/m^3$ for fall calculations. Over the three-year observation period, the annual balances are 0.1 ± 0.6 m w.e./yr. The winter and summer balances, and the annual balances for each glacier are summarized in Table 3.1.2.4.2-1.

Glacier runoff was compared to stream gauges in the Susitna River at Gold Creek, Susitna River at the Denali Highway, and at the MacLaren River on the Denali Highway gauge (Figure 3.1.2.4.2-1; Table 3.1.2.4.2-2). Approximately 34% of the runoff measured north of the Denali Highway (using Susitna River at Denali and MacLaren River at Denali stream gauges) was attributed to the glacierized area. The average runoff from the melting of snow, firn and ice was 1.3 m/yr, nearly 1.4 times greater than the runoff contribution from the non-glacierized area above the Denali Highway (0.95 m/yr). The glacier runoff component was approximately 2.5 times greater (13% of total runoff) than the volume contribution from the non-glacierized basin upstream of the Gold Creek stream gauge (Clarke *et al.* 1985a). The primary glacier melt season during the period of study was during July and August, when 75% of the glacier meltwater was generated. The remainder was produced during the late spring in May and June, and in the fall before the winter freeze-up in November (Clarke *et al.* 1985a).

Runoff from liquid precipitation was calculated from the high elevation Susitna Glacier climate station monitored by R&M Consultants, Inc. (Figure 3.1.2.4.2-1). This station was located at 1433 m on a nunatak between Susitna Glacier and its Northwest Tributary. Several assumptions used in

calculating rainfall over the glacierized basin are described in more detail in Clarke *et al.* (1985a). From this rain gauge, a lower-limit on the precipitation runoff is 0.25 m/yr.

## 3.2. Permafrost

Permafrost is defined as any parent material that remains below 0˚C for more than two consecutive years. About 85% of Alaska is within permafrost zones, while glaciers cover ~5% of the state. There are four permafrost distribution classes that are typically used: continuous, where >90% of the land surface is underlain by permafrost; discontinuous, between 50 and 90%; sporadic, between 10 and 50%; and isolated, between 0 and 10% (Figure 3.2-1; Jorgenson *et al.* 2008). The majority of the upper Susitna basin is estimated to be underlain by discontinuous and continuous permafrost.

### 3.2.1. Trends in Permafrost

Permafrost distribution and conditions are forced by upper (air) and lower (geothermal) boundary conditions, which are modified by snow, vegetation, and soil properties. During past glacial periods, air and permafrost temperatures were much lower than today. The last event that cooled the ground significantly was the Little Ice Age (LIA; ca. 1600-1800). Most shallow permafrost (<100 m) that exists in Interior Alaska were formed during the LIA (Romanovsky *et al.* 2010). Evidence suggests that permafrost warming and degradation in Interior Alaska began about 250 years ago (mid-1700s) and was associated with periods of relatively warm climate during the mid-late 1700s and 1900s (Jorgenson *et al.* 2001). Measurements and model simulations of the 19$^{th}$ and 20$^{th}$ centuries show periods of warming and stagnation of permafrost temperatures in Interior Alaska. Numerical model simulations suggest that permafrost warmed in the late 1960s and early 1970s in response to warmer air temperature and an increase in snow cover, but were nearly stable in the 1980s (Osterkamp and Romanovsky 1999). Measurements show permafrost warming since the late 1980s in Interior Alaska throughout the Tanana River region, in the region south of the Alaska Range from Tok westward to Gulkana (in the Copper River Valley) and beyond to the Talkeetna Mountains (Osterkamp 2005). Near Healy, this permafrost warming (since the late 1980s) also resulted in thawing from the top of the permafrost of about 10 cm/yr (Osterkamp 2005), which was almost entirely attributed to increased snow cover (Osterkamp 2007). In Gulkana, however, permafrost has been thawing from the bottom at a rate of 4 cm/yr since the 1980s and has accelerated to 9 cm/yr after 2000 (Osterkamp 2005). Interior Alaska permafrost has also experience degradation from both the top and bottom. Although initiated in the 1700s, permafrost degradation (from the top) has increased rapidly in the recent decades (Jorgenson *et al.* 2001). Continued thawing of permafrost will significantly alter the soil moisture, and the biogeochemical and hydrological cycles in Interior and south-central Alaska (Wolken *et al.* 2011).

### 3.2.2. Permafrost Modeling

Basic permafrost models include only two variables to simulate the soil thermal regime, the mean annual air temperature and the geothermal temperature gradient. From these two variables, permafrost temperatures can be estimated for any place where the mean annual air temperature is below freezing. This approach ignores most of the aspects of what controls permafrost distribution (see the modifiers described above), but could be used when no other data are available. Ultimately, knowledge is required about the geothermal heat flux, soil, surface properties, snow

depth and density (Jafarov *et al.* 2012). Over the last few decades, the amount of data available to develop such datasets has increased dramatically due to the use of remote sensing techniques.

Surface and groundwater movement and storage is controlled by permafrost distribution. Current theory on the behavior of thermo-hydrological coupled models is advancing, but insufficient computational capability still represents a major challenge to creating simulations of large regions at a fine enough resolution to fully couple the two processes. Daanen *et al.* (2008) modeled the water movement in the active layer with a fully coupled three dimensional model during freezing in order the better understand the behavior of non-sorted circles at the decimeter scale. A coarser approach was taken to simulate the Alaska and circumpolar permafrost domain to develop an understanding of the water balance in the active layer (Rawlins *et al.* 2013).

## 3.3. Hydrology

The hydrology of Interior and south-central Alaska is strongly influenced by seasonal to centennial variations in cryospheric components (i.e., snow, ice and permafrost). Permafrost and frozen ground are relatively impermeable layers (if ice rich) that restrict recharge, discharge, infiltration and movement of groundwater, by acting as a confining layer (Williams 1970). Glaciers are frozen reservoirs of water that can modify the streamflow from seasonal to centennial time scales (Fountain and Tangborn 1985). Both glaciers and permafrost are abundant in the upper Susitna basin and are expected to modify its hydrologic cycle as they continue to respond to climate change.

### 3.3.1. Runoff

Like other major river systems in Interior Alaska, the streamflow in the Susitna River is characterized by a high rate of discharge from May through September and by low flows from October through April. About 86% of the total annual flow of the upper Susitna occurs from May through September (Alaska District, Corps of Engineers 1975). Winter snowpack in the Alaska Range determines the magnitude of early spring discharge; summer temperatures and precipitation determine the magnitude and duration of summer flow, and precipitation during the late summer/early autumn promotes any elevated magnitude or duration of late-season discharge (Ford and Bedford 1987). In large rivers that have their headwaters in mountainous, glacierized regions, e.g. the Susitna River, the timing of peak flows is not restricted to the spring snowmelt as heavy rainfall in summer and early fall add to high-elevation glacial wastage and snowmelt contributions (MacKay *et al.* 1973). Variations in the timing of river break-up, freeze-up and magnitude of snowmelt peaks in the Susitna River have been linked to shifts in the PDO (Pacific Decadal Oscillation; Curran 2012).

Although glaciers cover only ~4 % of the Susitna basin, together with the adjacent mountain terrain, they contribute a disproportionate fraction of the average annual streamflow (see section 3.1.2.4.2). Roughly 38% of the streamflow at Gold Creek originates above the gauging stations on the MacLaren River near Paxson and on the Susitna River near Denali, although these gauging sites cover only 20% of the basin area (R&M Consultants and Harrison 1981). The Susitna glaciers alone (snow, firn and ice) are estimated to contribute about 13% of the annual runoff measured at the Devils Canyon (Figure 3.1.2.4.2-1; Bowling 1982 and Table 3.1.2.4.2-2; Clarke *et al.* 1985a).

The presence of permafrost leads to reduced basin storage and an increases surface runoff (Dingman *et al.* 1971; Haugen *et al.* 1982; Slaughter *et al.* 1983), and its distribution strongly controls groundwater movement. Flood hydrographs for catchments underlain by permafrost tend to be flashier and more responsive than those from permafrost-free catchments (Slaughter and Kane 1979) due to the limited storage capacity of the active layer. Current theory on the behavior of thermo-hydrological coupled models is advancing, but insufficient computational capability still represents a major challenge to creating simulations of large regions, such as the upper Susitna basin, at a fine enough resolution to fully couple the two processes.

### 3.3.2. Surface Water and Wetlands

Surface water, groundwater and permafrost play a major role in nourishing wetlands in the Susitna basin. The presence of permafrost supports extensive wetlands in areas that are otherwise considered semi-arid as water is retained near the ground surface due to the limited subsurface storage capacity of the active layer (Callegary *et al.* 2013). In discontinuous permafrost regions, aspect can determine the presence or absence of permafrost, which in turn influences the distribution of wetlands (Dingman and Koutz 1974).

Artesian discharge of subpermafrost groundwater is known to occur in several regions and to be related to both lake and wetland formation in Interior Alaska (Cederstrom 1963; Kane and Slaughter 1973; Racine and Walters 1994). If permafrost degrades, surface water may either increase or decrease depending on the pressure of the underlying groundwater. In many cases, subpermafrost groundwater is artesian, which results in lake-levels rising. If the hydraulic gradient is downwards, the lake-levels will drop and permafrost can aggrade.

### 3.3.3. Groundwater and Infiltration

Groundwater in permafrost zones occurs above (suprapermafrost), below (subpermafrost), and locally within (talik) permafrost. Groundwater recharge, whether it is to an aquifer above (within the active layer) or below the permafrost, is controlled by the amount of surface water that is available for infiltration and by the hydraulic conductivity of the soils. Frozen soils with high ice content have substantially lower infiltration rates than thawed soils and frozen soils with low pore ice content and (Kane and Stein 1983a; 1983b). Accordingly, soils that have ice-saturated pores are nearly impermeable. Ice saturated soils typically occur at the top of the permafrost or in near-surface soils that experience a snowmelt that is preceded by a wet fall season. However, frozen silts with low moisture content can readily accept snowmelt at rates greater than the snow can melt (Kane and Stein 1983b). The partitioning of the snowmelt water into groundwater recharge or surface runoff is, therefore, partly controlled by the moisture status of the frozen soils.

Recharge and discharge of water to and from the larger regional aquifers located below the permafrost are limited to the unfrozen zones that perforate the permafrost such as beneath streams, snowbanks, lakes, glaciers and south-facing slopes. The Tanana River, north of the Alaska Range, has a permafrost-free zone beneath it (Williams 1970), due to the local thermal anomaly caused by the river. Susitna River is most likely experiencing a similar phenomenon, which would allow the surface water in the river to connect with the underlying aquifer. Headwaters draining the north facing slopes of the Alaska Range, such as the Delta River and Jarvis Creek, are elevated above the regional aquifer with wells having static water levels as much as 61 m below the streambeds

(Dingman *et al.* 1971; Wilcox 1980). Both Delta River and Jarvis Creek are influent, e.g. they lose water to the aquifer, once the rivers enter more permeable sediments (Wilcox 1980). It is possible that a similar hydrologic system is encountered in the upper Susitna basin.

In Interior Alaska, heat from groundwater may contribute to permafrost degradation because the groundwater is relatively warm (2–4 °C) year-round (Jorgenson *et al.* 2001). Similar to the lowlands of the Tanana River basin, groundwater springs surface in numerous places in the upper Susitna basin and are easily identifiable in the winter due to localized melt.

### 3.3.4. Evapotranspiration

Evapotranspiration (ET) represents the water loss from the surface to the atmosphere via evaporation and transpiration. Refined ET assessments are difficult to obtain due to the expensive techniques (eddy covariance) used in directly measuring ET (Aubinet *et al.* 2012), and to the rough assumptions that are built into simpler techniques, which are typically used in estimating ET. The most widely used approaches calculate the potential evapotranspiration (PET), e.g. the upper limit for water losses to the atmosphere. PET should not be confused with actual evapotranspiration (AET), which can be dramatically lower than PET. The loss of water from the surface to the atmosphere is driven by available energy and vapor gradients, but modified by a series of complex processes such as leaf stomata, soil moisture, etc. The most commonly used equations for calculating ET include: (1) Thornthwaite's potential evapotranspiration as it only relies on air temperature; (2) Hamon, which in addition to air temperature requires day length; and (3) closing the water balance equation with ET, which builds in the assumption of no storage change and integrates all errors associated with precipitation, runoff and storage change into the estimated ET. Iwata *et al.* (2012) measured the ET of a black spruce forest near Fairbanks, Alaska using the eddy covariance technique and found cumulative ET (snow-free period) ranging from 195 mm to 234 mm (average of 211 mm) with a typical maximum of 2.5 mm $day^{-1}$ in July (year 2003-2009). In comparison, PET estimates of the upper Susitna basin ranges between 300 to 450 mm $yr^{-1}$ (Patrick and Black 1968; http://www.snap.uaf.edu/data.php). The range in total precipitation is documented to be much larger than both measured evapotranspiration and estimated potential evapotranspiration in Interior Alaska (Iwata *et al.* 2012), suggesting an annual 1D water balance (precipitation minus potential evapotranspiration) to range between 25 and 300 mm in the upper Susitna basin (Ford and Bedford 1987).

## 3.4. Climate

Mean annual surface air temperature over northern high-latitude land areas (>60 °N) has increased by ~2.0 °C since the mid-1960s (Overland *et al.* 2012). In Alaska, weather station observations from 1949-2012 show a mean annual surface air temperature increase of 1.6 °C, a warming that appears to be unprecedented in at least the last 400 years (Overpeck *et al.* 1997; Kaufman *et al.* 2009). Mean annual air temperature has increased by ~1.3 °C during the past 50 years in Interior Alaska and by ~2.0 °C in inland south-central Alaska, with the greatest warming occurring in winter (Hartmann and Wendler 2005; Shulski and Wendler 2007). Regional climate models indicate that by the end of the 21st century, air temperature in this region of Alaska is projected to increase by 3 to 7 °C (Walsh *et al.* 2008). Projected increases in winter precipitation during this same time period could be offset by less summer precipitation (Karl *et al.* 2009; ACIA 2005).

# 4. STUDY AREA

## 4.1. Upper Susitna Basin

The headwaters of the Susitna River are distributed across the south side of the central Alaska Range. The upper Susitna basin (i.e. the study area), as referred to in this study, comprises the 13,289 km$^2$ watershed above the proposed Susitna-Watana dam (62.822523º, -148.538986º; Figure 4.1-1) and ranges 450-4,200 m above sea level (a.s.l.). About 4% of the upper Susitna basin is glacierized, and the remainder of the catchment is characterized by sparse vegetation, discontinuous permafrost, and little human development.

The northern boundary of the upper Susitna basin is formed by the spine of the Alaska Range. This area is characterized by high relief, and supports icefields and numerous glaciers (Figures 2-1 and 4.1-1). The Talkeetna Mountains form the southwest boundary of the basin and support few small glaciers. Modern glaciers in the upper Susitna basin are well within the limit of the Late Wisconsinan glacial advance (20-25 ka), during which this part of the Alaska Range hosted the northern extent of the Cordilleran Ice Sheet (Kaufman and Manley 2004).

The area of all glaciers in the upper Susitna basin was 678.37 km$^2$ in 2009 (Pfeffer *et al.* 2014; Figure 4.1-1). Most glaciers in the study area are located in the Alaska Range, but a few small glaciers exist in the Talkeetna Mountains. The glacierized area in the Alaska Range is comprised of 127 glaciers (Figure 4.1-2), as identified in satellite imagery from 3/7/2009. The five largest glaciers in the study area were the focus of our glacier monitoring work and include, West Fork Glacier (193.423 km$^2$), Susitna Glacier (209.63 km$^2$), East Fork Glacier (39.764 km$^2$), MacLaren Glacier (56.531 km$^2$), and Eureka Glacier (34.046 km$^2$). Apart from a former tributary of the West Fork Glacier (32.959 km$^2$), which is now disconnected, the remainder of the glaciers are smaller than 7 km$^2$. Ninety-three glaciers in the upper Susitna basin are smaller than 1 km$^2$. Figure 4.1-3 clearly shows that the few large glaciers include much more area than the many small glaciers. Table 4.1-1 gives the percentage of glacier cover in each sub-basin of the upper Susitna basin (Figure 4.1-4).

The Talkeetna Mountains currently have 9 glaciers that flow into the upper Susitna watershed. These nine glaciers have a combined area of 8.9 km$^2$, and are dominated by a single glacier, with an area of 7.3 km$^2$, located at the head of Black River.

Using a population of glaciers (>100) around the world, Bahr *et al.* (1997) established a scaling relationship between glacier area ($S$ in m$^2$) and glacier volume ($V$ in m$^3$) that allows us to estimate the total volume (and mass) of the glaciers in the upper Susitna basin. In this empirical relationship

$$V = cS^{\gamma}$$

we assume scaling coefficients for mountain glaciers ($c$ = 0.2055 m$^{3-2\gamma}$ and $\gamma$ = 1.375) after Radić and Hock (2010). The total volume of the upper Susitna basin Alaska Range glaciers is estimated to be 136.897 km$^3$. If we assume an ice density of 900 kg/m$^3$, this represents 123.207 Gt of water equivalent. Glaciers in the Talkeetna Mountains have an estimated volume of less than 0.6 km$^3$.

Mean annual surface velocities of glaciers in the upper Susitna basin are estimated to range 0-0.73 m/day (Burgess *et al.* 2013), with the highest velocities occurring on Susitna and West Fork glaciers (Figure 4.1-5). Some glaciers experience brief periods of acceleration in spring, which have been linked to enhanced basal lubrication caused by meltwater (Macgregor *et al.* 2005; Bartholomaus *et al.* 2008), while periods of deceleration in late summer have been connected to warm summers and greater meltwater production (Sundal *et al.* 2011).

Surge-type glaciers experience episodic acceleration of flow at many times their normal velocities, transferring tremendous amounts of ice to lower elevation, and usually resulting in rapid terminus advance and outburst floods. Both Susitna and West Fork glaciers have a history of surging. The last surge of the Susitna Glacier is estimated to have occurred in 1952 or 1953, yielding a terminus advance of about 4 km (Post 1960). West Fork glacier is known to have surged in 1935 or 1937 and in 1987/88, the latter of which produced a terminus displacement of 4 km with a maximum surface elevation change of 120 m (Clarke 1991; Harrison *et al.* 1994). Harrison *et al.* (1994) report that the termination of the 1987/88 surge was accompanied by high sediment production and sharply increased runoff.

Rock debris covers of many of the glaciers in the upper Susitna basin, and can have an impact on melt because of its influence on surface energy fluxes (Reid and Brock 2010). Debris cover is most extensive on the termini of surge-type glaciers (Susitna and West Fork glaciers) as a result of melt-induced debris concentration following the transfer of mass from higher parts of the glacier after a surge. Also linked to surge behavior is the accumulation of supraglacial debris associated with concentrically looped medial moraines, such as on Susitna Glacier (Figure 2-1). Debris cover can also accumulate through mass movements sourced from adjacent slopes. This form of supraglacial debris entrainment is common in the upper Susitna basin, and is enhanced by active tectonic processes in the Alaska Range.

# 5. DATA SOURCES

A large array of modern and historic observational and derived datasets were used in this study. All datasets were collected or compiled in support of the hydrological modeling in the Upper Susitna basin for which we used the grid-based Water Flow and Balance Simulation Model (WaSiM). Modern observational data include field-based measurements and meteorological data acquired in the upper Susitna basin during the period 2012-2014. Data sources described below are subdivided into spatial, time series, and climatological and meteorological data categories.

## 5.1. Spatial Data

All Northings and Eastings given in this report are for NAD83 UTM Zone 6N, GRS80 ellipsoid.

### 5.1.1. IFSAR DEM

Topographic data used in this study were from the interferometric synthetic aperture radar (IfSAR) digital terrain model (2010), produced by the U.S. Geological Survey (USGS) Alaska Mapping Initiative and the Alaska Statewide Digital Mapping Initiative (SDMI). The IfSAR DEM has a 5

m grid post spacing and a vertical accuracy of 3 m LE90 (0-10 degree slope) and horizontal accuracy of 12.2-meter CE90.

### 5.1.2. Land Use

Land cover properties were specified for a land cover map obtained from the National Land Cover Database 2001 (NLCD2001). The dataset, produced through a cooperative project conducted by the Multi-Resolution Land Characteristics (MRLC) Consortium, is derived from 30 m resolution Landsat Thematic Mapper (TM) and Enhanced Thematic Mapper-plus (ETM+) circa 2001 satellite imagery and is available since 2008 (Selkowitz and Stehman, 2011). In their accuracy assessment, Selkowitz and Stehman (2011) evaluated this dataset to be reasonable for a wide variety of research, analysis, and modeling efforts.

The original land use dataset differentiates 19 land use classes in the study area (see Table 5.1.2-1, left). These were grouped according to their hydrologic implications into 9 land use classes for input into WaSiM (see Table 5.1.2-1, right; Figure 5.1.2-1). The dataset was resampled to 300 m and 1 km resolution.

### 5.1.3. Soils

Information on the soil properties within the Upper Susitna Basin was obtained from U.S. General Soil Map (STATSGO) Data, a digital general soil association map developed by the National Cooperative Soil Survey and distributed by the Natural Resources Conservation Service of the U.S. Department of Agriculture. The soil map units, in Esri digital format, are linked to tabular data stored in an Access Database, containing estimated data on the physical and chemical soil properties, soil interpretations, and static and dynamic metadata (USDA-NRCS Alaska, 2011).

Among others, the Access Database contains information on the particle size distribution of sand, silt and clay for each polygon. As soil characteristics, such as saturated hydraulic conductivity, saturated and residual soil water content and the Van Genuchten parameters are in WaSiM specified by different soil texture classes, the information on the particle size distribution was transferred into the corresponding soil textures on the basis of the classification according to the Food and Agriculture Organization and the World Reference Base for soils (Blume *et al.* 2014; Figure 5.1.3-1). The resulting soil texture map can be seen in Figure 5.1.3-2. In order to enhance the hydrological and heat transfer modeling, this soil texture map was further refined by incorporating information on organic layer depths for different sub-regions of the upper Susitna basin. Since organic substrate shows higher hydraulic conductivities compared to mineral substrate, information on estimated hydraulic conductivity (at different depths), accessed through the STATSGO Access Database, was used to receive an estimate of organic layer depth.

In a last step, bedrock locations overlain by vegetation were summarized in an additional soil texture class and assigned an organic soil layer. The resulting organic layer depths (Figure 5.1.3-2) lie well within the estimates of the Permafrost Laboratory at the University of Alaska, Fairbanks (personal communication with Elchin Jafarov).

For input into WaSiM, this vector dataset was transformed into raster datasets (resolution 300 m and 1 km).

### 5.1.4. Groundwater

The depth to water table for the Upper Susitna basin was accessed through the Soil Data Viewer 6.0 from the U.S. General Soil Map (STATSGO) Data Access Database (Figure 5.1.4-1).

### 5.1.5. Glaciers

#### *5.1.5.1. Glacier extent and spatial categorizations*

Glacier extents within the upper Susitna basin were obtained from the Randolph Glacier Inventory (RGI) 3.0 (Pfeffer *et al.* 2014; Figure 4.1-2), a global database of glacier outlines. Glacier outlines for this region were derived mainly from satellite optical instruments such as ASTER (Advanced Spaceborne Thermal Emission and reflection Radiometer) and Landsat during the first decade of the 21st century.

The glacier extent data were used to generate additional spatial information specific to the application of the dynamic glacier model within the hydrological model used for this study. A glacier identification grid was generated to identify individual glaciers in the same glacier complex in order to apply the volume-area scaling properly as ice cover evolves (Figure 5.1.5.1-1). Due to the different levels of spatial resolution used in the hydrological modeling (300 m and 1 km), ice fraction grids were generated to define the fraction of ice cover in each cell (Figure 5.1.5.1-2). Since many of the glaciers in the upper Susitna basin are partly covered with debris (see section 4.1), the hydrological model developer, implemented a scaling factor specifically for this study, which reduces glacier melt under this debris (see section 4.1). Debris covered areas of the glaciers were delineated using optical imagery (Landsat Path/Row: 68/15 and 68/16 from 9/15/2010), and categorized to reflect the estimated thickness of debris and associated melt reduction value, which was set to a constant value of 0.8 (i.e. melt in debris cover grid cells is reduced by 20%; Figure 5.1.5.1-3). Using the same optical imagery, the areal extents of firn and ice were digitized to provide a reference for model initialization (Figure 5.1.5.1-4).

## 5.2. Time Series Data

### 5.2.1. Glacier mass balance

#### *5.2.1.1. 2012-2014*

The mass balance of the West Fork, Susitna, East Fork, MacLaren, and Eureka glaciers was determined by the glaciological method. For each year during the period 2012-2014 between 27 and 29 stakes were distributed across the glaciers (Table 5.2.1.1-1). The stake distribution was designed to reoccupy the approximate stake positions used in the 1981-1983 study, and to reasonably sample the elevation range of each glacier (Figure 4.1-2). The amount of snow and ice that had accumulated and melted was measured at each stake in late April and early September.

The winter, summer, and annual balances for each glacier are summarized in Table 5.2.1.1-2, and annual mass balance profiles are shown in Figure 5.2.1.1-1. The basin-wide mass balance profiles show a typical pattern with negative annual mass balance at low elevation, where melt rates exceed 4 m w.e./year and winter accumulation is less than at higher elevations, and positive annual balances at high elevation, where low melt rates and high winter accumulation occur.

#### *5.2.1.2. Historic (1981-1983)*

From Susitna studies conducted in the 1980s, a total number of 109 mass balance measurements collected on West Fork, Susitna, East Fork, and MacLaren glaciers were recovered from Clarke (1985a; see section 3.1.2.4.1). Since the corresponding Station Coordinates of 1981 – 1983 stake measurements were not listed, they were derived from 2012 stake measurements from approximately the same locations (Table 5.2.1.2-1; Figures 3.1.2.4.2-1 and 4.1-2). The winter and summer balances, and the annual balances for each glacier are summarized in Table 3.1.2.4.2-1, and annual mass balance profiles are shown in Figure 5.2.1.1-1.

For glaciers monitored during both historic and recent periods, glacier-wide annual balances were significantly more negative in the interval 2012-2014 (-3.43 to -0.71 m w.e., Table 5.2.1.1-2) than in 1981-1983 (-0.30 to 0.40 m w.e., Table 3.1.2.4.2-1). Winter balances in 2012-2014 had a similar range (0.60-1.30 m w.e.) as the winter balances for 1981-1983 (0.65-1.44 m w.e.). Summer balances were significantly more negative in the recent interval (-4.17 to -1.95 m w.e.) compared to the earlier interval (-1.03 to -0.52 m w.e.). These recent, more negative summer balances strongly control the annual balance and can be observed at all elevations along the balance profile (Figure 5.2.1.1-1), and is consistent with a ~150-200 m increase in the height of the equilibrium-line on glaciers in the upper Susitna basin between the periods 1981-1983 and 2012-2014.

### 5.2.2. Winter snow accumulation

#### *5.2.2.1. Glacierized terrain*

Winter snow accumulation on glaciers was estimated as snow water equivalent (SWE; a volumetric measurement of water) at each stake by *in situ* probe and/or snow pit measurements (Figure 4.1-2). Unlike ablation, however, which tends to be spatially coherent and is commonly modeled (Hock 2005), snow accumulation tends to be highly spatially variable, making it difficult to accurately measure and model (Sold 2013). This is especially the case in complex terrain, where topography and meteorological processes vary over short distances (McGrath *et al.* accepted).

In order to more robustly validate model simulations of snow accumulation, we conducted helicopter-borne ground penetrating radar (GPR) common-offset surveys of snow accumulation over the five main glaciers and glacier foreland areas in the upper Susitna basin following Gusmeroli *et al.* (2014; Figure 5.2.2.1-1), and using *in situ* measurements of snow density to calculate end of winter SWE for each year during the period 2012-2014. Radar-derived estimates of winter snow accumulation (winter balance) illustrate the high spatial variability from glacier to basin scales (Figure 5.2.2.1-2). Elevation is the dominant influence on SWE at the upper Susitna basin scale, with snow accumulation on the glaciers at 2000 m measuring 2-3 times higher than at 1000 m. A notable south-north decrease in total SWE and accumulation gradient indicates a strong orographic influence. Over short spatial scales in the ablation zone, surface roughness is responsible for high spatial variability in SWE. While radar-derived estimates of winter snow accumulation show generally good agreement with traditional measurements (pit/probe), there is an obvious departure in high-elevation areas on some glaciers, likely resulting from the traditional measurement selecting a stratigraphically higher melt layer instead of the actual (deeper) summer melt surface.

#### *5.2.2.2. Non-glacierized terrain*

In non-glacierized settings (forest and tundra), snow surveys were made following the method by Rovansek et al (1993) using an Adirondack snow tube (2012) and a SnowHydro snow tube sampler (2014) for average snowpack densities. Five cores representing the entire snowpack were sampled for average site density. Average snow depth was calculated from 25 point measurements (Figure 5.2.2.2-1). The sites were reached by helicopter (April 4, 2012 and April 22-28, 2014) and via snow machine (April 8-12, 2014). No measurements were obtained in 2013. The compiled measurements are presented in Tables 5.2.2.2-1 and 5.2.2.2-2.

About 40 mm of SWE (25%) was lost due to a melting snowpack at the Lower Windy Cr. site from the early to late April snow surveys in 2014 (Table 5.2.2.2-2). Therefore, an adjusted SWE was calculated for the late April survey to account for any loss of end-of-winter snowpack (Table 5.2.2.2-2). Note that the data presented in Figures 5.2.2.2-2 and 5.2.2.2-3 do not represented the adjusted SWE.

The field measurements show variations in SWE according to elevation, region, and vegetation type. The SWE measurements illustrate a general increase with elevation in 2014, which becomes more significant in late April (Figure 5.2.2.2-2). Basin-wide SWE data distinguish three major regions (MacLaren, Clearwater and Talkeetna), where the MacLaren sites represent the highest SWE and the Talkeetna region the lowest (Figure 5.2.2.2-3). Within each region, the SWE data generally show a strong elevation dependence. Among the two main vegetation types, shrubs present larger SWE than the spruce locations (Tables 5.2.2.2-1 and 5.2.2.2-2).

#### *5.2.2.3. Historical measurements*

During the Susitna hydropower studies conducted in the early 1980s, a total of 165 snow depth measurements, at 16 location in both glacierized and non-glacierized terrain settings, were collected by R&M Consultants (1982) in 1981 and 1982. These measurements were recovered and used for hydrological model calibration purposes (Figure 5.2.2.3-1).

## 5.3. Climatological and Meteorological Data

Climate exerts the primary influence on glacier mass balance and river runoff. The meteorological and climatological knowledge of inter-mountain south-central Alaska, including the upper Susitna basin, is generally poor, largely due to the sparse and poorly distributed (mostly low elevation) data and the lack of consistent, long-term measurements. This study incorporates long-term records of climate from outside the basin as long-term coverage inside the basin is spatially and temporally very sparse, and monitoring at high elevation localities was nonexistent. To improve this coverage, we installed two multi-variable weather stations in the Alaska Range, and 25 small stations strategically placed throughout the entire watershed (Figure 5.3-1). Table 5.3-1 is a list of all meteorological stations used in this study.

Available meteorological measurements (historic and current) and gridded climate products applicable to the Susitna basin are summarized below.

### 5.3.1. Historical Observations in the Susitna Basin

As part of the early 1980s Susitna hydropower studies (as described above), many agencies participated in gathering field data to meet the FERC licensing requirements. These data were used to assess the hydrologic resources and aid the stream flow forecasting for future dam operations. In order to supplement climate data provided by NOAA, R&M Consultants, Inc. constructed six weather stations within the Susitna River Basin that recorded meteorological parameters in hourly time steps from 1980 to 1984 (Figure 3.1.2.4.2-1). One high-elevation climate station was installed in the Eastern Alaska Range near the confluence of the four major glaciers that contribute runoff to the Susitna River, two climate stations were installed in the Upper Susitna River Basin, one station was placed at the proposed Watana dam site, and two stations were installed downstream of the dam site (Table 5.3.1-1). At each climate station, meteorological observations of air temperature, wind speed and direction, relative humidity, precipitation, and solar energy were recorded. Air temperature at the six climate stations monitored from 1980 to 1984 is shown in Figure 5.3.1-1. Except for the climate data gathered between 1981- 1982, meteorological data were published in separate annual reports for each station (Table 5.3.1-2).

The historic data from the 1980s Susitna hydropower studies are important for calibrating the hydrological model for the current Glacier and Runoff Changes study.

### 5.3.2. National Climatic Data Center stations

The National Climatic Data Center (NCDC) maintains a network of weather stations across Alaska. We selected 34 stations close to the Susitna-Watana watershed for inclusion in our analysis. Most of these stations are outside of the basin, and all are at relatively low elevations compared to the range of elevations within the basin (Table 5.3-1; Figure 5.3.2-1). Figures 5.3.2-1 and 5.3.2-2 illustrate temperature and precipitation data availability timelines for each station. Temperatures for this interior Alaska area commonly range from -40 °C in the winter to 30 °C in the summer. Precipitation data were not recorded at as many stations as temperature; however, for the data that are available, precipitation rates often reach 2 cm/day, but are usually much less. More often than not, precipitation events occur across the whole region, rather than only in part of the basin.

Precipitation is an important influence on the basin hydrology of northern high-latitude watersheds. Biases towards systematic underestimation of precipitation are well known, largely due to the documented problem of undercatch with precipitation gauges, which is especially the case for solid precipitation (Black 1954; Hare and Hay 1971; Benson 1982). Since snow is such a significant part of the annual meteorologic input of water (Dingman *et al.* 1971), these errors strongly affect the uncertainty of water balance calculations. Further, despite the knowledge of orographic forcing of precipitation, most precipitation gauges (and especially long-term installations), are located in valley bottoms due to logistical constraints. Accordingly, it is challenging to construct total precipitation for a watershed that is dominated by complex topography (e.g. the Susitna River basin).

### 5.3.3. Gridded Climate Products

Weather and climate data can also be represented spatially in the form of continuous grids of pixels. These datasets typically describe basic statistics of meteorological variables over a daily or monthly time step, and are generated by combining observations of meteorological variables at ground- and ocean-based stations. Gridded datasets are particularly useful in Alaska, where few ground observations exist. Table 5.3.3-1 lists some of the most commonly used gridded datasets for Alaska.

### 5.3.4. Susitna-Watana Hydrological Network stations

The Susitna-Watana Hydrological Data Network (SWHDN) includes weather stations set up for the Susitna-Watana Hydroelectric Project. They record air temperature (and often stream temperature or stage) but not precipitation. They were installed in spring of 2012 and maintained through 2014 (Table 5.3-1; Figure 5.3.2-1).

### 5.3.5. On-Ice station (ESG-1)

To facilitate detailed glacier mass balance modeling described below (see section 6.), we installed a multi-variable weather station on West Fork Glacier (Figures 5.3-1 and 5.3.5-1). The station recorded all the variables listed in Table 5.3.5-1 during the summers of 2013 and 2014. For winter 2013/2014, the station measured temperature, relative humidity, snow temperature, and ice temperature.

### 5.3.6. Off-Ice station (ESG-2)

A second multi-variable weather station was installed on land at an elevation of 1516 m between two branches of Susitna Glacier (Figures 5.3-1 and 5.3.6-1). The station was installed in 2012 and continues to operate under DGGS custodianship. The station records all the variables listed in Table 5.3.5-1. Liquid precipitation data are unavailable for the 2012-2014 record as the rain gauge was removed each fall and reinstalled in spring.

### 5.3.7. Glacier and tundra weather stations

To supplement the stations described above and constrain the spatial patterns of temperature and precipitation within the basin, we installed 25 additional stations at strategic location across the basin (Table 5.3.7-1; Figures 5.3-1 and 5.3.7-1). The stations on (EF1, EF2, EF3, Mac1, Mac2, Mac3, SU1, SU3, WF1, WFTranB, WF5) or near (Off-Ice and Repeater) the glaciers measured temperature and relative humidity (T/RH) at a nominal height of 1.75 m above the glacier surface (Table 5.3.7-1). The sensor mounts were designed to slide down the ablation stake as the glacier surface melted, thereby maintaining approximately the same sensor height relative to the ice surface for the entire ablation season (Figure 5.3.7-2). The typical off-glacier station measured temperature, relative humidity, rainfall, and soil temperature at depths of 10 cm and 1 m (Figures 5.3.7-3 and 5.3.7-4).

### 5.3.7.1. Calibration

The HOBO sensors were set up next to each other for calibration in April of 2013. Temperatures during the 2013 calibration period ranged from -5 °C to -22 °C. The offset of the HOBOs relative to a reference HOBO station is typically ±0.1 °C, with excursions out to ±0.3 °C; the 'reference station' is an arbitrarily chosen HOBO sensor. The calibration data show subtle resolution changes with temperature. When using a Campbell T/RH sensors as the reference, it is clear that midday HOBO temperatures are often 1 °C colder than the Campbell T/RH. Nighttime HOBO temperature is typically 0.3 °C colder than Campbell. When looking at data with a fine time-resolution (e.g. 5 minutes), it is clear that the response time of the HOBO sensors is slower than the Campbell sensors, but this should not be a problem when considering the hourly or daily averages, as we do for the modeling in this study.

Measured relative humidity during the April 2013 calibration period ranged from 25% to just under 90%. The offset in temperature (HOBO is colder than Campbell) may explain the discrepancy seen here between the HOBO and Campbell relative humidity sensors. Temperatures during the calibration period ranged from -5 °C to -22 °C, but relative humidity values calculated here are still with respect to water, not ice.

The calibration in April 2014 yielded similar results to the 2013 calibration. Temperatures ranged from -15 to +10 °C over the calibration interval. The average offset among HOBO sensors was on the order of 0.1 °C, and they had a larger offset compared to the Campbell sensors. Relative humidity values ranged from about 20% up to 90% during the calibration interval.

#### 5.3.7.1.1. Precipitation calibration and correction

When performing a calibration of the precipitation gauges, we noticed that some tips of the tipping bucket rain gauge were counted twice in the data. All HOBO stations have some double tips, some stations have up to 10% double tips (Kosina Creek Upper, Kosina Creek Lower, and Windy Lower). The time difference between tips of the bucket (Figure 5.3.7.1.1-1) illustrates the 'double tip' problem. For every pair of tips that occurred within 2 seconds, we decided to zero out the second tip. The lower panel of Figure 5.3.7.1.1-2 shows cumulative precipitation with the uncorrected data (red) and with double tips removed (blue). The analysis done in this report uses the corrected data.

### 5.3.7.2. Basic weather variables

Graphs of cumulative measured precipitation (rainfall) for all HOBO stations for hydrologic years 2012, 2013, and 2014 show that precipitation events tend to occur at the same time at all stations, but the rainfall totals vary across space (Figures 5.3.7.2-1, 5.3.7.2-2, and 5.3.7.2-3). Precipitation lapse rates illustrate that precipitation varies significantly across small distances as well, and that timing of the events is consistent among stations (Figures 5.3.7.2-4, 5.3.7.2-5, 5.3.7.2-6, 5.3.7.2-7, and 5.3.7.2-8).

Temperature lapse rates for just the upper Susitna Basin show a larger temperature gradient for the off-ice stations compared to the on-ice stations (Figures 5.3.7.2-9, 5.3.7.2-10, 5.3.7.2-11, 5.3.7.2-12, and 5.3.7.2-13). In summer, when air temperatures are above freezing, the ice surface cools air

descending over the glacier, partially offsetting adiabatic warming. Table 5.3.7.2-1 shows on-ice (glacier) and off-ice (tundra) lapse rates for the summer months of 2013 and 2014.

## 5.4. Hydrology

Within the watershed of the proposed dam (i.e. upper Susitna basin), there are three gauges (USGS 15291500 SUSITNA R NR CANTWELL AK, USGS 15291000 SUSITNA R NR DENALI AK, USGS 15291200 MACLAREN R NR PAXSON AK; Figures 3.1.2.4.2-1 and 5.4-1 through 5.4-3). The Gold Creek gauge (USGS 15292000 SUSITNA R AT GOLD CREEK AK), however, located 75 km downstream from the proposed dam location, is relevant to the study area, and offers a more continuous record (Figures 3.1.2.4.2-1 and 5.4-4). The Denali and Paxson gauges monitor independent watersheds, both of which subsequently flow into the Cantwell gauge and later the Gold Creek gauge. The area of these watersheds depends to some extent on the method used to define the watershed boundaries. The USGS estimates of area are derived from maps. The watershed areas we use in WaSiM (labeled EZG) were derived using ArcGIS's watershed tools on a digital elevation model with a 1 km horizontal grid-resolution (Figure 5.4-5). A higher resolution watershed boundary calculation (on a 30 m grid), with gauge locations placed more accurately, revealed relatively small differences compared to the USGS and 1 km (EZG) boundaries (Figure 5.4-6). In the 30m version, Windy Creek is in Denali instead of Cantwell, Eureka Glacier is missing instead of present, Cantwell has extra area along the southern boundary of the watershed, and the Dam Site basin is more extensive along the eastern boundary with the Cantwell basin. The areas of "dispute" tend to have flat topography where a subtle difference in the DEM can shift an area from one drainage to another.

### 5.4.1. Discharge data

Total annual discharge at Gold Creek for the hydrologic years 1950-1996 and 2001-2013 had a mean of 8.74 Gt (277 $m^3/s$, 9,790 cfs) and a range of 5.00 - 11.63 Gt (159 - 369 $m^3/s$, 5,600 - 13,000 cfs). Figure 5.4-4 shows the variation in peak flows over the years of record, from about 25,000 cfs in 1978 to almost 90,000 cfs in 1964 and 2013.

## 5.5. Projections of Future Climate

General circulation models (GCMs) are the most widely used tools to help understand and assess climate variability and change. However, the enormous mathematical complexity and limited computational resources generally prevent GCMs from resolving processes at a high spatial resolution.

The coarse resolution (100s of km) of the GCMs hinders their capability to capture detailed mesoscale weather systems and finer scale meteorological conditions. A comparison (Figure 5.5-1) of the annual mean precipitation resolved by the National Centers for Environmental Prediction - National Center for Atmospheric Research (NCEP-NCAR) global reanalysis (Kalnay *et al.* 1996) and mesoscale model downscaling at different resolutions over Alaska (Zhang et al 2007a,b) further demonstrates that the finer scale structures associated with terrain effects can only be captured in the high-resolution simulations. This discrepancy caused by the coarse resolution of GCMs limits their application and suitability for understanding and assessing regional and local scale climate variability and changes.

Downscaling methodologies (e.g., statistical or dynamical) are used to quantitatively obtain regional and local scale climate change information from coarse resolution GCM outputs. Statistical downscaling techniques such as those used in Scenarios Network for Alaska and Arctic Planning (SNAP) climate dataset. The SNAP dataset include years 1980-2099 and are downscaled to 2 km grid cells. Future projections from SNAP are derived from a composition of the five best-ranked GCMs (out of 15 used by the Intergovernmental Panel on Climate Change; IPCC) models for Alaska. Dynamical downscaling techniques are commonly applied to better represent and understand the local weather systems and associated impacts (Bengtsson *et al.* 1996, Lynch *et al.* 1998, Zhang *et al.* 2007a, b). The Coordinated Regional Climate Downscaling Experiment (CORDEX, http://www.cordex.org/) and the North American Regional Climate Change Assessment Program (NARCCAP, http://www.narccap.ucar.edu) are such efforts. The downscaled domains included in CORDEX are mainly for the continental regions around the world and the NARCCAP covers most of North America. Unfortunately, a downscaling domain over the entirety of Alaska is not included in either the CORDEX or NARCCAP efforts, thus necessitating further dynamical downscaling activities focused specifically on Alaska.

### 5.5.1. Dynamic downscaling over the upper Susitna basin

The Coupled Model Intercomparison Project 5$^{th}$ phase (CMIP5) global climate simulations and projections represent the latest coordinated effort climate modeling around the world and provide important resources for the IPCC 5$^{th}$ Assessment Report (AR5; 2013). In order to better assess regional climate changes and impacts in Alaska, driven in large part by this study (Glacier and Runoff Changes in the upper Susitna basin), dynamic downscaling of CMIP5/IPCC AR5 GCM simulations for Alaska and its surrounding areas were conducted by J. Zhang and colleagues (Figure 5.5.1-1).

Hindcasts and projections of future climate used to force the hydrology model (see section 7.0) derive from the Community Climate System Model 4.0 (CCSM4, Gent *et al.* 2011). The 20$^{th}$-century all-forcing CCSM4 simulations from the MOAR (mother of all runs) ensemble member were downscaled to the modeling domain for the period 1970–2005. As part of CMIP5, many runs of CCSM were made using different forcing parameters (scenarios) for the future. For this study, a mid-range scenario, Representative Concentration Pathways (RCP) 6.0, was chosen, under which the entire 21$^{st}$-century (2006–2100) CCSM4 projection was dynamically downscaled to a 20 km-5 km nested grid over central Alaska using a physically optimized version of the Weather Research and Forecasting (WRF) modeling system (Skamarock *et al.* 2008). The entire upper Susitna basin study area falls within the 5 km grid. A summary of the downscaling simulations conducted by the WRF model is shown in Figure 5.5.1-2.

### 5.5.2. Downscaled future climate over the upper Susitna basin

Dynamic downscaling of CMIP5/IPCC AR5 GCM simulations was successfully conducted with a physically optimized version of WRF for Alaska and its surrounding areas. WRF downscaling of the 20th-century simulations from CCSM4 for the period 1991–2005 fundamentally captures reality. Strong seasonal variations are present in all three major surface climate parameters: temperature, wind speed, and precipitation. The downscaled 20th-century 15-year results are calibrated with in situ observations archived by the NCDC. A cold bias exists across most of the domain, except for a weak warm bias along the western and northern Alaskan coasts. In addition,

downscaled winds are stronger than observations and precipitation is overestimated along the southeast coast. Downscaling results over Alaska and its surrounding areas indicate that from 2010-2029 to 2080-2099, under the RCP6 climate change scenario, the upper Susitna basin will experience a 2.5 C increase in the mean-annual surface air temperature (Figure 5.5.2-1), and total annual precipitation will rise 2%, with a 13% decrease in snowfall and a 20% increase in rainfall (Figure 5.5.2-2).

### 5.5.3. Bias correction

We compared the 5km WRF downscaled climate product with local observational data for the climatology 1971-2000. Since the WRF output is not a reanalysis, we cannot compare individual years in the two datasets; however, we can reasonably compare the 30-year averages (climatologies) of temperature and precipitation. Of the 34 weather stations that surround the Susitna basin (Figure 5.3.2-1), we chose the 10 stations with the longest records (Figure 5.5.3-1) for this comparison. The 10 stations are spatially well-distributed around the basin.

For each station, we found the closest grid cell within the WRF output and calculated the daily climatology for both records. An example is shown in Figure 5.5.3-2. For temperature, the bias (difference) between station data and WRF was consistent among all ten stations. To remove the bias from the WRF data for the whole basin, we chose to average the bias of all 10 stations and then smooth the result with a triangular filter which weights the central point highest and considers 15 points (days) on either side. Due to the characteristics of precipitation data (no negative values) the bias correction of precipitation used a ratio instead of a difference.

$$T_{bias,i} = \langle T_{data,i} \rangle - \langle T_{WRF,i} \rangle$$

$$T_{corrected,i} = T_{WRF,i} + T_{bias,i}$$

$$P_{bias,i} = \langle P_{data,i} \rangle / \langle P_{WRF,i} \rangle$$

$$P_{corrected,i} = P_{WRF,i} \times P_{bias,i}$$

for day *i*, where < > denotes the average over the whole record 1971-2000.

# 6. GLACIER MASS BALANCE MODELING

In addition to the hydrological model WaSiM, we also applied the Distributed Temperature-Index Model DETIM, an open-access glacier mass-balance and runoff model (Hock, 1999). WaSiM's glacier mass balance and runoff module is similar to DETIM, but running DETIM separately allows us to independently evaluate the performance of WaSiM's glacier module, and to model the surface energy balance in order to determine the individual sources available for melt.

## 6.1. Temperature-index Model (DETIM)

The model computes the short-term mass balance variations (ablation and accumulation) of ice and snow with hourly to daily resolution and simulates resulting discharge. Processes outside the glacier are only considered crudely, hence, the model is only applicable in highly glacierized

catchments where discharge is dominated by glacier melt water. Therefore we apply the model only to the Denali sub-basin (24 % glacierized).

The mass balance model is fully distributed, i.e. calculations are performed for each grid cell of a digital elevation model. The model is run with the daily time step and forced with daily near-surface air temperature and precipitation from one weather station.

### 6.1.1. Model description

Melt, M (mm $d^{-1}$), at the glacier surface is calculated by:

$$M = (MF + r_{snow/ice} I_{pot})T : T > 0$$
$$M = 0 : T \leq 0,$$

where *MF* is an empirical melt factor (mm $d^{-1}$ $K^{-1}$), $r_{snow/ice}$ is an empirical radiation coefficient (mm $m^2$ $W^{-1}$ $h^{-1}$ $K^{-1}$), different for snow and ice to account for their differences in albedo, $I_{pot}$ is potential direct solar radiation at the inclined glacier surface (W $m^{-2}$) and *T* is daily mean air temperature (°C) extrapolated to each grid cell using a constant lapse rate. *Ipot* is computed as a function of top of atmosphere solar radiation, an assumed atmospheric transmissivity, solar geometry and topographic characteristics such as shading, aspect and slope angles, and set to zero if the considered grid cell is shaded by surrounding topography. By varying the degree-day factor according to *Ipot* a distinct spatial element is introduced considering these effects without the need of additional meteorological input data. The model has been developed on Storglaciären (Hock, 1999) and successfully been applied on many other glaciers (e.g. Schneeberger *et al.* 2001, Flowers and Clarke 2002, and Schuler *et al.* 2005a,b) and snow-covered areas (Hock *et al.*, 2002). Snow accumulation is computed from precipitation observations. Rain and snow are discriminated using a threshold temperature. One degree below/above this temperature all precipitation is assumed to fall as snow/rain. Within the two degree range the percentage of rain and snow is obtained from linear interpolation.

Glacier retreat is modeled using volume-area scaling (see section 4.1). Since total glacier volume is unknown, changes in volume are related to changes in area. The glacier area is adjusted at the end of each mass-balance year. Discharge is calculated from the water provided by melt plus liquid precipitation by three linear reservoirs corresponding to the different storage properties of firn, snow, and glacier ice.

Six model parameters are optimized using observed discharge data: temperature lapse rate, melt factor (*MF*), radiation coefficient for snow/firn ($r_{snow}$), radiation coefficient for ice ($r_{ice}$), precipitation versus elevation gradient, and precipitation correction factor.

### 6.1.2. Input data

We run DETIM for the period 1955 to 2010 using data from nearby long-term weather stations, and make projections until 2100 using the SNAP data (see section 5.5). For the hindcast we run the model with the daily ESG2 temperature record from the off-ice weather station (ESG2), which is located in the drainage basin. Since the record is short we derive a transfer function between the ESG2 (1516 m a.s.l.) and Talkeetna Airport station (907 m a.s.l.) daily air temperatures for the

overlapping period and use this function to extend the ESG2 record. While a precipitation gauge was operated at ESG2 during the melt seasons 2012-2014, we used the longer precipitation record from the Talkeetna Airport station, assuming precipitation fell on the same days at ESG2. In DETIM, a precipitation correction factor is applied to correct for gauge under-catch and expected regional differences between the precipitation values recorded at both stations.

For the future we force the model with the SNAP temperature and precipitation data of the grid cell closest to ESG2 (ID 197, 1514 m a.s.l.). We choose three climate scenarios (A1B, A2, and B1). The SNAP data are downscaled applying simple bias corrections following Radić and Hock, 2006). We determine the monthly averaged biases in temperature between the SNAP data and the observations at Talkeetna and the monthly averaged factor by which the two precipitation records differ. For example, for all years of overlap (2005-2012) the SNAP data shows considerably higher precipitation sums than the station at Talkeetna. We corrected the SNAP data for those biases prior to running the model.

### 6.1.3. Model calibration

Daily mean discharge data from the Susitna River near Denali Highway, covering the period 1957-1966, 1968-1986 and 2012 and 109 mass balance point measurements for years 1980-1983 and 2011-2012 were used to calibrate the model. The model parameters were calibrated maximizing the agreement between measured and modeled discharge and point glacier mass balances. Overall, modeled and measured daily discharge agree well for all years with existing observations despite the simplicity of the model (Figure 6.1.3-1). A detailed view of the early 1980s period is given in Figure 6.1.3-2. There is also good agreement between the modeled and measured glacier mass balances at individual locations on the glaciers ($r^2 = 0.78$; Figure 6.1.3-3).

### 6.1.4. Future projections

All simulations show an increase in runoff ranging from 22 to 39% over the period 2005-2100, depending on the climate scenario (Table 6.1.4-1 and Figure 6.1.4-1). By 2100 the glacier area is reduced by 10 to 14 % depending on the climate scenario. The climate scenarios project an increase in temperature of 3 to 5 °C and an increase in precipitation between 20 and 35%. Increased glacier melt due to higher temperatures is not compensated for by a decrease in area since the glacier area only declines relatively little.

The future projections show no trend in winter balance but show a trend towards more negative specific summer balances indicating that the increase in glacier runoff is largely caused by an increase in glacier ice melt volume.

## 6.2. Energy balance model (DEBAM)

A multi-variable automatic weather station was operated on the West Fork Glacier (ESG1) during the summers 2013 – 2014 (Table 5.3.5-1). The data allows us to estimate the individual sources of energy available for melt. We used the data for the 2013 melt season (15 April – 2 September) to compute all components of the energy balance based on air temperature, relative humidity, wind speed and radiation. The energy is converted into mass change, which then is compared to

available observations close to the weather station. The energy at the surface available for melt, $Q_M$, is given by

$$Q_M = Q_N + Q_H + Q_L + Q_G + Q_R$$

where $Q_N$ is net radiation, $Q_H$ is the sensible heat flux, $Q_L$ is the latent heat flux, $Q_G$ the heat flux into the ice and $Q_R$, the rain heat flux. The net radiation is defined as the sum of the shortwave incoming and reflected solar radiation, longwave incoming and longwave outgoing radiation, and is computed from the radiation measurements. The turbulent heat fluxes ($Q_H$, $Q_E$) are calculated as a function of wind speed, air temperature and humidity using the bulk aerodynamic method (Hock and Holmgren, 2005). The rain heat flux is computed as a function of air temperature and rainfall rate. The ground heat flux is assumed small and, thus, neglected here.

The turbulent heat fluxes depend on surface roughness. We obtain the roughness length necessary for the computation of the turbulent fluxes from tuning, i.e. we choose values that result in the best match to observations of mass change.

### 6.2.1. Model simulations

The cumulative mass changes modeled by the energy balance approach are shown in Figure 6.2.1-1. The net mass change between 15 April and 2 September 2013 is -3.18 m w.e. of which 0.63 m w.e. is melt of winter snow and the remainder is ice melt. The cumulative melt is in good agreement with the shorter period of available measurements.

Net radiation is the largest source of energy contributing 87% of the energy available for melt, followed by sensible and latent heat fluxes. The energy contributed by rain is generally very small. The time series of the energy balance components is shown in Figure 6.2.1-2. Negative latent heat fluxes occur during the first half of the study period indicative of sublimation while later in the season the latent heat contributes energy for melt (condensation). The melt energy strongly increases when the glacier surface transitions from snow to ice on 28 June.

## 7. HYDROLOGICAL MODELING

The study of hydrological issues, such as the seasonal and long-term regimes of rivers, the potential impact of climate change on water resources, or the potential impacts of land use change on flooding has led to the development of various hydrological models over the past several decades (Wainwright and Mulligan 2004). Watershed models are employed to understand dynamic interactions between climate and land-surface hydrology or to simulate hydrologic responses of catchments under a changing environment in order to better cope with potential future challenges (Singh and Wollhiser 2002; Biftu and Gan 2001).

From the long history of hydrological modeling, three different types of deterministic hydrological models have evolved over the years: empirical models, conceptual models, and physically based models.

While empirical and conceptual models were, in general, developed for runoff simulations under steady state conditions, and are not applicable to heterogeneous catchments under non-stationary conditions, most physically based models were developed to address exactly these non-stationary conditions, i.e., the impact of human activities or changing climatic conditions on catchment processes. Thus, physically based models are able to address a wider range of hydrological issues (Abbott and Refsgaard 1996; Wairnwright and Mulligan 2004). Further, all parameters of a fully distributed, physically based model can be assessed by means of field measurements and so, in theory, they do not need to be calibrated to observed data. Nevertheless, because model codes are often applied at scales on which important hydrological parameters cannot be directly assessed, model calibration is often necessary (Abbott and Refsgaard 1996).

Note that empirical, conceptual, and physically based models are deterministic models in which a given set of inputs will always produce the same output. Hydrological models may also be stochastic, attempting to handle some of the inherent uncertainty in modeling and in data by representing the variability of processes or events on the basis of probability distributions (Wairnwright and Mulligan 2004).

Since the goal of this study is to assess the effect of future climate change on glacier runoff and how this might change the seasonal flow regime as well as peak flows, the physically based, fully distributed model WaSiM was chosen. As described below (section 7.1), it incorporates a dynamic glacier model and a 1-D heat transfer model, respectively, which allows us to specifically address two important hydrological components of the Upper Susitna Basin that will most likely change under future climatic conditions.

## 7.1. Water Flow and Balance Simulation Model (WaSiM)

The hydrological modeling in the Upper Susitna Basin is carried out using the grid-based Water Flow and Balance Simulation Model (WaSiM), developed by Jörg Schulla. The physically based, spatially distributed model enables the investigation of the spatial and temporal variability of hydrological processes in complex watersheds, simulating water flows above and beneath the surface. The model's flexibility concerning its spatial and temporal scaling enables the modeling of small (<1 km²) and large (> 10,000 km²) watersheds in time steps from minutes to several days. Due to the preferential employment of physically based model approaches and the sophisticated model design, which allows the model to be performed also in regions with relatively limited data availability, it is applicable to various watersheds and is currently being used by over 50 institutions worldwide (Schulla 2012a).

Figure 7.1-1 shows the modular design of WaSiM displaying the different modules that simulate vertical and lateral water flows. The modules shown on a grey background simulate the water flow per grid cell while the remaining modules are calculated on the basis of sub-catchments (Schulla 2012b). The modular design enables WaSiM to run at different levels of complexity.

For this study, the following sub-models were run: Meteorological Data Interpolation; Evapotranspiration Model, Snow Model; Dynamic Glacier Model; Interception Model; Infiltration Model; Unsaturated Zone Model (Soil model); 1-D Soil Heat transfer Model (for a select few runs); 2-D Groundwater Model; and Routing Model. The model was run in daily time steps. The input files for the sub-models were produced in two spatial resolutions: 300 m and 1 km. In

addition, the model grids were prepared for two spatial extents. This is due to a peculiarity of Eureka glacier, which straddles the drainage divide between the Susitna and Delta River basin (Clarke *et al.* 1985). Periodically, Eureka glacier either drains entirely into Delta River basin (orange boundary in Figure 7.1-2), or about half of Eureka drains into Susitna River basin (red boundary in Figure 7.1-2; see also section 5.4 and Figures 5.4-1 and 5.4-2.).

### 7.1.1. Dynamic Glacier Model

WaSiM offers two possibilities to incorporate glaciers into the hydrological system of the Basin: A static and a dynamic model approach.

Since one goal of this study is to simulate potential changes in glacier wastage under future climatic conditions, the dynamic glacier model was applied. This method calculates glacier mass balance and, by applying a simple volume-area scaling (Bahr *et al.*, 1997; see section 4.1), enables the simulation of glacier advance or retreat. This allows the specific evaluation of the role of glacier melt on river runoff during the lifespan of the proposed dam.

The glaciological and hydrological modeling conducted in this study ignores the glaciers in the Talkeetna Mountains due to their small size and subsequent small effect on the total runoff. In addition, while it is acknowledged that variations in glacier velocity can have in impact on mass balance and runoff, the dynamics controlling both stable and unstable (surging) velocity changes are poorly understood (see section 4.1), and their successful incorporation into hydrological models, including the one used in this study, remains elusive.

#### *7.1.1.1. Process description mass balance*

On the basis of the glacier outlines (RGI; section 5.1.5.1), the volume of the glaciers is initialized by volume-area scaling after Bahr (1997; see section 4.1). At the end of each mass balance year (Oct 1$^{st}$ – Sep 30$^{th}$), the new volume $V_1$ and subsequently the new glacier area $A_1$ is calculated from the old volume $V_0$ and the annual mass balance $b$

$$V_1 = V_0 + b / \rho$$

$$A_1 = (V_1 / c)^{1/1.36}$$

where $\rho$ is 918 kg/m$^3$. To assure that glacier area change occurs only in the glacier ice facies, this zone is divided into bands of equal elevation (the upper limit is the ELA); glacier fractions are removed (or added) iteratively within this zone according to annual mass balance.

The dynamic glacier model also incorporates a dynamic firn model that accounts for changes in firn depth using a simple approach of metamorphosis of snow to firn to ice. Unmelted snow automatically becomes firn after the balancing period. Eventually, different firn layers are stacked over each other. After seven years (adjustable), the lowermost firn layer finally becomes ice. The firn stack must be initialized in cold start using the number of years it takes for snow to convert to ice, the ELA, and the change in water equivalent of firn with height.

### 7.1.1.2. Melt from glacierized areas

WaSiM offers several methods for glacier melt calculation ranging from simple degree-day approaches to an energy-balance approach. Due to data limitations, this study implemented the traditional degree-day approach. Melt is calculated for snow, firn, and ice separately using degree-day-factors in the following melt equation:

$$M = \begin{cases} \frac{1}{n} * DDF_{snow/firn/ice} * (T - T_0) & T > T_0 \\ 0 & T \leq T_0 \end{cases}$$

With $M$ = melt [mm/time step]
$n$ = number of time steps per day [day$^{-1}$]
$DDF$ = Three degree-day-factors for snow, firn and ice, respectively [mm*°C$^{-1}$*day$^{-1}$]
$T$ = air temperature in a standard elevation of 2 m [°C]
$T_0$ = threshold temperature for melt [°C]

According to the WaSiM manual, the relation $DDF_{ice} > DDF_{firn} > DDF_{snow}$ usually holds. All three parameters are constant in space and time for the entire model domain. The parameter values range between 2 and 10 mm °C$^{-1}$ day$^{-1}$. The default settings are 5, 4, 3 mm °C$^{-1}$ day$^{-1}$, respectively.

### 7.1.1.3. Routing runoff through the glacier

The three runoff components were superimposed and routed to the sub-basin outlets (Figure 4.1-4) using a set of parallel single linear reservoirs.

Each reservoir (snow, firn, and ice) has specific storage coefficients $k_i$ [hours] and inflow rates $R_i$ [mm/time step], representing the areal means of the three melt components. The total runoff during time step t was calculated using:

$$Q(t) = \sum_{i=1}^{3} (Q_i\,(t-1) * e^{-\frac{1}{k_i}} + R_i(t) * (1 - e^{-\frac{1}{k_i}}))$$

with $Q(t)$ total runoff during time step $t$ [mm/time step]
$i$ reservoir index (1 reservoir for snow melt, 1 for firn melt and 1 for ice melt)
$Q_i(t-1)$ outflow of reservoir $i$ during the last time step $t$-1 [mm/time step]
$R_i(t)$ input into reservoir $i$ in the actual time step $t$, i.e. the sum of melt and additional rain [mm/time step]
$k_i$ storage coefficient (recession constant) for reservoir i

The storage coefficients for ice, snow and firn typically range:

$k_{ice}$: 1 to 20 hours (default is 3)
$k_{snow}$: 10 to 100 hours (default is 30)
$k_{firn}$: 100 to 1000 hours (default is 300)

### 7.1.2. Evapotranspiration

In WaSiM, evapotranspiration (ETR) is computed for each grid cell by two different methods, first as potential ETR, and subsequently as real ETR.

#### *7.1.2.1. Potential evapotranspiration*

Three different methods are implemented in WaSiM for the computation of potential ETR, i.e. the maximum volume of water that can be transferred back to the atmosphere, directly from the soil and/or through the plant canopy, under the occurring meteorological and plant physiological conditions (Hamon 1963; Monteith 1975; Wendling 1975; Brutsaert 1982; and Schulla 1997).

The most sophisticated equation is the one after Penman-Monteith which specifies potential ETR as a latent heat flux (in $KJ*m^{-2}$). This equation (Schulla 2012a,b), requires the highest amount of input data, namely precipitation, air temperature, global radiation, wind speed and air humidity, ideally on an hourly basis (Schulla 2012b). As this data requirement cannot be fulfilled for the area under examination, it cannot be applied.

In the case of only limited meteorological data availability, the equations after Wendling (1975) or Hamon (1963) can be employed. They represent a simplified approximation of potential ETR, based solely on temperature and global radiation data or exclusively on temperature data, respectively. They do not consider vegetation (e.g. phenological stages) as is the case in the equation after Penman-Monteith.

Both equations include empirical factors to account for missing meteorological input data and, thus, enable calibration. They are only applicable to model set-ups running in daily time steps.

Within this study, potential ETR is computed by the equation after Hamon (1963), as the data requirements for the application of the equation after Wendling (1975) (see Schulla 2012b) cannot be met. However, in case global radiation data becomes available, the employment of the equation after Wendling (1975) is favorable over the approach after Hamon (1963), since sensitivity analyses have shown that results based on the equation after Wendling (1975) only differ marginally from the reference ETR after Penman-Monteith (Schulla 1997). By contrast, potential ETR values based on the Hamon (1963) equation can differ substantially, resulting from the lack of radiation data, which is a primary driver of evaporation (Schulla 1997). The computation of potential ETR after Hamon is therefore, and as a result of not considering vegetation conditions into the calculation, a potential source of error.

The Hamon (1963) equation, as it is used in WaSiM, was first applied by Federer and Lash (1978) in their hydrologic simulation model BROOK. BROOK was developed to study the response of streamflow to forest land harvesting activities in the eastern United States. The equation considers potential ETR as an index to the demand of the atmosphere for water (Federer and Lash 1978), where

$$ETP = 0.1651 * f_i * \frac{h_d}{12} * \frac{216.7 * e_s}{T + 273.3}$$

with

$$e_s = 6.108 * \text{EXP}\left(\frac{17.26939 \ * \ T}{T \ + \ 237.3}\right)$$

with

| | | |
|---|---|---|
| | $ETP$ | potential evapotranspiration [mm] |
| | $f_i$ | empirical factor, monthly values (see Table 7.1.2.1-1) |
| | $h_d$ | day length [h] from sunrise to sunset |
| | $e_s$ | saturation vapor pressure at temperature $T$ [hPa] |
| | $T$ | temperature [°C] |

### *7.1.2.2. Real Evapotranspiration*

As mentioned above, potential ETR is defined as the maximum volume of water that can be transferred back to the atmosphere from the soil and/or through the plant canopy under unrestricted water supply. As completely unrestricted water supply rarely occurs, the computation of real ETR reduces the potential amount of ETR by accounting for water deficiencies in the soil. WaSiM offers two approaches to calculating real ETR from potential ETR, both reducing real ETR as a function of soil moisture.

Within the first WaSiM version, in which the soil module is based on the TOPMODEL-approach, real ETR is obtained by a relatively simple, linear reduction of potential ETR if the content of the soil moisture storage drops below a specified level (Schulla 2012b).

The calculation of real ETR used in the Susitna Study is realized by the more physically based RICHARDS-equation, implemented in WaSiM version 2. Depending on the relation between the soil water content $\theta$ and the actual capillary pressure $\psi$, real ETR is either set zero, equals potential rates, or is calculated as a portion of potential ETR as given by the following:

$$ETR_i = 0 \qquad \theta\,(\psi) < \theta_{wp}$$

$$ETR_i = ETP_i * (\theta_{\psi_g} - \ \theta_{wp}) \ / \ (\theta_{\psi_g} - \ \theta_{wp}) \qquad \theta_{wp} \leq \theta(\psi) \leq \ \theta_{\psi_g}$$

$$ETR_i = ETP_i \qquad \theta_{\psi_g} \leq \ \eta * \ \theta_{sat}$$

$$ETR_i = ETP_i * \ (\theta_{sat} - \ \theta\,(\psi)_i\,) \ / \ (\theta_{sat} - \ \eta * \theta_{sat}) \qquad \eta * \ \theta_{sat} \leq \theta\,(\psi) \leq \ \theta_{sat}$$

with

| | | |
|---|---|---|
| | $i$ | index of the soil layer |
| | $ETR$ | real evaporation [mm] |
| | $ETP$ | potential evaporation [mm] |
| | $\theta\,(\psi)$ | actual relative soil water content at suction $\psi$ [-] |
| | $\psi$ | actual suction (capillary pressure) [m] |
| | $\eta$ | maximum relative water content without partly or total anaerobe |

conditions (≈ 0.9…0.95)

$\theta_{sat}$ saturation water content of the soil [-]

$\theta_{wp}$ water content of the soil at permanent wilting point ($\psi$ = 1.5 MPa ≈ 150 m)

$\theta_{\psi_g}$ soil water content at a given suction $\psi_g$

### 7.1.3. Soil Model

WaSiM offers two different approaches to modeling the soil water balance and runoff generation: the conceptual TOPMODEL approach implemented in WaSiM version 1, and the more physically based Richards approach in WaSiM version 2. In this study, the more sophisticated RICHARDS approach was applied. It models the vertical fluxes within the unsaturated soil zone, which is discretized into several soil layers, in a one-dimensional manner. The continuity equation

$$\frac{\partial \theta}{\partial t} = \frac{\partial q}{\partial z} = \frac{\partial}{\partial z}\left(-k\,(\theta)\frac{\partial \psi(\theta)}{\partial z}\right)$$

with $\theta$ water content [$m^3/m^3$]

$t$ time [s]

$k$ hydraulic conductivity [m/s]

$\psi$ hydraulic head as sum of the suction $\psi$ and geodetic altitude $h$ [m]

$q$ specific flux [m/s]

$z$ vertical coordinate [m]

can be discretized as the difference between the inflow into and the outflow from a soil layer. The flux between two soil layers is given by the following:

$$q = k_{eff} * \frac{h_h\,(\theta_u) - h_h\,(\theta_l)}{0.5 * (d_u + d_l)} \qquad \text{with } \frac{1}{k_{eff}} = \frac{d_u}{d_l + d_u} * \frac{1}{k\,(\theta)_u} + \frac{d_u}{d_l + d_u} * \frac{1}{k\,(\theta)_l}$$

with $q$ flux between two discrete layers [m/s]

$k_{eff}$ effective hydraulic conductivity [m/s]

$h_h$ hydraulic head, dependent on the water content and given as sum of suction $\psi(\theta)$ and geodetic altitude $h_{geo}$ [m]

$d$ thickness of the layers under consideration [m], whereby $u$ is the upper and $l$ is the lower layer

The hydraulic properties of the soil can either be specified by look-up-tables with a free amount of entries describing the relationship between the hydraulic head $h_h$ and $\theta$ and between the hydraulic conductivity $k$ and $\theta$ (for each soil type), respectively, or, when less data is available, as is the case in this study, by applying a method after Van Genuchten (1976). The suction of the soil, as a function of water content, is then approximated based on its actual and residual water content, saturation water content, saturated hydraulic conductivity and three empirical parameters ($\alpha$, $n$ and $m$). The decrease in saturated hydraulic conductivity is accounted for by a recession constant *krec*

(Schulla 2012b). The soil module also accounts for water inflows by infiltration from the surroundings or exfiltration from groundwater, and water losses due to ETR and groundwater recharge.

## 7.2. Data Inputs

Input data to WaSiM generally consists of two different data types, spatially distributed data and time series data and are described in section 5. At a minimum, the model requires the following data as input:

1. Spatial distributed (grid) data, including digital elevation model (DEM), land use, and soil type. All datasets were resampled to 300 m and 1 km resolution by bilinear interpolation.
2. Meteorological data, including hourly or daily time series of precipitation and air temperature.

## 7.3. Calibration and Validation

Before future glacier and runoff projections can be simulated, the ability of the hydrological model WaSiM to reproduce historical records (e.g. river discharge) must first be tested. This was accomplished through two iterative approaches of combining meteorological (method 1) and climatological (method 2) forcing and hydrological model settings that accurately represents the historic runoff observations.

Even though physically based models theoretically should not have to be calibrated, it is often necessary nevertheless, as important model parameters are often not representative of the spatio-temporal scale applied. As a result of the frequent under-representation of the physical structure and processes in the system under study, initial parameter estimates need to be adjusted by an iterative process of model calibration in order to achieve model outputs that are in agreement with observed data (Wainwright and Mulligan 2004). As a first step (method 1), the model was adapted to the upper Susitna basin by the means of model calibration using detailed in situ data from a historic period and nearby weather station data as forcing. In a second step, the model was calibrated to a downscaled 21$^{st}$ century climate dataset (see sections 5.5.2 and 5.5.3) using a climatological approach.

### 7.3.1. Method 1

The calibration period was set to the water balance years 1981 – 1983, i.e. starting 1$^{st}$ Oct 1980 and ending 30$^{th}$ Sept 1983, since this period not only holds historic discharge records at all three gauging stations, but also a wealth of data on glacier mass balance and snow depths exists for this period thanks to the Susitna studies conducted in the 1980s. Data on river discharge, snow depth, glacier mass balance, and soil temperatures were compiled to support calibration and validation (Table 7.3.1-1). Calibration was conducted using 1 km resolution grids with the extent including half of Eureka glacier (Figure 7.1-2).

During the calibration process, a considerable amount of time was spent on optimizing meteorological forcing data, implementing different interpolation methods and applying different precipitation correction factors in order to accurately represent the historic temperature and

precipitation patterns for good discharge simulations. Simultaneously, our goal was to reproduce glacier mass balances, end-of-winter snow depths throughout the whole basin, and singular precipitation events that generated observed runoff peaks.

A great deal of time also went into the calibration of the heat transfer model since it was a newly implemented model in WaSiM and had not been applied at the scale of this study. Further, this heat transfer model requires long spin-up runs until soil temperatures reach a semi-equilibrium state, which lengthens the calibration process. Greater than 100 model configurations were run for this calibration phase, and nearly 200 configurations were run for calibration method 1.

The degree of goodness between simulated and measured variables was assessed by the means of the coefficient of determination ($R^2$) and the Nash-Sutcliffe coefficient (NSE; 1970). The latter is a common quality criteria used in hydrological modeling and reflects the mean square error in relation to the observed variance (Wainwright and Mulligan 2004), where

$$NSE = \frac{\sum_{i=1}^{n}(O_i - M_i)^2}{\sum_{i=1}^{n}(O_i - \bar{O})^2}$$

With $O_i$ = observed variable at time step i
$\bar{O}$ = mean observed variable
$M_i$ = modeled variable at time step i
$n$ = number of time steps

The NSE can take on values ranging from $-\infty$ (no agreement) to 1, which represents a perfect adaptation of the model to the measured data.

Since, in glacierized basins, ice-melt can lead to error compensation in discharge modeling by providing an additional source of runoff (apart from precipitation), model calibration and validation was conducted using a multi-criteria approach. As has been shown in several studies (e.g. Braun and Renner 1992 and Huss *et al.* 2008), this has proven to enhance the modeling effort.

#### *7.3.1.1. Downscaling of historic climate data*

Since historical meteorological data in the study area is spatially not well distributed, different forcing approaches were tested using both measured daily time series and gridded (monthly) meteorological datasets, which were temporally downscaled to fit the model requirements.

Based on the Hill *et al.* (2015) climate grids, daily time series for temperature and precipitation were computed for the upper Susitna basin in the following way:

Monthly means (temperature) and monthly sums (precipitation) were calculated for Gulkana and Talkeetna stations since these showed the fewest data gaps for the time period 1961 – 2009 (Figure 5.5.3-1).

Daily temperature and precipitation anomalies were computed based on following equations:

Calculation of Temperature Anomalies

$$\Delta T_{day} = T_{day} - T_{month}$$

Calculation of Precipitation Anomalies

$$_{fraction}P_{day} = P_{day} / P_{month}$$

The resulting anomaly time series for Gulkana and Talkeetna stations can be seen in Figures 7.3.1.2-1 and 7.3.1.2-2, respectively.

Time series from the Hill *et al.* (2015) grids were generated as follows:

Calculation of Temperature time series for each 2 x 2 km grid point

$$T_{day\,(i,j)} = T_{month\,(i,j)} - \Delta T_{day}$$

Calculation of Precipitation time series for each 2 x 2 km grid point

$$P_{day\,(i,j)} = P_{month\,(i,j)} * {}_{fraction}P_{day}$$

The downscaling of the Hill *et al.* (2015) grids led to 4187 time series, referred to as "virtual climate stations" from here onward.

The downscaled climate record of the virtual climate stations were validated via the incomplete data observed at selected climate stations within the upper Susitna basin by the means of the coefficient of determination ($R^2$). The distance of these climate stations to Gulkana Airport Climate Station is as follows: Lake Louise (60.5 km), Lake Susitna (71.1 km), Tyone Lake (75.6 km), MacLaren (120 km), Gracious House (151.9 km), Monahan Flat (170.2 km).

Although the deviation of daily temperature from the monthly mean was superimposed on the whole upper Susitna basin, relatively good results ($R^2 >= 0.9$, except for MacLaren Station) were attained for the downscaled temperature records (Figure 7.3.1.2-3).

This statistical downscaling method, however, is not appropriate for spatially distributing precipitation over the upper Susitna basin on a daily basis. For example, if no precipitation was recorded at Gulkana Airport station for a given day, then precipitation amounts to zero at every virtual station for that day. Conversely, precipitation will occur at every virtual station whenever daily precipitation was recorded at Gulkana Airport station. Consequently, there is little or no correlation of the downscaled daily precipitation amounts when compared to observed amounts at weather stations (Figure 7.3.1.2-4). Instead, monthly sums of downscaled daily precipitation were used to represent the spatial distribution of precipitation during the calibration period (Figure 7.3.1.2-5).

### *7.3.1.2. Interpolation methods and module settings*

Throughout the calibration phase, different interpolation methods were applied to meteorological data. These range from Inverse Distance Weighting and Elevation Dependent Regression over the application of Lapse Rates and finally, the Regional Superposition of these three methods. Each application was influenced strongly by the spatial distribution of the meteorological input data sets.

#### *7.3.1.2.1. Inverse Distance Weighting (IDW)*

When using the first meteorological forcing with very limited measured data which were only representative for low elevations (50 – 800 m), the Inverse Distance Weighting interpolation method was applied. This led to a very poor spatial representation and led to the temporal downscaling of the Hill *et al*. (2015) data sets. IDW was also used when running WaSiM with the virtual climate stations produced by the temporal downscaling, since they are representative on a 2 x 2 km grid.

#### *7.3.1.2.2. Elevation dependent Regression (EDR)*

As high elevation temperature and precipitation data became available through the Hill downscaling the interpolation method combining IDW with an elevation dependent regression (EDR) was tested. The analysis of the temperature and precipitation data led to following inversion layers: 500 m (lower) and 1200 m (upper) for temperature; and 2500 m (lower) and 2800 m (upper) for precipitation.

#### *7.3.1.2.3. Lapse Rate*

When only very limited data is available, WaSiM can also be forced by only one climate station and a specified lower lapse rate, an upper limit, and an upper lapse rate. Since the upper Susitna basin covers an area of >13,000 $km^2$, this option was initially not taken into account. During the calibration process, however, this interpolation method proved to be the only possibility to notably increase the amount of precipitation at high altitudes, which was crucial for the enhancement of the mass balance modeling.

#### *7.3.1.2.4. Regional Superposition*

In order to incorporate both the higher effective precipitation values produced by the lapse rate in high elevations and the valuable measured data by which the spatial-temporal representation throughout the entire basin is enhanced, the upper Susitna basin was divided into sub-basins to which different interpolation methods can be applied (Figure 4.1-4).

### *7.3.1.3. Calibration results*

In this section we describe the modeled runoff results stemming from the combination of climate forcing data and WaSiM module settings that yielded the best overall agreement with data from the calibration period (1981-1983).

#### *7.3.1.3.1. Runoff – daily*

Daily modeled runoff at all three gauging stations for which runoff records exist, namely Susitna River near Cantwell, Susitna River near Denali and MacLaren River near Paxson show high correlations, with efficiency values (NSE) of 0.87, 0.84 and 0.84 (Figures 7.3.1.4.1-1, 7.3.1.4.1-2, and 7.3.1.4.1-3). While runoff is slightly underestimated in water balance (WB) years 1981 and 1983, 1982 shows an overestimation of total runoff, particularly in late September. Note that the second runoff peak June/July 1983 is modeled quite accurately for MacLaren River near Paxson, but is highly underestimated in Susitna River near Denali, and as a result, also at Susitna River near Cantwell. This is possibly due to an underestimation of glacier runoff (see section 7.3.1.4.4).

#### *7.3.1.3.2. Runoff – monthly*

Modeled monthly discharge measurements for the calibration period 1981-1983 show generally good agreement with the observed runoff pattern (Figures 7.3.1.4.2-1, 7.3.1.4.2-2, and 7.3.1.4.2-3). Monthly plots of the modeled runoff for 1982, however, clearly illustrate the overestimation of runoff during summer months. The 3-year mean monthly runoff for the period 1981-1983 reveals good agreement between the modeled and observed hydrographs, despite an overestimate in annual runoff. This is likely due to the fact that the heat transfer model was not activated in these calibration runs, resulting in too high groundwater flow during the winter, and, since this leads to higher water saturation in the soils, higher river runoffs during the entire year. This overestimation likely can be addressed by implementing the heat transfer model; however, the coupling of groundwater and heat transfer models remains problematic, and leads to an underestimation of both winter and summer runoffs.

#### *7.3.1.3.3. Glacier discharge*

Modeled mean annual runoff for the period 1981-1983 can be partitioned in to four contribution categories (snow, firn, ice, and rain) for each of the sub-basins in the upper Susitna basin (Figure 7.3.1.4.3-1). With a glacierized area of 24%, the Susitna River near Denali sub-basin shows the highest ice and firn runoff (26.2% and 20.7%, respectively) followed by MacLaren River near Paxson (14.9% and 14.7%), in which 15% of the watershed was covered by glaciers. At Susitna River near Cantwell (6% glacierized), roughly 12.3% of total runoff can be attributed to glacier ice, while runoff from firn accounts for 10.1%. The modeled contribution of runoff from glacierized areas (ice and firn) at the proposed dam site (Susitna River at Watana) during the calibration period is 19.2%.

#### *7.3.1.3.4. Glacier Mass Balance*

Modeled point mass balance values were compared to those acquired using the glaciological method during early 1980s (see section 5.2.1.2). Overall, the modeled mass balance values show only moderate correlation with the measured values ($R^2 = 0.52$ and NSE = 0.37; Figure 7.3.1.4.4-1). A closer look at the correlations for the different locations at which mass balances were measured during the Susitna studies conducted in the 1980s (Clarke 1986), and their partitioning into the years in which they were measured, can provide some insight about the lack of agreement.

Poorly correlated low elevation (< 1200 m) mass balances are associated with specific locations on East Fork and MacLaren glaciers (Figure 7.3.1.4.4-1). On East Fork Glacier, the lowest mass balance stake from the 1980s measurements was located on the western margin of the glacier (Figure 3.1.2.4.2-1) and likely recorded very high melt rates due to this position. In addition, the low spatial resolution of the model (1 km) probably misrepresents the elevation and hydro-meteorological processes occurring in this narrow, deeply incised valley. MacLaren Glacier shows four modeled mass balances that are in good agreement with measured values and only one model result that differs considerably from the measured result.

In the mid elevation mass balance plots (1400 – 1670 m), a systematic underestimation of the 1981 mass balance can be observed for all stations except for Susitna Glacier. This is attributed to the lack of an accurate "starting date" for the computation of mass balance, which always refers to a period. The first measurements made in 1981 refer to a previous summer surface to which no specific date is identified (Clarke 1986); consequently, a starting date of 1 Oct 1980 was defined,

which could be the reason for the value offset. The lack of correlation at Susitna Glacier is attributed to measurement errors.

While many low and mid elevations show relatively good correlations, mass balance at high elevations (1950 m – 2350 m) consistently have efficiencies (NSE) of below 0. Susitna Glacier at 2350 m shows the most striking offset, with highly overestimated mass balances, which is attributed to an overestimate of the precipitation lapse rate applied. Since all measurements stem from 1981, they might also be affected by the lack of a specific starting date for the mass balance computation in WaSiM.

#### *7.3.1.3.5. Snow depth*

Figure 7.3.1.4.5-1 show modeled and measured snow depths for the period 1981-1983. Snow depths are reproduced very well in low elevation, topographically simple settings in the upper Susitna basin. Correlations decrease with increasing elevation as reliable meteorological forcing data are absent.

## 7.3.2. Method 2

To make accurate projections of future runoff from the upper Susitna basin, we used downscaled climate model projections of the 21st century (see sections 5.5.2 and 5.5.3) to force the hydrological model. To find the best set of model parameters for the bias-corrected CCSM WRF 5 km product, we used multiple evaluation criteria: annual runoff; runoff climatology; glacier mass balance; and snow depths. Using a systematic approach, we varied the following parameters to find the best match to the measured runoff for the historical period: the degree day factors for ice, firn, and snow; the time constants for the linear reservoirs of ice, firn, and snow used to move melt water into the river network; the temperature threshold above which precipitation is considered rain and below which it is considered ice; and the temperature threshold above which ice, firn, and snow begin to melt. The parameters, value ranges, and optimized results for this calibration approach are shown Table 7.3.2-1. During the optimization phase, we ensured that the degree day factor (DDF) for ice was larger than that for firn and the DDF for firn was larger than that for snow. The time constants of the linear reservoirs for meltwater derived from ice, firn, and snow also maintained a physically-plausible ordering; the ice reservoir is the fastest because it allows essentially no infiltration of meltwater, snow is second fastest, and firn is slowest because it allows the most infiltration and thus meltwater takes the longest to run out from that reservoir. The temperature thresholds that gave the best fit were also plausible; $T_{rain}$ controls whether precipitation falls as rain or snow and was set to 0.6 °C. The melt temperature threshold $T_{melt}$, which sets the limit for calculating degree days was set to the standard 0.0 °C.

### *7.3.2.1. Hydrological model setup*

Hydrological model setup was consistent with calibration method 1. For our initial tests, however, the heat transfer module (used for permafrost modeling) in WaSiM failed to integrate with the groundwater module. The input parameters for the heat transfer module were also some of the least well-constrained parameters in the model. Therefore, we chose to disable the heat transfer module for the remainder of the runs discussed in this report; the groundwater module remained on. The most uncertain parameters from the calibration phases included the degree day factors for ice, firn, and snow. We used those parameters to tune WaSiM with WRF (Table 7.3.2-1).

### *7.3.2.2. Calibration results*

Because historical periods in the bias-corrected CCSM WRF 5 km product are hindcasts and not reanalysis, annual comparisons of modeled values and historic data are not possible. Instead, we used a climatology-based calibration approach where we compared the aggregate statistics of many years of data and model output, covering approximately the same interval of time. Specifically, we compare the distributions of annual total runoff, climatology of runoff, annual net glacier mass balance, and snow depth.

The tuned model accurately reproduces both the mean and variability of annual specific runoff (Figure 7.3.2.2-1). The difference between the modeled mean annual runoff and the measured is less than 10% for all sub-basins of the Upper Susitna watershed (Table 7.3.2.2-1). The inter-annual variability is also well-represented, as shown by the histograms in (Figure 7.3.2.2-1). Using these metrics, the model performs better using the bias-corrected CCSM WRF 5 km downscaled climate forcing than it does with the station data forcing used in calibration method 1 (Figure 7.3.2.2-2). This contrasts with the match between the time series of daily modeled runoff and measured where, of course, the local station data forcing provides a better match.

The annual cycle of runoff, as represented in the daily climatology plots of Figure 7.3.2.2-3 show that the modeled runoff starts to rise in the spring a few days earlier than the data, but again, the match is not far off. For the MacLaren near Paxson gauge, there is a significant discrepancy later in the summer, where the modeled runoff is lower than the measured. No combination of model parameters that we tried were able to remove this bias and simultaneously maintain a reasonable glacier mass balance. The signal of slightly low late summer flow from the model propagates downstream to the Cantwell gauge and the proposed dam site location. The bias is much smaller when the model is forced with local station data Figure 7.3.2.2-4, indicating that the physically-based model is well calibrated.

Annual net point mass balance measurements are in the same range as calculated mass balance for the same grid cell in the model (Figure 7.3.2.2-5). The measurement locations are the same as the field measurement locations described above (all glaciers are combined in the plot). The mass balance gradients across the elevation range of the glaciers are also reasonable, as evidenced by the slope of the line in figure 7.3.2.2-5. There is a bias where the modeled mass balance is more negative (or less positive) than the measured, but it is difficult to directly compare the modeled with the data as the modeled values are not representative of actual individual years, which can have considerable inter-annual variability. In addition, the model output is averaged over 1 $km^2$, whereas the data are representative of a specific point on the glacier (i.e. 1 $m^2$).

Modeled snow depths over glaciers in the upper Susitna basin generally achieve the correct range (Figure 7.3.2.2-5), indicating that the model reasonably reproduces the distribution of snow depths across the basin for the 1980s data (Figure 7.3.2.2-6).

## 7.4. Future Runoff

### 7.4.1. Glacier change projections

The total glacier area in the upper Susitna basin at the start of the WaSiM run in 1971 was 666 $km^2$. At the end of the run in 2100, the area remaining was 398 $km^2$, a loss of 40.2% of the original area. The original glacier cover input grid for 1971 shows many cells with 100% glacier cover (Figure 7.4.1-1). However, by as early as 2015, many cells have been reduced to 50% cover or less. By 2060, only the main trunks of large glaciers remain, along with a few small, high elevation, glaciers. Even less glacier cover is predicted by 2100.

Simulated average annual glacier-wide mass balance becomes increasingly negative for all glaciers over the period 1970-2080 (Figures 7.4.1-2 and 7.4.1-3). After 2080, the mass balance of glaciers in the Denali sub-basin becomes positive because only small, high elevation, glaciers remain; large trunk glaciers that occupy low elevation valleys disappear. In the Paxson basin after 2070, all the glaciers have disappeared except for a few grid cells in the main trunk areas, leaving the remaining cells with very negative mass balance.

Glacier runoff in the upper Susitna basin holds relatively steady for the first 30 or 40 years of the simulation (1971-2010), but thereafter starts a steady decline nearly to zero by the end of the 21st century (Figure 7.4.1-4), in accordance with the reduction of glacier area and increasingly negative glacier-wide mass balance rates (Figures 7.4.1-1, 7.4.1-2, and 7.4.1-3).

### 7.4.2. Runoff projections

Projected temperature increases over the 21st century will lead to a reduction in basin-wide runoff (Figure 5.5.2-1 and Figure 7.4.2-1). Modeled mean specific runoff for the Dam site, Susitna near Cantwell, and Susitna near Denali increases between the intervals 1976-1995 and 2016-2035 (Table 7.4.2-1). Runoff decreases in those basins between 2016-2035 and 2080-2099. In the MacLaren near Paxson basin, runoff increases slightly between all intervals. At the Dam site, the mean specific runoff is 1.36 mm/day for 1976-1995, 1.38 mm/day for 2016-2035, and 1.28 mm/day for 2080-2099, a rise of 1.5% between the first two intervals, and a decline of 7.3% between the last two intervals. Evapotranspiration rates increases ~40-45% in each sub-basin over the simulation period (1976-2099; Figure 7.4.2-2), further reducing total runoff and gaining importance as a contributing hydrologic flux. Glacier runoff in the Denali and Paxson sub-basins are projected to diminish considerably over the interval 2010-2099 as glacier wastage and retreat accelerate (Table 7.4.2-2 and Figure 7.4.1-4). This pattern is superimposed on the time series of projected total annual runoff at the dam site (Figure 7.4.2-1), which simultaneously shows large inter-annual variability over the coming century.

The daily climatology of runoff shows a distinct shift to earlier peak runoff by the end of the 21st century in all sub-basins (Figure 7.4.2-3). Measured data from the higher elevation basins Susitna near Denali and MacLaren near Paxson exhibit a broad summer-long peak in runoff, while the lower basins peak earlier in the year and trail off gradually over the summer. For the overlapping period 1976-1995, spring runoff in the model rises earlier than in the measured data, and late summer runoff is generally underestimated. A more robust comparison can be made from one time period in the model to another model period. In this case, we see that peak runoff at the proposed

dam site is nearly one month earlier by the end of the century than it was for 1976-1995 (Figure 7.4.2-1 and Table 7.4.2-3). Also between these intervals, the spring snow melt runoff peak is up to 40% larger for the Paxson sub-basin and marginally larger for the other sub-basins (Figure 7.4.2-3), consistent with projected changes in total snow storage (Figure 7.4.2-4). Late-summer runoff (August) for 2080-2099 at the dam site is about half of what it was for 1976-1995.

#### *7.4.2.1. Flow frequency analysis*

A flow frequency analysis was conducted to examine the frequency of simulated events on the Susitna and MacLaren rivers near existing gaging stations. Analyses were conducted according to the Interagency Advisory Committee on Water Data, Hydrology Subcommittee, Bulletin 17B (Log Pearson III distribution) using U.S. Army Corps of Engineers Hydrologic Engineering Center software, and were performed using annual maximum daily flow data from the WaSiM model simulations (discussed above) over the period 1971-2100. USGS instantaneous peak flow data was available at two stations, the MacLaren River near Paxson and Susitna River near Denali; analysis was performed on these data for evaluation against the flow frequency analysis of the model simulations. Due to the complexity of this watershed, the annual maximum flow event may be generated by snowmelt, rainfall, or glacial melt, or a combination of these processes, thus the peak event for any given year may not be independent and homogenous. The standard frequency approach was used for the mixed population; only one annual maximum flow event was examined regardless of whether it was generated by rainfall, snowmelt, or glacier melt. A weighted skew was calculated based on the regional generalized skew for Alaska Region 6.

The analysis was divided into five periods of approximately 20-30 year increments: Period-1 (1971-2000); Period-2 (2001-2030); Period-3 (2031-2060); Period-4 (2061-2080); Period-5 (2081-2100). The analysis was also completed for the entire time series (1971-2100) and for the USGS instantaneous peak flow data from each station (period of record varies).

Tables 7.4.2.1-1 and 7.4.2.1-2 present each analysis and the skewness for each analysis period. A positive skewness indicates the mean peak flow exceeds the median peak flow. A negative skewness indicates the median peak flow exceeds the mean peak flow. The skewness (weighted) was generally positive for each simulation.

Figures 7.4.2.1-1 through 7.4.2.1-14 show the results of the flow frequency analysis. The "predicted" flow frequency curves generally show higher discharges and an increase in the variation of annual maximum flow (steeper slope) with increasing time.

The annual peak flows on the two rivers are a result of rain events during the snowmelt period or rain events during the late summer when glacial melt is also occurring. Results of the flow frequency analysis for runoff simulations 1971-2100 indicate that the annual maximum daily flows may increase slightly and occur earlier in the year for both rivers (Figure 7.4.2.1-15). In other words, there may be less frequent flood events in late summer and less contribution to the annual peak flow from glacial sources (Figures 7.4.2.1-16 and 7.4.2.1-17). This trend is notable for the MacLaren River, where there are no simulated annual maximum flows occurring after July 1 beginning in 2073. For the Susitna River near Denali, the simulated annual maximum discharge occurs after July 1 in 25 out of 30 years for the analysis period 1971-2000, but by the analysis period of 2081-2100, only 6 of the 20 years the annual maximum flow occurs after July 1.

# 8. CONCLUSIONS

With the anticipated changes in future climate, the hydrology of the upper Susitna basin in south-central Alaska is also expected to change. These changes would impact the quantity and seasonality of river flow into the proposed Susitna-Watana hydroelectric dam, if it were to be built. In this study, we combined field measurements and computational modeling to provide estimates of the effects of future glacier wastage and retreat on 21st century river discharge into the proposed reservoir of the Susitna-Watana Hydroelectric Project.

In the upper Susitna basin catchment (13,289 km²; 450-4200 m a.s.l), we collected new hydrometeorological data over the period 2012-2014 and combined these with historic data from measurements collected in the 1980s. These data were used to calibrate and validate the physically-based hydrological model Water Flow and Balance Simulation Model (WaSiM). Traditional glacier mass balance measurements show that the glaciers lost more mass in 2012-2014 than in 1981-1983. Springtime snow radar surveys of the glaciers allowed us to extrapolate from point measurements of snow depth to the whole glacier area. Snow depth measurements at tundra sites as well as tundra vegetation and soil characterizations helped us choose appropriate model parameters for the tundra portions of the basin. Meteorological data (temperature, humidity, and precipitation) from over 20 stations in the basin show the summertime temperature lapse rate to be smaller over glacier surfaces compared to ice-free surfaces, and show high spatial variability in precipitation across the basin. Energy balance measurements from two meteorological stations, one located on West Fork Glacier and one on a nunatak near Susitna Glacier, were used for more detailed modeling of summertime glacier melt and runoff.

The hydrological model, WaSiM, was forced with climate inputs from a CCSM CMIP5 RCP6.0 scenario downscaled to a 20km-5km nested grid using the Weather Research and Forecasting (WRF) Model. Climate model projections indicate that from 2010-2029 to 2080-2099 the basin-wide mean-annual temperature will rise 2.5º C and total precipitation will rise 2%, with a 13% decrease in snowfall and a 20% increase in rainfall. Hydrological simulations over the 21st century indicate that glaciers will retreat, evapotranspiration will increase, and permafrost will thaw. Mean specific runoff at the proposed dam site will increase slightly (+1.5%) from 1976-1995 to 2016-2035. From 2016-2035 to 2080-2099, mean specific runoff is projected to decrease (-7.3%), coincident with a strongly reduced contribution from glaciers. By the end of the 21st century, peak spring runoff occurs ~1 month earlier than it did at the beginning of the century, and late summer runoff reduces to about half its original volume during this same interval.

# 9. LITERATURE CITED


ACIA. 2005. *Arctic climate impact assessment*. Cambridge, Cambridge University Press.

Aðalgeirsdóttir, G., T. Jóhannesson, H. Björnsson, F. Pálsson and O. Sigurðsson. 2006. Response of Hofsjökull and southern Vatnajökull, Iceland, to climate change. *Journal of Geophysical Research: Earth Surface*. **111**(F3), doi: 10.1029/2005JF000388.

Alaska District, Corps of Engineers 1975. Hydroelectric power development, upper Susitna River basin Southcentral Railbelt area, Alaska. Revised draft environmental impact statement. No. 2962. Department of the Army. Office of the Chief of Engineers, Anchorage, Alaska

Arendt, A.A., K.A. Echelmeyer, W.D. Harrison, C.S. Lingle and V.B. Valentine. 2002. Rapid wastage of Alaska glaciers and their contribution to rising sea level. *Science*. **297**(5580), 382-386. doi: 10.1126/science.1072497.

Arendt, A.A., J. Walsh and W.D. Harrison. 2009. Changes of glaciers and climate in Northwestern North America during the late twentieth century. *Journal of Climate*. **22**(15), 4117-4134. doi: 10.1175/2009JCLI2784.1.

Arnold, N., K. Richards, I. Willis and M. Sharp. 1998. Initial results from a distributed, physically based model of glacier hydrology. *Hydrological Processes*. **12**(2), 191-219. doi: 10.1002/(SICI)1099-1085(199802)12:2<191::AID-HYP571>3.0.CO;2-C.

Aubinet, M., T. Vesala and D. Papale. 2012. *Eddy covariance: a practical guide to measurement and data analysis*. Springer Science & Business Media.

Bahr, D., M. Meier and S. Peckham. 1997. The physical basis of glacier volume-area scaling. *Journal of Geophysical Research-Solid Earth*. **102**(B9), 20355-20362. doi: 10.1029/97JB01696.

Baraer, M., B.G. Mark, J.M. McKenzie, T. Condom, J. Bury, K.-I. Huh, C. Portocarrero, J. Gómez and S. Rathay. 2012. Glacier recession and water resources in Peru's Cordillera Blanca. *Journal of Glaciology*. **58**(207), 134-150. doi: http://dx.doi.org/10.3189/2012JoG11J186.

Bartholomaus, T.C., R.S. Anderson and S.P. Anderson. 2008. Response of glacier basal motion to transient water storage. *Nature Geoscience*. **1**, 33-37. doi: 10.1038/ngeo.2007.52.

Bengtsson, L., M. Botzet and M. Esch. 1996. Will greenhouse gas-induced warming over the next 50 years lead to higher frequency and greater intensity of hurricanes? *Tellus A*. **48**(1), 57-73. doi: 10.1034/j.1600-0870.1996.00004.x.

Benson, C.S. 1982. *Reassessment of winter precipitation on Alaska's Arctic Slope and measurements on the flux of wind blown snow*. Geophysical Institute, University of Alaska Fairbanks.

Berthier, E., E. Schiefer, G.K.C. Clarke, B. Menounos and F. Remy. 2010. Contribution of Alaskan glaciers to sea-level rise derived from satellite imagery. *Nature Geoscience*. **3**(2), 92-95. doi: 10.1038/ngeo737.

Bhatia, M.P., E.B. Kujawinski, S.B. Das, C.F. Breier, P.B. Henderson and M.A. Charette. 2013. Greenland meltwater as a significant and potentially bioavailable source of iron to the ocean. *Nature Geoscience*. **6**(4), 274-278. doi: 10.1038/ngeo1746.

Biftu, G. and T. Gan. 2001. Semi-distributed, physically based, hydrologic modeling of the Paddle River Basin, Alberta, using remotely sensed data. *Journal of Hydrology*. **244**(3), 137-156. doi: 10.1016/S0022-1694(01)00333-X.

Bjornsson, H. 2003. Subglacial lakes and jokulhlaups in Iceland. *Global and Planetary Change*. **35**(3-4), 255 - 271. doi: 10.1016/S0921-8181(02)00130-3.

Black, R.F. 1954. Precipitation at Barrow, Alaska, greater than recorded. *Transactions, American Geophysical Union*. **35**(2), 203-207. doi: 10.1029/TR035i002p00203.

Blume, H.-P., P. Felix-Henningsen, W. Fischer, H.-G. Frede, G. Guggenberger and R. Horn. 1995-2014. *Handbuch der Bodenkunde*. K. Stahr (Ed.). Weinheim, Wiley-VCH.

Brutsaert, W. 1982. *Evaporation into the Atmosphere: Theory, History and Applications. In*, Volume 1 of Environmental Fluid Mechanics. Dordrecht-Boston-London: Springer Netherlands.

Bodvarsson, G. 1983. Temperature/flow statistics and thermomechanics of low-temperature geothermal systems in Iceland. *Journal of volcanology and geothermal research*. **19**(3), 255-280. doi: 10.1016/0377-0273(83)90114-2.

Bowling, S.A. (1982). Task 3 – Hydrology, 1982 Susitna Basin glacier studies. *In* W. D. Harrison and R. Consultants (Eds.), *Task 3 – Hydrology, 1982 Susitna Basin glacier studies* p. 22. Alaska Power Authority, Susitna Hydroelectric Project.

Braun, L. and C. Renner. 1992. Application of a conceptual runoff model in different physiographic regions of Switzerland. *Hydrological Sciences Journal*. **37**(3), 217-231. doi: 10.1080/02626669209492583.

Braun, L.N., M. Weber and M. Schulz. 2000. Consequences of climate change for runoff from Alpine regions. *Annals of Glaciology*. **31**(1), 19-25. doi: 10.3189/172756400781820165.

Burgess, E.W., R.R. Forster and C.F. Larsen. 2013. Flow velocities of Alaskan glaciers. *Nature communications*. **4**, doi: 10.1038/ncomms3146.

Callegary, J.B., C.P. Kikuchi, J.C. Koch, M.R. Lilly and S.A. Leake. 2013. Review: Groundwater in Alaska (USA). *Hydrogeology Journal*. **21**(1), 25-39. doi: 10.1007/s10040-012-0940-5.

Casassa, G., P. Lopez, B. Pouyaud and F. Escobar. 2009. Detection of changes in glacial run-off in alpine basins: examples from North America, the Alps, central Asia and the Andes. *Hydrological Processes*. **23**(1), 31-41. doi: 10.1002/hyp.7194.

Cederstrom, D.J. 1963. *Ground-water resources of the Fairbanks area, Alaska*. United States, Government Printing Office.

Chen, J. and A. Ohmura. (1990). On the influence of Alpine glaciers on runoff. *In* H. Lang and A. Musy (Eds.), *Hydrology in Mountainous Regions I. Hydrological Measurements; The Water Cycle. Lausanne Symposia* (Vol. 193, p. 117-125). Oxfordshire, UK: IAHS Press.

Chow, V.T., D.R. Maidment and L.W. Mays. 1988. *Applied hydrology*. Tata McGraw-Hill Education.

Clarke, T.S., D. Johnson and W.D. Harrison. (1985). *Glacier runoff in the upper Susitna and MacLaren river basins, Alaska.* Paper presented at the Resolving Alaska's water resources conflicts proceedings, Fairbanks, Alaska.

Clarke, T.S., D. Johnson and W.D. Harrison. 1985. *Glacier Mass Balances and Runoff in the Upper Susitna and Maclaren River Basins, 1981-1983*. Geophysical Institute, University of Alaska Fairbanks.

Clarke, T.S. (1986). *Glacier runoff, balance and dynamics in the upper Susitna River Basin, Alaska.* (M.S.), University of Alaska, Fairbanks.

Clarke, T.S. 1991. Glacier dynamics in the Susitna River basin, Alaska, USA. *Journal of Glaciology*. **37**(125), 97-106. http://www.igsoc.org:8080/journal/37/125/igs_journal_vol37_issue125_pg97-106.pdf

Cogley, J., R. Hock, L. Rasmussen, A. Arendt, A. Bauder, R. Braithwaite, P. Jansson, G. Kaser, M. Moller, L. Nicholson and others. 2011. Glossary of glacier mass balance and related terms. UNESCO-IHP, Paris

Comeau, L.E.L., A. Pietroniro and M.N. Demuth. 2009. Glacier contribution to the North and South Saskatchewan Rivers. *Hydrological Processes*. **23**(18), 2640-2653. doi: 10.1002/hyp.7409.

Curran, J.H. 2012. Streamflow Record Extension for Selected Streams in the Susitna River Basin, Alaska. U.S. Department of the Interior, U.S. Geological Survey.

Daanen, R.P., D. Misra, H. Epstein, D. Walker and V. Romanovsky. 2008. Simulating nonsorted circle development in arctic tundra ecosystems. *Journal of Geophysical Research: Biogeosciences*. **113**(G03S06), doi: 10.1029/2008JG000682.

Dingman, S.L., H. Samide, D. Saboe, M. Lynch and C. Slaughter. 1971. Hydrologic reconnaissance of the Delta River and its drainage basin, Alaska. U.S. Army Cold Regions Research and Engineering Laboratory. United States

Dingman, S.L. and F.R. Koutz. 1974. Relations among vegetation, permafrost, and potential insolation in central Alaska. *Arctic and Alpine Research*. **6**(1), 37-47. doi: 10.2307/1550368

Escher-Vetter, H. and O. Reinwarth. 1994. Two decades of runoff measurements (1974 to 1993) at the Pegelstation Vernagtback/Oetztal Alps. *Zeitschrift fur Gletscherkunde und Glazialgeologie*. **30**, 53-98. doi: 10013/epic.38520.d001.

Escher-Vetter, H. 2000. Modeling meltwater production with a distributed energy balance method and runoff using a linear reservoir approach-Results from Vernagtferner, Oetztal Alps, for the ablation. *Zeitschrift fur Gletscherkunde und Glazialgeologie*. **36**, 119-150.

Federer, C.A. and D. Lash. 1978. *BROOK: A hydrologic simulation model for eastern forests*. University of New Hampshire, Water Resource Research Center.

Fleming, S.W. and G.K. Clarke. 2003. Glacial control of water resource and related environmental responses to climatic warming: empirical analysis using historical streamflow data from northwestern Canada. *Canadian Water Resources Journal*. **28**(1), 69-86. doi: 10.4296/cwrj2801069.

Flowers, G.E. and G.K.C. Clarke. 2002. A multicomponent coupled model of glacier hydrology 1. Theory and synthetic examples. *Journal of Geophysical Research: Solid Earth*. **107**(B11), ECV 9-1-ECV 9-17. doi: 10.1029/2001JB001122.

Ford, J. and B.L. Bedford. 1987. The hydrology of Alaskan wetlands, USA: a review. *Arctic and Alpine Research*. **19**(3), 209-229. doi: 10.2307/1551357

Fountain, A.G. and W.V. Tangborn. 1985. The Effect of Glaciers on Streamflow Variations. *Water Resources Research*. **21**(4), 579-586. doi: 10.1029/WR021i004p00579.

Gardner, A.S., G. Moholdt, J.G. Cogley, B. Wouters, A.A. Arendt, J. Wahr, E. Berthier, R. Hock, W.T. Pfeffer, G. Kaser, S.R.M. Ligtenberg, T. Bolch, M.J. Sharp, J.O. Hagen, M.R. van den Broeke and F. Paul. 2013. A Reconciled Estimate of Glacier Contributions to Sea Level Rise: 2003 to 2009. *Science*. **340**(6134), 852-857. doi: 10.1126/science.1234532

Gusmeroli, A., G.J. Wolken and A.A. Arendt. 2014. Helicopter-borne radar imaging of snow cover on and around glaciers in Alaska. *Annals of Glaciology*. **55**(67), 78-88. doi: 10.3189/2014AoG67A029.

Hagg, W., L.N. Braun, M. Weber and M. Becht. 2006. Runoff modeling in glacierized Central Asian catchments for present-day and future climate. *Nordic Hydrology*. **37**(2), 93-105. http://epub.ub.uni-muenchen.de/13563/

Hamon, W.R. 1963. *Computation of direct runoff amounts from storm rainfall*. Publisher not

identified.

Hare, F.K. and J.E. Hay. 1971. Anomalies in the large-scale annual water balance over Northern North America. *Canadian Geographer*. **15**(2), 79-94. doi: 10.1111/j.1541-0064.1971.tb00145.x.

Harrison, W.D., B.T. Drage, S. Bredthauer, D. Johnson, C. Schoch and A.B. Follett. 1983. Reconnaissance of the glaciers of the Susitna River basin in connection with proposed hydroelectric development. *Annals of Glaciology*. **4**, 99-104. http://www.igsoc.org:8080/annals/4/igs_annals_vol04_year1983_pg99-104.pdf

Harrison, W., K. Echelmeyer, E. Chacho, C. Raymond and R. Benedict. 1994. The 1987-88 surge of West Fork Glacier, Susitna Basin, Alaska, USA. *Journal of Glaciology*. **40**(135), 241-254. http://www.igsoc.org:8080/journal/40/135/igs_journal_vol40_issue135_pg241-254.pdf

Harrison, W.D., D.H. Elsberg, K.A. Echelmeyer and R.M. Krimmel. 2001. On the characterization of glacier response by a single time-scale. *Journal of Glaciology*. **47**(159), 659-664. doi: 10.3189/172756501781831837.

Hartmann, B. and G. Wendler. 2005. The significance of the 1976 pacific climate shift in the climatology of Alaska. *Journal of Climate*. **18**(22), 4824-4839. doi: 10.1175/JCLI3532.1.

Haugen, R.K., C.W. Slaughter, K.E. Howe and S.L. Dingman. 1982. Hydrology and climatology of the Caribou-Poker creeks research watershed, Alaska. U.S. Army Cold Regions Research and Engineering Laboratory.

Hill, D.F., N. Bruhis, S.E. Calos, A. Arendt and J. Beamer. 2015. Spatial and temporal variability of freshwater discharge into the Gulf of Alaska. *Journal of Geophysical Research: Oceans*. **120**(2), 634-646. doi: 10.1002/2014JC010395.

Hock, R. and C. Noetzli. 1997. Areal melt and discharge modeling of Storglacieiren, Sweden. *Annals of Glaciology*. **24**, 211-217. http://www.igsoc.org:8080/annals/24/igs_annals_vol24_year1997_pg211-216.pdf

Hock, R. 1999. A distributed temperature-index ice- and snowmelt model including potential direct solar radiation. *Journal of Glaciology*. **45**(149), 101-111. http://www.igsoc.org:8080/journal/45/149/igs_journal_vol45_issue149_pg101-111.pdf

Hock, R., M. Johansson, P. Jansson and L. Bärring. 2002. Modeling climate conditions required for glacier formation in cirques of the Rassepautasjtjåkka Massif, northern Sweden. *Arctic, Antarctic, and Alpine Research*. 3-11. doi: 10.2307/1552502

Hock, R. 2003. Temperature index melt modeling in mountain areas. *Journal of Hydrology*. **282**(1-4), 104-115. doi: 10.1016/S0022-1694(03)00257-9.

Hock, R. 2005. Glacier melt: a review of processes and their modeling. *Progress in Physical Geography*. **29**(3), 362-391. doi: 10.1191/0309133305pp453ra

Hock, R. and B. Holmgren. 2005. A distributed surface energy-balance model for complex topography and its application to Storglaciären, Sweden. *Journal of Glaciology*. **51**(172), 25-36. doi: 10.3189/172756505781829566.

Hock, R., P. Jansson and L. Braun. (2005). Global Change and Mountain Regions - An Overview of Current Knowledge. *In* U. Huber, H. M. Bugmann and M. Reasoner (Eds.), *Global Change and Mountain Regions* (Vol. 23., p. 243-252): Springer, Netherlands.

Hock, R. and P. Jansson. (2006). Encyclopedia of Hydrological Sciences. *In* M. G. Anderson and J. McDonnell (Eds.), *Encyclopedia of Hydrological Sciences*: John Wiley \& Sons, Ltd.

Hodson, A., A.M. Anesio, M. Tranter, A. Fountain, M. Osborn, J. Priscu, J. Laybourn-Parry and B. Sattler. 2008. Glacial ecosystems. *Ecological Monographs*. **78**(1), 41-67. doi: 10.1890/07-0187.1.

Hood, E. and D. Scott. 2008. Riverine organic matter and nutrients in southeast Alaska affected by glacial coverage. *Nature Geoscience*. **1**, 583-587. doi: 10.1038/ngeo280.

Hood, E. and L. Berner. 2009. Effects of changing glacial coverage on the physical and biogeochemical properties of coastal streams in southeastern Alaska. *Journal of Geophysical Research: Biogeosciences*. **114**(G3), doi: 10.1029/2009JG000971.

Hood, E., J. Fellman, R.G. Spencer, P.J. Hernes, R. Edwards, D. D'Amore and D. Scott. 2009. Glaciers as a source of ancient and labile organic matter to the marine environment. *Nature*. **462**(7276), 1044-1047. doi: 10.1038/nature08580.

Hopkinson, C. and G.J. Young. 1998. The effect of glacier wastage on the flow of the Bow River at Banff, Alberta, 1951-1993. *Hydrological Processes*. **12**(10-11), 1745-1762. doi: 10.1002/(SICI)1099-1085(199808/09)12:10/11<1745::AID-HYP692>3.0.CO;2-S.

Horton, P., B. Schaefli, A. Mezghani, B.t. Hingray and A. Musy. 2006. Assessment of climate-change impacts on alpine discharge regimes with climate model uncertainty. *Hydrological Processes*. **20**(10), 2091-2109. doi: 10.1002/hyp.6197.

Huss, M., A. Bauder, M. Funk and R. Hock. 2008. Determination of the seasonal mass balance of four Alpine glaciers since 1865. *Journal of Geophysical Research: Earth Surface (2003–2012)*. **113**(F1), doi: 10.1029/2007JF000803.

Huss, M., D. Farinotti, A. Bauder and M. Funk. 2008. Modeling runoff from highly glacierized alpine drainage basins in a changing climate. *Hydrological Processes*. **22**(19), 3888-3902. doi: 10.1002/hyp.7055.

Huss, M., G. Jouvet, D. Farinotti and A. Bauder. 2010. Future high-mountain hydrology: a new

parameterization of glacier retreat. *Hydrology and Earth System Sciences Discussions*. **7**(1), 345-387. doi: 10.5194/hessd-7-345-2010.

Huss, M. 2011. Present and future contribution of glacier storage change to runoff from macroscale drainage basins in Europe. *Water Resources Research*. **47**(7), doi: 10.1029/2010WR010299.

Huss, M., R. Hock, A. Bauder and M. Funk. 2012. Conventional versus reference-surface mass balance. *Journal of Glaciology*. **38**(208), 278-286. doi: 10.3189/2012JoG11J216.

Immerzeel, W. 2008. Historical trends and future predictions of climate variability in the Brahmaputra basin. *International Journal of Climatology*. **28**(2), 243-254. doi: 10.1002/joc.1528.

Immerzeel, W.W., F. Pellicciotti and M.F.P. Bierkens. 2013. Rising river flows throughout the twenty-first century in two Himalayan glacierized watersheds. *Nature Geoscience*. **6**, 742-745. doi: 10.1038/ngeo1896.

IPCC. 2013. Climate Change 2013: The Physical Science Basis. Contribution of Working Group I to the Fifth Assessment Report of the Intergovernmental Panel on Climate Change. Cambridge University Press, Cambridge, United Kingdom and New York, USA doi: 10.1017/CBO9781107415324

Iwata, H., Y. Harazono and M. Ueyama. 2012. The role of permafrost in water exchange of a black spruce forest in Interior Alaska. *Agricultural and Forest Meteorology*. **161**, 107-115. doi: 10.1016/j.agrformet.2012.03.017.

Jafarov, E.E., S.S. Marchenko and V.E. Romanovsky. 2012. Numerical modeling of permafrost dynamics in Alaska using a high spatial resolution dataset. *The Cryosphere Discussions*. **6**, 89-124. doi: 10.5194/tcd-6-89-2012.

Jansson, P., R. Hock and T. Schneider. 2003. The concept of glacier storage: a review. *Journal of Hydrology*. **282**(1-4), 116-129. doi: 10.1016/S0022-1694(03)00258-0.

Jensen, H. and H. Lang. 1973. Forecasting discharge from a glaciated basin in the Swiss Alps. *In Role of Snow and Ice in Hydrology*. International Association of Hydrological Sciences Publication. Vol. 107(2). p. 1047-1057. IAHS Press. Oxfordshire, UK.

Johannesson, T., C.F. Raymond and E.D. Waddington. 1989. Time-scale adjustments of glaciers to changes in mass balance. *Journal of Glaciology*. **35**, 355-369. http://www.igsoc.org:8080/journal/35/121/igs_journal_vol35_issue121_pg355-369.pdf

Jorgenson, M.T., C.H. Racine, J.C. Walters and T.E. Osterkamp. 2001. Permafrost degradation and ecological changes associated with a warming climate in Central Alaska. *Climatic Change*. **48**(4), 551-579. doi: 10.1023/A%3A1005667424292.

Jorgenson, M.T., K. Yoshikawa, M. Kanevskiy, Y. Shur, V. Romanovsky, S. Marchenko, G. Grosse, J. Brown and B. Jones. 2008. *Permafrost characteristics of Alaska*. Institute of Northern Engineering, University of Alaska Fairbanks.

Juen, I., G. Kaser and C. Georges. 2007. Modeling observed and future runoff from a glacierized tropical catchment (Cordillera Blanca, Peru). *Global and Planetary Change*. **59**(1-4), 37 - 48. doi: 10.1016/j.gloplacha.2006.11.038.

Kade, A., V.E. Romanovsky and D.A. Walker. 2006. The n-factor of nonsorted circles along a climate gradient in Arctic Alaska. *Permafrost and Periglacial Processes*. **17**(4), 279-289. doi: 10.1002/ppp.563.

Kalnay, E., M. Kanamitsu, R. Kistler, W. Collins, D. Deaven, L. Gandin, M. Iredell, S. Saha, G. White, J. Woollen, Y. Zhu, A. Leetmaa, R. Reynolds, M. Chelliah, W. Ebisuzaki, W. Higgins, J. Janowiak, K.C. Mo, C. Ropelewski, J. Wang, R. Jenne and D. Joseph. 1996. The NCEP/NCAR 40-Year Reanalysis Project. *Bulletin of the American Meteorological Society*. **77**(3), 437-471. doi: 10.1175/1520-0477(1996)077<0437:TNYRP>2.0.CO;2.

Kane, D. and C. Slaughter. (1973). Recharge of a central Alaska lake by sub-permafrost groundwater. *In. Permafrost-North American Contribution to Second International Conference on Permafrost, Yakutsk, Siberia, July 13-18.* p. 458-462. National Academy of Sciences. Washington, D.C.

Kane, D. and J. Stein. 1983a. Field evidence of groundwater recharge in interior Alaska. *In, Fourth international conference on permafrost Fairbanks Alaska, July 17-22, final proceedings*. Vol. 2. p. 572-577. National Academy Press. Washington, D.C.

Kane, D.L. and J. Stein. 1983b. Water movement into seasonally frozen soils. *Water Resources Research*. **19**(6), 1547-1557. doi:10.1029/WR019i006p01547.

Karl, T.R. 2009. *Global climate change impacts in the United States.* Cambridge University Press.

Kaser, G., M. Grosshauser and B. Marzeion. 2010. Contribution potential of glaciers to water availability in different climate regimes. *Proceedings of the National Academy of Sciences of the United States of America*. **107**(47), 20223-20227. doi: 10.1073/pnas.1008162107.

Kaufman, D.S., D.P. Schneider, N.P. McKay, C.M. Ammann, R.S. Bradley, K.R. Briffa, G.H. Miller, B.L. Otto-Bliesner, J.T. Overpeck, B.M. Vinther and A.L. 2k Project Members. 2009. Recent Warming Reverses Long-Term Arctic Cooling. *Science*. **325**(5945), 1236-1239. doi: 10.1126/science.1173983

Kauman, D.S. and W.F. Manley. (2004). Pleistocene Maximum and Late Wisconsinan glacier extents across Alaska, U.S.A. *In* J. Ehlers and P. L. Gibbard (Eds.), *Developments in Quaternary Sciences*. **2**(Part B), p. 9-27. Elsevier.

Kobierska, F., T. Jonas, M. Zappa, M. Bavay, J. Magnusson and S.M. Bernasconi. 2013. Future

runoff from a partly glacierized watershed in Central Switzerland: A two-model approach. *Advances in Water Resources*. **55**, 204-214. doi: 10.1016/j.advwatres.2012.07.024.

Koboltschnig, G.R., W. Schoner, M. Zappa, C. Kroisleitner and H. Holzmann. 2008. Runoff modeling of the glacierized Alpine Upper Salzach basin (Austria): multi-criteria result validation. *Hydrological Processes*. **22**(19), 3950-3964. doi: 10.1002/hyp.7112.

Kyle, R.E., T.P. Brabets and others. 2001. Water temperature of streams in the Cook Inlet basin, Alaska, and implications of climate change. U.S. Department of the Interior, U.S. Geological Survey.

Lang, H. 1968. Relations between glacier runoff and meteorological factors observed on and outside the glacier. *In Snow and Ice. Reports and Discussions*. International Association of Hydrological Sciences Publication. No. 79. p. 439-439. IAHS Press. Oxfordshire, UK.

Lang, H. 1986. Forecasting meltwater runoff from snow-covered areas and from glacier basins. In Kraijenhoff DA; Moll, J. (eds.), *River flow modeling and forecasting*. p. 99-127. Springer.

Larsen, C.F., R.J. Motyka, A.A. Arendt, K.A. Echelmeyer and P.E. Geissler. 2007. Glacier changes in southeast Alaska and northwest British Columbia and contribution to sea level rise. *Journal of Geophysical Research: Earth Surface*. **112**(F1), doi: 10.1029/2006JF000586.

Larsen, C., E. Burgess, A. Arendt, S. O'Neel, A. Johnson and C. Kienholz. 2015. Surface melt dominates Alaska glacier mass balance. *Geophysical Research Letters*. doi: 10.1002/2015GL064349.

Lliboutry, L., B. Morales Arnao, A. Pautre and B. Schneider. 1977. Glaciological problems set by the control of dangerous lakes in Cordillera Blanca, Peru. *Journal of Glaciology*. **18**(79), 239-290. http://www.igsoc.org:8080/journal/19/81/igs_journal_vol19_issue081_pg673-674.pdf

Lynch, A.H., D.L. McGinnis and D.A. Bailey. 1998. Snow-albedo feedback and the spring transition in a regional climate system model: Influence of land surface model. *Journal of Geophysical Research: Atmospheres*. **103**(D22), 29037-29049. doi: 10.1029/98JD00790.

MacDougall, A.H., B.A. Wheler and G.E. Flowers. 2011. A preliminary assessment of glacier melt-model parameter sensitivity and transferability in a dry subarctic environment. *The Cryosphere*. **5**, 1011-1028. doi: 10.5194/tc-5-1011-2011.

MacGregor, K.R., C.A. Riihimaki and R.S. Anderson. 2005. Spatial and temporal evolution of rapid basal sliding on Bench Glacier, Alaska, USA. *Journal of Glaciology*. **51**(172), 49-63. doi: 10.3189/172756505781829485.

MacKay, D.K., S. Fogarasi and M. Spitzer. 1973. Documentation of an extreme summers storm in the Mackenzie Mountains, N.W.T. In on Northern Oil Development, N.P.T.F. (eds.),

Hydrologic Aspects of Norhern Pipeline Development - A Series of 16 Reports. Vol. 73(3). p. 191-222. Water Resources Branch. Ottawa, Canada.

Mark, B.G. and G.O. Seltzer. 2003. Tropical glacier meltwater contribution to stream discharge: a case study in the Cordillera Blanca, Peru. *Journal of Glaciology*. **49**(165), 271-281. doi: 10.3189/172756503781830746.

Mark, B.G. and J.M. Mckenzie. 2007. Tracing Increasing Tropical Andean Glacier Melt with Stable Isotopes in Water. *Environmental Science \& Technology*. **41**(20), 6955-6960. doi: 10.1021/es071099d.

McGrath, D., L. Sass, S. O'Neel, A. Arendt, G. Wolken, A. Gusmeroli, C. Kienholz and C. McNeil. 2015. End-of-winter snow depth variability on glaciers in Alaska. *Journal of Geophysical Research: Earth Surface*. doi: 10.1002/2015JF003539.

Meier, M. and W. Tangborn. 1961. Distinctive characteristics of glacier runoff. *U.S. Geological Survey Professional Paper*. Vol. 424(B). U.S. Department of the Interior, U.S. Geological Survey. Milner, A.M., E.E. Knudsen, C. Soiseth, A.L. Robertson, D. Schell, I.T. Phillips and K. Magnusson. 2000. Colonization and development of stream communities across a 200-year gradient in Glacier Bay National Park, Alaska, U.S.A. *Canadian Journal of Fisheries and Aquatic Sciences*. **57**(11) 2319-2335. doi:10.1139/f00-212.

Milner, A.M., E.E. Knudsen, C. Soiseth, A.L. Robertson, D. Schell, I.T. Phillips and K. Magnusson. 2000. Colonization and development of stream communities across a 200-year gradient in Glacier Bay National Park, Alaska, U.S.A. *Canadian Journal of Fisheries and Aquatic Sciences*. **57**(11), 2319-2335. doi: 10.1139/f00-212.

Monteith, J.L. (Ed.). (1975). *Vegetation and the atmosphere. Vol. 1. Principles. Vol. 2. Case studies 1975* (Vol. 1). Leicestershire, UK: University of Nottingham.

Nash, J. and J.V. Sutcliffe. 1970. River flow forecasting through conceptual models part I—A discussion of principles. *Journal of Hydrology*. **10**(3), 282-290. doi: 10.1016/0022-1694(70)90255-6.

Neal, E.G., M.T. Walter and C. Coffeen. 2002. Linking the pacific decadal oscillation to seasonal stream discharge patterns in Southeast Alaska. *Journal of Hydrology*. **263**(1-4), 188-197. doi: 10.1016/S0022-1694(02)00058-6.

Neal, E.G., E. Hood and K. Smikrud. 2010. Contribution of glacier runoff to freshwater discharge into the Gulf of Alaska. *Geophysical Research Letters*. **37**(6), doi: 10.1029/2010GL042385.

Osterkamp, T.E. and V.E. Romanovsky. 1999. Evidence for warming and thawing of discontinuous permafrost in Alaska. *Permafrost and Periglacial Processes*. **10**, 17-37. doi: 10.1002/(SICI)1099-1530(199901/03)10:1<17::AID-PPP303>3.0.CO;2-4.

Osterkamp, T.E. 2005. The recent warming of permafrost in Alaska. *Global and Planetary Change*. **49**(3-4), 187-202. doi: 10.1016/j.gloplacha.2005.09.001.

Osterkamp, T.E. 2007. Causes of warming and thawing permafrost in Alaska. *Eos, Transactions American Geophysical Union*. **88**(48), 522-523. doi: 10.1029/2007EO480002.

Ostrem, G. 1973. Runoff forecasts for highly glacierized basins. *In Role of snow and ice in hydrology*. International Association of Hydrological Sciences Publication. Vol. 107(2). p. 1111-1132. IAHS Press. Oxfordshire, UK.

Overland, J., J. Key, B.M. Kim, S.J. Kim, Y. Liu, J. Walsh, M. Wang and U. Bhatt. (2012). Air temperature, atmospheric circulation and clouds. In M. Jeffries, J. Overland and J. Richter-Menge (Eds.), *Arctic Report Card 2012*: NOAA.

Overpeck, J., K. Hughen, D. Hardy, R. Bradley, R. Case, M. Douglas, B. Finney, K. Gajewski, G. Jacoby, A. Jennings, S. Lamoureux, A. Lasca, G. MacDonald, J. Moore, M. Retelle, S. Smith, A. Wolfe and G. Zielinski. 1997. Arctic Environmental Change of the Last Four Centuries. *Science*. **278**(5341), 1251-1256. doi: 10.1126/science.278.5341.1251

Patrick J.H. and P. Black. 1968. Potential evapotranspiration and climate in Alaska by Thornthwaites classification. *U.S. Department of Agriculture Forest Service Research Paper*. No. PNW-71. Institute of Northern Forestry.

Pellicciotti, F., B. Brock, U. Strasser, P. Burlando, M. Funk and J. Corripio. 2005. An enhanced temperature-index glacier melt model including the shortwave radiation balance: development and testing for Haut Glacier d'Arolla, Switzerland. *Journal of Glaciology*. **51**(175), 573-587. doi: 10.3189/172756505781829124.

Pfeffer, W.T., A.A. Arendt, A. Bliss, T. Bolch, J.G. Cogley, A.S. Gardner, J.-O. Hagen, R. Hock, G. Kaser and C. Kienholz. 2014. The Randolph Glacier Inventory: a globally complete inventory of glaciers. *Journal of Glaciology*. **60**(221), 537-552. doi: 10.3189/2014JoG13J176.

Post, A.S. 1960. The exceptional advances of the Muldrow, Black Rapids, and Susitna glaciers. *Journal of Geophysical Research*. **65**(11), 3703-3712. doi: 10.1029/JZ065i011p03703.

Pouyaud, B., M. Zapata, J. Yerren, J. Gomez, G. Rosas, W. Suarez and P. Ribstein. 2005. On the future of the water resources from glacier melting in the Cordillera Blanca, Peru. *Hydrological Sciences Journal.* **50**(6), 999-1022. doi: 10.1623/hysj.2005.50.6.999.

Quick, M. and A. Pipes. 1977. U.B.C Watershed Model. *Hydrological Sciences Bulletin*. **22**(1), 153-161. doi: 10.1080/02626667709491701.

R&M Consultants, Inc. and W.D. Harrison. 1981. Task 3, Hydrology. Glacier Studies. Susitna Hydroelectric Project, Document 211. Report for Acres American Incorporated. Alaska Power Authority, Buffalo, NY.

R&M Consultants, Inc. 1982. Task 3, Hydrology. Field data collection and processing, Supplement 1, 1982 field data. Susitna Hydroelectric Project, Document 23. Report for Acres American Incorporated. Alaska Power Authority, Buffalo, NY.

R&M Consultants, Inc. and under contract to Harza-Ebasco Susitna Joint Venture. 1983. Task 4, Hydrology. Processed climatic data (1983). October 1982-September 1983. Susitna Hydroelectric Project, Document 1088-1094. Report for Acres American Incorporated. Alaska Power Authority, Buffalo, NY.

R&M Consultants, Inc. and under contract to Harza-Ebasco Susitna Joint Venture. 1983. Task 4, Hydrology. Processed climatic data October 1983 - December 1984: final report. Susitna Hydroelectric Project, Document 2767 - 2773. Report for Acres American Incorporated. Alaska Power Authority, Buffalo, NY.

Racine, C.H. and J.C. Walters. 1994. Groundwater-discharge fens in the Tanana Lowlands, interior Alaska, USA. *Arctic and Alpine Research*. **26**(4), 418-426. doi: 10.2307/1551804

Radić, V., A. Bliss, A.C. Beedlow, R. Hock, E. Miles and J.G. Cogley. 2013. Regional and global projections of twenty-first century glacier mass changes in response to climate scenarios from global climate models. *Climate Dynamics*. **April**, 1-22. doi: 10.1007/s00382-013-1719-7.

Radić, V. and R. Hock. 2006. Modeling future glacier mass balance and volume changes using ERA-40 reanalysis and climate models: A sensitivity study at Storglaciären, Sweden. *Journal of Geophysical Research: Earth Surface (2003–2012)*. **111**(F3), doi: 10.1029/2005JF000440.

Radić, V., and R. Hock. 2010. Regional and global volumes of glaciers derived from statistical upscaling of glacier inventory data. *Journal of Geophysical Research: Earth Surface (2003–2012)*, **115**(F1).

Radić, V. and R. Hock. 2011. Regionally differentiated contribution of mountain glaciers and ice caps to future sea-level rise. *Nature Geoscience*. **4**(2), 91-94. doi: 10.1038/ngeo1052.

Radić, V. and R. Hock. 2014. Glaciers in the Earth's hydrological cycle: assessments of glacier mass and runoff changes on global and regional scales *The Earth's Hydrological Cycle*. p. 813-837: Springer.

Ragettli, S., F. Pellicciotti, R. Bordoy and W.W. Immerzeel. 2013. Sources of uncertainty in modeling the glaciohydrological response of a Karakoram watershed to climate change. *Water Resources Research*. doi: 10.1002/wrcr.20450.

Rawlins, M.A., D.J. Nicolsky, K.C. McDonald and V.E. Romanovsky. 2013. Simulating soil freeze/thaw dynamics with an improved pan-Arctic water balance model. *Journal of Advances in Modeling Earth Systems*. **5**, doi: 10.1002/jame.20045.

Raymond, P.A., J. McClelland, R. Holmes, A. Zhulidov, K. Mull, B. Peterson, R. Striegl, G. Aiken and T. Gurtovaya. 2007. Flux and age of dissolved organic carbon exported to the Arctic Ocean: A carbon isotopic study of the five largest arctic rivers. *Global Biogeochemical Cycles*. **21**(4), doi: 10.1029/2007GB002934.

Rees, H.G. and D.N. Collins. 2006. Regional differences in response of flow in glacier-fed Himalayan rivers to climatic warming. *Hydrological Processes*. **20**(10), 2157-2169. doi: 10.1002/hyp.6209.

Reid, T.D. and B.W. Brock. 2010. An energy-balance model for debris-covered glaciers including heat conduction through the debris layer. *Journal of Glaciology*. **56**(199), 903-916. doi: 10.3189/002214310794457218.

Robinson, C.T., U. Uehlinger and M. Hieber. 2001. Spatio-temporal variation in macroinvertebrate assemblages of glacial streams in the Swiss Alps. *Freshwater Biology*. **46**(12), 1663-1672. doi: 10.1046/j.1365-2427.2001.00851.x.

Romanovsky, V.E., S.L. Smith and H.H. Christiansen. 2010. Permafrost thermal state in the polar Northern Hemisphere during the international polar year 2007-2009: a synthesis. *Permafrost and Periglacial Processes*. **21**(2), 106-116. doi: 10.1002/ppp.689.

Rothlisberger, H. and H. Lang. (1987). Glacio-Fluvial Sediment Transfer: An Alpine Perspective. In A. M. Gurnell and M. J. Clark (Eds.), p. 207-284. New York, USA: John Wiley & Sons, Ltd.

Rovansek, R., D. Kane and L. Hinzman. (1993). *Improving estimates of snowpack water equivalent using double sampling.* Paper presented at the Proceedings of the 61st Western snow conference.

Schneeberger, C., O. Albrecht, H. Blatter, M. Wild and R. Hock. 2001. Modeling the response of glaciers to a doubling in atmospheric CO2: a case study of Storglaciären, northern Sweden. *Climate Dynamics*. **17**(11), 825-834. doi: 10.1007/s003820000147.

Schuler, T., K. Melvold, J. Hagen and R. Hock. 2005. Assessing the future evolution of meltwater intrusions into a mine below Gruvefonna, Svalbard. *Annals of Glaciology*. **42**(1), 262-268. doi: 10.3189/172756405781812970.

Schuler, T.V., R. Hock, M. Jackson, H. Elvehøy, M. Braun, I. Brown and J.-O. Hagen. 2005. Distributed mass-balance and climate sensitivity modeling of Engabreen, Norway. *Annals of Glaciology*. **42**(1), 395-401. doi: 10.3189/172756405781812998.

Schulla, J. (1997). *Hydrologische Modellierung von Flussgebieten zur Abschätzung der Folgen von Klimaänderungen.* Diss. Naturwiss. ETH Zürich, Nr. 12018, 1997. Ref.: H. Lang; Korref.: W. Kinzelbach; Korref.: R. Schulze.

Schulla, J. (2012). Model Description WaSiM (Water balance Simulation Model), completely

revised version 2012. Zürich, Switzerland: Hydrology Software Consulting. Retrieved from http://www.wasim.ch/downloads/doku/wasim/wasim_2012_ed2_en.pdf

Schulla, J. (2012). The hydrological model system WaSiM. Retrieved from http://www.wasim.ch/en/index.html

Selkowitz, D.J. and S.V. Stehman. 2011. Thematic accuracy of the National Land Cover Database (NLCD) 2001 land cover for Alaska. *Remote Sensing of Environment*. **115**(6), 1401-1407. doi: 10.1016/j.rse.2011.01.020.

Sharp, M. and G. Wolken. 2011. Arctic Glaciers and ice caps (outside Greenland). *In* Blunden, J., D.S. Arndt and M. Baringer (eds.), *State of the Climate in 2010*. Bulletin of the American Meteorological Society. Vol. 92(6). p. S155–S156.

Shulski, M. and G. Wendler. 2007. *The climate of Alaska*. Fairbanks, Alaska, University of Alaska Press.

Singh, V.P. and D.A. Woolhiser. 2002. Mathematical modeling of watershed hydrology. *Journal of hydrologic engineering*. **7**(4), 270-292. doi: 10.1061/(ASCE)1084-0699(2002)7:4(270)

Slaughter, C.W. and D.L. Kane. 1979. Hydrologic role of shallow organic soils in cold climates. *In, Canadian hydrology symposium 79 - cold climate hydrology proceedings*. Report No. 17834. p. 380-389. Vancouver, B.C., Canada.

Slaughter, C.W., J.W. Hilgert and E.H. Culp. 1983. Summer streamflow and sediment yield from discontinuous permafrost headwater catchments. *In, Fourth international conference on permafrost Fairbanks Alaska, July 17-22, final proceedings*. Vol. 2. p. 1172-1177. National Academy Press. Washington, D.C.

Sold, L., M. Huss, M. Hoelzle, H. Andereggen, P.C. Joerg and M. Zemp. 2013. Methodological approaches to infer end-of-winter snow distribution on alpine glaciers. *Journal of Glaciology*. **59**(218), 1047-1059. doi: 10.3189/2013JoG13J015.

Staff, S.S. U.S. General Soil Map (STATSGO2) http://sdmdataaccess.nrcs.usda.gov/. Retrieved 07/05/2012, from Natural Resources Conservation Service, United States Department of Agriculture http://sdmdataaccess.nrcs.usda.gov/

Stahl, K. and R.D. Moore. 2006. Influence of watershed glacier coverage on summer streamflow in British Columbia, Canada. *Water Resources Research*. **42**(6), doi: 10.1029/2006WR005022.

Stahl, K., R.D. Moore, J.M. Shea, D. Hutchinson and A.J. Cannon. 2008. Coupled modeling of glacier and streamflow response to future climate scenarios. *Water Resources Research*. **44**(2), doi: 10.1029/2007WR005956.

Stahl, K., H. Hisdal, J. Hannaford, L. Tallaksen, H.v. Lanen, E. Sauquet, S. Demuth, M. Fendekova and d. J\'o, J. 2010. Streamflow trends in Europe: evidence from a dataset of near-natural

catchments. *Hydrology and Earth System Sciences Discussions*. **7**(4), 5769-5804. doi: 10.5194/hess-14-2367-2010.

Suarez, W., P. Chevallier, B. Pouyayd and P. Lopez. 2008. Modeling the water balance in the glacierized Paron Lake basin (White Cordillera, Peru). *Hydrological Sciences Journal*. **53**(1), 266-277. doi: 10.1623/hysj.53.1.266.

USGS Survey (2012). USGS Surface-Water Daily Data for the Nation. Retrieved from: http://waterdata.usgs.gov/nwis/dv?referred_module=sw&state_cd=ak&huc2_cd=19&format=station_list&sort_key=site_no&group_key=NONE&range_selection=days&period=365&date_format=YYYY-MM-DD&rdb_compression=file&list_of_search_criteria=state_cd%2Chuc2_cd%2Crealtime_parameter_selection.
http://waterdata.usgs.gov/nwis/dv?referred_module=sw&state_cd=ak&huc2_cd=19&format=station_list&sort_key=site_no&group_key=NONE&range_selection=days&period=365&date_format=YYYY-MM-DD&rdb_compression=file&list_of_search_criteria=state_cd%2Chuc2_cd%2Crealtime_parameter_selection

Tangborn, W.V. 1984. Prediction of glacier derived runoff for hydroelectric development. *Geografiska Annaler*. **66**(A), 257-265. doi: 10.2307/520699

Van Genuchten, M.T., F. Leij and S. Yates. 1991. *The RETC code for quantifying the hydraulic functions of unsaturated soils.* Robert S. Kerr Environmental Research Laboratory.

VanLooy, J., R. Forster and A. Ford. 2006. Accelerating thinning of Kenai Peninsula glaciers, Alaska. *Geophysical Research Letters*. **33**(21), doi: 10.1029/2006GL028060.

Vuille, M., B. Francou, P. Wagnon, I. Juen, G. Kaser, B.G. Mark and R.S. Bradley. 2008. Climate change and tropical Andean glaciers: Past, present and future. *Earth-Science Reviews*. **89**(3-4), 79-96. doi: 10.1016/j.earscirev.2008.04.002.

Wainwright, J. and M. Mulligan. 2005. *Environmental modeling: finding simplicity in complexity*. John Wiley & Sons.

Walsh, J.E., W.L. Chapman, V. Romanovsky, J.H. Christensen and M. Stendel. 2008. Global climate model performance over Alaska and Greenland. *Journal of Climate*. **21**, 6156-6174. doi: 10.1175/2008JCLI2163.1.

Weber, M., L. Braun, W. Mauser and M. Prasch. 2010. Contribution of rain, snow-and icemelt in the upper Danube discharge today and in the future. *Geografia Fisica e Dinammica Quaternaria*. **33**(2), 221-230. http://gfdq.glaciologia.it/33_2_12_2010/

Wendling, U. 1975. Zur Messung und Schätzung der potentiellen Verdunstung. *Zeitschrift für Meteorologie*. **25**(2), 103-111.

Wilcox, D.E. 1980. Geohydrology of the Delta-Clearwater Area, Alaska. *U.S. Geological Survey Water-Resources Investigation Report*. No. 80-92. U.S. Department of the Interior, U.S. Geological Survey.

Williams, J.R. 1970. Ground water in the permafrost regions of Alaska. *U.S. Geological Survey Professional Paper*. No. 696. U.S. Department of the Interior, U.S. Geological Survey.

Willis, I.C., N.S. Arnold and B.W. Brock. 2002. Effect of snowpack removal on energy balance, melt and runoff in a small supraglacial catchment. *Hydrological Processes*. **16**(14), 2721-2749. doi: 10.1002/hyp.1067.

Wolken, J.M., T.N. Hollingsworth, T.S. Rupp, F.S. Chapin III, S.F. Trainor, T.M. Barrett, P.F. Sullivan, A.D. McGuire, E.S. Euskirchen, P.E. Hennon and others. 2011. Evidence and implications of recent and projected climate change in Alaska's forest ecosystems. *Ecosphere*. **2**(11), 1-35. doi: 10.1890/ES11-00288.1.

Wolken, G., M. Sharp, M.L. Geai, D. Burgess, A. Arent and B. Wouters. 2013. Arctic Glaciers and ice caps (outside Greenland). In Blunden, J. and D.S. Arndt (eds.), *State of the Climate in 2012*. Bulletin of the American Meteorological Society. Vol. 94(8). p. S119–S121.

Yao, T., J. Pu, A. Lu, Y. Wang and W. Yu. 2007. Recent Glacial Retreat and Its Impact on Hydrological Processes on the Tibetan Plateau, China, and Surrounding Regions. *Arctic, Antarctic, and Alpine Research*. **39**(4), 642-650. doi: 10.1657/1523-0430(07-510)[YAO]2.0.CO;2.

Zhang, J., U.S. Bhatt, W.V. Tangborn and C.S. Lingle. 2007. Climate downscaling for estimating glacier mass balances in northwestern North America: Validation with a USGS benchmark glacier. *Geophysical Research Letters*. **34**(21), doi: 10.1029/2007GL031139.

Zhang, J., U.S. Bhatt, W.V. Tangborn and C.S. Lingle. 2007. Response of glaciers in northwestern North America to future climate change: an atmosphere/glacier hierarchical modeling approach. *Annals of Glaciology*. **46**(1), 283-290. doi: 10.3189/172756407782871378.

# 10. TABLES

**Table 3.1.1-1. Reported studies of regional-scale glacier mass changes in Alaska (including the adjacent glaciers in northwestern Canada).** Assuming, where necessary, an ice/firn/snow density of 900 kg m-3 and rounding to whole years.

| Reference | Original unit | Mass change (Gt $yr^{-1}$) | Specific mass change (m w.e. $yr^{-1}$) | Domain (area, $km^2$) | Period | Method |
|---|---|---|---|---|---|---|
| *Alaska and NW Canada* | | | | | | |
| Arendt et al. 2002 | –52±15 $km^3 yr^{-1}$ w.e. | –52±15 | -0.57 | Alaska (90,000) | 1955-5/1995 | Laser altimetry/maps |
| Arendt et al. 2002 | –96±35 $km^3 yr^{-1}$ w.e. | –96±35 | -1.07 | Alaska (90,000) | 5/1995-5/2000 | Laser altimetry |
| Tamisiea et al. 2005 | -110±30 $km^3 yr^{-1}$ w.e. | -110±30 | -1.26 | Alaska (87,000) | 4/2002-6/2004 | GRACE |
| Chen et al. 2006 | -101±22 $km^3 yr^{-1}$ w.e. | -101±22 | -1.11 | Alaska (90,957) | 4/2002-11/2005 | GRACE |
| Luthcke et al. 2008 | -84±5 Gt $yr^{-1}$ | -84±5 | -1.02 | Gulf of Alaska (82,505)* | 4/2003-9/2007 | GRACE |
| Berthier et al. 2010 | -41.9±8.6 $km^3 yr^{-1}$ w.e. | -41.9±8.6 | -0.48 | Alaska (87,860) | 1962-2006 | geodetic |
| Wu et al. 2010 | -101±23 Gt $yr^{-1}$ | -101±23 | | Alaska ** | 4/2002-12/2008 | GRACE |
| Luthcke et al. 2013 | -68.8±11 Gt $yr^{-1}$ | -68.8±11 | -0.91 | Alaska (76,000) | 12/2003-12/2010 | GRACE |
| Gardner et al. 2013 | -50±17 Gt $yr^{-1}$ | -50±17 | -0.57 | Alaska (87,100) | 2003-2009 | GRACE |
| Arendt et al. 2013 | -65±11 Gt $yr^{-1}$ | -65±11 | -0.79 | Gulf of Alaska (82,505) | 12/2003-12/2010 | GRACE |
| Arendt et al. 2013 | -61±11 Gt $yr^{-1}$ | -61±11 | -0.74 | Gulf of Alaska (82,505) | 10/2003-10/2009 | GRACE |
| Arendt et al. 2013 | -65±12 Gt $yr^{-1}$ | -65±12 | -0.79 | Gulf of Alaska (82,505) | 10/2003-10/2009 | ICESat |
| *Subregions in Alaska* | | | | | | |
| Adalgeirsdottir 1998 | -34 $km^3$ ice | -0.71 | -0.39 | Harding Icefield (1,800) | 1950/52-1994/96 | Laser altimetry/map |
| Arendt et al. 2002 | -5.3 $km^3 yr^{-1}$ w.e. | -5.3 | | Alaska Range ** | 1955-5/1995 | Laser altimetry/maps |
| Arendt et al. 2002 | -1.0 $km^3 yr^{-1}$ w.e. | -1.0 | | Brooks Range ** | 1955-5/1995 | Laser altimetry/maps |
| Arendt et al. 2002 | -5.4 $km^3 yr^{-1}$ w.e. | -5.4 | | Coast Range ** | 1955-5/1995 | Laser altimetry/maps |
| Arendt et al. 2002 | -2.7 $km^3 yr^{-1}$ w.e. | -2.7 | | Kenai Mountains ** | 1955-5/1995 | Laser altimetry/maps |
| Arendt et al. 2002 | -25.7 $km^3 yr^{-1}$ w.e. | -25.7 | | St. Elias Mountains ** | 1955-5/1995 | Laser altimetry/maps |
| Arendt et al. 2002 | -6.8 $km^3 yr^{-1}$ w.e. | -6.8 | | Western Chugach Mountains ** | 1955-5/1995 | Laser altimetry/maps |
| Arendt et al. 2002 | -1.3 $km^3 yr^{-1}$ w.e. | -1.3 | | Wrangell Mountains ** | 1955-5/1995 | Laser altimetry/maps |
| Arendt et al. 2002 | -4.2 $km^3 yr^{-1}$ w.e. | -4.2 | | Tidewater glaciers ** | 1955-5/1995 | Laser altimetry/maps |
| Arendt et al. 2006 | -7.4 ± 1.1 $km^3 yr^{-1}$ weq | -7.4 ± 1.1 | -0.80 | Western Chugach Mts (9,300) | 1955-5/1995 | Laser altimetry/maps |
| Larsen et al. 2007 | -16.7 ± 4.4 $km^3$ ice $yr^{-1}$ | -15.0±4.0 | -1.03 | Southeast Alaska (14,580) | 8/1948-2/2000 | geodetic |
| Arendt et al. 2008 | -0.43±0.12 m w.e. $yr^{-1}$ | -21.2±3.8 | -0.64 | St Elias Mtns (32,900) | 9/2003-8/2007 | Laser altimetry |
| Arendt et al. 2008 | -0.63±0.09 m w.e. $yr^{-1}$ | -20.6±3.0 | -0.63 | St Elias Mtns (32,900) | 9/2003-8/2007 | GRACE |
| Johnson et al. 2013 | 3.93±0.89 Gt $yr^{-1}$ | 3.93±0.89 | -0.61 | Glacier Bay (6,428) | 1995-2011 | Laser altimetry |
| Das et al. in press | -0.07±0.19 m w.e. $yr^{-1}$ | -0.34±0.93 | -0.07 | Wrangell Mountains (4,900) | 1957-2000 | Laser altimetry/DEM |
| Das et al. in press | -0.24±0.16 m w.e. $yr^{-1}$ | -1.18±0.78 | -0.24 | Wrangell Mountains (4,900) | 2000-2007 | Laser altimetry/DEM |

* "32,900$km^2$, about 40% of the area" yields 82,250. So here we assume the area is equal to Arendt *et al.* 2013.

** Area not defined in the reference.

**Table 3.1.2.4.2-1. Summary of winter, summer, and annual mass balances of four main glaciers in the upper Susitna basin during the period 1981-1983.**

| | Mass Balance Measurements for Susitna River Basin Glaciers (m w.e.) | | | | | | | | |
|---|---|---|---|---|---|---|---|---|---|
| | Winter Balance $b_w$ October 1 to May 14 | | | Summer Balance $b_s$ May 15 to September 30 | | | Annual Balance $b_a$ October 1 to September 30 | | |
| Glacier Name | 1981 | 1982 | 1983 | 1981 | 1982 | 1983 | 1981 | 1982 | 1983 |
| West Fork | 0.86 | 0.78 | 0.93 | -0.87 | -1.02 | -0.81 | -0.01 | -0.24 | 0.12 |
| Susitna | 0.76 | 0.65 | 0.78 | -1.03 | -0.87 | -0.38 | -0.3 | -0.22 | 0.4 |
| East Fork | -- | 0.77 | 0.78 | -- | -0.97 | -0.69 | --* | -0.2 | 0.09 |
| Maclaren | 0.83 | 1.44 | 1.07 | -0.52 | -1 | -0.7 | 0.3 | 0.14 | 0.37 |
| *Average* | *0.8* | *0.81* | *0.89* | *-0.85* | *-0.96* | *-0.63* | *0.05* | *-0.15* | *0.26* |

* Assumed annual balance at East Fork Glacier was -0.3 m in 1981. Data provided from Clarke *et al.* (1985).

**Table 3.1.2.4.2-2. Total specific runoff measured at several stream gauges and the estimated runoff contributions from the glacierized area in the Susitna River Basin.**

All data and averages are for the period 1981 to 1983 and are taken from Clarke *et al.* (1985a): (a) the total flow above the Denali Highway is compiled from the Maclaren River near Paxson and Susitna River near Denali Highway stream gauges; (b) the total glacier runoff contribution does not include runoff from glaciers in the Talkeetna Mountains at the Susitna River at Gold Creek stream gauge; (c) the glacierized area is not known accurately because the meltwater contribution from Eureka Glacier changes from the Delta River to the Susitna River at unknown intervals (R&M Consultants, Inc. 1981).

| | Runoff in Susitna River Basin | | | | | |
|---|---|---|---|---|---|---|
| Stream Gauge Name | Average Total Specific Runoff at Stream Gauge (m/yr) | Total Specific Glacier Runoff (m/yr) (snow, firn, ice, rain) | | | Glacier Runoff Component % of Total Runoff[c] | Glacierized Area ($km^2$)[c] |
| | 1981 - 1983 | 1981 | 1982 | 1983 | 1981 – 1983 | 1981 - 1983 |
| Paxson | 1.22 | 1.3 | 1.4 | 1.2 | 24% | 160[c] |
| Denali | 1.07 | 1.7 | 1.7 | 1.4 | 38% | 628 |
| Total flow above Denali Hwy[a] | 1.1 | -- | -- | -- | 34% | 790[c] |
| Gold Creek[b] | 0.59 | 1.6 | 1.6 | 1.4 | 13% | 790[c] |

**Table 4.1-1. Fraction of area covered by glaciers for each sub-basin (Dam site and Cantwell sub-basins include the Denali and Paxson sub-basins).**

| | Glacier Area of Sub-basins | | |
|---|---|---|---|
| Sub-basin | Area ($km^2$) | Glacier Area ($km^2$) | Fraction (%) |
| Dam site | 13296 | 638 | 4.8 |
| Cantwell | 10673 | 638 | 6.0 |

| | | | |
|---|---|---|---|
| Denali | 2215 | 522 | 23.6 |
| Paxson | 778 | 116 | 15.0 |

**Table 5.1.2-1. Land use classes before and after resampling.**

| Original Classification | | Classification after Resampling | |
|---|---|---|---|
| 1 | Open Water | 1 | Water |
| 2 | Perennial Ice/snow | 2 | Ice/snow |
| 3 | Developed, Open Space | 3 | Barren Land |
| 4 | Developed, Low Intensity | | |
| 5 | Developed, Medium Intensity | | |
| 6 | Developed, High Intensity | | |
| 7 | Barren Land | | |
| 8 | Deciduous Forest | 4 | Deciduous Forest |
| 9 | Evergreen Forest | 5 | Evergreen/Coniferous Forest |
| 10 | Mixed Forest | 6 | Mixed Forest |
| 11 | Dwarf Scrub | 7 | Shrub |
| 12 | Shrub/Scrub | | |
| 13 | Grassland/Herbaceous | 8 | Grassland/Tundra |
| 14 | Sedge/Herbaceous | | |
| 15 | Moss | | |
| 16 | Hay/Pasture | | |
| 17 | Cultivated Crops | | |
| 18 | Woody Wetlands | 9 | Wetland |
| 19 | Emergent Herbaceous Wetland | | |

**Table 5.2.1.1-1. List of mass balances stakes and their locations on glaciers in the upper Susitna basin during the 2012-2014 study period.**

| Station<br>West Fork Glacier | Northing (m) | Easting (m) | Latitude | Longitude | Elev (m) |
|---|---|---|---|---|---|
| WF1 | 7.05303e+06 | 496062 | 63.6052 | -147.079 | 1971 |
| WF2 | 7.04618e+06 | 491531 | 63.5437 | -147.17 | 1505 |
| WFTranA | 7.04542e+06 | 488026 | 63.5368 | -147.241 | 1409 |
| WFTranB | 7.04452e+06 | 488236 | 63.5287 | -147.237 | 1413 |
| WFTranC | 7.04381e+06 | 488777 | 63.5223 | -147.226 | 1402 |
| On-ice | 7.04491e+06 | 487788 | 63.5322 | -147.246 | 1398 |
| WF4 | 7.04237e+06 | 481372 | 63.5091 | -147.374 | 1221 |
| WF5 | 7.03988e+06 | 477642 | 63.4865 | -147.449 | 1123 |

| | | | | | |
|---|---|---|---|---|---|
| WF6 | 7.03706e+06 | 475379 | 63.4611 | -147.494 | 1025 |
| WF7 | 7.0312e+06 | 473647 | 63.4084 | -147.528 | 874 |
| WFNorth | 7.05089e+06 | 486187 | 63.5858 | -147.278 | 1638 |
| WFSouth | 7.04144e+06 | 488081 | 63.5011 | -147.239 | 1727 |
| WTrib1 | 7.05087e+06 | 505929 | 63.5859 | -146.881 | 2289 |
| WTrib2 | 7.04641e+06 | 505443 | 63.5458 | -146.89 | 1417 |
| Susitna Glacier | | | | | |
| SU1South | 7.03847e+06 | 514710 | 63.4743 | -146.705 | 1958 |
| SU1 | 7.04056e+06 | 519096 | 63.4929 | -146.617 | 1858 |
| SU2 | 7.04251e+06 | 512733 | 63.5107 | -146.744 | 1513 |
| SU3 | 7.0426e+06 | 505625 | 63.5116 | -146.887 | 1245 |
| SU4 | 7.04149e+06 | 498941 | 63.5017 | -147.021 | 1041 |
| SU5 | 7.03682e+06 | 493946 | 63.4597 | -147.121 | 908 |
| TURKEY1 | 7.04968e+06 | 514055 | 63.5749 | -146.717 | 2114 |
| TURKEY2 | 7.0457e+06 | 512825 | 63.5393 | -146.742 | 1700 |
| NWTrib1 | 7.05217e+06 | 500703 | 63.5976 | -146.986 | 2075 |
| East Fork Glacier | | | | | |
| EF1 | 7.03421e+06 | 520153 | 63.4358 | -146.596 | 2133 |
| EF2 | 7.03418e+06 | 510895 | 63.4359 | -146.782 | 1328 |
| EF3 | 7.03159e+06 | 509419 | 63.4127 | -146.811 | 1073 |
| MacLaren Glacier | | | | | |
| MAC1 | 7.03201e+06 | 520038 | 63.416 | -146.599 | 2104 |
| MAC2 | 7.02522e+06 | 522529 | 63.355 | -146.55 | 1396 |
| MAC3 | 7.0197e+06 | 523689 | 63.3054 | -146.527 | 1018 |
| Eureka Glacier | | | | | |
| EU1 | 7.02382e+06 | 531923 | 63.3417 | -146.362 | 1417 |
| Others | | | | | |
| Off-ice | 7.04473e+06 | 505561 | 63.5307 | -146.888 | 1516 |
| Repeater_1 | 7.04174e+06 | 490842 | 63.5038 | -147.184 | 2079 |
| Tundra Stations | | | | | |
| Valdez Cr (Round Mtn) | 7.00821e+06 | 491438 | 63.2029 | -147.17 | 1676 |
| Windy Cr Lower | 6.99889e+06 | 480303 | 63.1188 | -147.39 | 941 |
| Windy Cr Upper | 6.99998e+06 | 491975 | 63.129 | -147.159 | 1177 |
| MacLaren Lower | 7.00451e+06 | 514754 | 63.1695 | -146.707 | 1016 |
| MacLaren Upper | 7.00347e+06 | 513262 | 63.1602 | -146.737 | 1315 |
| Two Plate Creek | 7.01911e+06 | 518467 | 63.3004 | -146.632 | 1555 |
| Kosina Cr Lower | 6.94888e+06 | 450373 | 62.6671 | -147.969 | 919 |
| Kosina Cr Upper | 6.93702e+06 | 451553 | 62.5609 | -147.942 | 1274 |
| Oshetna Lower | 6.90172e+06 | 475705 | 62.2464 | -147.468 | 1263 |
| Oshetna Upper | 6.90072e+06 | 458336 | 62.2359 | -147.802 | 1583 |
| Tyone Creek | 6.90381e+06 | 498150 | 62.2659 | -147.036 | 954 |

**Table 5.2.1.1-2. Summary of winter, summer, and annual mass balances of the five main glaciers in the upper Susitna basin during the period 2012-2014.**

Site visits were conducted in the following date ranges: 2012/4/26-5/2, 2012/9/26-9/28, 2013/4/15-4/21, 2013/9/6-9/15, 2014/4/22-4/27, and 2014/9/7-9/9. Point mass balance measurements were linearly interpolated across elevations between measurements. Elevations beyond the above and below the measurement range were assigned the value of the nearest neighbor. The elevation profile of mass balance was distributed to the entire glacier area based on the glacier hypsometry.

| | Mass Balance Measurements for upper Susitna Basin Glaciers (m w.e.) | | | | | | | | |
|---|---|---|---|---|---|---|---|---|---|
| | Winter Balance $b_w$ October to May | | | Summer Balance $b_s$ May to September | | | Annual Balance $b_a$ October to September | | |
| Glacier Name | 2012 | 2013 | 2014 | 2012 | 2013 | 2014 | 2012 | 2013 | 2014 |
| West Fork | 0.86 | 0.85 | 0.97 | -2.96 | -3.35 | -2.28 | -2.10 | -2.50 | -1.31 |
| Susitna | 0.88 | 0.60 | 1.17 | -1.95 | -2.37 | -2.10 | -1.07 | -1.77 | -0.93 |
| East Fork | 0.74 | 1.04 | 1.30 | -4.17 | -2.55 | -2.04 | -3.43 | -1.51 | -0.74 |
| Maclaren | 0.94 | 1.17 | 1.09 | -3.86 | -2.88 | -1.81 | -2.92 | -1.70 | -0.71 |
| Eureka | -- | 0.74 | 0.89 | -- | -4.42 | -3.32 | -- | -3.67 | -2.43 |
| *Average* | *0.86* | *0.88* | *1.09* | *-3.24* | *-3.11* | *-2.31* | *-2.38* | *-2.23* | *-1.22* |

**Table 5.2.1.2-1. Ablation stake IDs and locations for the periods 1981-1983 and 2012-2014.**

| ID's in 1981-1983 | Corres-ponding ID's in 2012 | Elevation [m] measured 1980s | Elevation [m] measured 2012 | Latitude | Longitude | Northing * | Easting * |
|---|---|---|---|---|---|---|---|
| East Fork Glacier, 2050 m | EF1 | 2050 | 2133.089 | 63.44° N | -146.60° E | 7034211.15 | 520151.60 |
| East Fork Glacier, 1460 m | EF2 | 1460 | 1328.113 | 63.44° N | -146.78° E | 7034175.32 | 510893.69 |
| East Fork Glacier, 1080 m | EF3 | 1080 | 1073.249 | 63.41° N | -146.81° E | 7031586.17 | 509417.42 |
| Maclaren Glacier, 2030 m | MAC1 | 2030 | 2103.941 | 63.42° N | -146.60° E | 7032005.36 | 520036.31 |
| Maclaren Glacier, 1430 m | MAC2 | 1430 | 1396.162 | 63.35° N | -146.55° E | 7025220.60 | 522527.48 |
| Maclaren Glacier, 1100 m | MAC3 | 1100 | 1018.191 | 63.31° N | -146.53° E | 7019700.07 | 523687.57 |
| Main branch of Susitna Glacier, 2010 m | SU1south | 2010 | 1958.253 | 63.47° N | -146.70° E | 7038466.25 | 514709.07 |
| Main branch of Susitna Glacier, 1530 m | SU2 | 1530 | 1512.611 | 63.51° N | -146.74° E | 7042513.95 | 512731.46 |
| Main branch of Susitna Glacier, 1110 m | SU4 | 1110 | 1040.803 | 63.50° N | -147.02° E | 7041489.03 | 498939.61 |
| Turkey tributary of Susitna Glacier, 2200 m | TURKEY1 | 2200 | 2114.057 | 63.57° N | -146.72° E | 7049676.96 | 514053.88 |

| | | | | | | | |
|---|---|---|---|---|---|---|---|
| Turkey tributary of Susitna Glacier, 1670 m | TURKEY2 | 1670 | 1700.109 | 63.54° N | -146.74° E | 7045699.73 | 512824.22 |
| West Fork Glacier, 1950 m | WF1 | 1950 | 1971.166 | 63.61° N | -147.08° E | 7053029.06 | 496060.76 |
| West Fork Glacier, 1120 m | WF6 | 1120 | 1024.58 | 63.46° N | -147.49° E | 7037064.38 | 475377.28 |
| West Fork Glacier, 1460 m | WFTransB | 1460 | 1413.139 | 63.53° N | -147.24° E | 7044519.06 | 488234.31 |
| Northwest tributary of Susitna Glacier, 2350 m | WTrib1 | 2350 | 2289.413 | 63.59° N | -146.88° E | 7050872.60 | 505927.41 |
| Northwest tributary of Susitna Glacier, 1400 m | WTrib2 | 1400 | 1416.734 | 63.55° N | -146.89° E | 7046405.40 | 505441.60 |

* Projection: WGS 1984 UTM Zone 6N

**Table 5.2.2.2-1. Snow depths and density measurements in non-glacierized terrain (April 2012).**
Snow depths are averages of 50 measurements in the vicinity of the site. Snow density is sampled with an Adirondack tube that captures the full snow depth. Numbers presented here are the average of three or four samples at each site.

| Date | E | N | Elevation (m) | Site | Veg. Class | Depth (cm) | Density ($g/cm^3$) | Depth (mm w.e.) |
|---|---|---|---|---|---|---|---|---|
| 4/4/2012 | 516825 | 7003216 | 941 | MacLaren R | Shrub | 130 | 0.29 | 371 |
| 4/4/2012 | 492008 | 6999971 | 1185 | Windy Cr. Upper | Shrub | 88 | 0.28 | 248 |
| 4/4/2012 | 480035 | 6998884 | 939 | Windy Cr. Lower | Shrub | 76 | 0.27 | 202 |
| 4/4/2012 | 478016 | 6992239 | 817 | Spruce forest | Spruce | 105 | 0.13 | 141 |
| | | | | | Average | 100 | 0.24 | 240 |

**Table 5.2.2.2-2. Snow depth and density measurements in non-glacierized terrain (April 2014).**

Estimated average snow pack density represent the average measured snow density for all sites. The snow surveys were performed during two separate periods (early and late April). Late April estimated snow water equivalent (SWE) was adjusted for melt that may have occurred by applying the percentage of change that was observed at the Lower Windy Cr site.

| Date | E | N | Elevation (m) | Site | Veg. Class | Depth (cm) | Density (kg/m$^3$) | SWE (mm) | *Depth, Adjust.* | *SWE, Adjust.* | SWE shrub (mm) | SWE spruce (mm) | Depth shrub (cm) | Depth spruce (cm) |
|---|---|---|---|---|---|---|---|---|---|---|---|---|---|---|
| 4/8/2014 | 466122 | 7009898 | 911 | Shrub/Tundra | Shrub | 51 | 0.28 | 141 | - | - | 141 | | 51 | |
| 4/8/2014 | 478023 | 6992232 | 809 | Open spruce forest | Spruce | 72 | 0.24 | 173 | - | - | | 173 | | 72 |
| 4/9/2014 | 491995 | 6999971 | 1198 | Upper Windy Cr. | Shrub | 100 | 0.33 | 328 | - | - | 328 | | 100 | |
| 4/9/2014 | 480306 | 6998893 | 946 | Lower Windy Cr. | Shrub | 69 | 0.22 | 153 | - | - | 153 | | 69 | |
| 4/9/2014 | 468969 | 6986486 | 931 | Low sparse shrubs | Shrub | 109 | 0.28 | 306 | - | - | 306 | | 109 | |
| 4/9/2014 | 470690 | 6992367 | 781 | Spruce Forest | Spruce | 68 | 0.22 | 150 | - | - | | 150 | | 68 |
| 4/10/2014 | 493626 | 6974167 | 711 | Clearwater Cr. | Spruce | 63 | 0.21 | 134 | - | - | | 134 | | 63 |
| 4/11/2014 | 523593 | 7014353 | 943 | Lower Maclaren Glacier | Shrub | 143 | 0.31 | 440 | - | - | 440 | | 143 | |
| 4/11/2014 | 520732 | 7001006 | 996 | Maclaren Glacier Trail | Shrub | 132 | 0.33 | 435 | - | - | 435 | | 132 | |
| 4/11/2014 | 507510 | 6990546 | 942 | Clearwater/Denali Hwy | Shrub | 86 | 0.24 | 202 | - | - | 202 | | 86 | |
| 4/11/2014 | 526340 | 7003041 | 1023 | Upper 7mile Lake Trail | Shrub | 94 | 0.25 | 234 | - | - | 234 | | 94 | |
| 4/11/2014 | 526655 | 7000569 | 965 | Lower 7mile Lake Trail | Shrub | 79 | 0.25 | 197 | - | - | 197 | | 79 | |
| 4/12/2014 | 528779 | 6995546 | 1207 | Top of Denali Hwy | Shrub | 95 | 0.30 | 287 | - | - | 287 | | 95 | |
| | | | | | *Average* | 89 | 0.27 | 245 | - | - | 272 | 152 | 96 | 67 |
| 4/22/2014 | 513239 | 7003457 | 1266 | Maclaren Upper | Shrub | 176 | 0.35 | 610 | 225 | 781 | 610 | | 176 | |
| 4/22/2014 | 514754 | 7004506 | 1016 | Maclaren Lower | Shrub | 131 | *0.27* | 348 | 168 | 445 | 348 | | 131 | |
| 4/22/2014 | 518464 | 7019108 | 1555 | Two Plate Cr. | Rock | 259 | *0.27* | 687 | 331 | 878 | - | - | - | - |
| 4/22/2014 | 480306 | 6998893 | 946 | Lower Windy Cr. | Shrub | 54 | 0.21 | 114 | 69 | 146 | 114 | | 54 | |
| 4/28/2014 | 498152 | 6903793 | 954 | Tyone Cr. | Spruce | 11 | *0.27* | 30 | 14 | 38 | | 30 | | 11 |
| 4/28/2014 | 475712 | 6901721 | 1263 | Lower Oshetna Cr. | Shrub | 57 | *0.27* | 152 | 73 | 195 | 152 | | 57 | |
| 4/28/2014 | 458329 | 6900723 | 1583 | Upper Oshetna Cr. | Shrub | 43 | *0.27* | 113 | 55 | 145 | 113 | | 43 | |
| 4/28/2014 | 451554 | 6937020 | 1274 | Upper Kosina Cr. | Shrub | 32 | 0.23 | 72 | 41 | 93 | 72 | | 32 | |
| 4/28/2014 | 450371 | 6948876 | 919 | Lower Kosina Cr. | Shrub | 23 | *0.27* | 60 | 29 | 77 | 60 | | 23 | |
| | | | | | *Average* | *87* | *0.26* | *243* | *112* | *311* | *210* | *30* | *74* | *11* |
| | | | | | *AVERAGE ALL* | *88* | *0.27* | *244* | *98* | *272* | *247* | *121* | *87* | *53* |

**Table 5.3-1. All meteorological station used in this study.**

| Station name | Station type | Latitude | Longitude | Northing | Easting | Elevation |
|---|---|---|---|---|---|---|
| WestForkOnIceESG1 | AWS | 63.5322 | -147.246 | 7.04491e+06 | 487787 | 1398 |
| SusitnaOffIceESG2 | AWS | 63.5307 | -146.888 | 7.04473e+06 | 505559 | 1516 |
| RepeaterESR9 | AWSlite | 63.5038 | -147.184 | 7.04174e+06 | 490839 | 2079 |
| EF1 | HOBOglacier | 63.4358 | -146.596 | 7.03421e+06 | 520153 | 2133.09 |
| EF2 | HOBOglacier | 63.4359 | -146.782 | 7.03417e+06 | 510895 | 1328.11 |
| EF3 | HOBOglacier | 63.4127 | -146.811 | 7.03159e+06 | 509419 | 1073.25 |
| KosinaCreekLower | HOBO | 62.6671 | -147.969 | 6.94887e+06 | 450373 | 918.824 |
| KosinaCreekUpper | HOBO | 62.5609 | -147.942 | 6.93702e+06 | 451553 | 1274.06 |
| Mac1 | HOBOglacier | 63.416 | -146.599 | 7.03201e+06 | 520038 | 2103.94 |
| Mac2 | HOBOglacier | 63.355 | -146.55 | 7.02522e+06 | 522529 | 1396.16 |
| Mac3 | HOBOglacier | 63.3054 | -146.527 | 7.0197e+06 | 523689 | 1018.19 |
| MacLarenLower | HOBO | 63.1695 | -146.707 | 7.00451e+06 | 514754 | 1016 |
| MacLarenUpper | HOBO | 63.1602 | -146.737 | 7.00347e+06 | 513262 | 1315 |
| NWTrib1 | HOBOglacier | 63.5976 | -146.986 | 7.05217e+06 | 500703 | 2075 |
| OffIce | HOBO | 63.5307 | -146.888 | 7.04473e+06 | 505561 | 1516 |
| OshetnaRiverLower | HOBO | 62.2464 | -147.468 | 6.90172e+06 | 475705 | 1262.6 |
| OshetnaRiverUpper | HOBO | 62.2359 | -147.802 | 6.90072e+06 | 458336 | 1582.91 |
| Repeater | HOBOglacier | 63.5038 | -147.184 | 7.04174e+06 | 490842 | 2079 |
| SU1 | HOBOglacier | 63.4929 | -146.617 | 7.04056e+06 | 519096 | 1857.64 |
| SU3 | HOBOglacier | 63.5116 | -146.887 | 7.0426e+06 | 505625 | 1245.24 |
| TwoPlateCreek | HOBO | 63.3004 | -146.632 | 7.01911e+06 | 518467 | 1554.74 |
| TyoneCreek | HOBO | 62.2659 | -147.036 | 6.90381e+06 | 498150 | 954 |
| ValdezCreek | HOBO | 63.2029 | -147.17 | 7.00821e+06 | 491438 | 1676.4 |
| WF1 | HOBOglacier | 63.6052 | -147.079 | 7.05303e+06 | 496062 | 1971.17 |
| WF5 | HOBOglacier | 63.4865 | -147.449 | 7.03988e+06 | 477642 | 1122.64 |
| WFTranB | HOBOglacier | 63.5287 | -147.237 | 7.04452e+06 | 488236 | 1413.14 |
| WindyCreekLower | HOBO | 63.1188 | -147.39 | 6.99889e+06 | 480303 | 940.61 |
| WindyCreekUpper | HOBO | 63.129 | -147.159 | 6.99998e+06 | 491975 | 1176.53 |
| ALPINE CREEK LODGE AK US | NCDC | 63.0429 | -147.248 | 6.99039e+06 | 487462 | 944.9 |
| BIG DELTA AIRPORT AK US | NCDC | 63.9944 | -145.721 | 7.09702e+06 | 562548 | 389.2 |
| CANTWELL 2 E AK US | NCDC | 63.3952 | -148.895 | 7.03102e+06 | 405324 | 649.8 |
| CANTWELL 4 E AK US | NCDC | 63.3724 | -148.844 | 7.02841e+06 | 407793 | 689.5 |
| GAKONA 1 N AK US | NCDC | 62.3 | -145.3 | 6.90876e+06 | 588157 | 445 |
| GLENNALLEN KCAM AK US | NCDC | 62.1086 | -145.533 | 6.88714e+06 | 576570 | 421.5 |
| GULKANA AIRPORT AK US | NCDC | 62.1591 | -145.459 | 6.89286e+06 | 580297 | 476.1 |
| GUNSIGHT AK US | NCDC | 61.9 | -147.3 | 6.86308e+06 | 484235 | 901.9 |
| HEALY AK US | NCDC | 63.8717 | -149.017 | 7.08428e+06 | 400909 | 448.1 |
| HIGH LAKE LODGE AK US | NCDC | 62.85 | -149.117 | 6.97065e+06 | 392250 | 732.1 |
| LAKE LOUISE AK US | NCDC | 62.3 | -146.583 | 6.90767e+06 | 521609 | 747.1 |
| LAKE SUSITNA AK US | NCDC | 62.4528 | -146.679 | 6.92466e+06 | 516569 | 723.9 |
| MACLAREN RIVER AK US | NCDC | 63.1167 | -146.533 | 6.99867e+06 | 523543 | 894 |
| MATANUSKA AGRICULTURAL EXPERIMENT STATION AK US | NCDC | 61.5663 | -149.254 | 6.82794e+06 | 380278 | 52.4 |

| | | | | | | |
|---|---|---|---|---|---|---|
| MCKINLEY PARK AK US | NCDC | 63.7175 | -148.969 | 7.06703e+06 | 402724 | 630.9 |
| MENTASTA LAKE 7 E BARTELL CREEK AK US | NCDC | 62.933 | -143.574 | 6.98275e+06 | 673867 | 720.5 |
| NELCHINA HIGHWAY CAM AK US | NCDC | 61.9833 | -146.867 | 6.87233e+06 | 506987 | 757.7 |
| PALMER JOB CORPS AK US | NCDC | 61.5888 | -149.099 | 6.83017e+06 | 388584 | 65.8 |
| PAXSON AK US | NCDC | 63.0322 | -145.498 | 6.99007e+06 | 575974 | 823 |
| PAXSON ALASKA AK US | NCDC | 62.9453 | -145.501 | 6.98038e+06 | 576045 | 813.8 |
| PAXSON RIVER AK US | NCDC | 62.95 | -145.5 | 6.98091e+06 | 576104 | 839.1 |
| RENEE ALASKA AK US | NCDC | 62.71 | -146.618 | 6.95334e+06 | 519536 | 792.5 |
| SHEEP MOUNTAIN LODGE AK US | NCDC | 61.8125 | -147.499 | 6.85339e+06 | 473693 | 847.3 |
| SNOWSHOE LAKE AK US | NCDC | 62.0302 | -146.693 | 6.87758e+06 | 516064 | 704.7 |
| SOURDOUGH 1 N AK US | NCDC | 62.5333 | -145.517 | 6.93447e+06 | 576326 | 597.4 |
| SUMMIT LAKE AK US | NCDC | 63.1483 | -145.541 | 7.00295e+06 | 573531 | 990.6 |
| SUSITNA MEADOWS AK US | NCDC | 62.75 | -149.7 | 6.96062e+06 | 362100 | 228.9 |
| SUTTON 1 W AK US | NCDC | 61.7138 | -148.909 | 6.84378e+06 | 399096 | 167.6 |
| TAHNETA PASS AK US | NCDC | 61.8167 | -147.55 | 6.85388e+06 | 471020 | 798.6 |
| TALKEETNA AIRPORT AK US | NCDC | 62.32 | -150.095 | 6.91367e+06 | 339639 | 106.7 |
| THE GRACIOUS HOUSE AK US | NCDC | 63.1333 | -147.533 | 7.00056e+06 | 473109 | 777.8 |
| TONSINA AK US | NCDC | 61.651 | -145.17 | 6.83666e+06 | 596925 | 481.3 |
| TRIMS CAMP AK US | NCDC | 63.4333 | -145.767 | 7.03446e+06 | 561541 | 734.9 |
| TYONE LAKE AK US | NCDC | 62.5167 | -146.7 | 6.93178e+06 | 515446 | 723 |
| Denali Station | SWHDN | 63.09 | -147.47 | 6.9957e+06 | 476267 | 822.96 |
| Devil Canyon Station | SWHDN | 62.814 | -149.314 | NaN | NaN | 457.2 |
| Kosina Creek Station | SWHDN | 62.69 | -147.97 | 6.95142e+06 | 450348 | 792.48 |
| Sherman Station | SWHDN | 62.703 | -149.831 | NaN | NaN | 182.88 |
| Susitna Glacier Station | SWHDN | 63.53 | -146.89 | 7.04465e+06 | 505471 | 1432.56 |
| Watana Station | SWHDN | 62.84 | -148.51 | 6.96866e+06 | 423102 | 701.04 |
| ESG2 | SWHDN | 63.5307 | -146.888 | 7.04473e+06 | 505560 | NaN |
| ESM1 | SWHDN | 62.8295 | -148.552 | 6.96754e+06 | 420944 | NaN |
| ESM2 | SWHDN | NaN | NaN | NaN | NaN | NaN |
| ESM3 | SWHDN | NaN | NaN | NaN | NaN | NaN |
| ESR1 | SWHDN | 61.4817 | -150.697 | 6.82203e+06 | 303147 | NaN |
| ESR2 | SWHDN | 62.8511 | -148.027 | 6.96941e+06 | 447710 | NaN |
| ESR3 | SWHDN | NaN | NaN | NaN | NaN | NaN |
| ESR4 | SWHDN | 62.5786 | -150.112 | 6.94249e+06 | 340126 | 609.6 |
| ESR5 | SWHDN | 62.809 | -149.789 | 6.96738e+06 | 357834 | NaN |
| ESR6 | SWHDN | 62.8 | -148.924 | 6.96477e+06 | 401891 | NaN |
| ESR7 | SWHDN | 62.8329 | -149.384 | 6.96922e+06 | 378581 | NaN |
| ESR8 | SWHDN | 62.6812 | -147.623 | 6.95023e+06 | 468121 | NaN |
| ESS10 | SWHDN | 61.4053 | -150.46 | 6.81284e+06 | 315303 | NaN |
| ESS15 | SWHDN | 61.4895 | -150.562 | 6.82249e+06 | 310392 | NaN |
| ESS20 | SWHDN | 61.5442 | -150.515 | 6.82844e+06 | 313228 | NaN |
| ESS30 | SWHDN | 62.2945 | -150.116 | 6.91088e+06 | 338418 | 106.07 |
| ESS35 | SWHDN | 62.3376 | -150.143 | 6.91575e+06 | 337252 | 100.58 |
| ESS40 | SWHDN | 62.3954 | -150.137 | 6.92216e+06 | 337882 | 109.73 |

| | | | | | | |
|---|---|---|---|---|---|---|
| ESS45 | SWHDN | 62.5264 | -150.116 | 6.93669e+06 | 339646 | 138.68 |
| ESS50 | SWHDN | 62.6172 | -150.015 | 6.94655e+06 | 345323 | 155.14 |
| ESS55 | SWHDN | 62.8305 | -149.384 | 6.96895e+06 | 378570 | 259.38 |
| ESS60 | SWHDN | 62.7918 | -148.994 | 6.96397e+06 | 398302 | 384.96 |
| ESS65 | SWHDN | 62.7649 | -148.777 | 6.96065e+06 | 409300 | 430.68 |
| ESS70 | SWHDN | 62.823 | -148.538 | 6.9668e+06 | 421613 | NaN |
| ESS10 | SWHDN | 61.4053 | -150.46 | 6.81284e+06 | 315303 | NaN |
| ESS15 | SWHDN | 61.4895 | -150.562 | 6.82249e+06 | 310392 | NaN |
| ESS20 | SWHDN | 61.5442 | -150.515 | 6.82844e+06 | 313228 | NaN |
| ESS30 | SWHDN | 62.2945 | -150.116 | 6.91088e+06 | 338418 | 106.07 |
| ESS35 | SWHDN | 62.3376 | -150.143 | 6.91575e+06 | 337252 | 100.58 |
| ESS40 | SWHDN | 62.3954 | -150.137 | 6.92216e+06 | 337882 | 109.73 |
| ESS45 | SWHDN | 62.5264 | -150.116 | 6.93669e+06 | 339646 | 138.68 |
| ESS50 | SWHDN | 62.6172 | -150.015 | 6.94655e+06 | 345323 | 155.14 |
| ESS55 | SWHDN | 62.8305 | -149.384 | 6.96895e+06 | 378570 | 259.38 |
| ESS60 | SWHDN | 62.7918 | -148.994 | 6.96397e+06 | 398302 | 384.96 |
| ESS65 | SWHDN | 62.7649 | -148.777 | 6.96065e+06 | 409300 | 430.68 |
| ESS70 | SWHDN | 62.823 | -148.538 | 6.9668e+06 | 421613 | NaN |
| ESS80 | SWHDN | 62.6978 | -147.547 | 6.95204e+06 | 471992 | 579.12 |

**Table 5.3.1-1. Meteorological stations used to record climatic data from 1980 to 1984 in the Susitna River Basin by R&M Consultants, Inc.**

| Climate Station Name | General Region | Land Cover Classification | Elevation (m) | Coordinates | Period of Record |
|---|---|---|---|---|---|
| Denali | Upper Susitna Basin | Shrubland | 828 | 63° 05' 24" N 147° 28' 12" W | July 1980 - Dec 1984 |
| Kosina Creek | Upper Susitna Basin | Shrubland | 792 | 62° 41' 24" N 147° 58' 12" W | Aug 1980 - Dec 1984 |
| Susitna Glacier | Alaska Range Mountains | Barren Land | 1433 | 63° 31' 48" N 146° 53' 24" W | July 1980 - Dec 1984 |
| Watana | Proposed Dam Site | Shrubland | 701 | 62° 50' 24" N 148° 30' 36" W | Apr 1980 - Dec 1984 |
| Devil Canyon | Downstream of Dam Site | Coniferous Forest | 457 | 62° 48' 50" N 149° 18' 50" W | Apr 1980 - Dec 1984 |
| Sherman | Downstream of Dam Site | Mixed Forest | 183 | 62° 42' 10" N 149° 49' 52" W | Oct 1981 - Dec 1984 |

**Table 5.3.1-2. Individual sources for recovered climate data from the Susitna basin during the period 1980-1984.**

| Denali Station | Source |
|---|---|

| | |
|---|---|
| Year 1980 – 1981 | R&M Consultants, Inc. (1982), Susitna Hydroelectric Project, Processed Climatic Data, Volume 2, Denali Station. Prepared for Acres American Inc. Susitna Hydroelectric Project, Federal Energy Regulatory Commission, Project No. 7114.<br>Available at: http://www.arlis.org/docs/vol2/hydropower/APA_DOC_no._200.pdf. |
| Year 1981 – 1982 | R&M Consultants, Inc. (1982), Susitna Hydroelectric Project 1982 Field Data, Collection and Processing, Supplement 1. Prepared for Acres American Inc. Susitna Hydroelectric Project, Federal Energy Regulatory Commission, Project No. 7114.<br>Available at: http://www.arlis.org/docs/vol1/Susitna/2/APA211.pdf. |
| Year 1982 – 1983 | R&M Consultants, Inc. (1984), Processed Climatic Data October 1982 - September 1983, Vol. 2, Denali Station. Final Report, Document No. 1089. Under Contract to Hazra-Ebasco Susitna Joint Venture. Prepared for Alaska Power Authority. Susitna Hydroelectric Project, Federal Energy Regulatory Commission, Project No. 7114.<br>Available at: http://www.arlis.org/docs/vol1/Susitna/10/APA1089.pdf. |
| Year 1983 – 1984 | R&M Consultants, Inc. (1985), Processed Climatic Data October 1983 - December 1984, Vol. 2, Denali Station. Final Report, Document No. 2768. Under Contracted to Hazra-Ebasco Susitna Joint Venture. Prepared for Alaska Power Authority. Susitna Hydroelectric Project, Federal Energy Regulatory Commission, Project No. 7114.<br>Available at: http://www.arlis.org/docs/vol1/Susitna/27/APA2768.pdf. |

| Devil Canyon Station | Source |
|---|---|
| Year 1980 – 1981 | R&M Consultants, Inc. (1982), Susitna Hydroelectric Project, Processed Climatic Data, Volume 6, Devil Canyon Station. Prepared for Acres American Inc. Susitna Hydroelectric Project, Federal Energy Regulatory Commission, Project No. 7114.<br>Available at: http://www.arlis.org/docs/vol2/hydropower/APA_DOC_no._208.pdf |
| Year 1981 – 1982 | R&M Consultants, Inc. (1982), Susitna Hydroelectric Project 1982 Field Data, Collection and Processing, Supplement 1. Prepared for Acres American Inc. Susitna Hydroelectric Project, Federal Energy Regulatory Commission, Project No. 7114.<br>Available at: http://www.arlis.org/docs/vol1/Susitna/2/APA211.pdf. |
| Year 1982 – 1983 | R&M Consultants, Inc. (1984), Processed Climatic Data October 1982 - September 1983, Vol. V, Devil Canyon Station. Final Report, Document No. 1092. Under Contract to Hazra-Ebasco Susitna Joint Venture. Prepared for Alaska Power Authority. Susitna Hydroelectric Project, Federal Energy Regulatory Commission, Project No. 7114.<br>Available at: http://www.arlis.org/docs/vol1/Susitna/10/APA1092.pdf. |
| Year 1983 – 1984 | R&M Consultants, Inc. (1985), Processed Climatic Data October 1983 - December 1984, Vol. 5, Devil Canyon Station. Final Report, Document No. 2771. Under Contracted to Hazra-Ebasco Susitna Joint Venture. Prepared for Alaska Power Authority. Susitna Hydroelectric Project, Federal Energy Regulatory Commission, Project No. 7114.<br>Available at: http://www.arlis.org/docs/vol1/Susitna/27/APA2771.pdf. |

| Kosina Creek Station | Source |
|---|---|
| Year 1980 – 1981 | R&M Consultants, Inc. (1982), Susitna Hydroelectric Project 1982 Field Data, Collection and Processing, Supplement 1. Prepared for Acres American Inc. Susitna Hydroelectric Project, Federal Energy Regulatory Commission, Project No. 7114.<br>Available at: http://www.arlis.org/docs/vol2/hydropower/APA_DOC_no._204.pdf. |
| Year 1981 – 1982 | R&M Consultants, Inc. (1982), Susitna Hydroelectric Project 1982 Field Data, Collection and Processing, Supplement 1. Prepared for Acres American Inc. Susitna Hydroelectric Project, Federal Energy Regulatory Commission, Project No. 7114.<br>Available at: http://www.arlis.org/docs/vol1/Susitna/2/APA211.pdf. |
| Year 1982 – 1983 | R&M Consultants, Inc. (1984), Processed Climatic Data October 1982 - September 1983, Vol. 3, Kosina Creek Station. Final Report, Document No. 1090. Under Contract to Hazra-Ebasco Susitna Joint Venture. Prepared for Alaska Power Authority. Susitna Hydroelectric Project, Federal Energy Regulatory Commission, Project No. 7114.<br>Available at: http://www.arlis.org/docs/vol1/Susitna/10/APA1090.pdf. |

| | |
|---|---|
| Year 1983 – 1984 | R&M Consultants, Inc. (1985), Processed Climatic Data October 1983 - December 1984, Vol. 3, Kosina Creek Station. Final Report, Document No. 2769. Under Contract to Hazra-Ebasco Susitna Joint Venture. Prepared for Alaska Power Authority. Susitna Hydroelectric Project, Federal Energy Regulatory Commission, Project No. 7114.<br>Available at: http://www.arlis.org/docs/vol1/Susitna/27/APA2769.pdf. |

| Sherman Station | Source |
|---|---|
| Year 1981 – 1982 | R&M Consultants, Inc. (1982), Susitna Hydroelectric Project 1982 Field Data, Collection and Processing, Supplement 1. Prepared for Acres American Inc. Susitna Hydroelectric Project, Federal Energy Regulatory Commission, Project No. 7114.<br>Available at: http://www.arlis.org/docs/vol1/Susitna/2/APA211.pdf. |
| Year 1982 – 1983 | R&M Consultants, Inc. (1984), Processed Climatic Data October 1982 - September 1983, Vol. 6, Sherman Station. Final Report, Document No. 1093. Under Contract to Hazra-Ebasco Susitna Joint Venture. Prepared for Alaska Power Authority. Susitna Hydroelectric Project, Federal Energy Regulatory Commission, Project No. 7114.<br>Available at: http://www.arlis.org/docs/vol1/Susitna/10/APA1093.pdf. |
| Year 1983 – 1984 | R&M Consultants, Inc. (1985), Processed Climatic Data October 1983 - December 1984, Vol. 6, Sherman Station. Final Report, Document No. 2772. Under Contract to Hazra-Ebasco Susitna Joint Venture. Prepared for Alaska Power Authority. Susitna Hydroelectric Project, Federal Energy Regulatory Commission, Project No. 7114.<br>Available at: http://www.arlis.org/docs/vol1/Susitna/27/APA2772.pdf. |

| Susitna Glacier Station | Source |
|---|---|
| Year 1980 – 1981 | R&M Consultants, Inc. (1982), Susitna Hydroelectric Project, Processed Climatic Data Volume 5 Susitna Glacier Station. Prepared for Acres American Inc. Susitna Hydroelectric Project, Federal Energy Regulatory Commission, Project No. 7114.<br>Available at: http://www.arlis.org/docs/vol2/hydropower/APA_DOC_no._198.pdf. |
| Year 1981 – 1982 | R&M Consultants, Inc. (1982), Susitna Hydroelectric Project 1982 Field Data, Collection and Processing, Supplement 1. Prepared for Acres American Inc. Susitna Hydroelectric Project, Federal Energy Regulatory Commission, Project No. 7114.<br>Available at: http://www.arlis.org/docs/vol1/Susitna/2/APA211.pdf. |
| Year 1982 – 1983 | R&M Consultants, Inc. (1984), Processed Climatic Data October 1982 - September 1983, Vol. 1, Susitna Glacier Station. Final Report, Document No. 1088. Under Contract to Hazra-Ebasco Susitna Joint Venture. Prepared for Alaska Power Authority. Susitna Hydroelectric Project, Federal Energy Regulatory Commission, Project No. 7114.<br>Available at: http://www.arlis.org/docs/vol1/Susitna/10/APA1088.pdf. |
| Year 1983 – 1984 | R&M Consultants, Inc. (1985), Processed Climatic Data October 1983 - December 1984, Vol. 1, Susitna Glacier Station. Final Report, Document No. 2767. Under Contract to Hazra-Ebasco Susitna Joint Venture. Prepared for Alaska Power Authority. Susitna Hydroelectric Project, Federal Energy Regulatory Commission, Project No. 7114.<br>Available at: http://www.arlis.org/docs/vol1/Susitna/27/APA2767.pdf. |

| Watana Station | Source |
|---|---|
| Year 1980 – 1981 | R&M Consultants, Inc. (1982), Susitna Hydroelectric Project, Processed Climatic Data, Volume 5, Watana Station. Prepared for Acres American Inc. Susitna Hydroelectric Project, Federal Energy Regulatory Commission, Project No. 7114.<br>Available at: http://www.arlis.org/docs/vol2/hydropower/APA_DOC_no._206.pdf. |
| Year 1981 – 1982 | R&M Consultants, Inc. (1982), Susitna Hydroelectric Project 1982 Field Data, Collection and Processing, Supplement 1. Prepared for Acres American Inc. Susitna Hydroelectric Project, Federal Energy Regulatory Commission, Project No. 7114. |

| | |
|---|---|
| | Available at: http://www.arlis.org/docs/vol1/Susitna/2/APA211.pdf. |
| Year 1982 – 1983 | R&M Consultants, Inc. (1984), Processed Climatic Data October 1982 - September 1983, Vol. 4, Watana Station. Final Report, Document No. 1091. Under Contract to Hazra-Ebasco Susitna Joint Venture. Prepared for Alaska Power Authority. Susitna Hydroelectric Project, Federal Energy Regulatory Commission, Project No. 7114.<br>Available at: http://www.arlis.org/docs/vol1/Susitna/10/APA1091.pdf. |
| Year 1983 – 1984 | R&M Consultants, Inc. (1985), Processed Climatic Data October 1983 - December 1984, Vol. 4, Watana Station. Final Report, Document No. 2770. Under Contract to Hazra-Ebasco Susitna Joint Venture. Prepared for Alaska Power Authority. Susitna Hydroelectric Project, Federal Energy Regulatory Commission, Project No. 7114.<br>Available at: http://www.arlis.org/docs/vol1/Susitna/27/APA2770.pdf. |

**Table 5.3.3-1. Overview of gridded climate products available for Alaska.**

| Gridded Products | Spatial Resolution | Temporal Resolution / Period covered |
|---|---|---|
| OSU's David Hill's Monthly Temperature and Precipitation grids for Alaska, British Columbia, and Yukon | 2 km | Monthly /1961 - 2009 |
| University of British Columbia NARR downscaled Temperature, Precipitation, and Solar grids (SE AK and BC at present) | < 2 km | Daily |
| SNAP Temperature and Precipitation historical (CRU TS 3.1 1901-2009) | 771 m / 2 km | Monthly /1901 - 2009 |
| OSU's PRISM (1971-2000) | 800 m / 4 km | Monthly /1971 - 2000 |
| NCEP Climate Forecast System Reanalysis (CFSR) (1979-2010) | 38 km – 2.5 deg | Hourly,6-hourly,monthly 1979 - 2010 |
| ECMEF ERA 40 Temperature and Precipitation (1958-2002) | 0.5 deg | 1958 - 2002 |
| ECMEF ERA Interim | 0.5 deg | 1979 – Present |
| NCEP and NCAR | 2.5 deg | 1948 – Present |
| NARR | 32 km | 1979 – Present |

**Table 5.3.5-1. Sensors list for On-Ice (ESG-1: 2013-2014) and Off-Ice (ESG-2; 2012-2014) weather stations.**

| Variable | Sensor | Unit | Accuracy |
|---|---|---|---|
| Temperature | Rotronic HygroClip2 Temperature/RH Probe* | C | |
| Relative humidity | Rotronic HygroClip2 Temperature/RH Probe* | % | |

| | | | |
|---|---|---|---|
| Barometric pressure | Vaisala PTB110 Barometer | mbar | 1 mb |
| Incoming longwave radiation | Hukseflux 4-Component Net Radiation | W/m^2 | |
| Outgoing longwave radiation | Hukseflux 4-Component Net Radiation | W/m^2 | |
| Incoming shortwave radiation | Hukseflux 4-Component Net Radiation | W/m^2 | |
| Outgoing shortwave radiation | Hukseflux 4-Component Net Radiation | W/m^2 | |
| Rainfall | Texas Electronics Rain Gage** | mm | 1% |
| Tilt of the radiation sensors | Turck Inclinometer B2N45H-Q20L60-2LU3-H1151 | degrees | 0.5 degrees |
| Wind direction | RM Young Wind Monitor, Alpine version | degrees | 5 degrees |
| Wind speed | RM Young Wind Monitor, Alpine version | m/s | 0.3 m/s or 1% |
| Distance to ice surface (ablation) | SR50A | M | 1 cm or 0.4% |
| Snow temperature | Thermistor 3K Ohm from Digikey | °C | 0.1 °C |
| Ice temperature | Thermistor 3K Ohm from Digikey | °C | 0.1 °C |
| Datalogger | Campbell Scientific CR1000 | - | - |

* shielded with a RM Young 10-plate Gill shield.
** shielded with a Novalynx Alter-type Rain Gage Wind Screen at the Off Ice station. Unshielded at the On Ice station.

**Table 5.3.7-1. Sensors list for glacier and tundra weather stations.**

| Variable | Sensor | Unit | Accuracy |
|---|---|---|---|
| Temperature | HOBO Pro v2 U23-001 * | °C | 0.21 °C |
| Relative humidity | HOBO Pro v2 U23-001 * | % | 3.5% |
| Rainfall | HOBO RG3-M ** | Mm | 1% |
| Soil temperature | HOBO Pro v2 U23-003 2x External Temp. | °C | 0.21 °C |

* shielded with a HOBO M-RSA Gill-type shield
** shielded with a Novalynx Alter-type Rain Gage Wind Screen

**Table 5.3.7.2-1. On-ice (glacier) and off-ice (tundra) lapse rates (°C/km) for the summer months of 2013 and 2014.**
Lapse rates were calculated by linear regression between monthly average data at all available HOBO stations and station elevations from Table 5.3-1.

| Sensor Group | Year | June | July | August | September |
|---|---|---|---|---|---|
| Tundra | 2013 | -- | 5.8 | 5.2 | 6.2 |
| Glacier | 2013 | -- | 2.7 | 3.7 | -- |
| Tundra | 2014 | 7.5 | 6.5 | 6 | 5.1 |
| Glacier | 2014 | 5 | 3.5 | 4 | -- |

**Table 6.1.4-1. Projected changes in annual runoff at the gauging station Susitna river near Denali Highway (ΔQ), cumulative mass balance, glacierized area in the catchment (ΔArea), temperature (ΔTemp), and precipitation change (ΔPrec) over the period 2003-2100 for three emission scenarios (A1B, A2, and B1).**

| Scenario | ΔQ (%) | Mass balance (m w.e.) | ΔArea (%) | ΔTemp (°C) | ΔPrec (%) |
|---|---|---|---|---|---|
| A1B | 39 | -100 | -11 | 4.4 | 34 |
| A2 | 38 | -128 | -14 | 4.9 | 33 |
| B1 | 22 | -92 | -10 | 3.0 | 23 |

**Table 7.1.2.1-1. Monthly correction factors ($f_i$) for potential ETR (based on values from northern Switzerland).**

| Month | Jan | Feb | Mar | Apr | May | Jun | Jul | Aug | Sep | Oct. | Nov | Dec |
|---|---|---|---|---|---|---|---|---|---|---|---|---|
| $f_i$ | 0.5 | 0.6 | 0.8 | 1.1 | 1.2 | 1.3 | 1.2 | 1.1 | 1.0 | 0.9 | 0.7 | 0.5 |

**Table 7.3.1-1. Overview of input data used to support model calibration and validation during historical time periods in the upper Susitna basin (see section 5).**

**River discharge**

U.S. Geological Survey (2012) and
NWS Flood Forecasting Center / Alaska River Forecast Center (*MacLaren River*, recent)

*Susitna River near Cantwell*
- 1961/05/01 – 1972/09/30
- 1980/05/29 – 1986/07/31

*Susitna River near Denali*
- 1957/05/30 – 1966/09/30
- 1968/07/01 – 1986/07/31
- 2012/05/28 – 2012/11/15

*Susitna River at Gold Creek*
- 1949/08/01 – 1996/09/30
- 2001/05/25 – 2012/11/21

*MacLaren River near Paxson*
- 1958/06/01 – 1986/07/31
- 2005/07/01 – 2009/06/19
- 2010/03/20 – 2012/11/21

**Snow depth measurements**

Recovered from Reports of 1980s, R&M Consultants, Inc. (1982)

- 1981 – 1982: Total of 165 snow depth measurements at 16 location (on and outside glacier)

**Glacier Mass Balance**

Clarke, T. (1986)

- 1981 – 1983: Total of 109 Mass Balance measurements on West Fork, East Fork, Susitna and MacLaren Glacier

**Soil Temperature**

Jafarov, E. E. et al (2012), Sergei Marchenko
Permafrost Laboratory UAF (2011)

- 1960, 1980: Modeled soil temperature profiles from Permafrost Lab (0 – 50 m)
- 2008 – 2011: Surface temperatures (0 – ca. 1 m) at 2 locations and borehole temperatures (depth ca. 1 – 30/40 m) at 3 locations. All measurements are outside but in proximity of the Upper Susitna Basin

**Table 7.3.2-1. Parameters and ranges used in the optimization of the hydrological model.**
Time step length was 1 day. Degree day factors (DDF) control the rate of ice, firn, and snow melt. Time constants ($t$) set the response of the linear reservoirs holding meltwater derived from ice, firn and snow. A threshold temperature ($T_{rain}$) controls whether precipitation falls as rain or snow. Another threshold temperature ($T_{melt}$) set the limit for calculating degree days.

| Parameter | Minimum | Maximum | Optimized |
|---|---|---|---|
| DDF ice | 5.5 mm w.e. day$^{-1}$ K$^{-1}$ | 10 mm w.e. day$^{-1}$ K$^{-1}$ | 6 mm w.e. day$^{-1}$ K$^{-1}$ |

| | | | |
|---|---|---|---|
| DDF firn | 3 mm w.e. day$^{-1}$ K$^{-1}$ | 7 mm w.e. day$^{-1}$ K$^{-1}$ | 3 mm w.e. day$^{-1}$ K$^{-1}$ |
| DDF snow | 1 mm w.e. day$^{-1}$ K$^{-1}$ | 4.5 mm w.e. day$^{-1}$ K$^{-1}$ | 2.5 mm w.e. day$^{-1}$ K$^{-1}$ |
| $t_{ice}$ | 0.125 time steps | 3 time steps | 0.125 time steps |
| $t_{firn}$ | 12.5 time steps | 300 time steps | 30 time steps |
| $t_{snow}$ | 1.25 time steps | 300 time steps | 1.25 time steps |
| $T_{rain}$ | -4.4 °C | 1.2 °C | 0.6 °C |
| $T_{melt}$ | -5 °C | 0 °C | 0 °C |

**Table 7.3.2.2-1 Annual specific discharge (mm) comparison of observations and model results for hydrologic years 1971 to 2014.**

The model results include all years; the measured data includes only those years with complete records. The model slightly underestimates the discharge at the dam site, but is within 5% at the Cantwell and Denali gauges.

| Station | Data | Model | Model to data ratio | Data to model ratio |
|---|---|---|---|---|
| DamSynthFromGoldByArea | 556 | 501 | 0.90 | 1.11 |
| Cantwell | 535 | 526 | 0.98 | 1.02 |
| Denali | 1136 | 1081 | 0.95 | 1.05 |
| Paxson | 1126 | 1023 | 0.91 | 1.10 |
| CantwellSynthFromGoldByArea | 551 | 526 | 0.96 | 1.05 |
| CantwellSynthFromGoldByRegr | 529 | 526 | 1.00 | 1.00 |

**Table 7.4.2-1 Modeled mean specific runoff (mm/day) for the Dam site, Cantwell, Denali, and Paxson for three 20-year intervals: 1976-1995, 2016-2035, and 2080-2099.**

The specific runoff is calculated based on the grid cells within the sub-basin, not including water that is routed into the basin from higher basins. For all basins but Paxson, runoff increases between the first and second interval and decreases from the second to the third. At the Paxson station, runoff increases between all intervals.

| Station | 1976-1995 | 2016-2035 | 2080-2099 |
|---|---|---|---|
| Dam site | 1.36 | 1.38 | 1.28 |
| Cantwell | 1.43 | 1.47 | 1.36 |
| Denali | 2.92 | 2.95 | 2.73 |
| Paxson | 2.78 | 2.80 | 2.81 |

**Table 7.4.2-2 Modeled mean runoff from glaciers, in specific units (mm/day) relative to the area of each sub-basin.**

The Dam and Cantwell sub-basins do not include glaciers in our model setup.

| Station | 1976-1995 | 2016-2035 | 2080-2099 |
|---|---|---|---|
| Dam site | 0 | 0 | 0 |
| Cantwell | 0 | 0 | 0 |
| Denali | 1.58 | 1.29 | 0.41 |
| Paxson | 0.85 | 0.55 | 0.089 |
| Whole basin | 0.31 | 0.25 | 0.074 |

**Table 7.4.2-3 Intervals of simulated runoff and the day of the year when runoff reaches its peak.**

Peak runoff occurs earlier with time over the 21st century.

| Source | Start date | End date | Dam site | Cantwell | Denali | Paxson |
|---|---|---|---|---|---|---|
| Data | 1949 | 2014 | 167 | 172 | 197 | 196 |
| Model | 1976 01 01 | 1995 12 31 | 155 | 156 | 201 | 159 |

| | | | | | | |
|---|---|---|---|---|---|---|
| Model | 2016 01 01 | 2035 12 31 | 165 | 166 | 171 | 164 |
| Model | 2080 01 01 | 2099 12 31 | 134 | 150 | 157 | 153 |

**Table 7.4.2.1-1 Simulated Mean Daily Peak Flows for Maclaren River near Paxson.**

| Analysis | Period of Record | Number of annual events | Number of low outliers | Number of high outliers | Weighted Skew | Station Skew |
|---|---|---|---|---|---|---|
| 1 | 1971-2000 | 30 | 0 | 0 | 0.010 | -0.118 |
| 2 | 2001-2030 | 30 | 0 | 0 | 0.073 | -0.037 |
| 3 | 2031-2060 | 30 | 0 | 0 | 0.644 | 0.656 |
| 4 | 2061-2080 | 20 | 0 | 0 | 0.648 | 0.667 |
| 5 | 2081-2100 | 20 | 0 | 0 | -0.022 | -0.225 |
| 6 | 1971-2100 | 130 | 0 | 1 | 0.537 | 0.532 |
| 7 | 1958-1985, USGS instantaneous peak flows | 28 | 0 | 0 | 0.548 | 0.533 |

**Table 7.4.2.1-2 Simulated Mean Daily Peak Flows for Susitna River near Denali.**

| Analysis | Period of Record | Number of annual events | Number of low outliers | Number of high outliers | Weighted Skew | Station Skew |
|---|---|---|---|---|---|---|
| 1 | 1971-2000 | 30 | 0 | 0 | -0.005 | -0.137 |
| 2 | 2001-2030 | 30 | 0 | 0 | 0.479 | 0.448 |
| 3 | 2031-2060 | 30 | 0 | 0 | -0.110 | -0.276 |
| 4 | 2061-2080 | 20 | 0 | 0 | 0.022 | -0.163 |
| 5 | 2081-2100 | 20 | 0 | 0 | 0.082 | -0.078 |
| 6 | 1971-2100 | 130 | 0 | 0 | 0.055 | 0.026 |
| 7 | 1957-1965, 1967, 1969-1985, 2003, 2012-2014 USGS instantaneous peak flows | 31 | 0 | 1 | 0.998 | 1.159 |

# 11. FIGURES

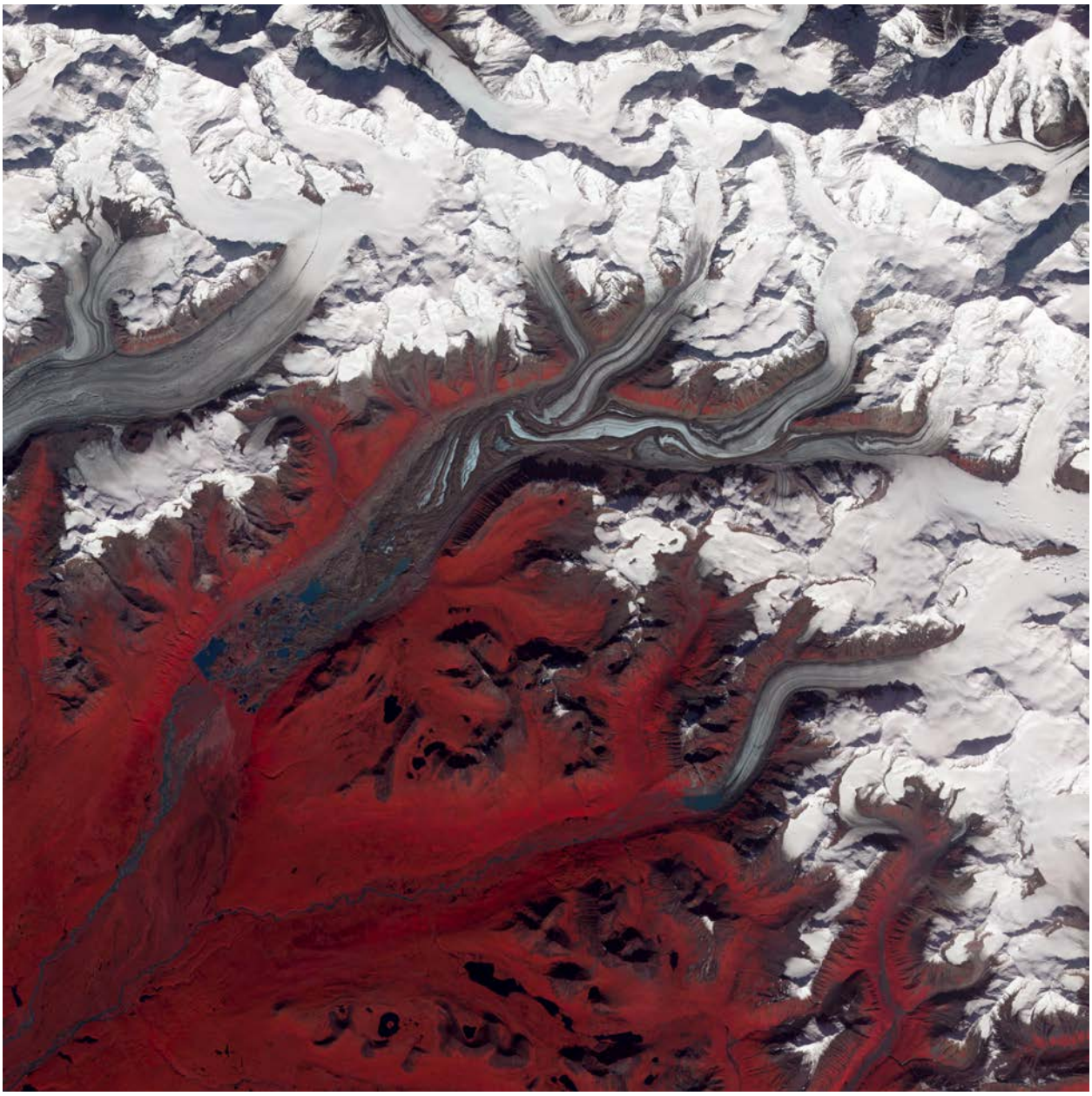

**Figure 2-1. Advanced Spaceborne Thermal Emission and Reflection Radiometer (ASTER) image of part of the glacierized Alaska Range portion of the upper Susitna drainage basin.**
Susitna Glacier (center), with its characteristic looped moraines, is one of the main glaciers in the watershed. Also visible here is East Fork Glacier (center right) and the upper portion of West Fork Glacier (upper left). In this false color image, red represents areas of vegetation cover.

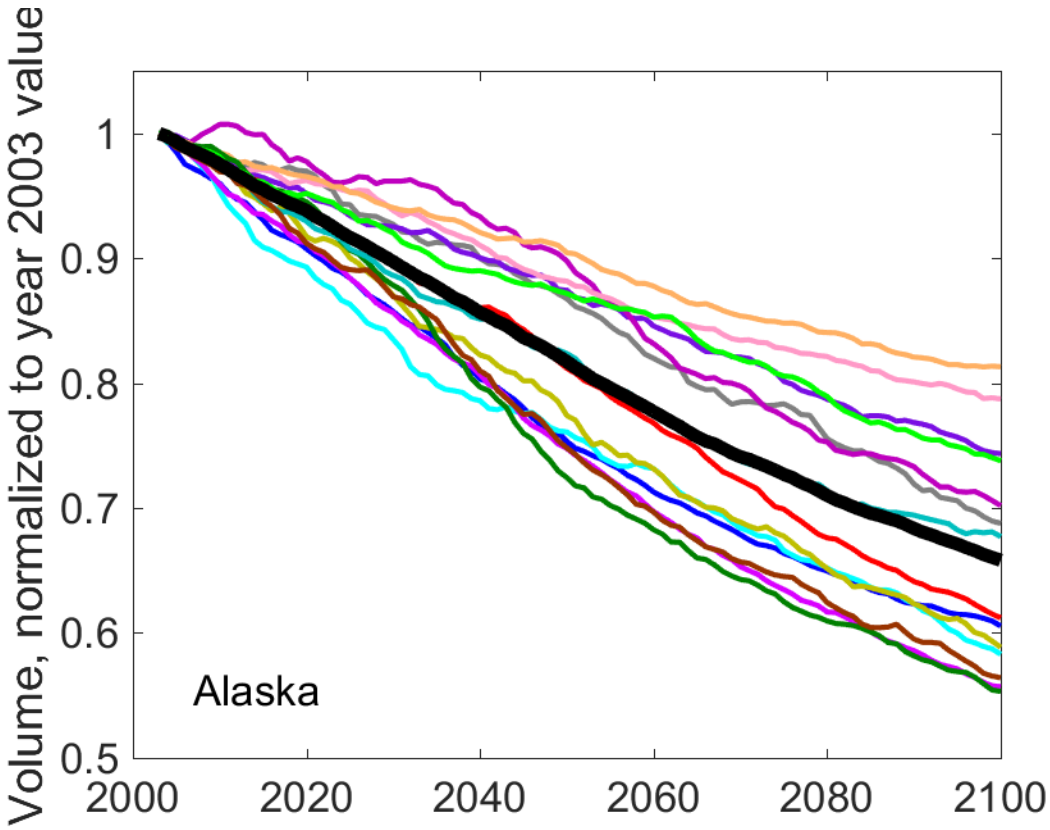


**Figure 3.1-1. 100-year projections of glacier volume in Alaska using 14 Global Climate Models forced by the RCP4.5 emission scenario.**
Glaciers in Alaska are expected to lose 18-45% (multi-model mean 32%) of their initial volume (2003) by the end of the century (Radić *et al.* 2013).

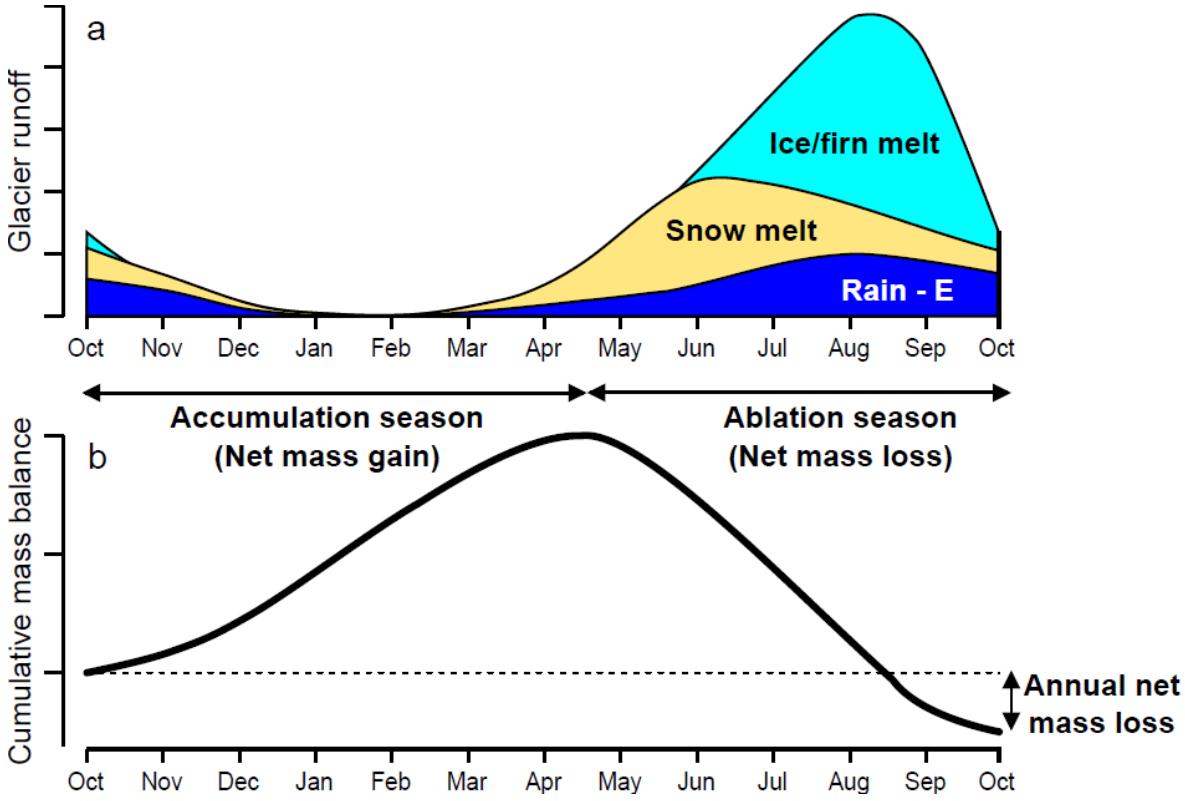


**Figure 3.1.2.1-1. Variations in glacier runoff and mass balance.**
(a) Schematic seasonal variation of total glacier runoff, defined as all water exiting a glacier, and its components, E is evaporation; (b) cumulative glacier mass balance in specific units (m w.e. year-1) showing a year with negative annual balance (Radić and Hock in press).

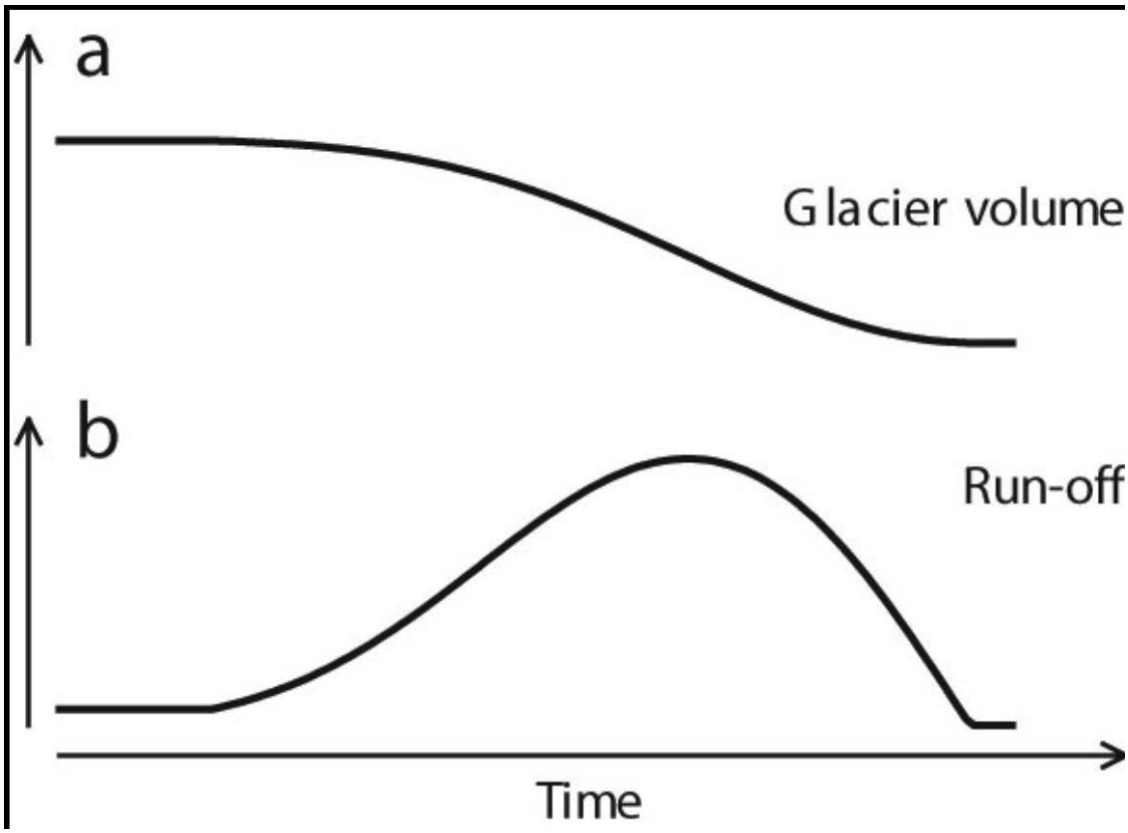


**Figure 3.1.2.2-1. Schematic representation of the long-term effects glacier mass loss on: a) glacier volume; and b) glacier runoff.**
Note that runoff initially increases as melt is enhanced but then reaches a 'turning point' beyond which runoff decreases as the glacier shrinks thus reducing the excess runoff from glacier storage (modified from Jansson *et al.* 2003).

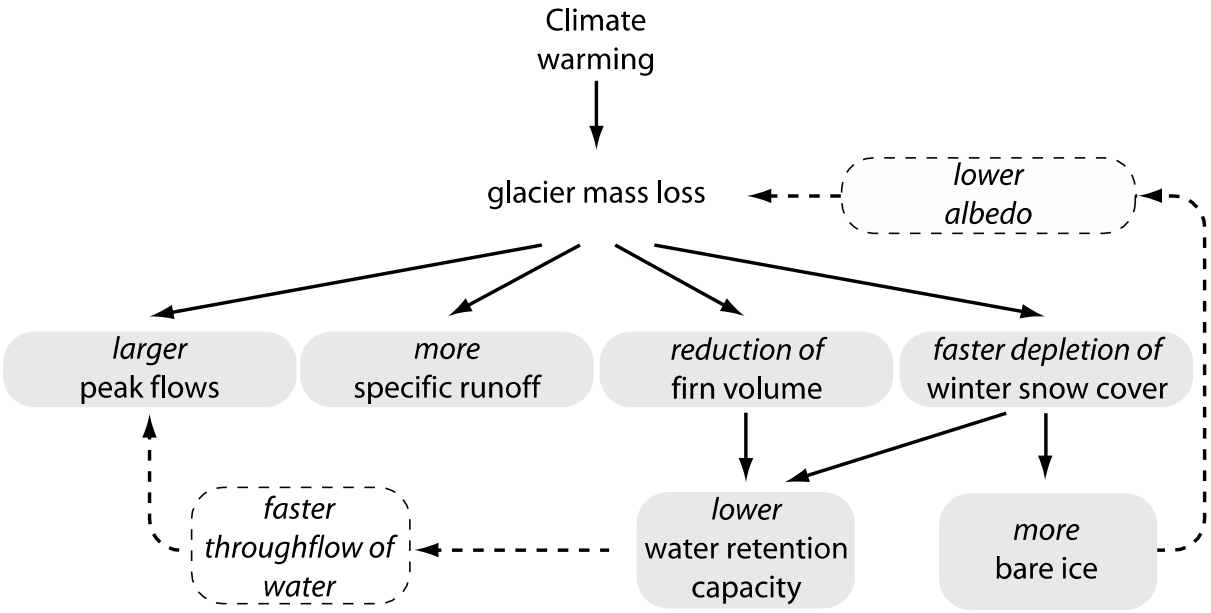


**Figure 3.1.2.2-2. Initial effects of atmospheric warming on glacier runoff including feedback mechanisms leading to further enhanced runoff totals and peak flows (Hock *et al.* 2005).**

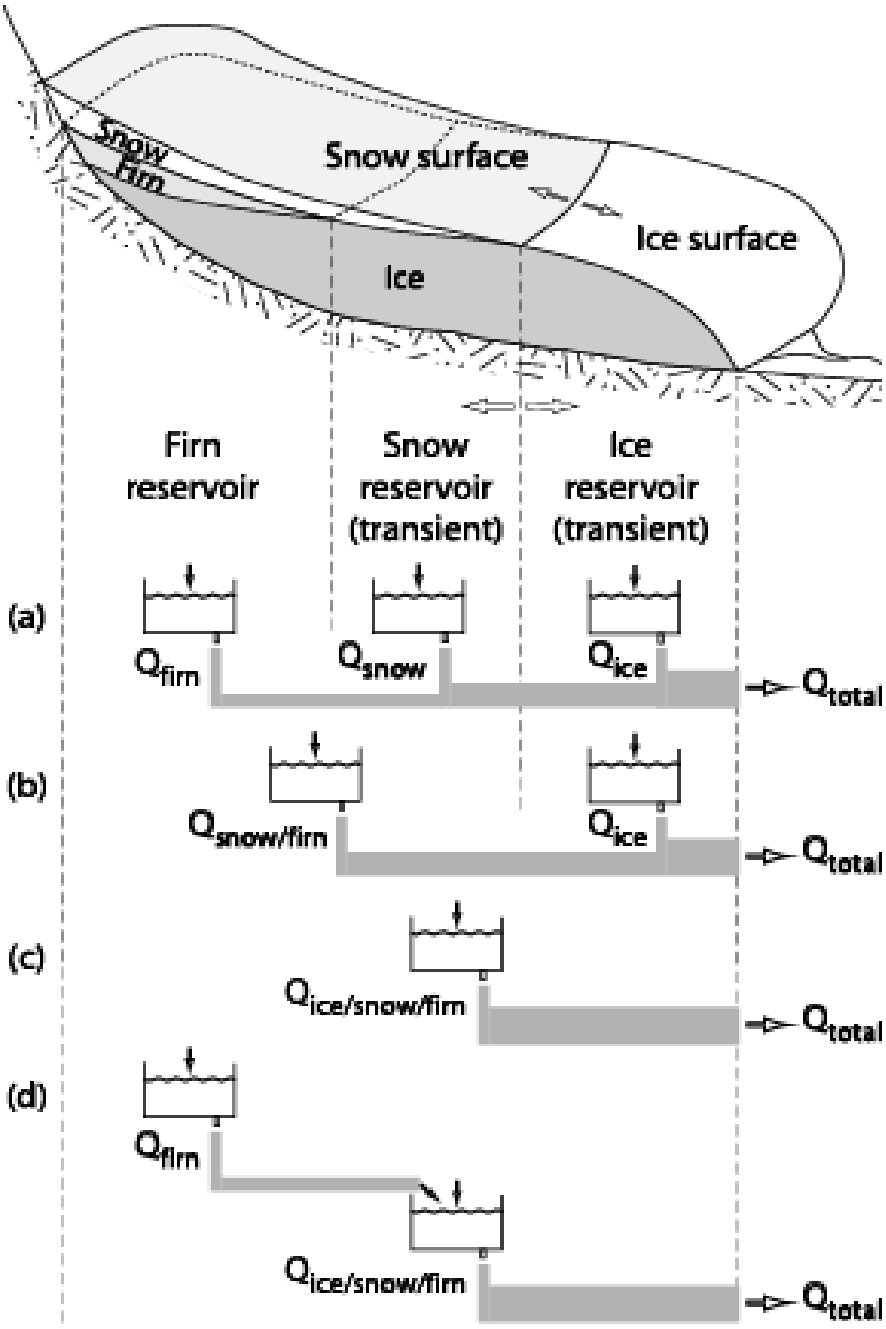


**Figure 3.1.2.3.3-1. Concept of linear reservoirs as applied to glaciers using one to three (c-a) different linear reservoirs.**

Reservoirs are coupled in parallel in (a-b), and in series in (d). Exact delineation of reservoirs varies between studies. Q is outflow from the reservoirs (Hock *et al.* 2005b).

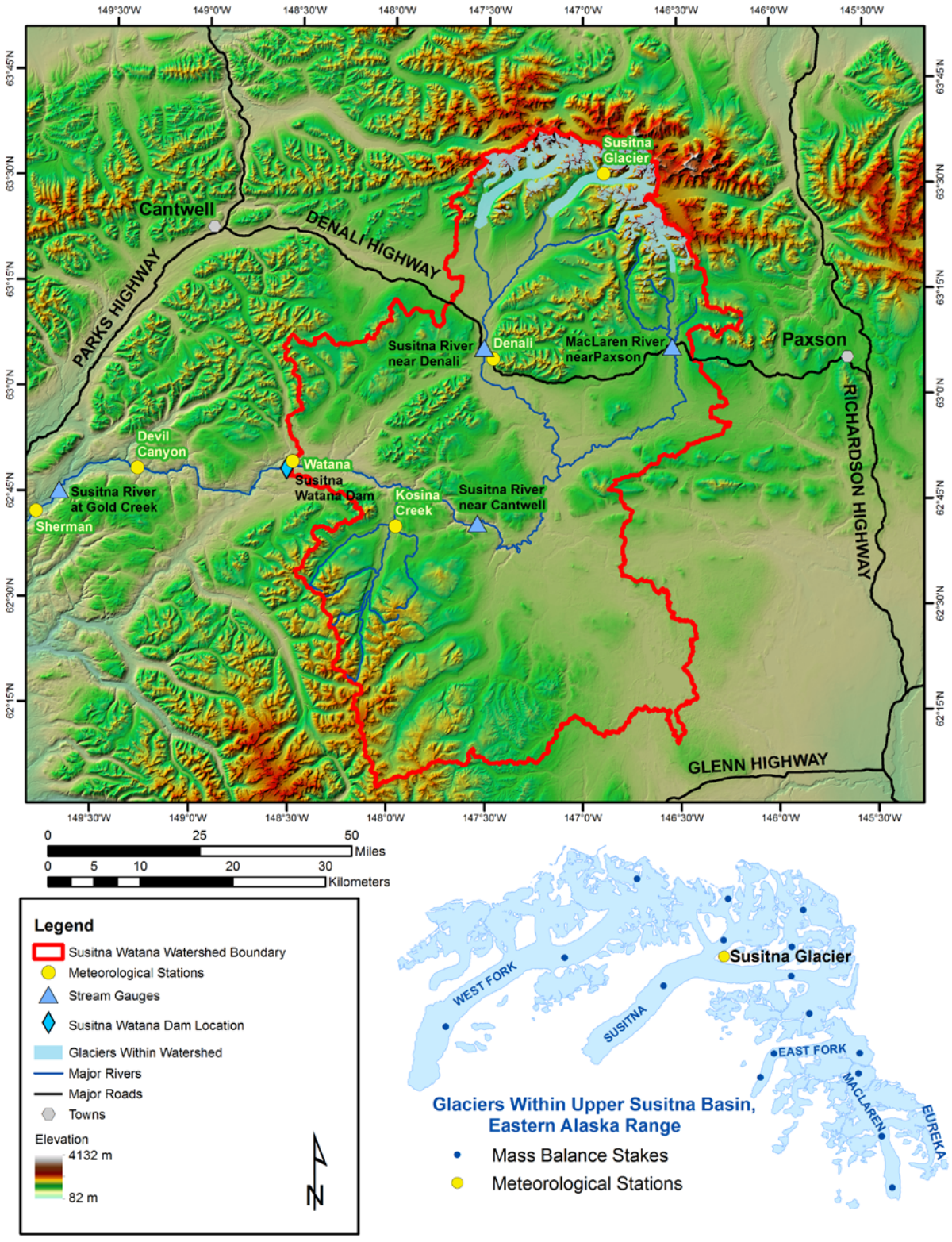


**Figure 3.1.2.4.2-1. Map of the upper Susitna basin, including the locations of historical meteorological, stream gauge and glacier monitoring stations.**

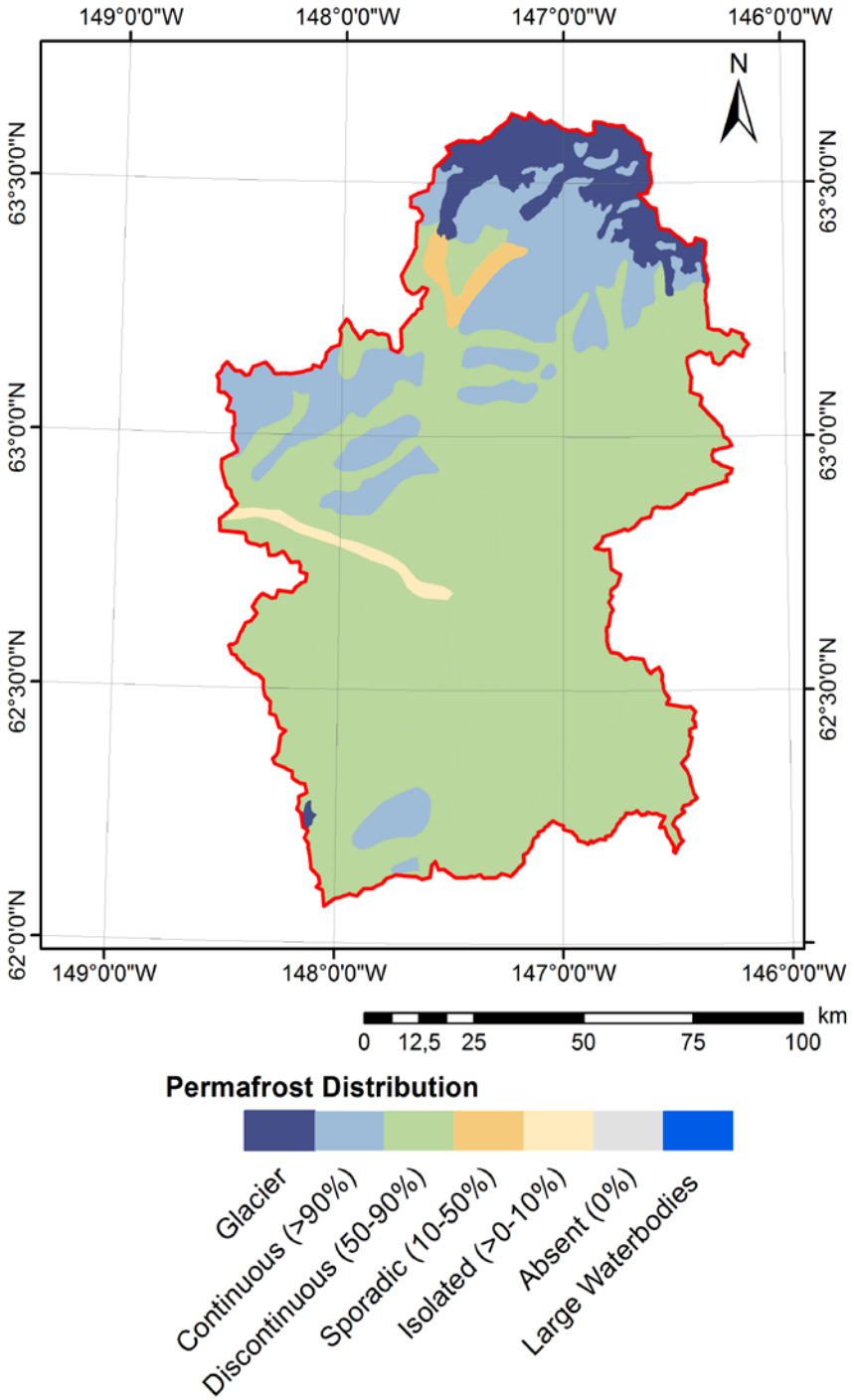


**Figure 3.2-1. Permafrost distribution in the upper Susitna basin.**
A majority of the area draining into the proposed dam is estimated to be underlain by discontinuous and continuous permafrost (modified after Jorgenson *et al.* 2008). Maximum depth to the base of permafrost in the Maclaren River junction with the Susitna River is about 200 m (Alaska District, Corps of Engineers 1975), while it is 40 m at Gulkana, which is just outside the basin to the southeast (Geophysical Institute permafrost lab).

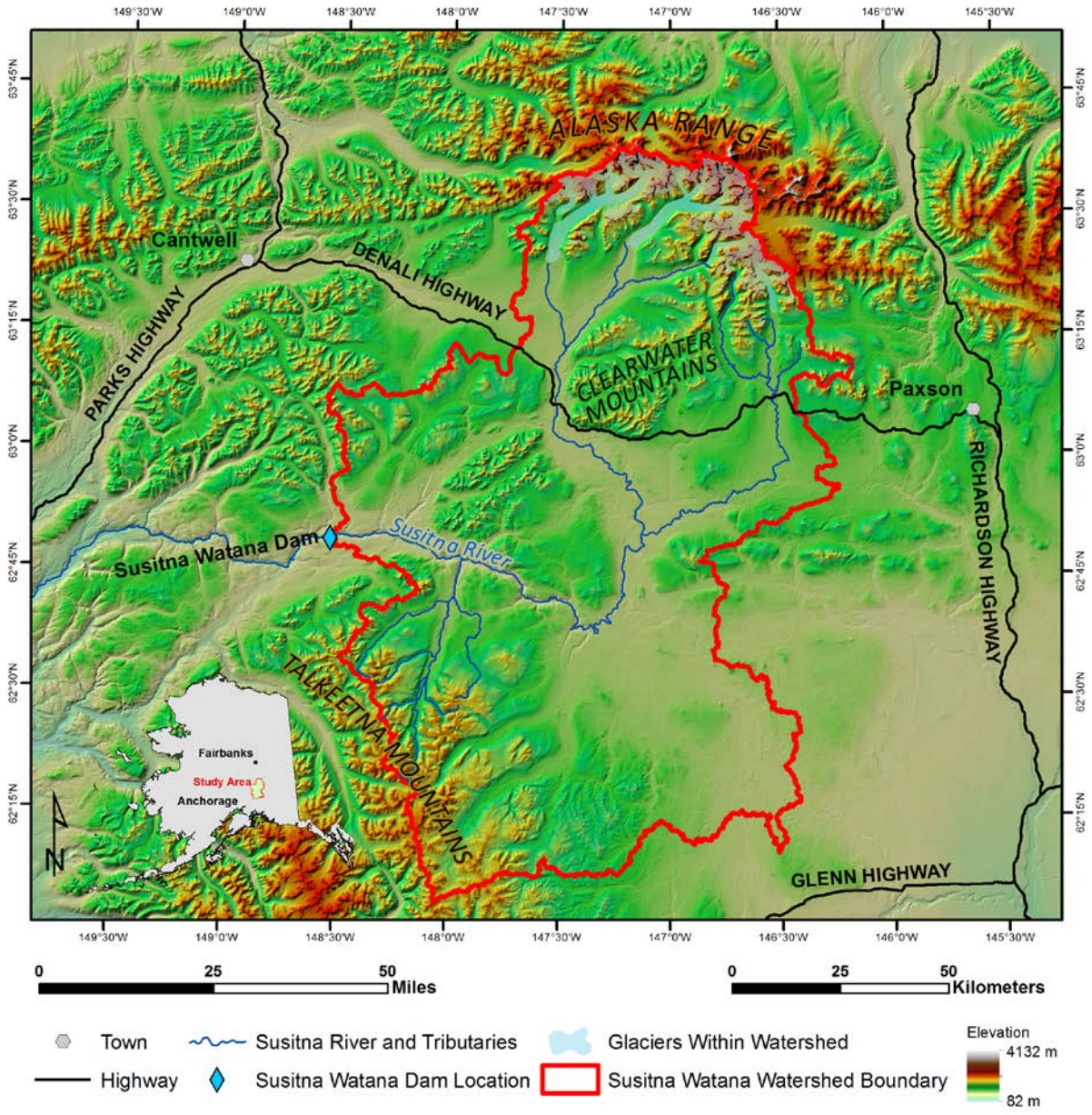


**Figure 4.1-1. Overview map of the upper Susitna basin.**

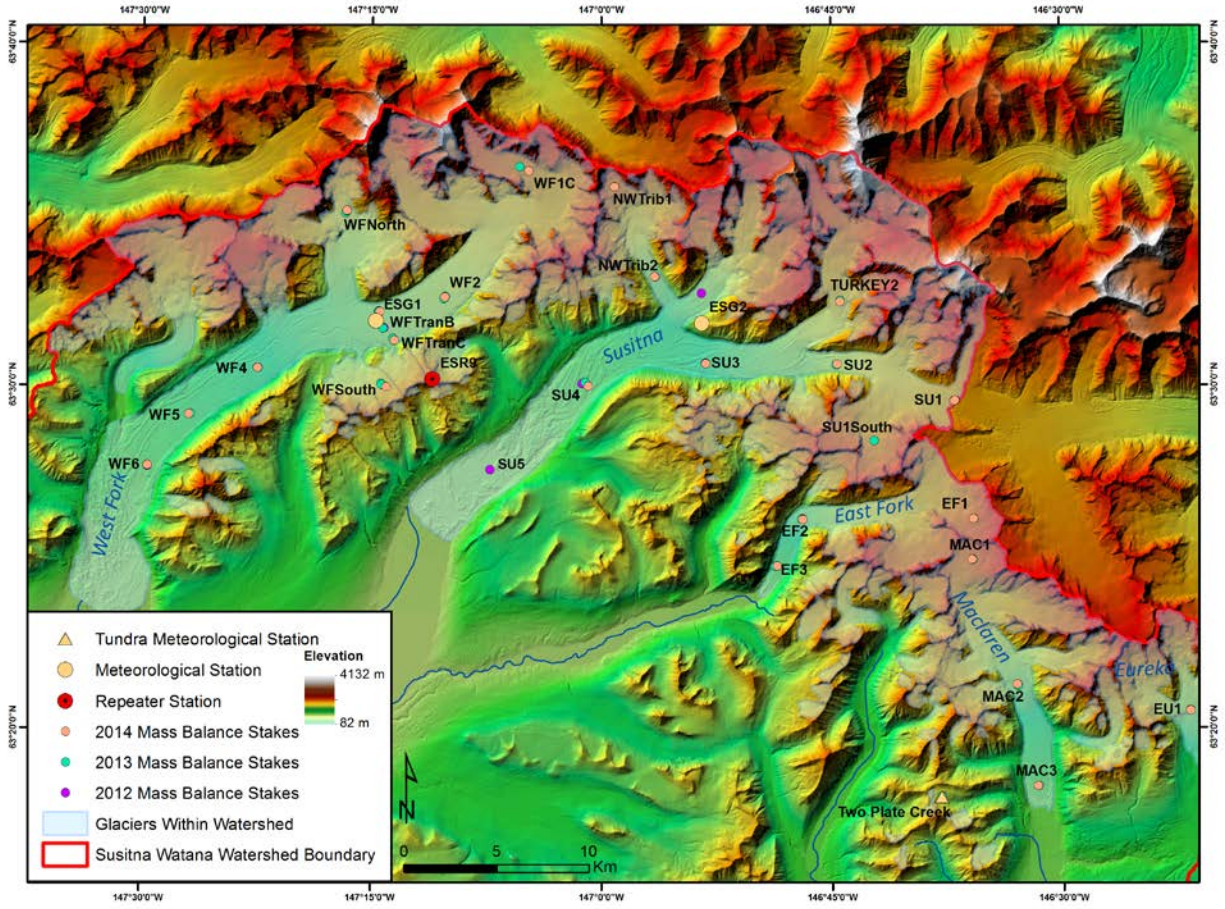


**Figure 4.1-2. Glaciers of the Alaska Range in the upper Susitna basin.**

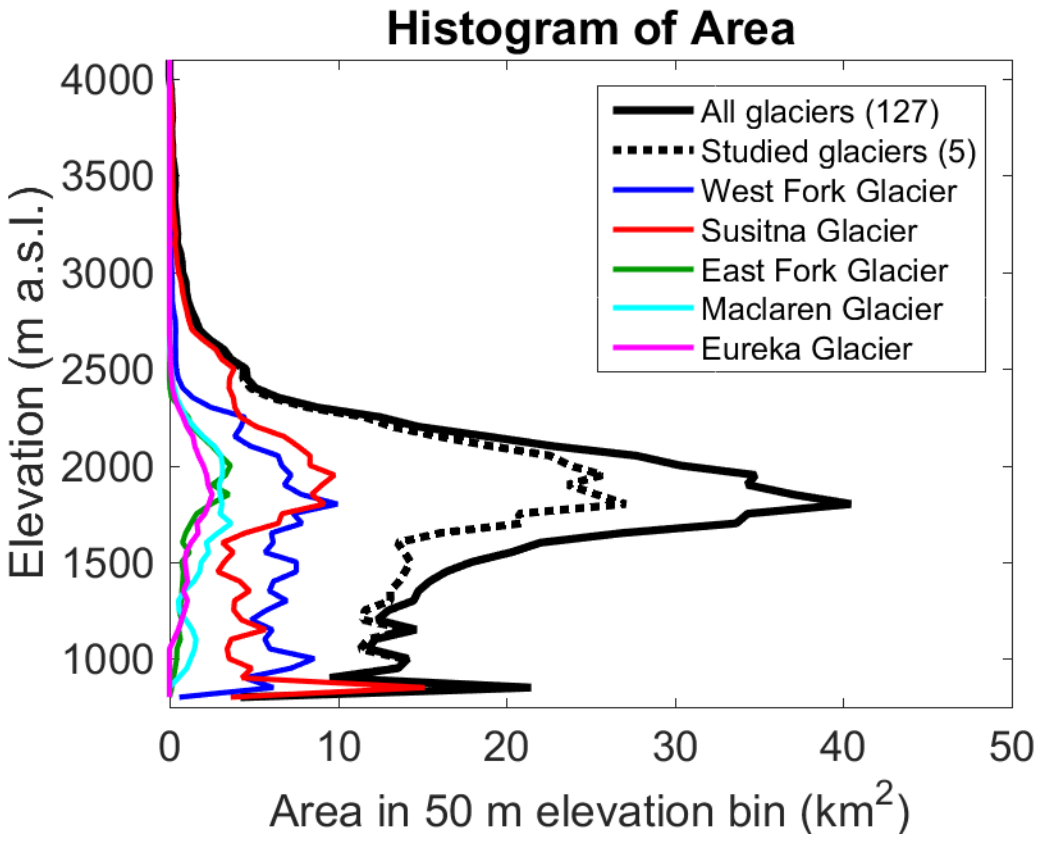


**Figure 4.1-3. Area-elevation distribution (hypsometry) of glaciers in the upper Susitna basin.**

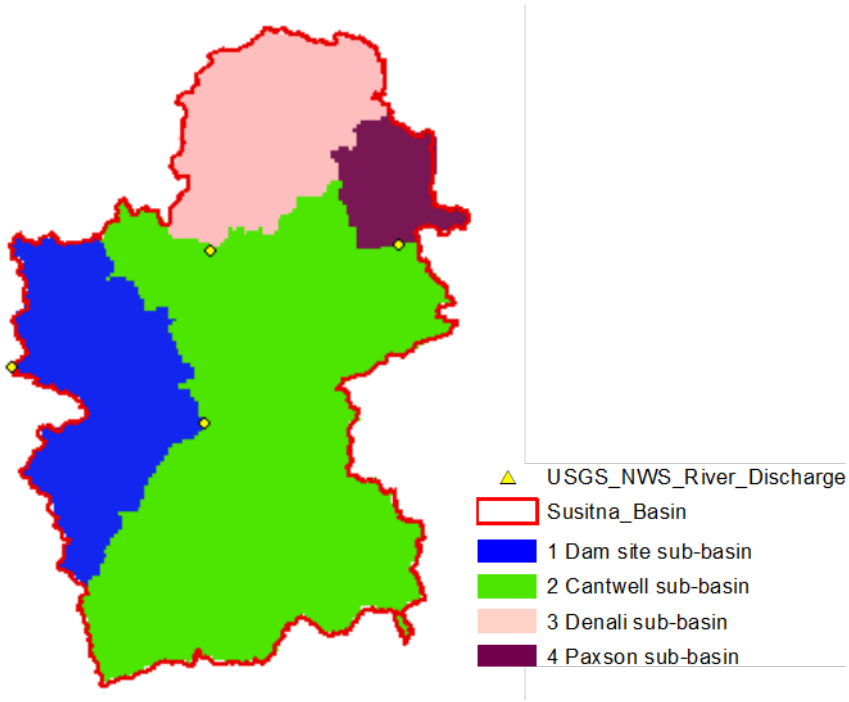


**Figure 4.1-4. Upper Susitna basin sub-basins and stream gauge locations.**

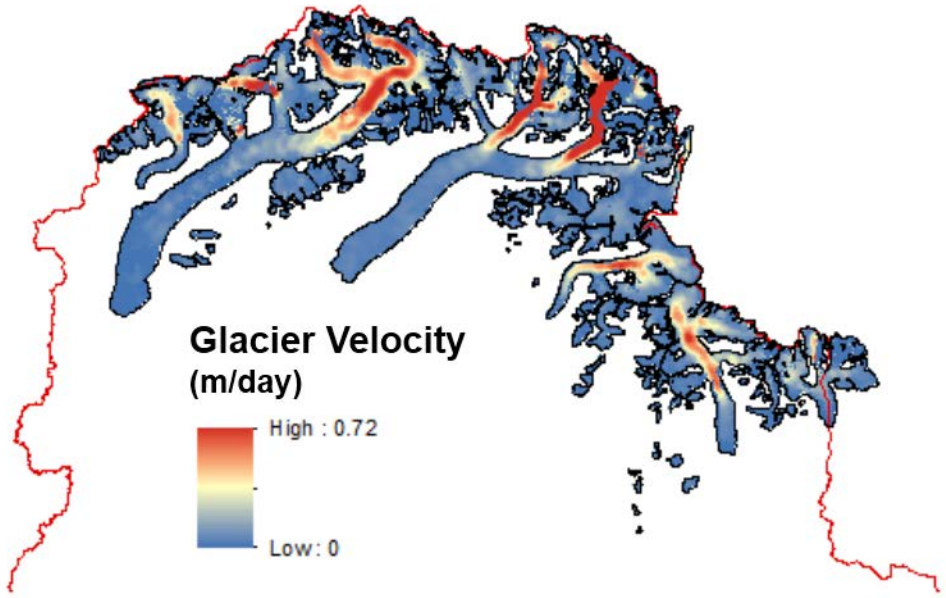


**Figure 4.1-5. Estimated mean annual surface velocities of glaciers in the upper Susitna basin from Burgess *et al.* (2013).**

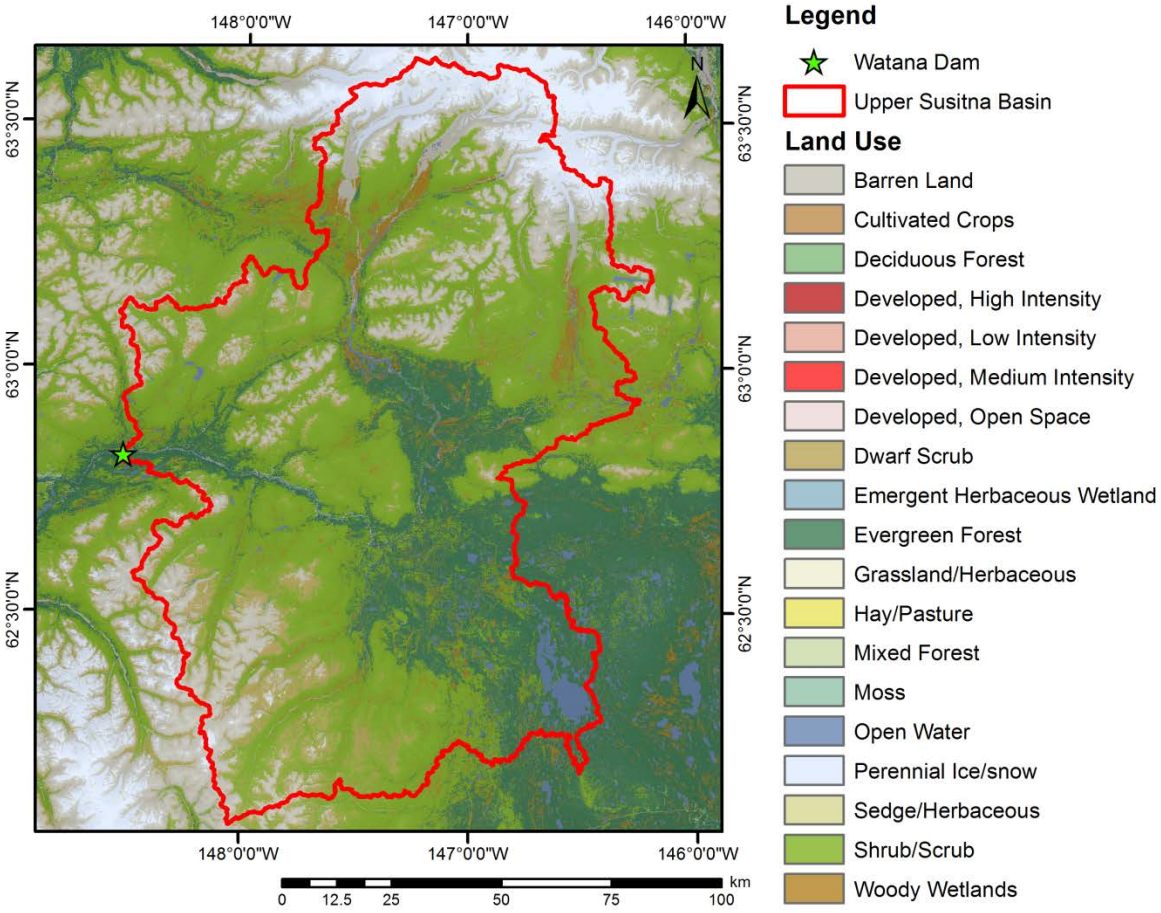


**Figure 5.1.2-1. Land use in the upper Susitna basin derived from Selkowitz and Stehman (2011).**

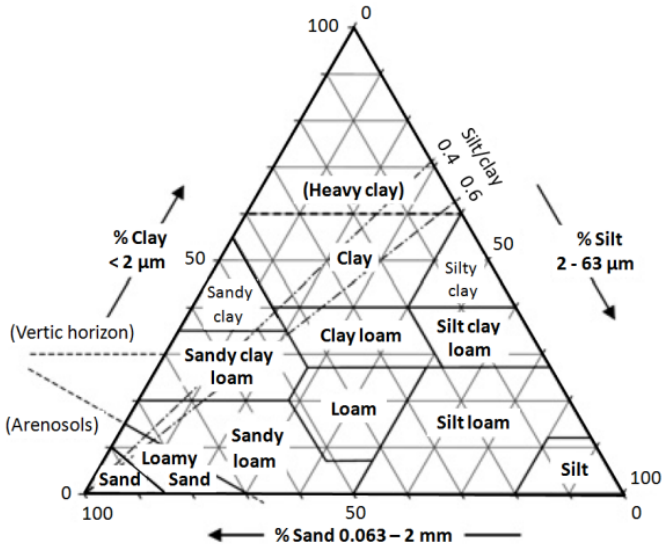


**Figure 5.1.3-1. Soil texture classification as a percentage of clay, silt and sand (Blume *et al.* 2010)**

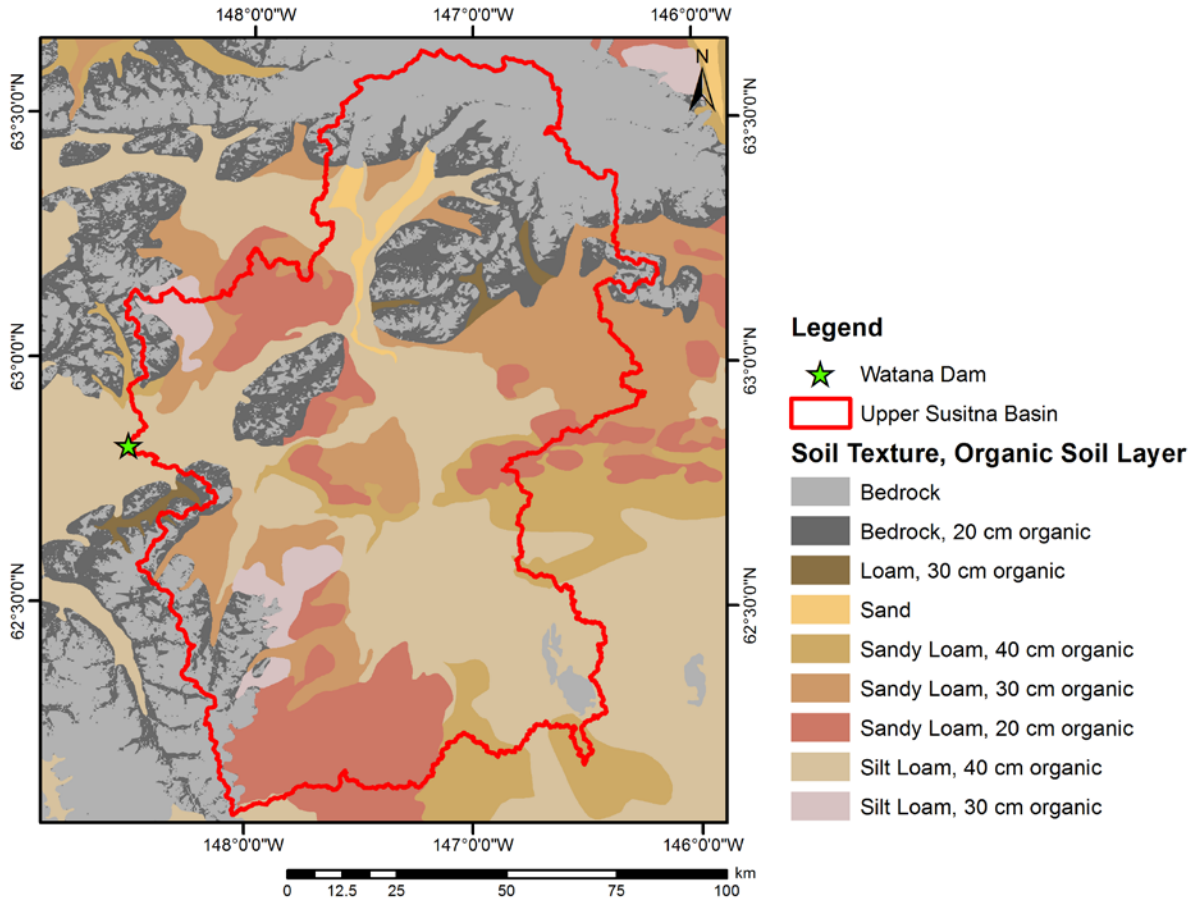


**Figure 5.1.3-2. Soil Texture, including estimates on organic layer depths.**

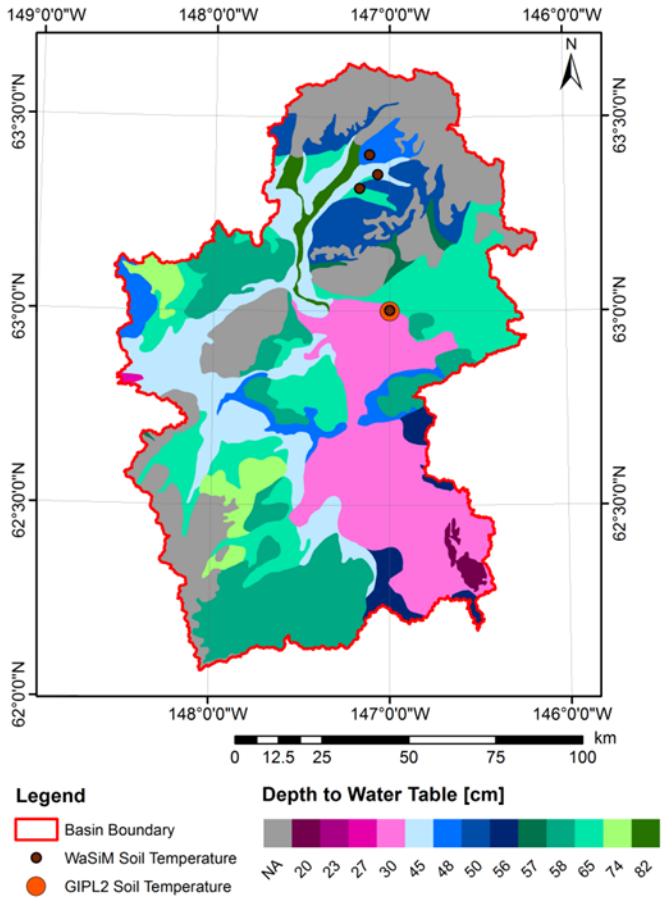


**Figure 5.1.4-1. Depth to water table.**

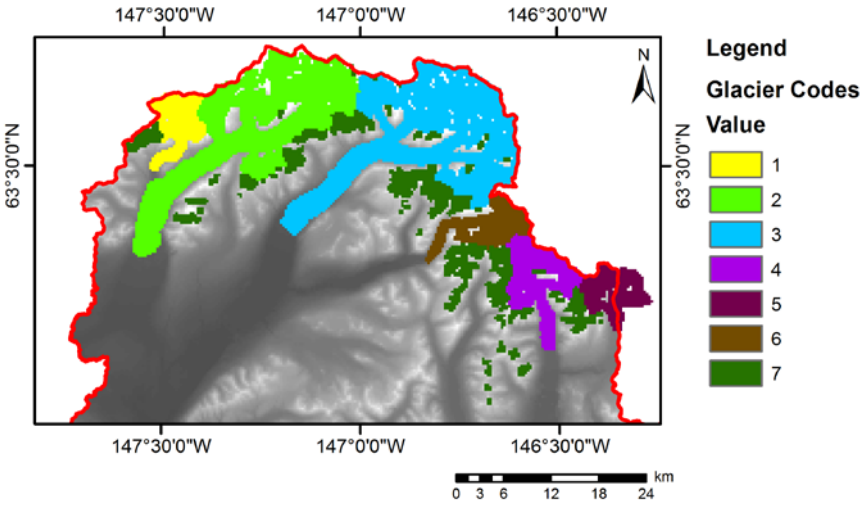


**Figure 5.1.5.1-1. Glacier classification codes (300 m resolution) for upper Susitna basin glaciers.**

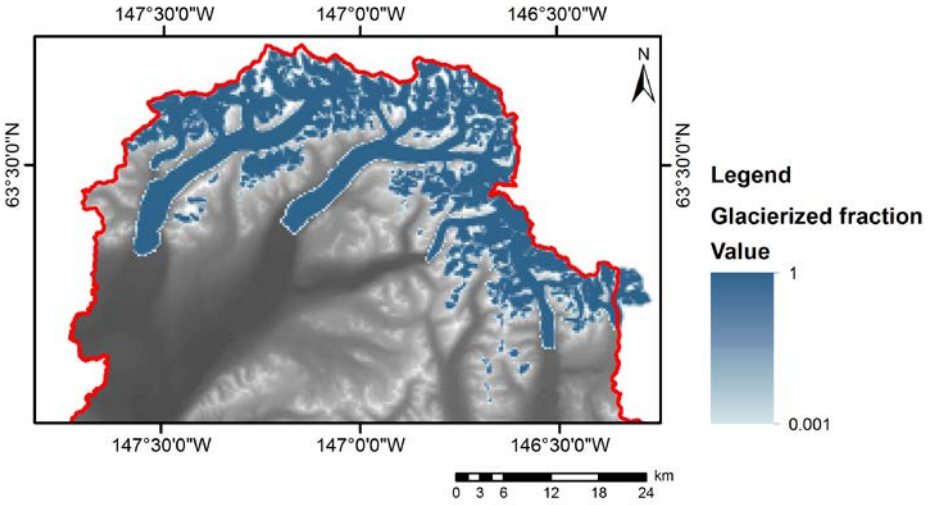


**Figure 5.1.5.1-2. Glacierized fraction of each cell (300 m resolution) in the upper Susitna basin glaciers.**

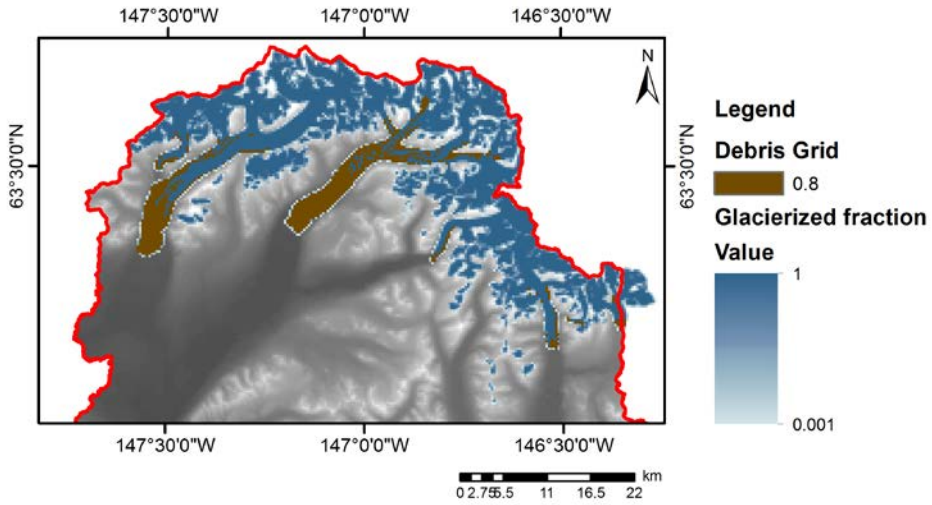


**Figure 5.1.5.1-3. Glacierized cell fraction and debris cover (300 m resolution) in the Upper Susitna Basin.**

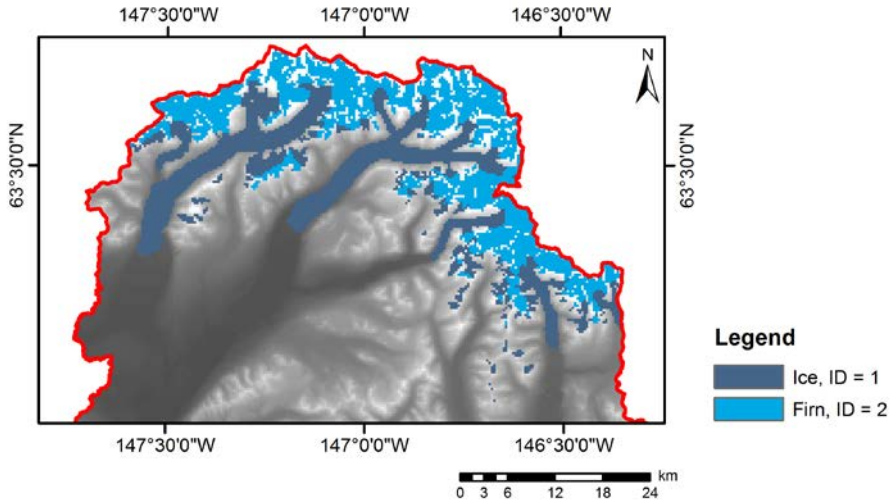


**Figure 5.1.5.1-4. Ice-firn delineation grid (300 m resolution) of glaciers in the upper Susitna basin.**

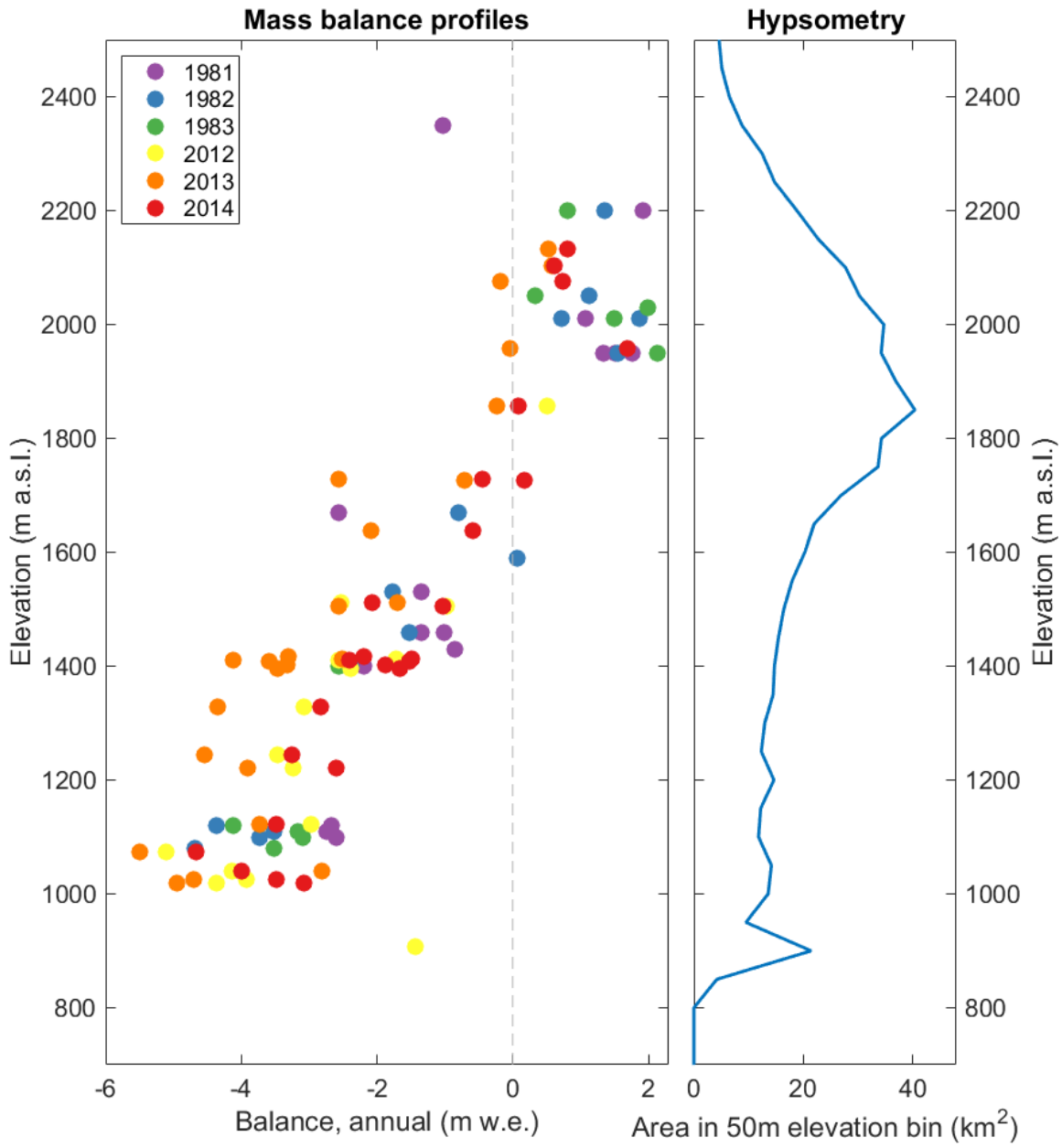


**Figure 5.2.1.1-1. Annual mass balance profiles for monitored glaciers in the upper Susitna basin for the periods 1981-1983 and 2012-2014.**

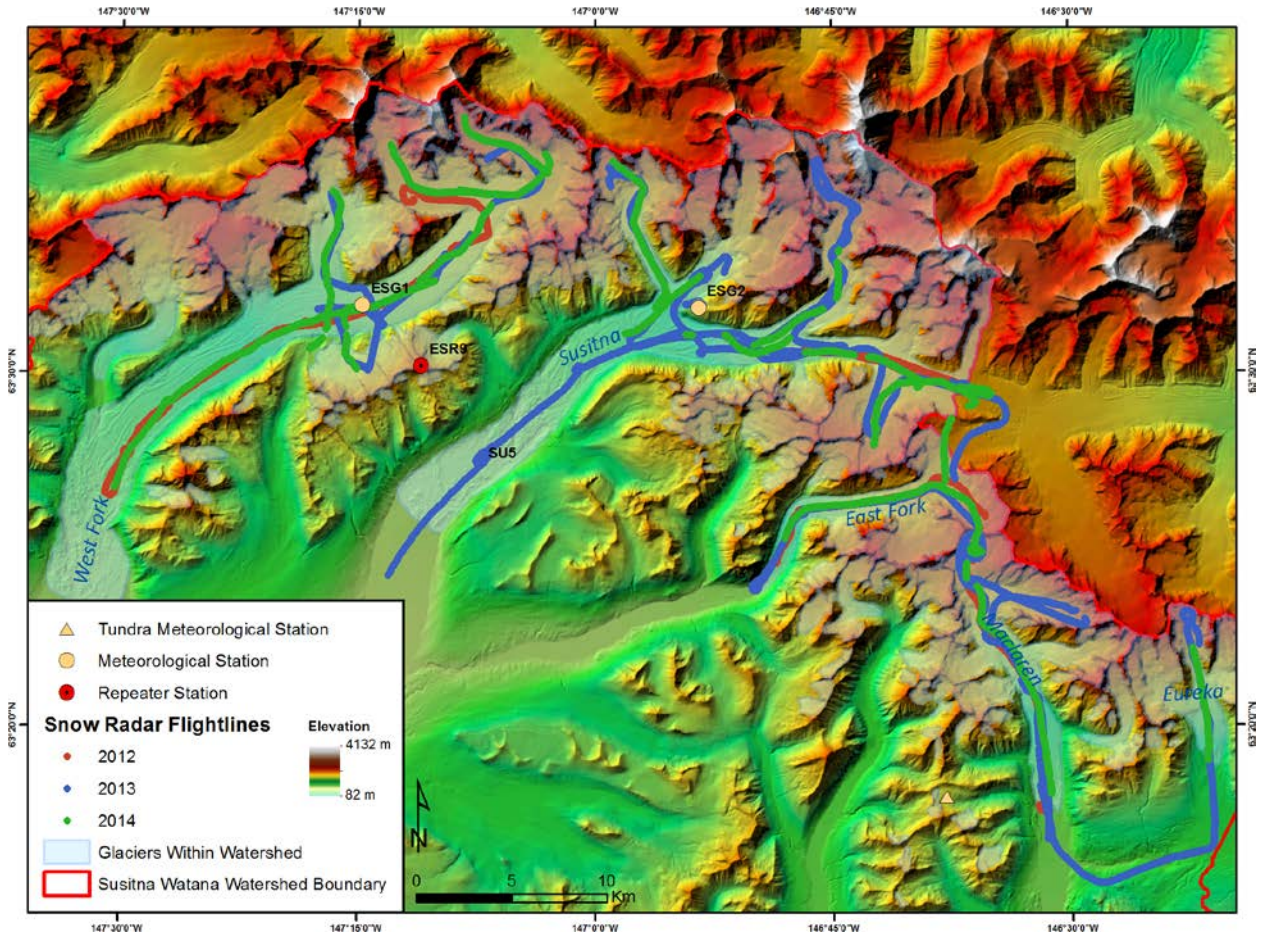


**Figure 5.2.2.1-1. Flight lines of helicopter-borne ground penetrating radar (GPR) common-offset surveys of snow accumulation over the five main glaciers in the upper Susitna basin during the period 2012-2014.**

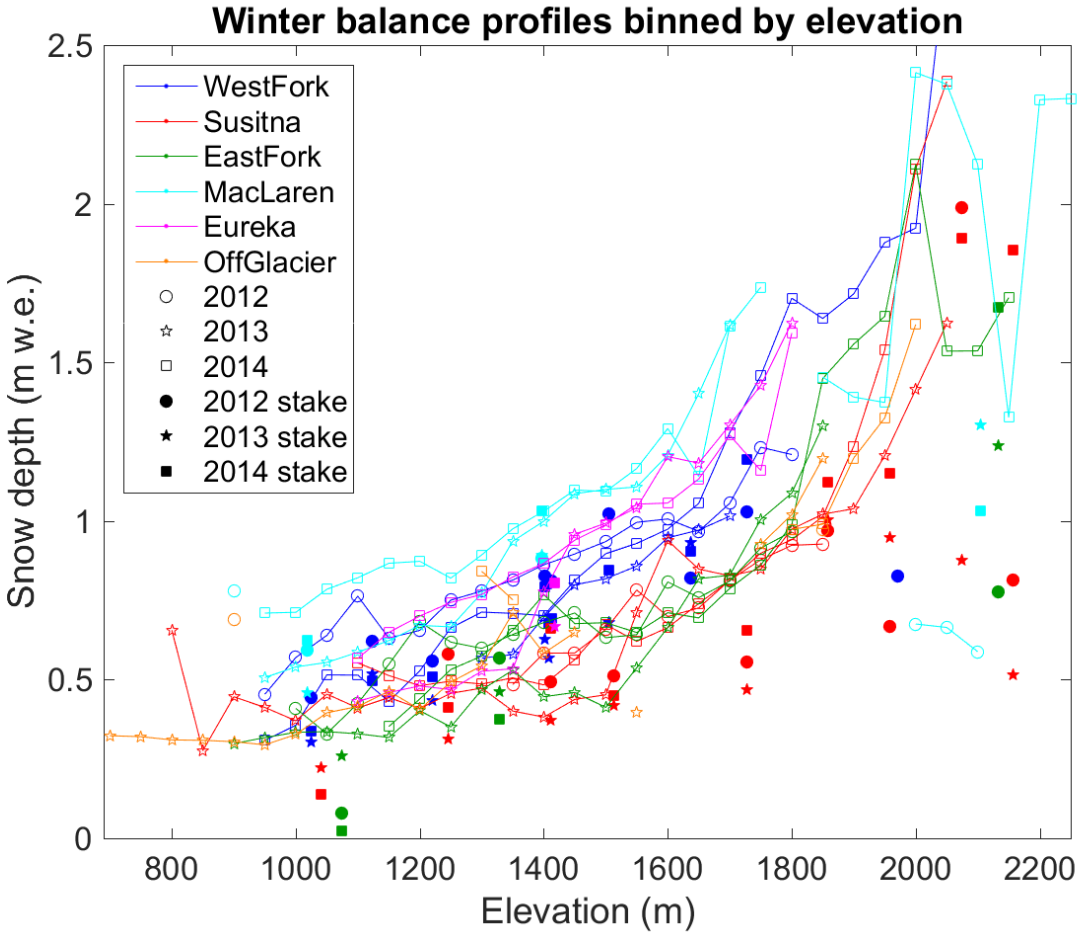


**Figure 5.2.2.1-2. Winter balance profiles derived from radar data (open symbols connected by lines) and from traditional mass balance measurements (filled symbols) for the period 2012-2014.**
The radar data are binned by elevation (50 m bands). The gradient in winter precipitation means that snow accumulation on the glaciers at 2000 m is 2 or 3 times higher than at 1000 m. There is good correspondence between the radar measurements and the traditional method. A few points at high elevation where the discrepancies are largest might be explained by the traditional (probe) measurements hitting a melt surface shallower than the true previous summer's surface. Or the radar may be catching the snow to ice boundary and not the previous summer's surface.

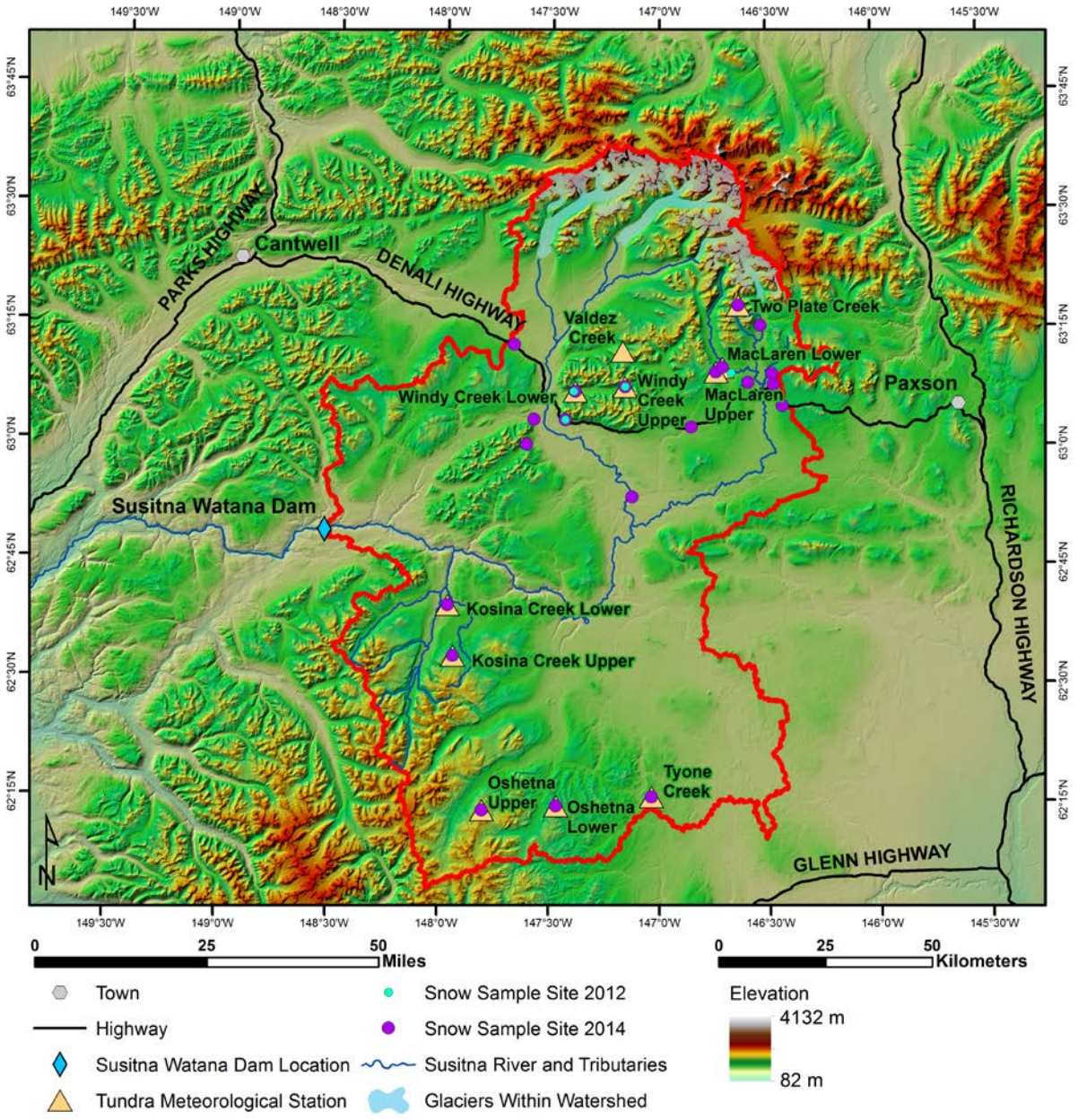


**Figure 5.2.2.2-1. Locations of snow sample sites in non-glacierized terrain (2012 and 2014).**

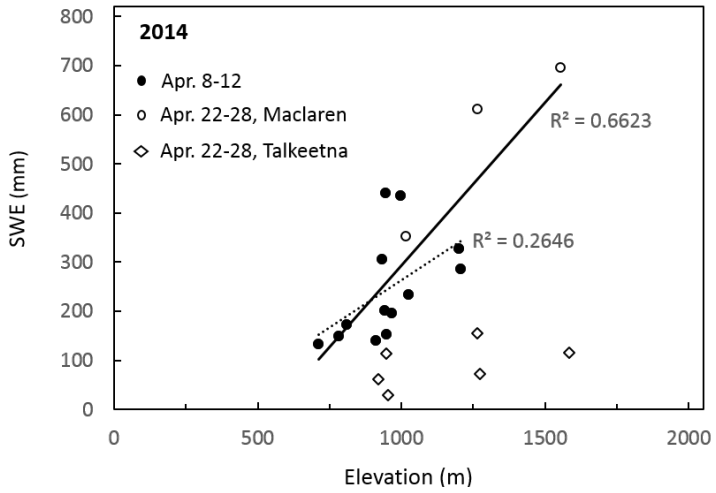


**Figure 5.2.2.2-2. Increase in snow water equivalent with elevation in 2014 over non-glacierized terrain.**
The higher R2 is achieved when excluding the April 22-28 Talkeetna sites, which likely had experienced significant melting by the time they were surveyed. The lower R2 represent only the Apr 8-12 measurements.

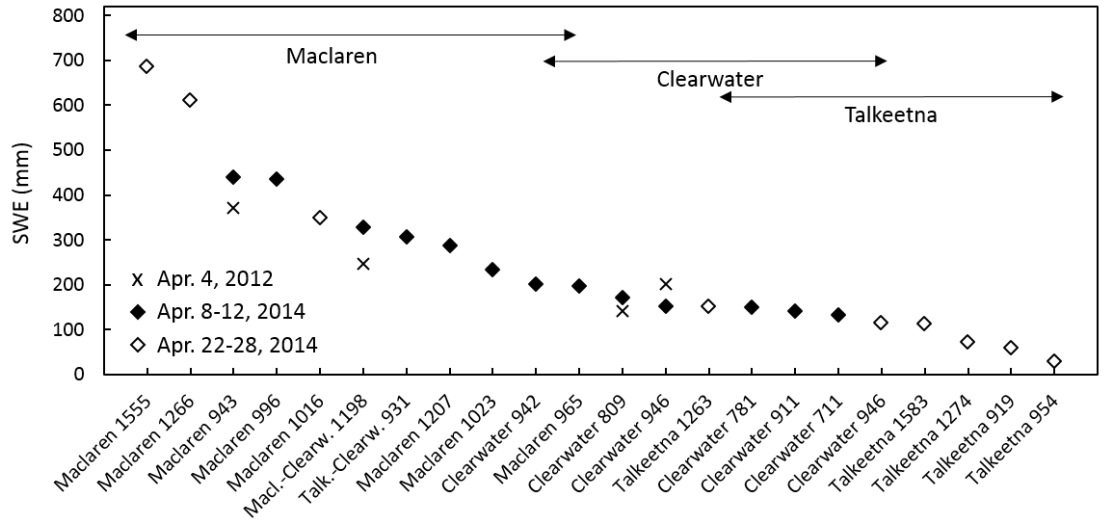


**Figure 5.2.2.2-3. End-of-winter snow water equivalent sorted according to decreasing value for field measurements in 2012 and 2014. Also marked are the three main regions (Maclaren, Clearwater and Talkeetna).**
The x-axis represent each site given a name according to respective region and elevation of the individual sites.

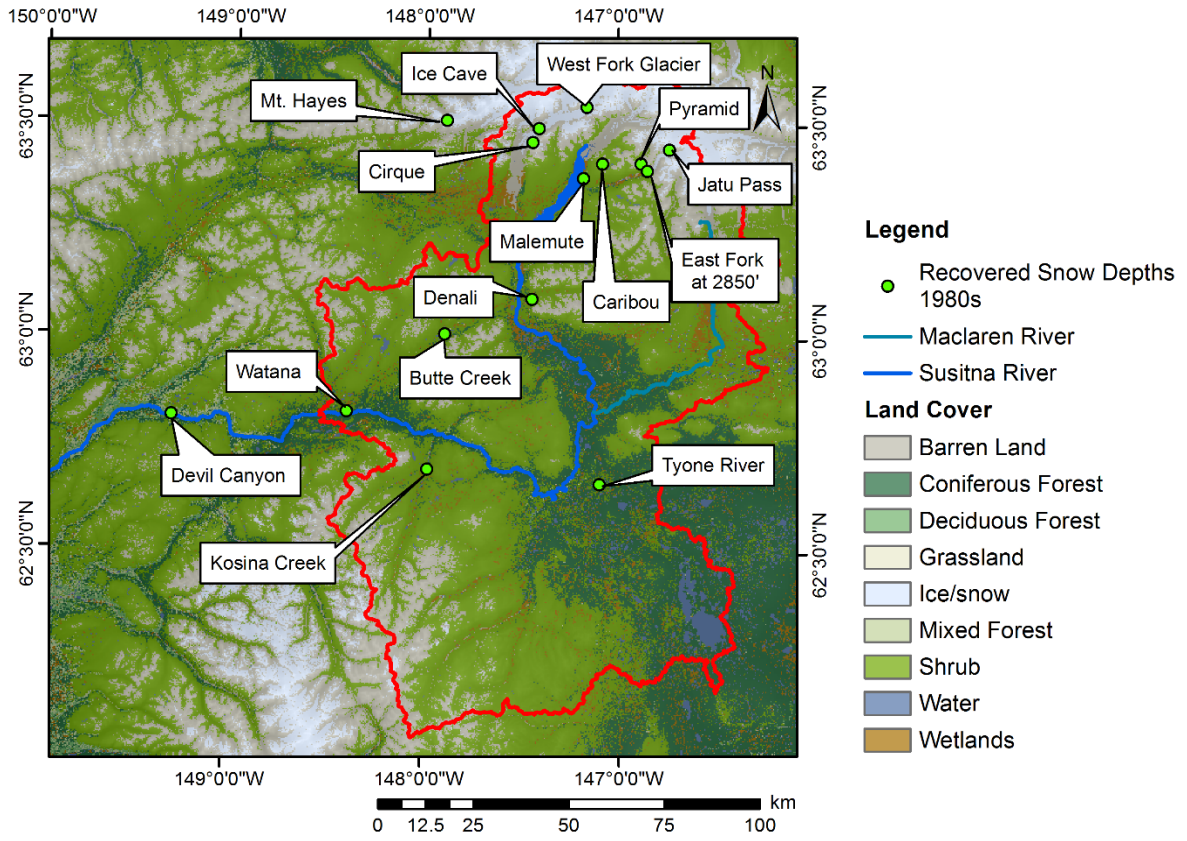


**Figure 5.2.2.3-1. Locations of snow depth measurements from 1981 and 1982.**

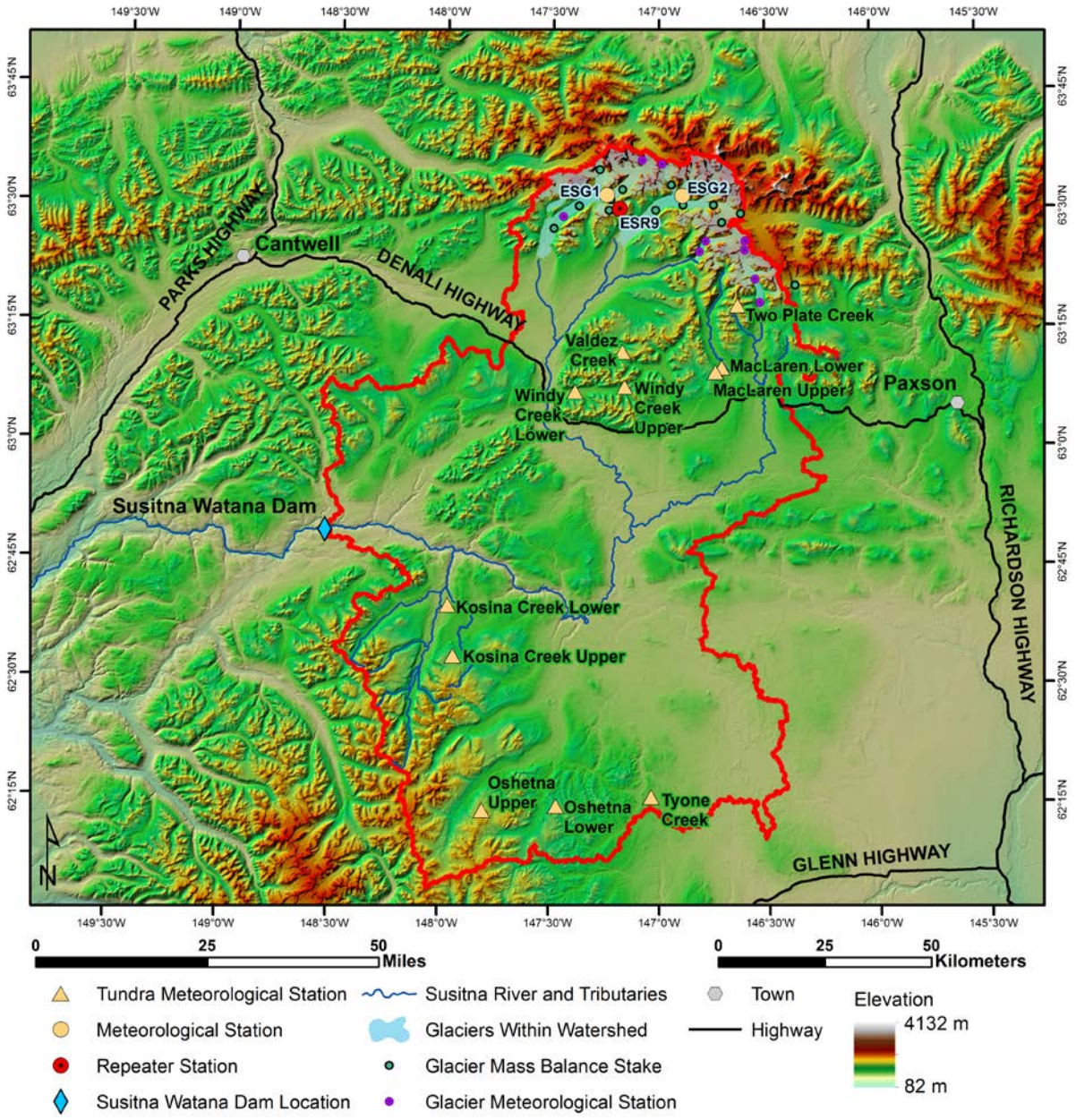


**Figure 5.3-1. Map of meteorological stations deployed during the 2012-2014 study period.**

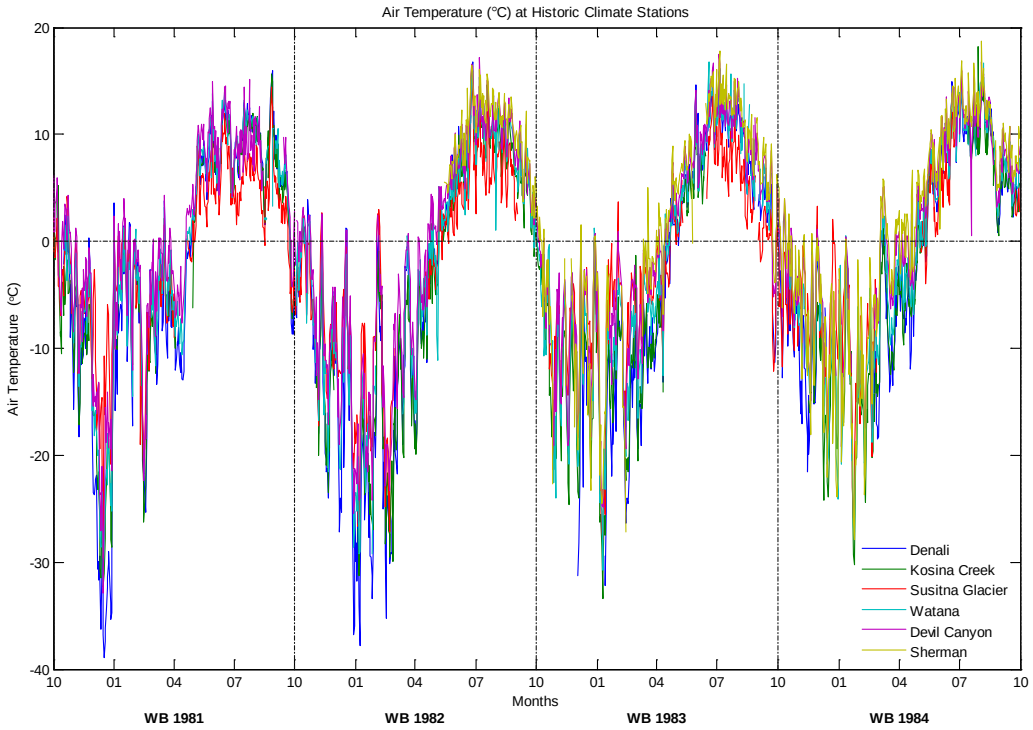


**Figure 5.3.1-1. Air temperature in degrees Celsius at the six climate stations monitored from 1980 to 1984.** The hydrologic year is indicated by the dashed black vertical lines. The hydrologic year runs from September 30th to October 1st of the following year.

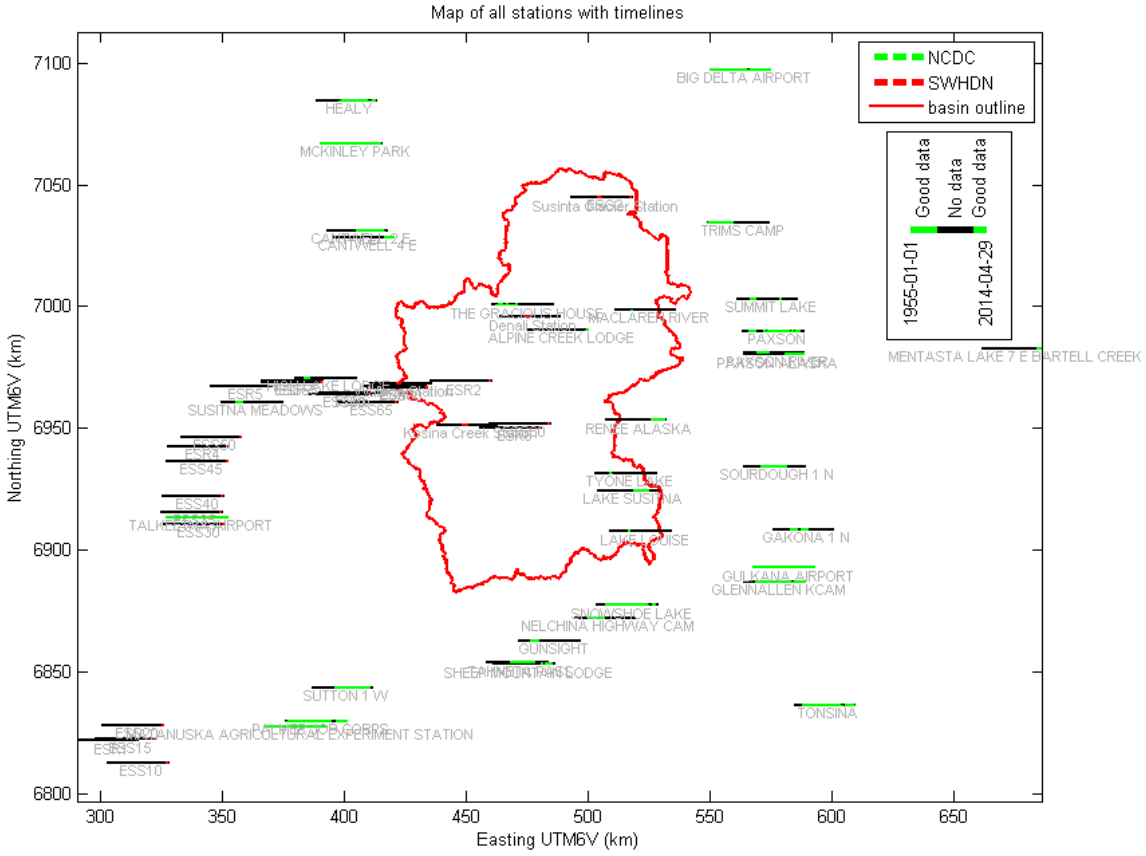


**Figure 5.3.2-1. A map of all climate stations in the vicinity of the upper Susitna basin, showing availability of temperature data.**
Each station has a time line (horizontal bar) that runs from 1955 to 2014. Times when that station has data are colored, and times with no data are black. NOAA NCDC stations use green for good data. SWHDN stations use red for good data.

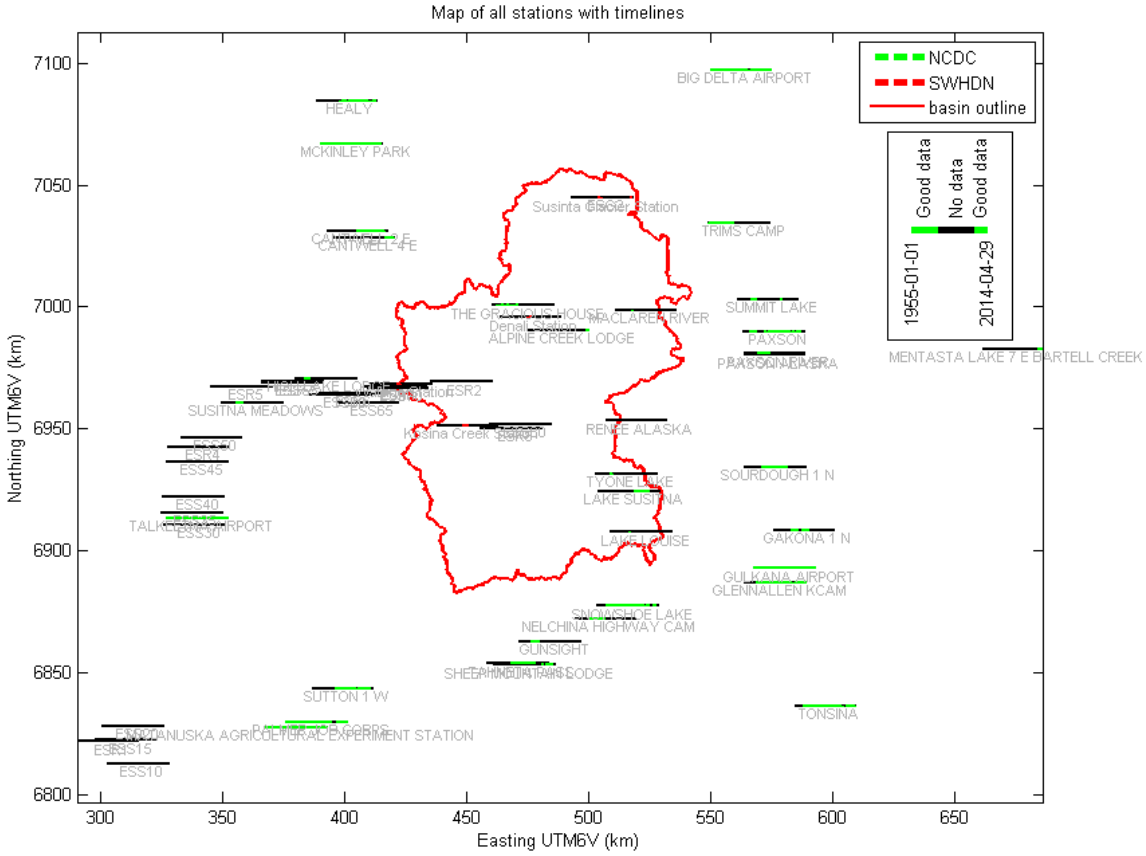


**Figure 5.3.2-2. A map of all climate stations in the vicinity of the upper Susitna basin, showing availability of precipitation data.**

Each station has a time line (horizontal bar) that runs from 1955 to 2014. Times when that station has data are colored, and times with no data are black. NOAA NCDC stations use green for good data. SWHDN stations use red for good data.

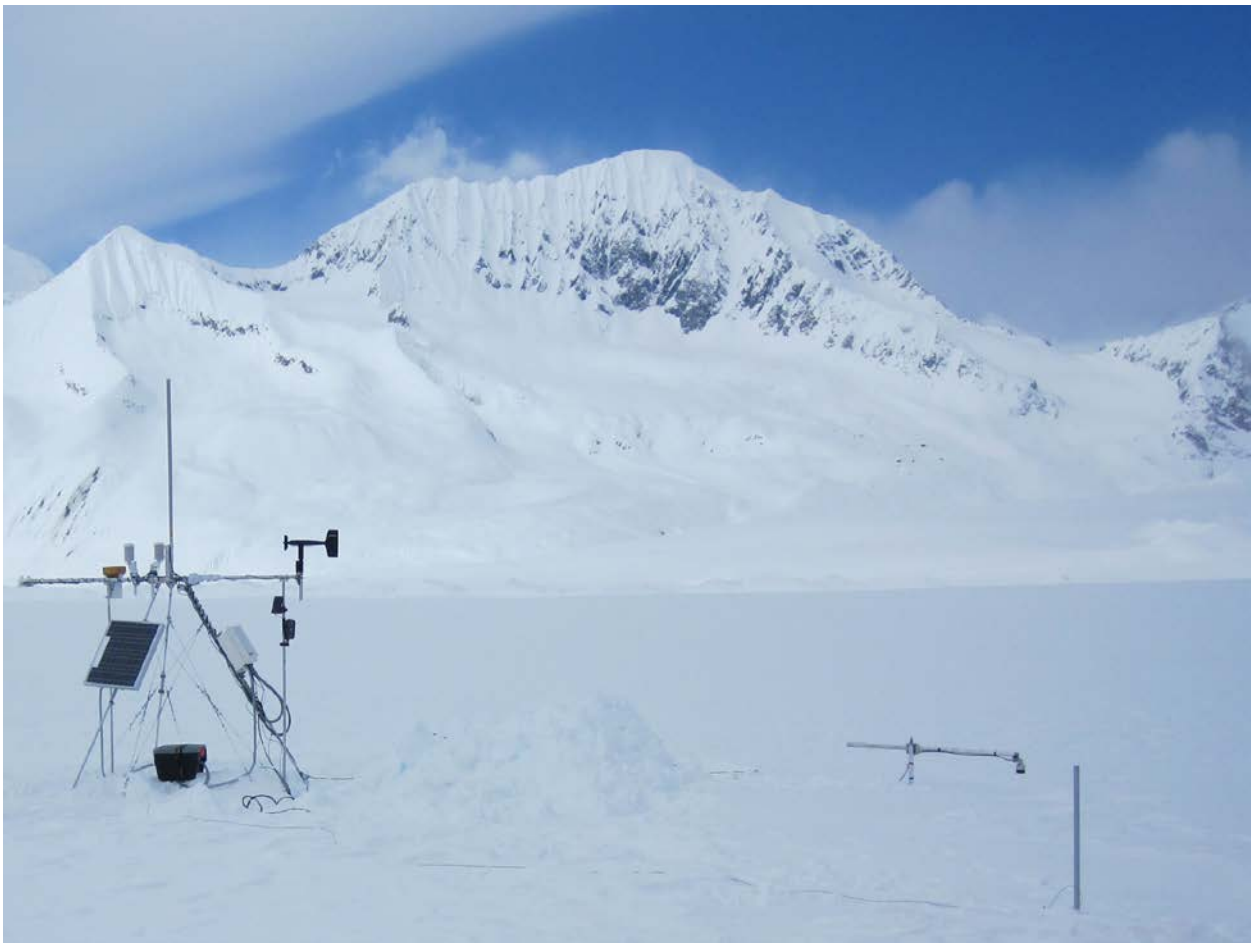

**Figure 5.3.5-1. A northwest-oriented view of the On-Ice weather station deployed on West Fork Glacier (2013-2014).**

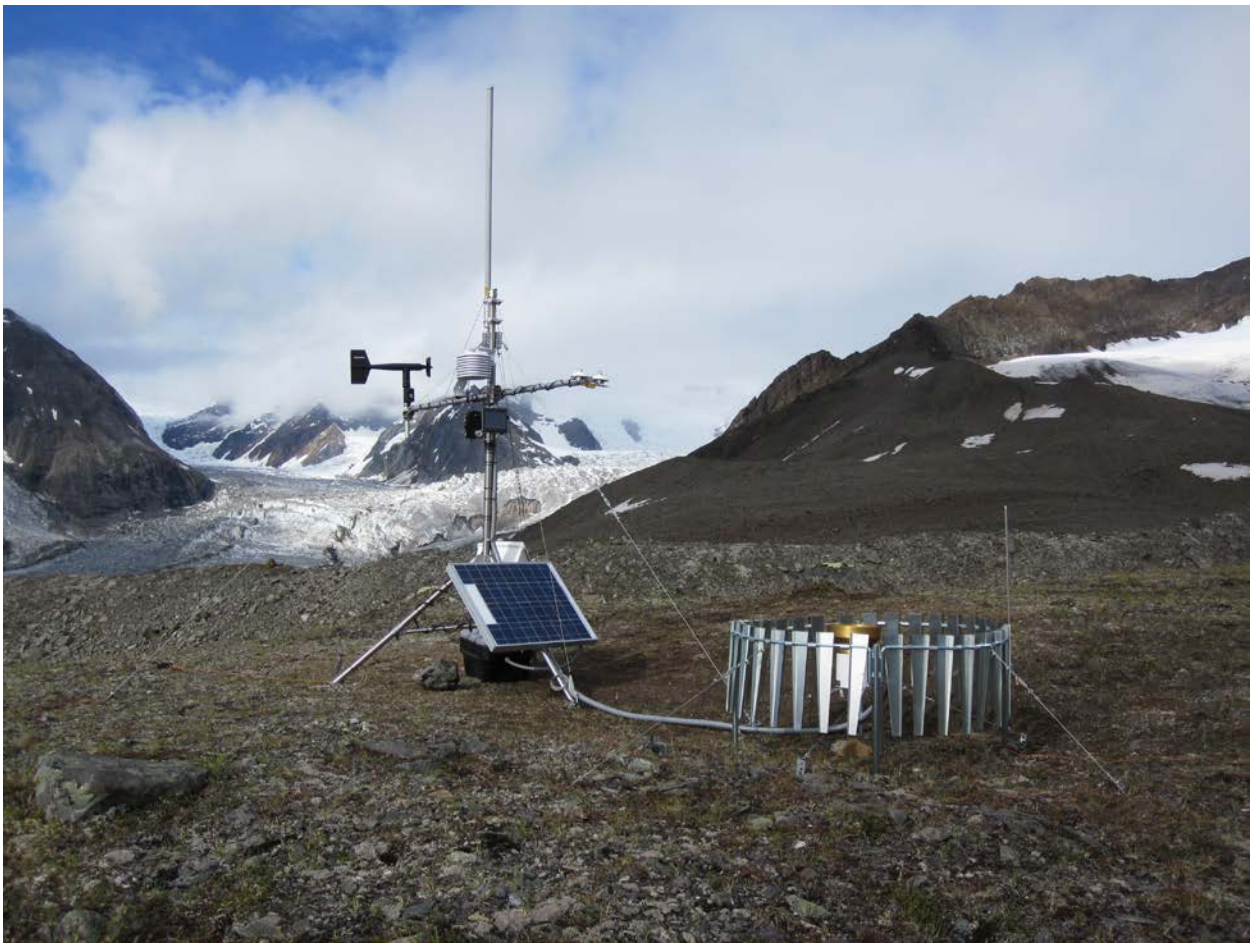

**Figure 5.3.6-1. A northeast-oriented view of the Off-Ice weather station deployed near Susitna Glacier (2012-2014).**

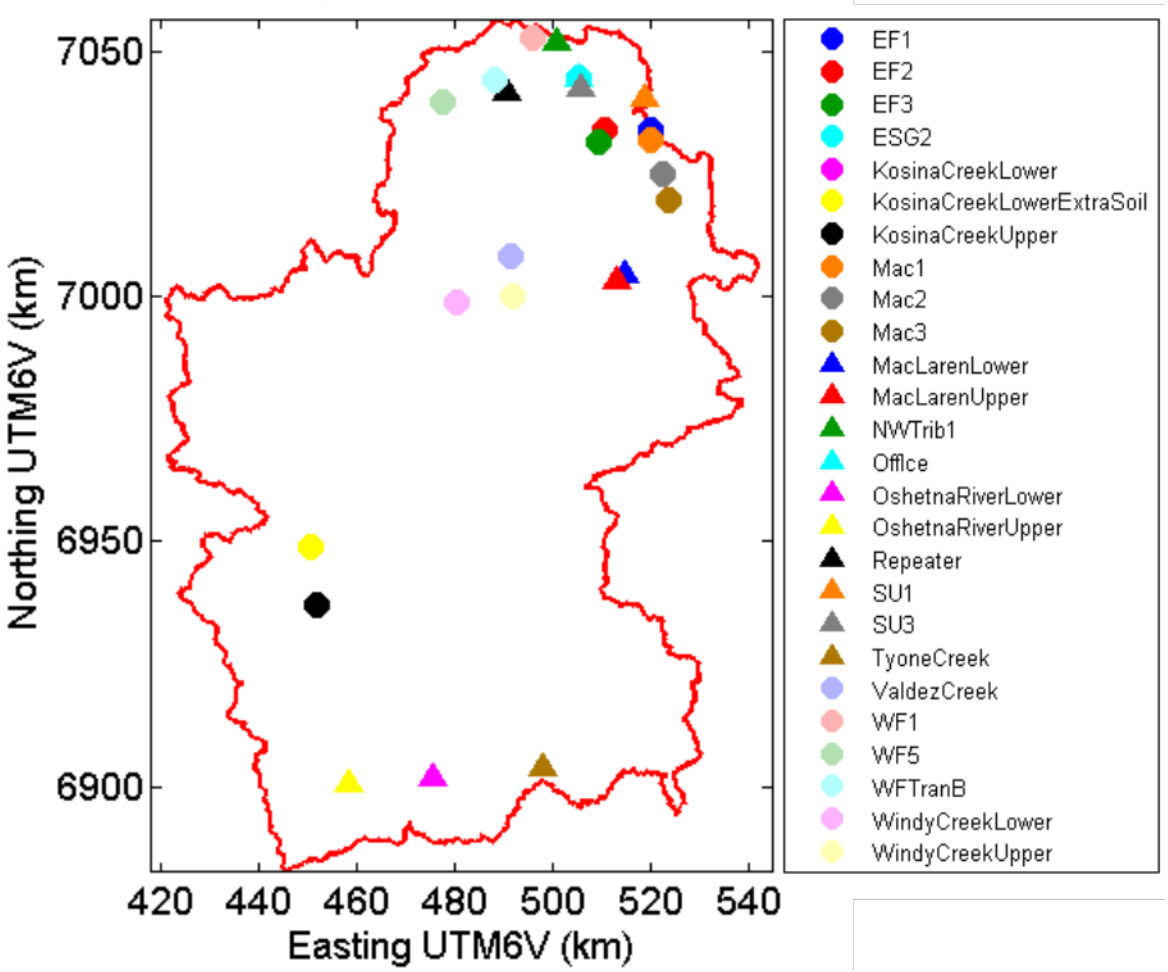


**Figure 5.3.7-1. The location of HOBO (glacier and tundra) weather stations in glacierized and non-glacierized terrain of the upper Susitna basin during the 2012-2014 period.**

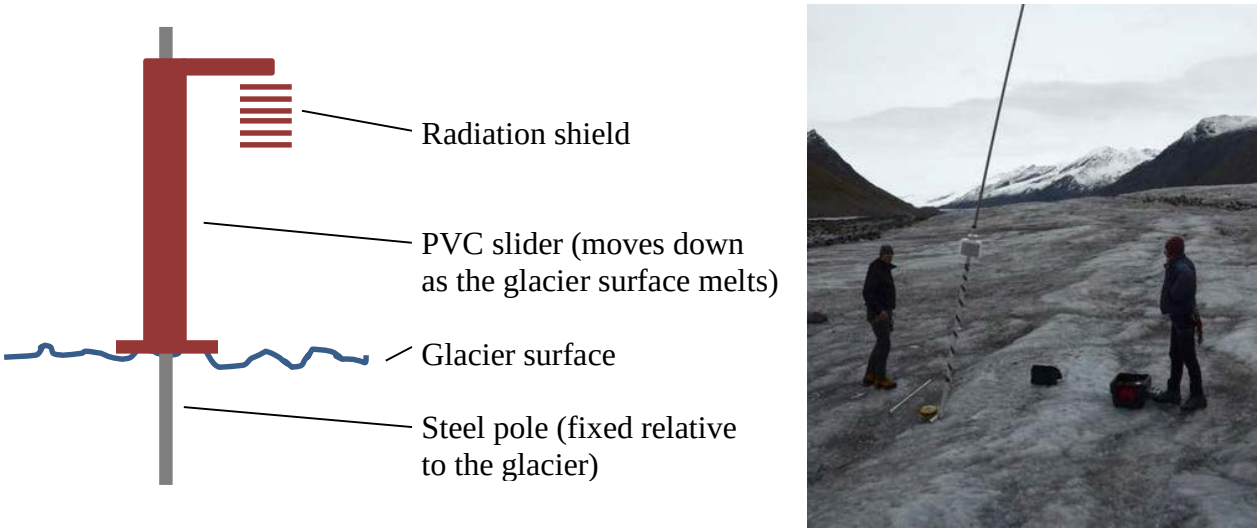


**Figure 5.3.7-2. The design of the glacier weather monitoring stations allowed the sensors to remain at approximately the same height relative to the glacier surface throughout the melt season.**

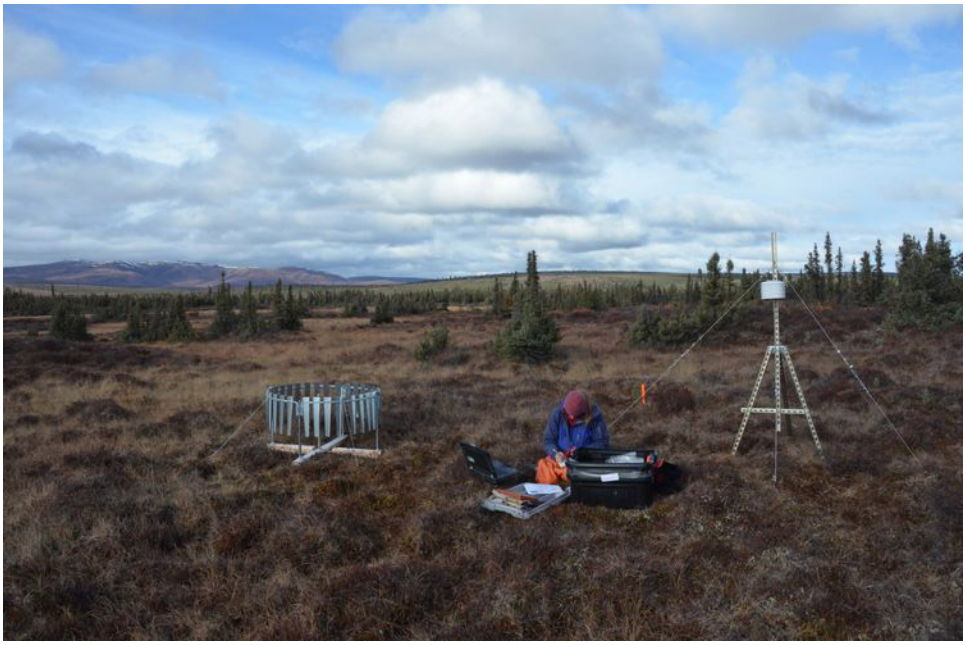

**Figure 5.3.7-3. The design of the typical tundra weather station deployed during the study period 2012-2014.**

**Figure 5.3.7-4. A typical soil pit dug at the tundra weather station locations. Pit depths were usually tens of centimeters deep.**

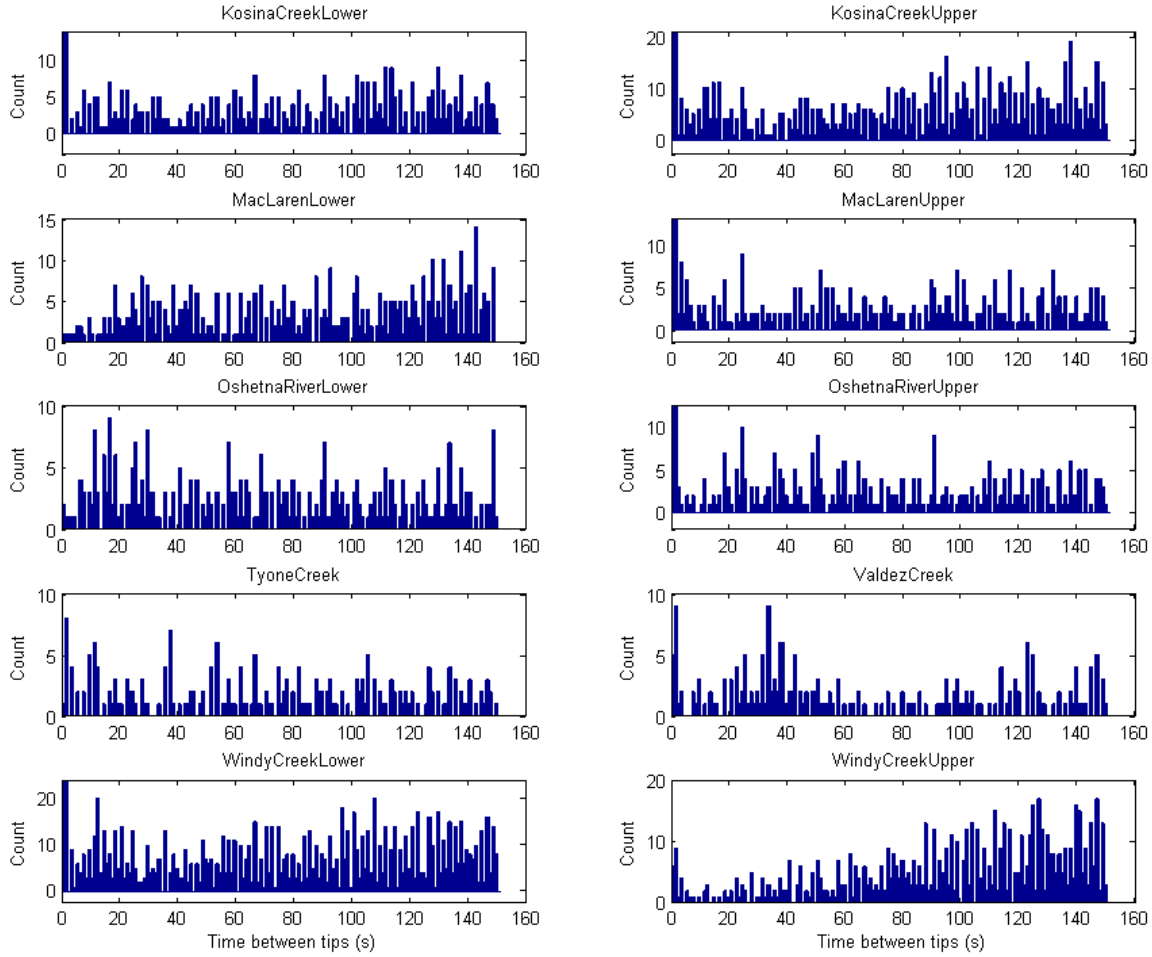


**Figure 5.3.7.1.1-1. Histograms of the time between tips of the precipitation gauges' tipping bucket.**
Tips within 2 seconds of each other were considered to be erroneous. All stations have some double tips, some stations have up to 10% double tips (e.g. both Kosina stations and Windy Lower). There are a number of tips in the range 1-36 seconds too, that are somewhat suspect. 36 seconds between tips is the maximum rainfall rate that can accurately be measured by the sensor. If it is raining harder than that, the water is pouring into the bucket rather than dripping, so some water is lost in the time it takes the bucket to tip.

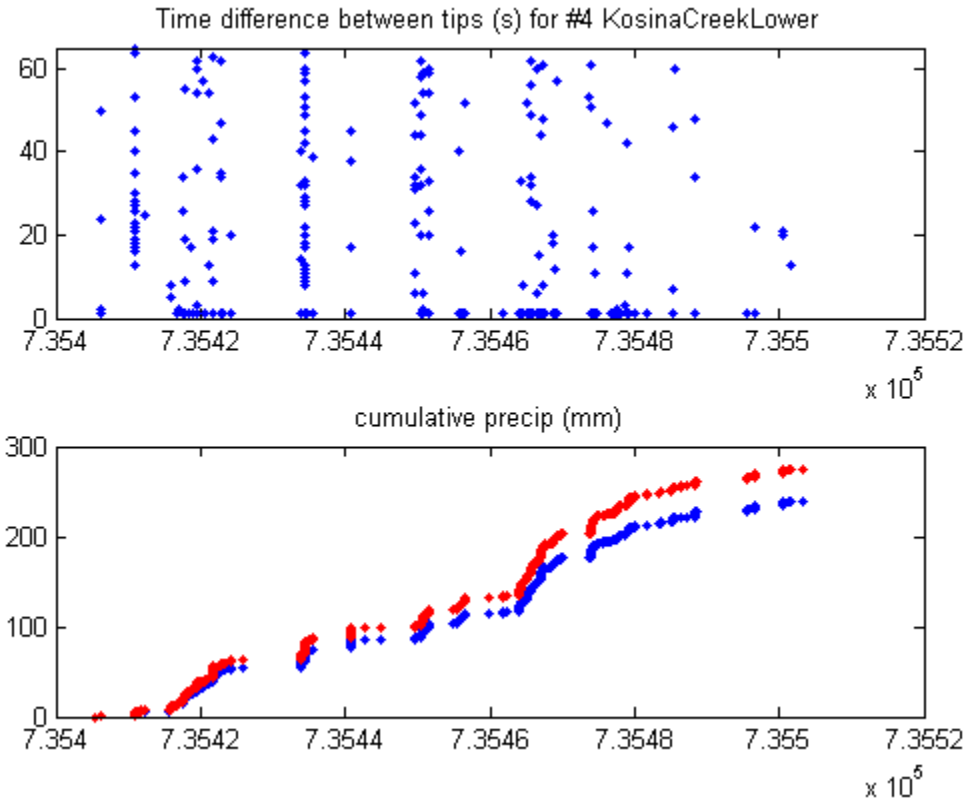


**Figure 5.3.7.1.1-2. Correcting HOBO precipitation gauge (tipping bucket) data.**
The time difference between tips of the tipping bucket rain gauge (upper panel, axis is cut off at 1 minute) illustrates the 'double tip' problem. The lower panel shows cumulative precipitation (uncorrected in red, double tips removed in blue). The analysis done in this report uses the corrected data.

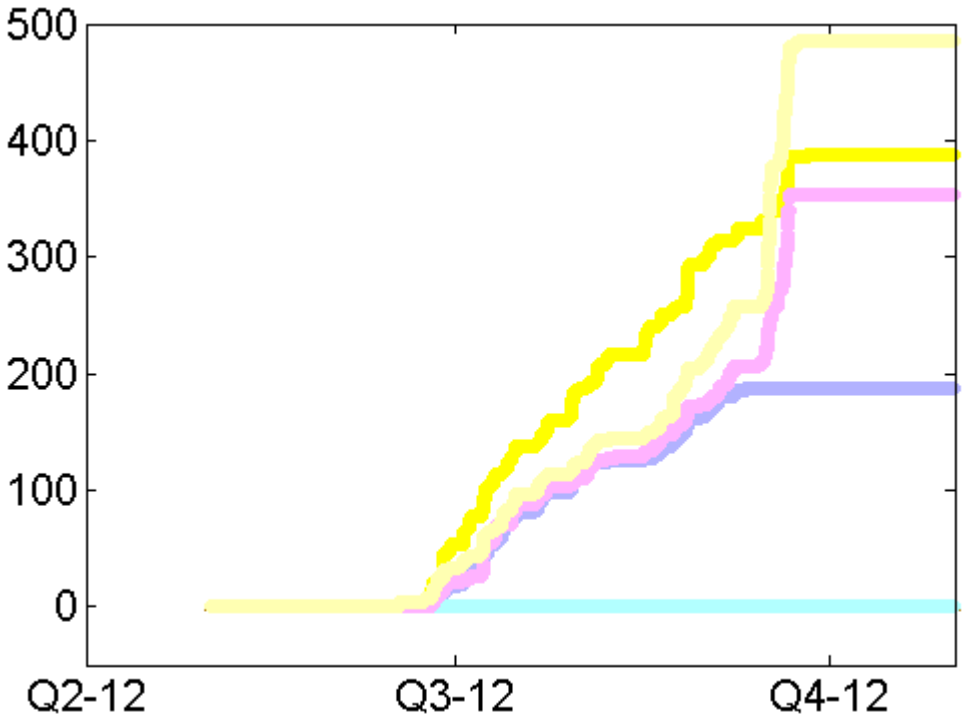


**Figure 5.3.7.2-1. Cumulative measured precipitation (rainfall) for hydrologic year 2012.**
Colors are coordinated with the symbols on the map of HOBO stations. The gauges were installed on June 17 and removed for winter at the end of September.

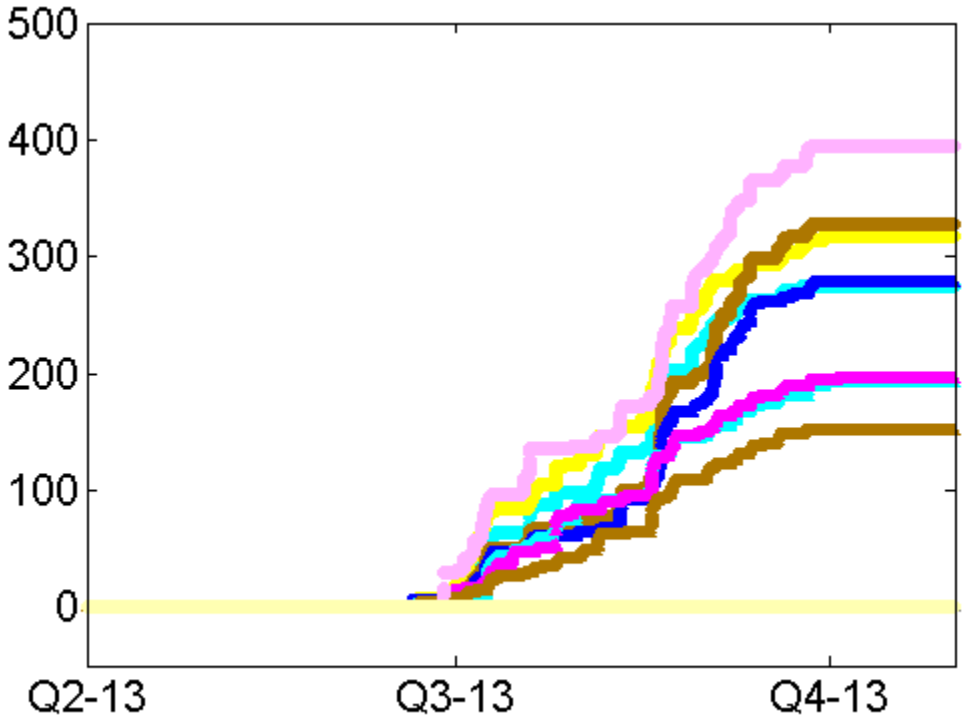


**Figure 5.3.7.2-2. Cumulative measured precipitation (rainfall) for hydrologic year 2013.**
Colors are coordinated with the symbols on the map of HOBO stations. The gauges were installed around June 20 and removed for winter in early October.

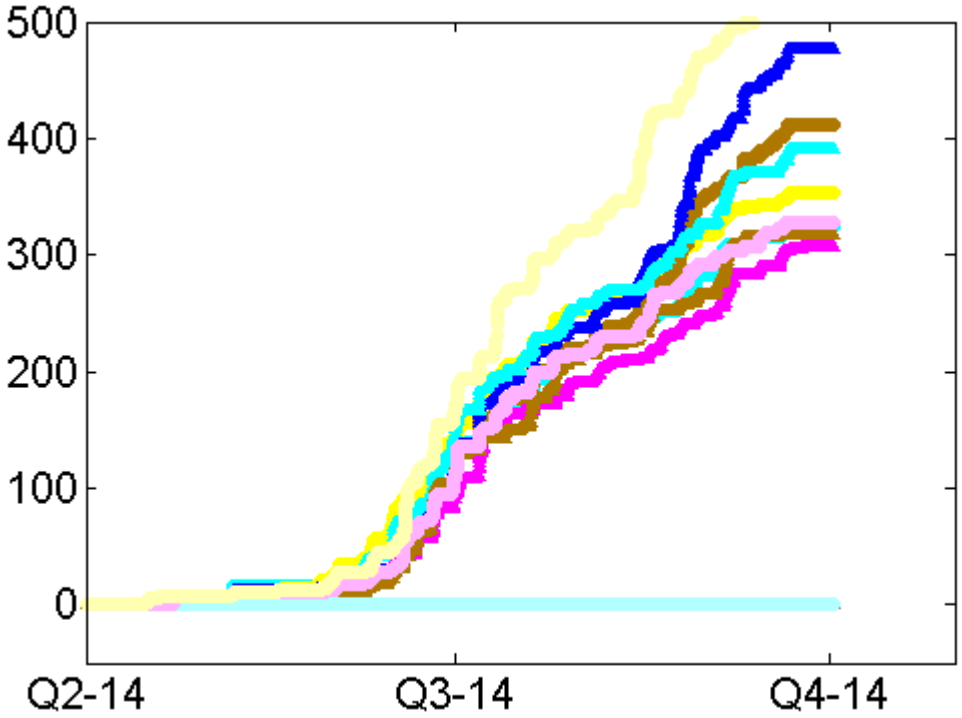


**Figure 5.3.7.2-3. Cumulative measured precipitation (rainfall) for hydrologic year 2014.**
Colors are coordinated with the symbols on the map of HOBO stations. The gauges were installed at the end of April and removed for winter at the end of September.

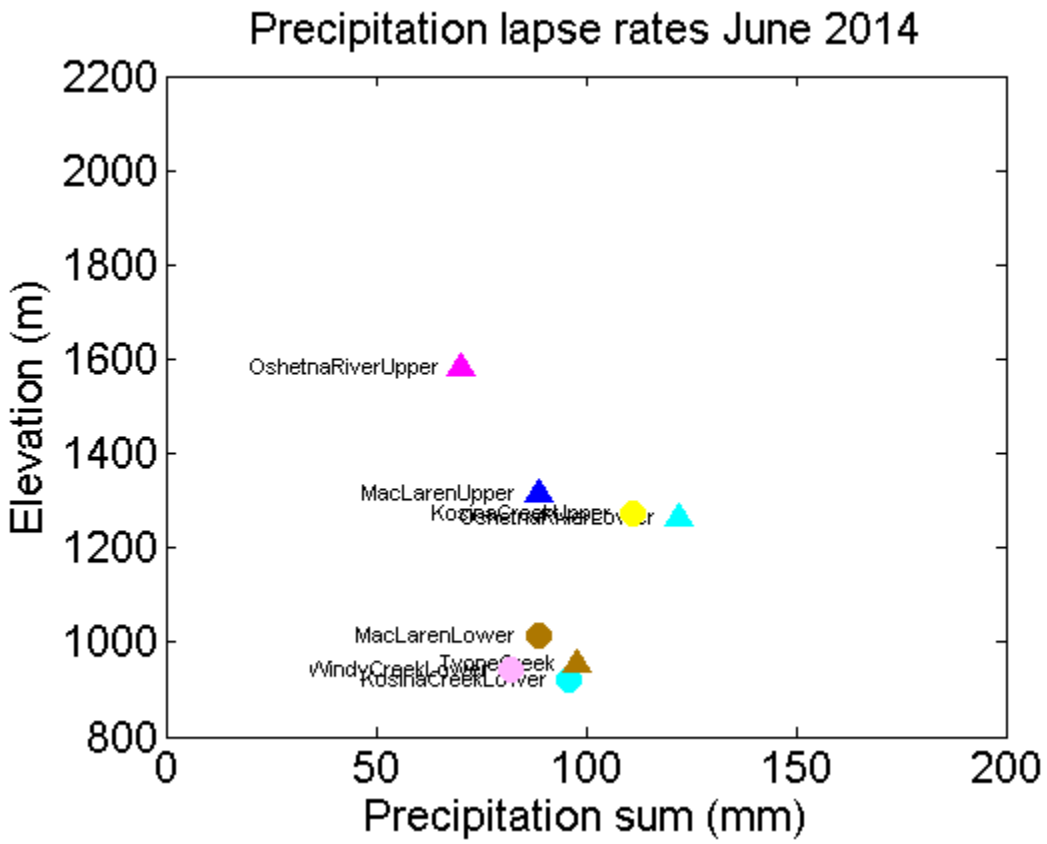


**Figure 5.3.7.2-4. Precipitation lapse rates for June 2014.**
Precipitation varies significantly across small distances. Timing of events is consistent among stations.

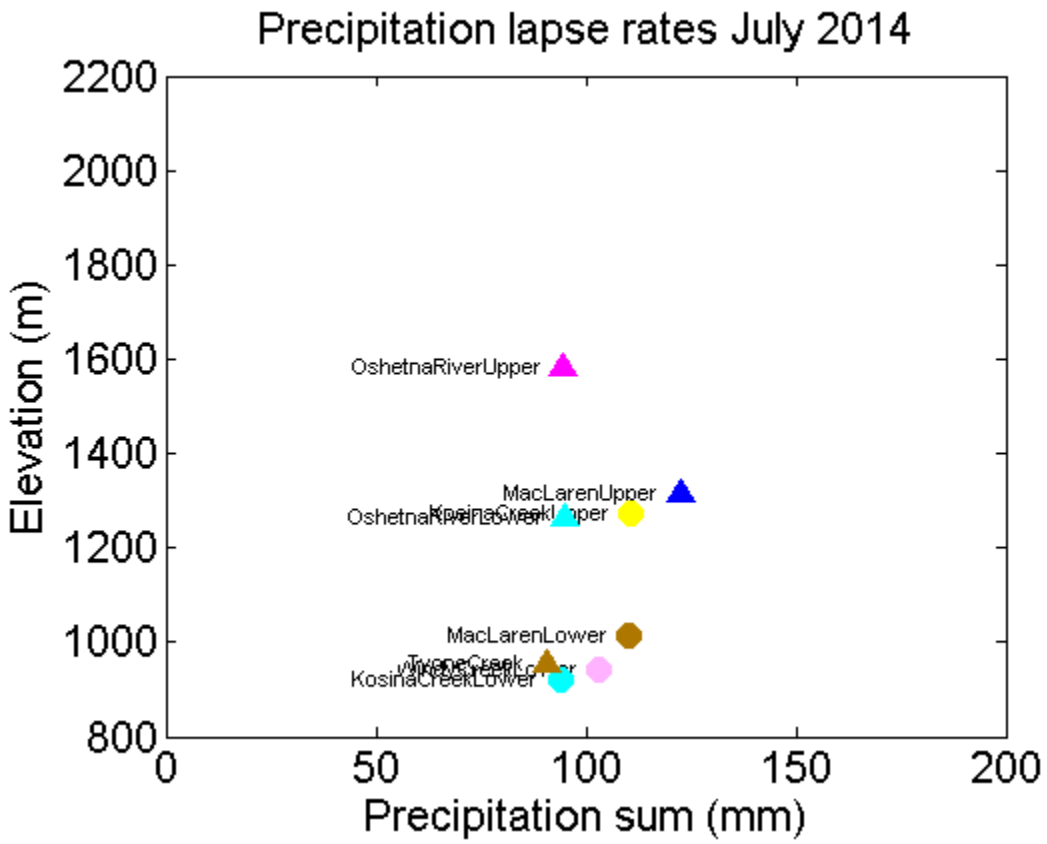


**Figure 5.3.7.2-5. Precipitation lapse rates for July 2014.**

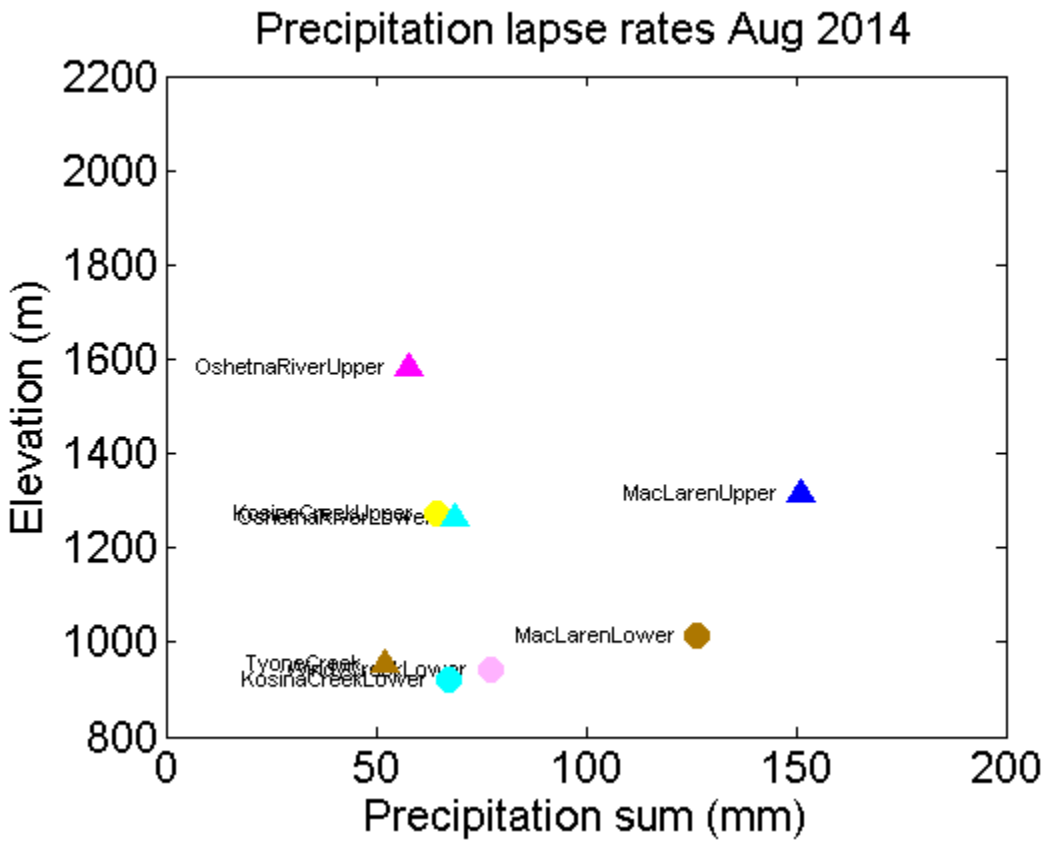


**Figure 5.3.7.2-6. Precipitation lapse rates for August 2014.**

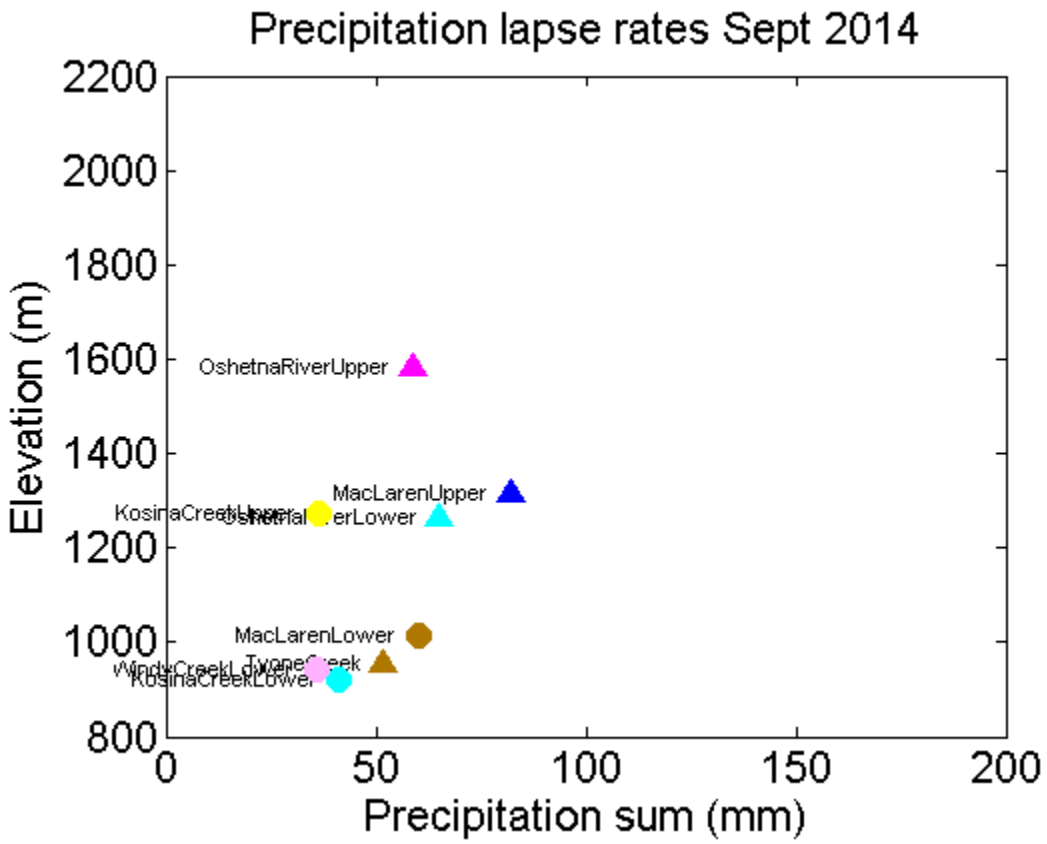


**Figure 5.3.7.2-7. Precipitation lapse rates for September 2014.**

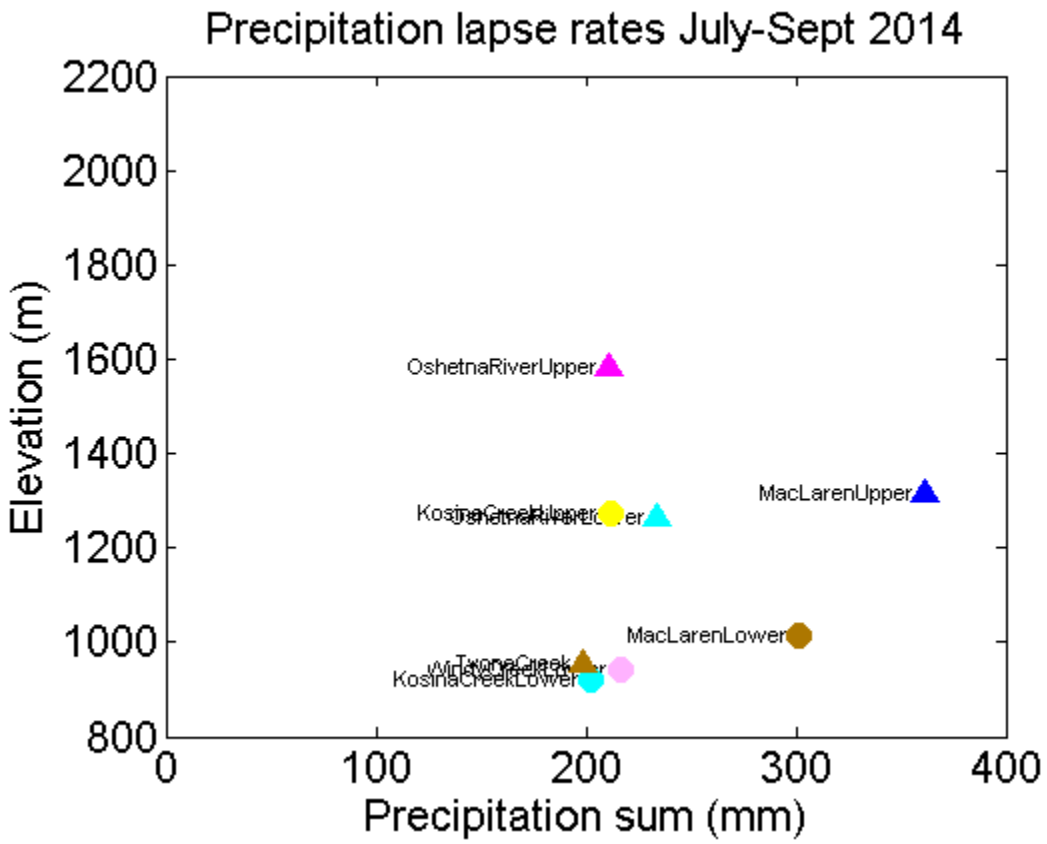


**Figure 5.3.7.2-8. Precipitation lapse rates for July-September 2014.**

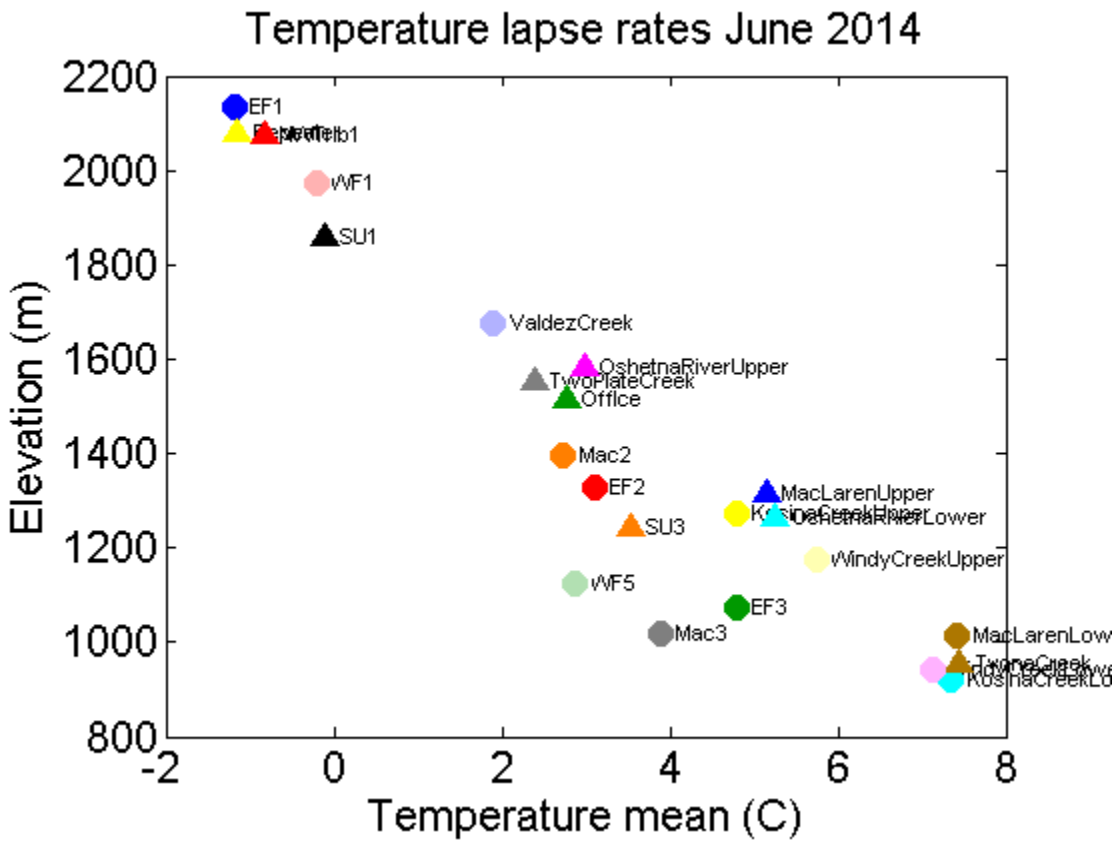


**Figure 5.3.7.2-9. Temperature lapse rates for June 2014.**
Temperature lapse rates for just the upper Susitna Basin show a larger temperature gradient for the off-ice stations compared to the on-ice stations. In summer, when air temperatures are above freezing, the ice surface cools air descending over the glacier, partially offsetting adiabatic warming.

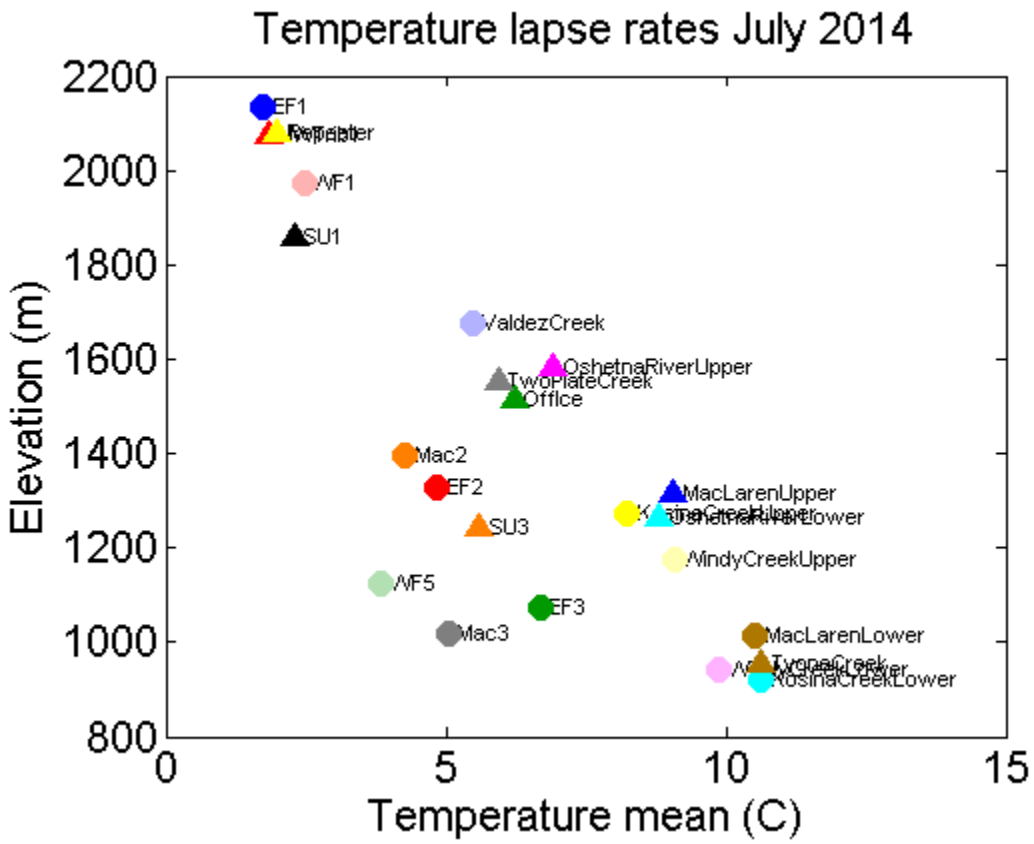


**Figure 5.3.7.2-10. Temperature lapse rates for July 2014.**

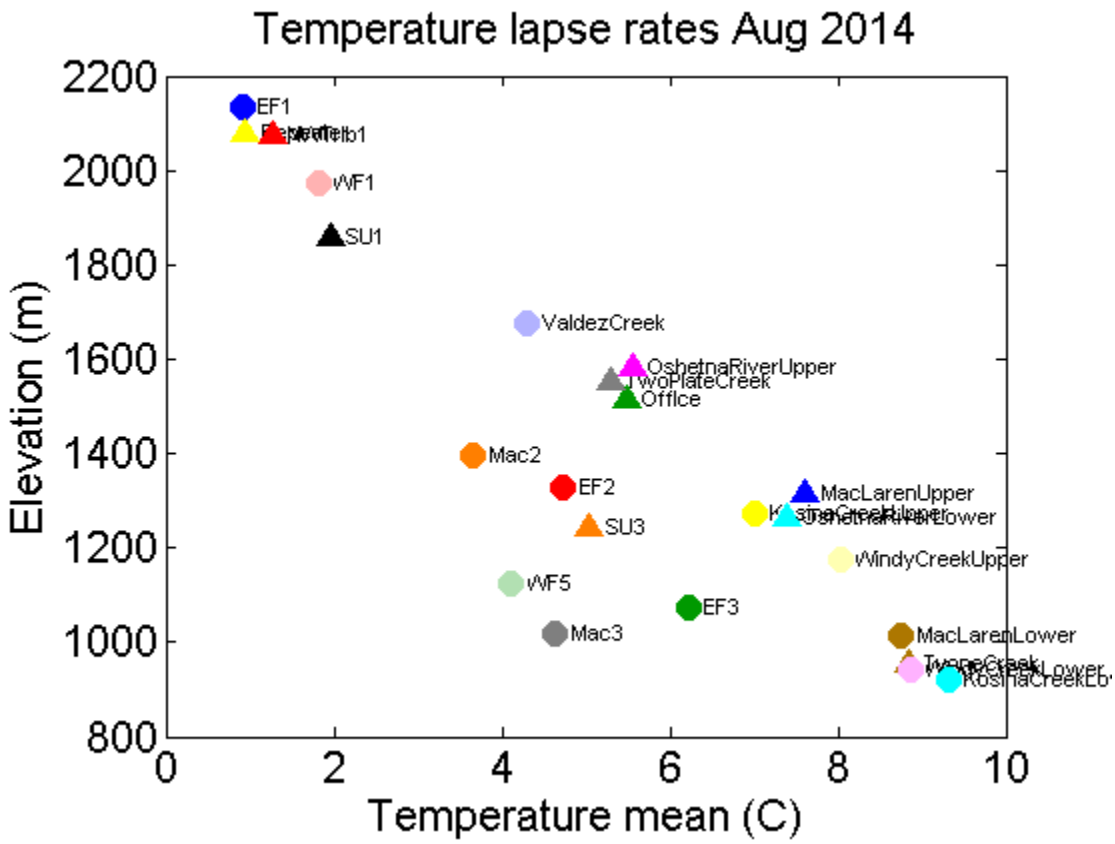


**Figure 5.3.7.2-11. Temperature lapse rates for August 2014.**

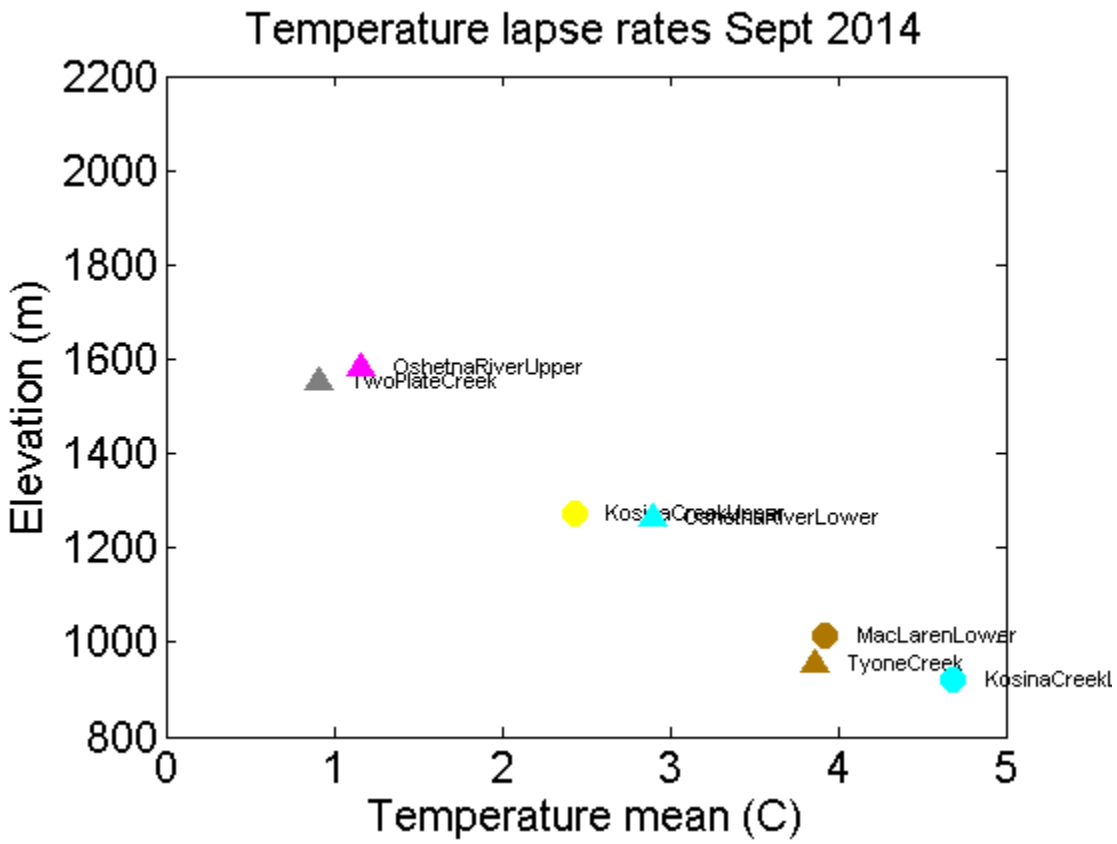


**Figure 5.3.7.2-12. Temperature lapse rates for September 2014.**

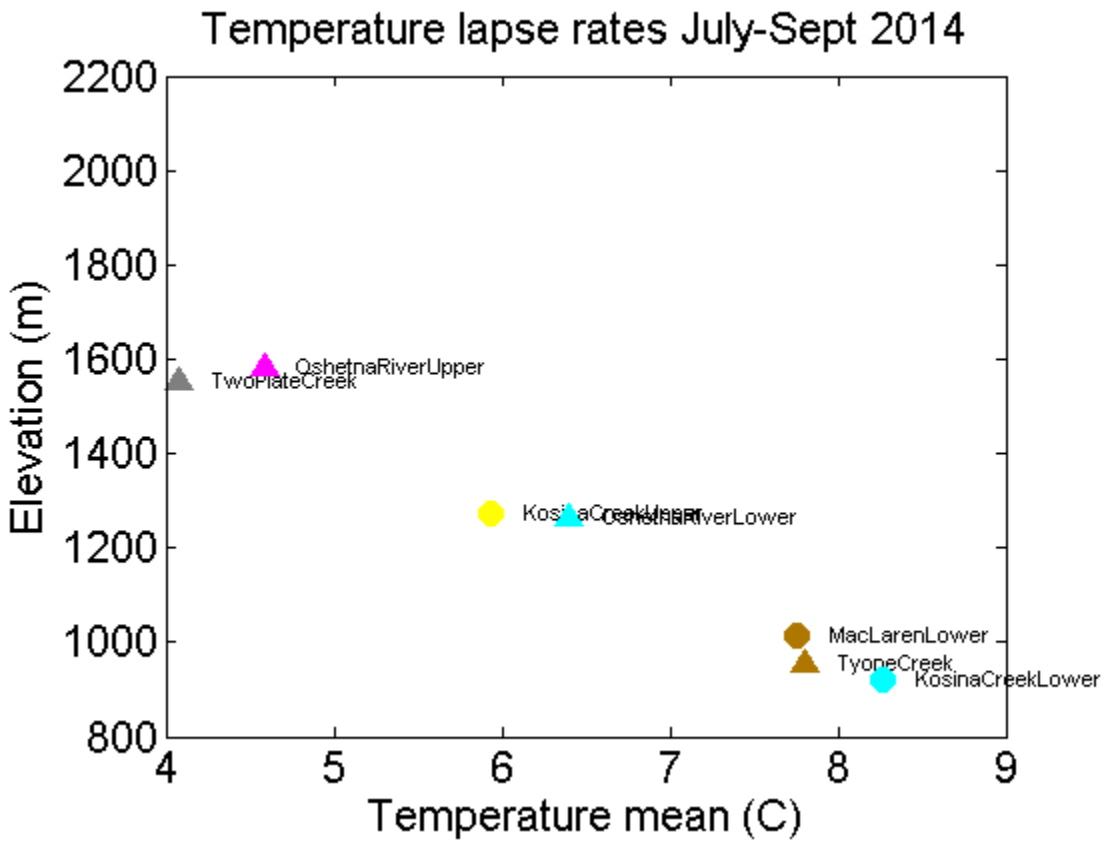


**Figure 5.3.7.2-13. Temperature lapse rates for July-September 2014.**

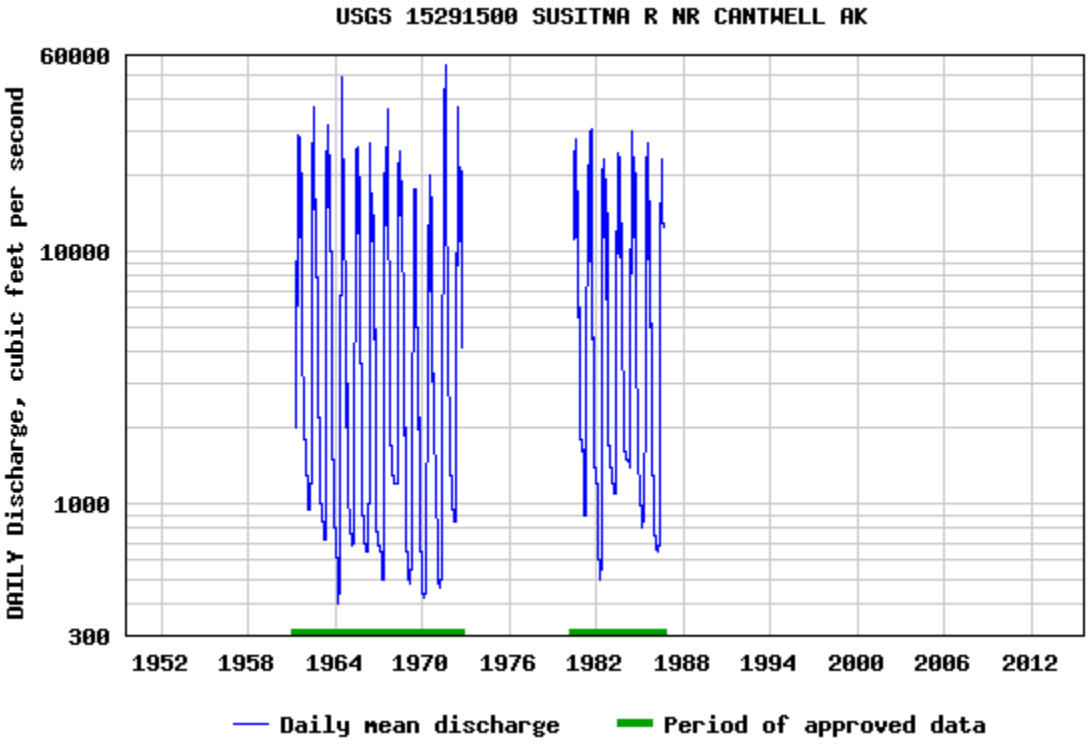


**Figure 5.4-1. Daily mean discharge record for station SUSITNA R NR CANTWELL AK.**

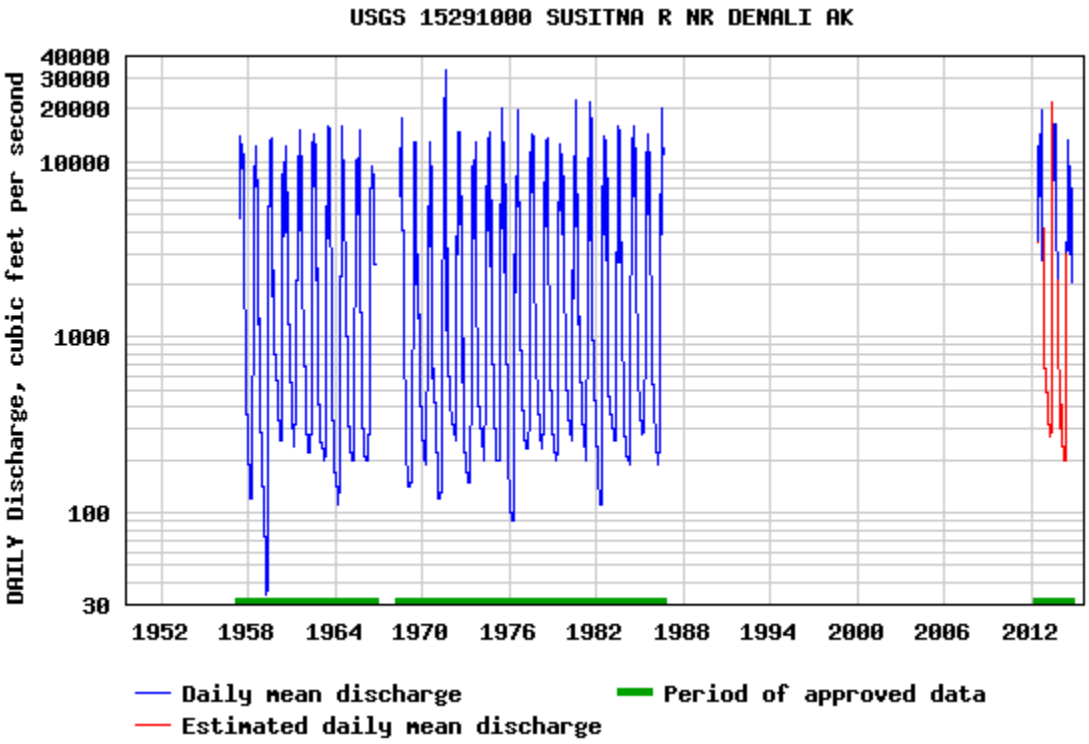


**Figure 5.4-2. Daily mean discharge record for station SUSITNA R NR DENALI AK.**

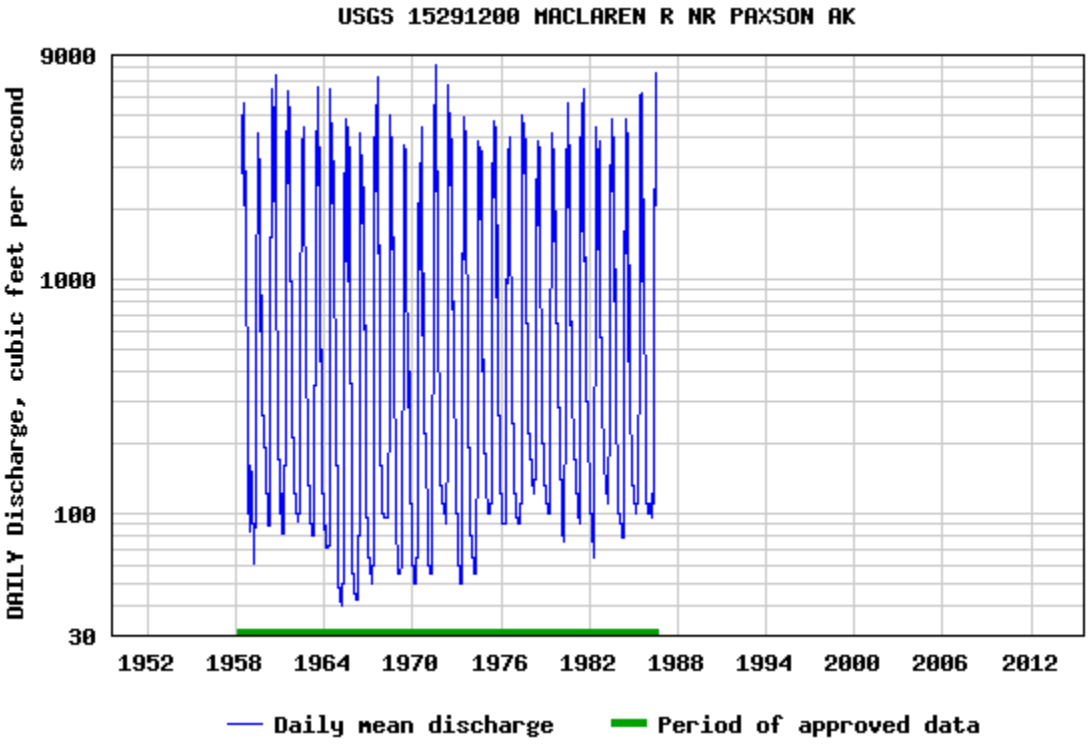


**Figure 5.4-3. Daily mean discharge record for station MACLAREN R NR PAXSON AK.**

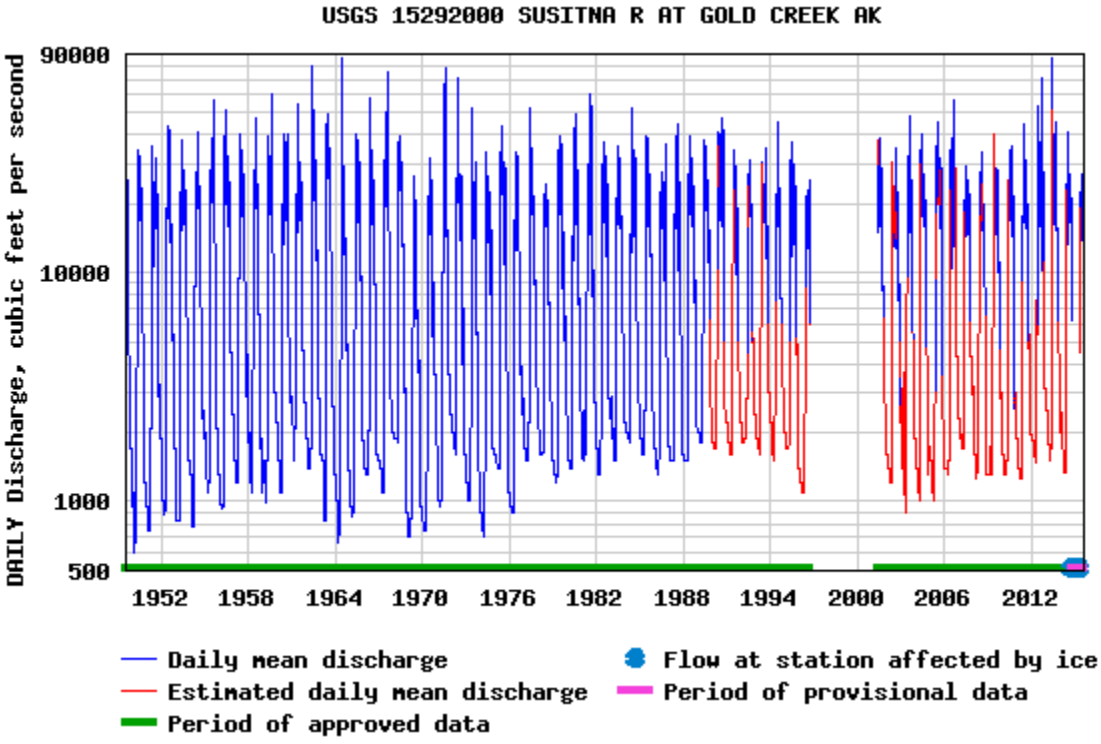


**Figure 5.4-4. Daily mean discharge record for station SUSITNA R AT GOLD CREEK AK.**

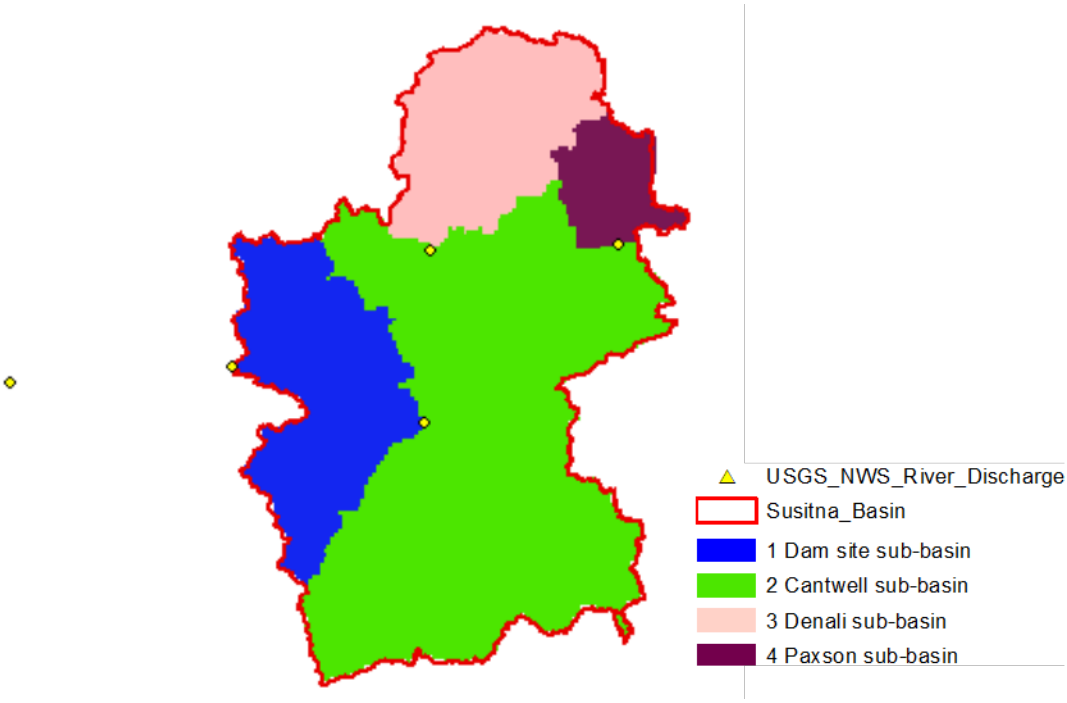


**Figure 5.4-5. Watershed boundaries calculated on a 1 km grid, and used for WaSiM modeling.** Relatively small differences exist compared to the USGS and 1 km grid boundaries (EZG).

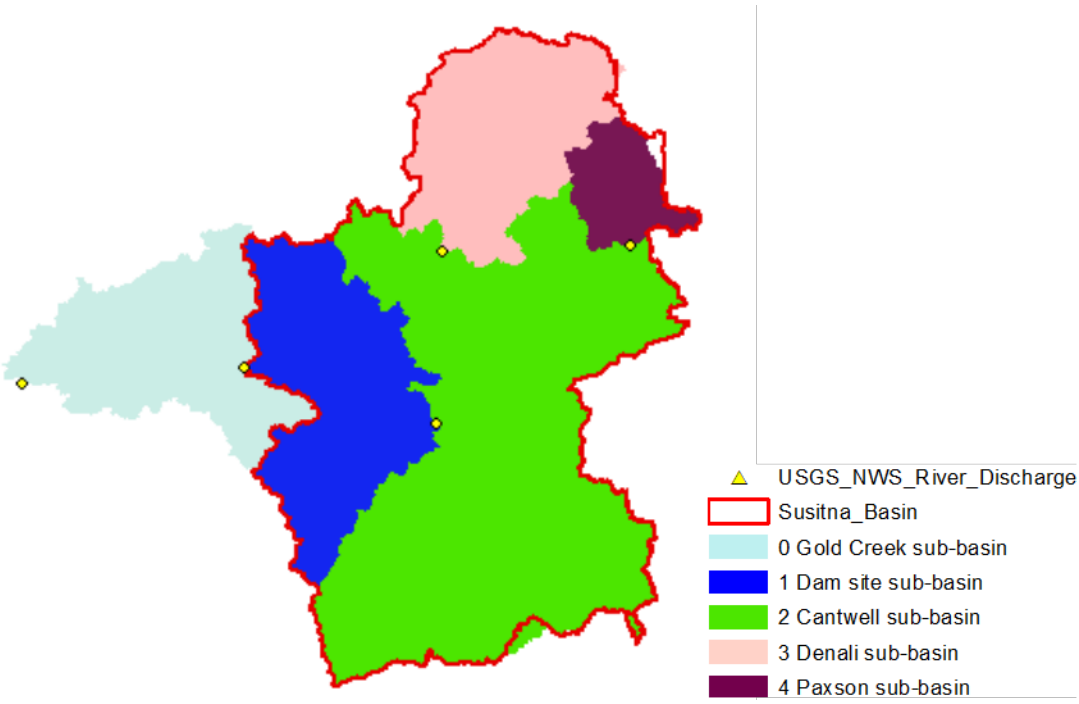


**Figure 5.4-6. Watershed and sub-basin boundaries calculated on a 30 m grid, with gauge locations placed as accurately as possible.**

In the 30 m version: Windy Creek is in Denali instead of Cantwell, Eureka Glacier is missing instead of present, Cantwell has extra area along the southern boundary of the watershed, the Dam Site basin is more extensive along the eastern boundary with the Cantwell basin. The areas of dispute tend to have flat topography where a subtle difference in the DEM can shift an area from one drainage to another.

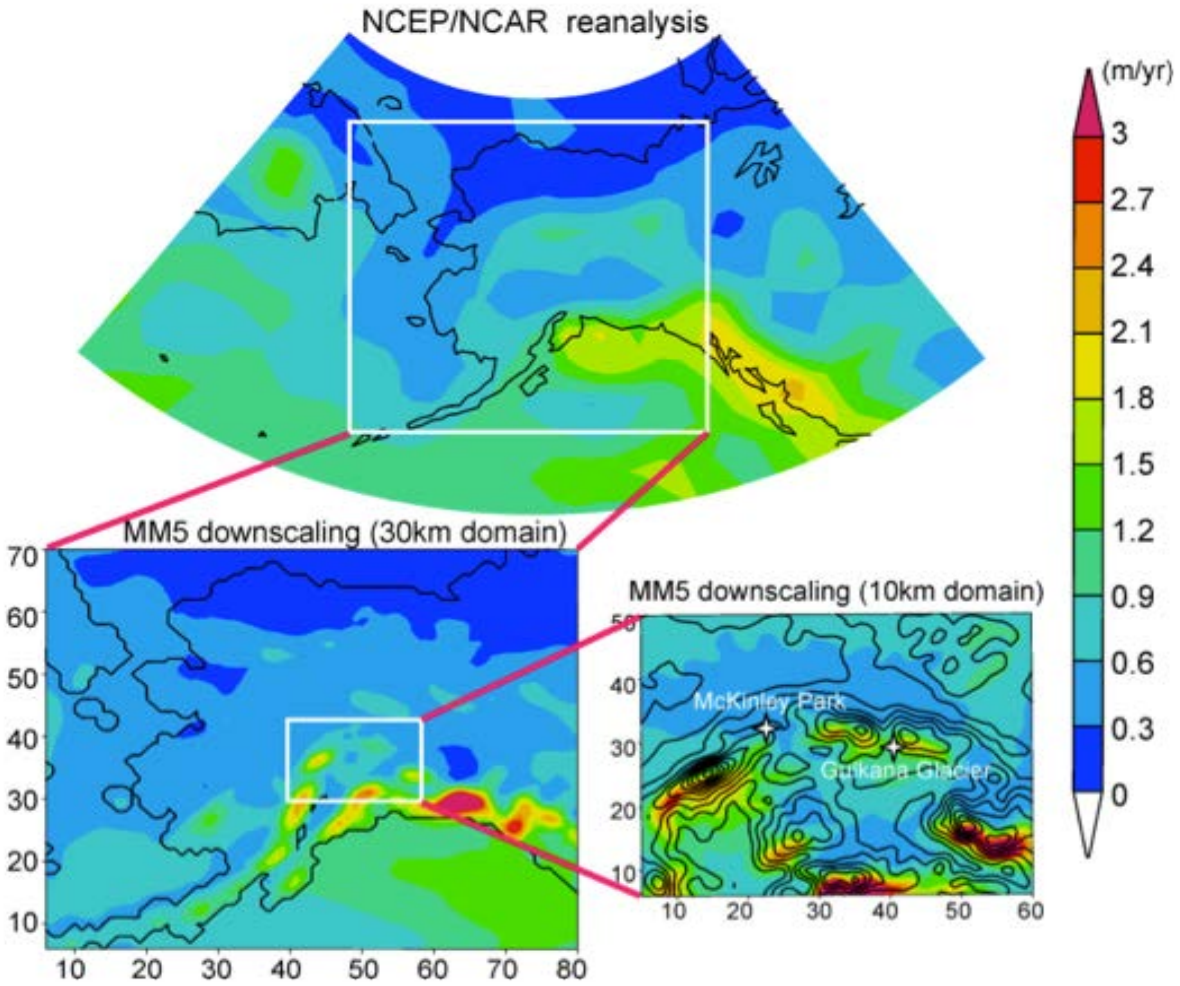


**Figure 5.5-1. Comparisons of annual mean precipitation during 1994-2004 from the global reanalysis (2.5ºx2.5º), 30km and 10km downscaling (topography in black contour and precipitation in color) (Zhang *et al.* 2007a).**

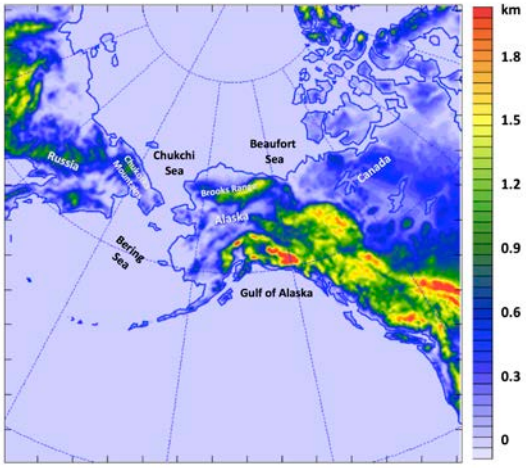


**Figure 5.5.1-1. The downscaling domain, including Alaska, northwest Canada, easternmost Russia, and the surrounding ocean including the Beaufort, Chukchi, and Bering Seas.**
The color bar indicates kilometers of elevation above sea level.

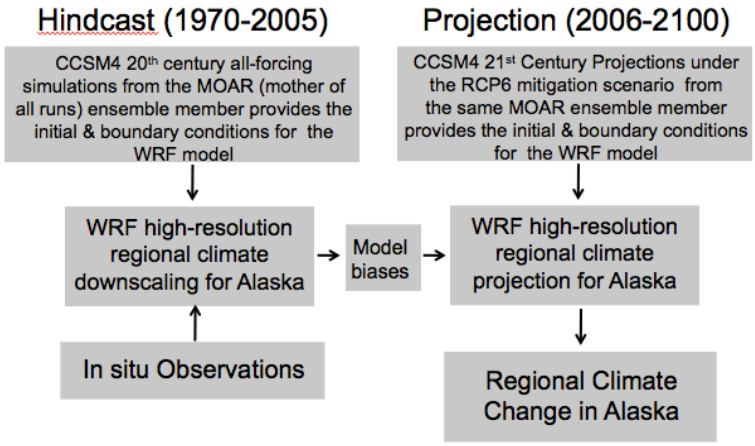


**Figure 5.5.1-2. The downscaling simulation design.**

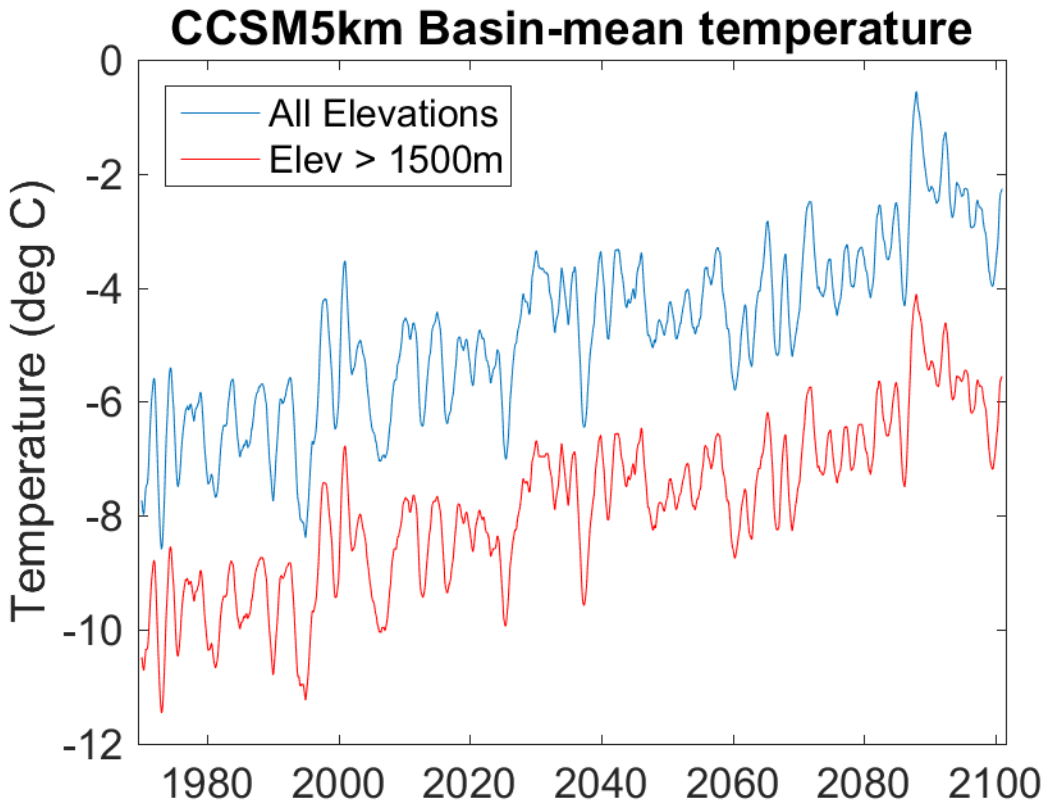


**Figure 5.5.2-1. Projected mean surface air temperature for the upper Susitna basin.**
Temperature averaged across the whole upper Susitna basin is increasing with time (blue). Projections from the 5 km resolution climate product downscaled from a CCSM4 (RCP6.0) run (see section 5.5). Data are smoothed with a triangular filter which weights the central point highest and considers 365 points (one year) on either side. Areas above 1500 m a.s.l. are also warming at approximately the same rates as the whole basin (red).

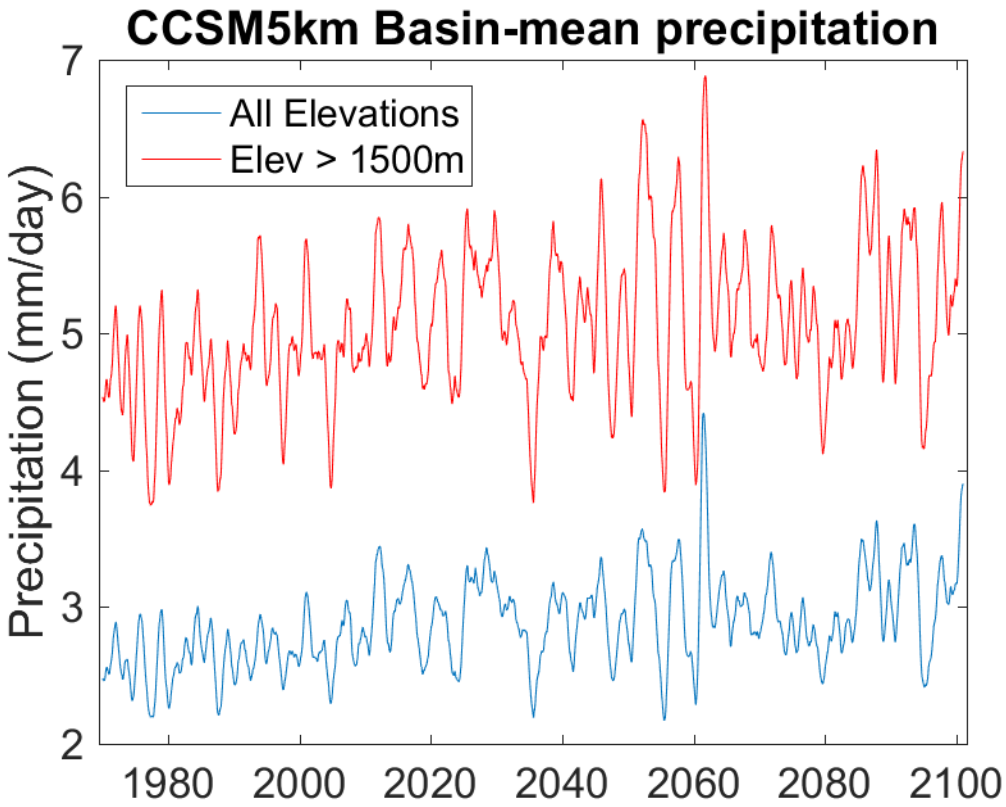


**Figure 5.5.2-2. Projected mean precipitation for the upper Susitna basin.**
Precipitation averaged across the whole upper Susitna basin exhibits a slight increase with time (blue). Projections from the 5 km resolution climate product downscaled from a CCSM4 (RCP6.0) run (see section 5.5). Data are smoothed with a triangular filter which weights the central point highest and considers 365 points (one year) on either side. Areas above 1500 m a.s.l. also show a slight increase in precipitation over time (red).

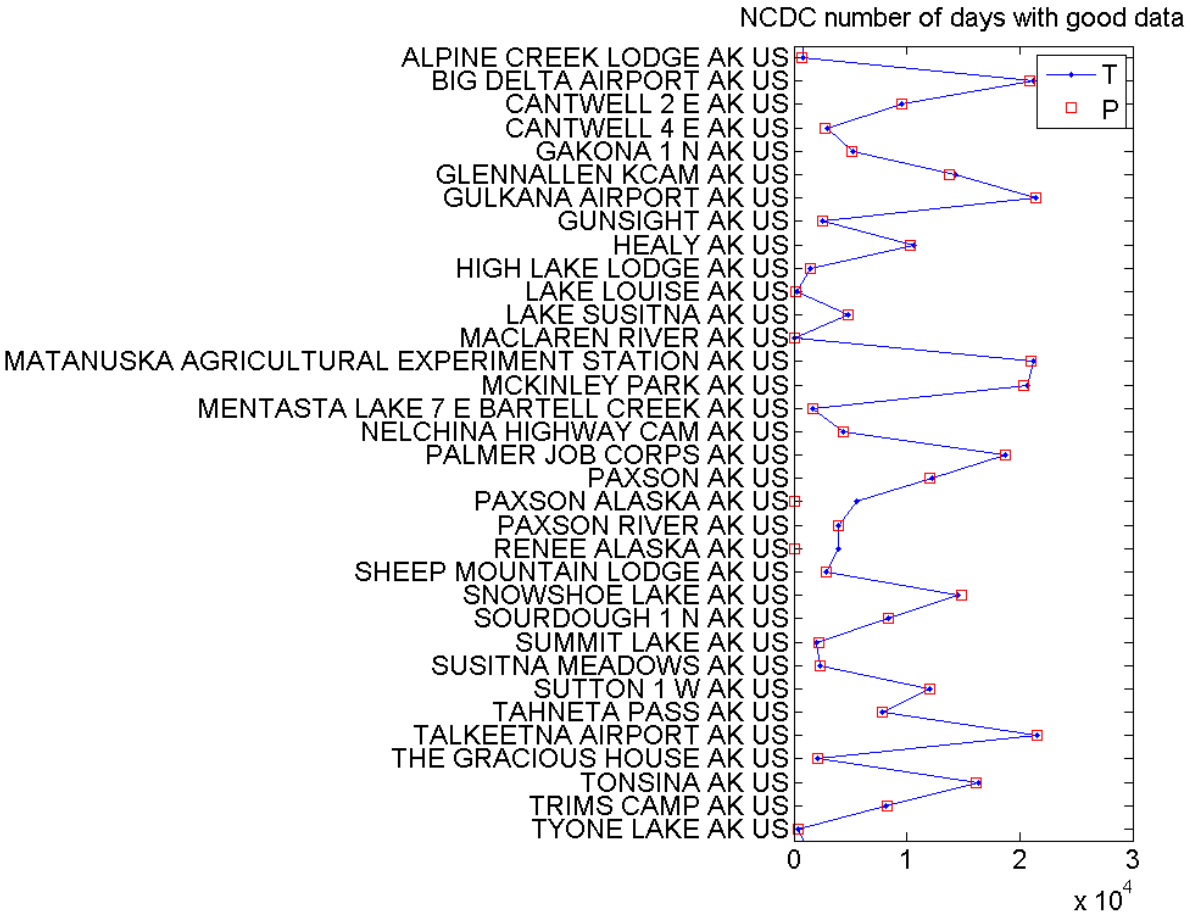


**Figure 5.5.3-1. The 10 longest records were identified from the NCDC stations near the upper Susitna Basin.** These 10 stations were used in the bias correction of the CCSM WRF 5 km climate product. The number of days with good data is shown for temperature (blue line) and precipitation (red squares).

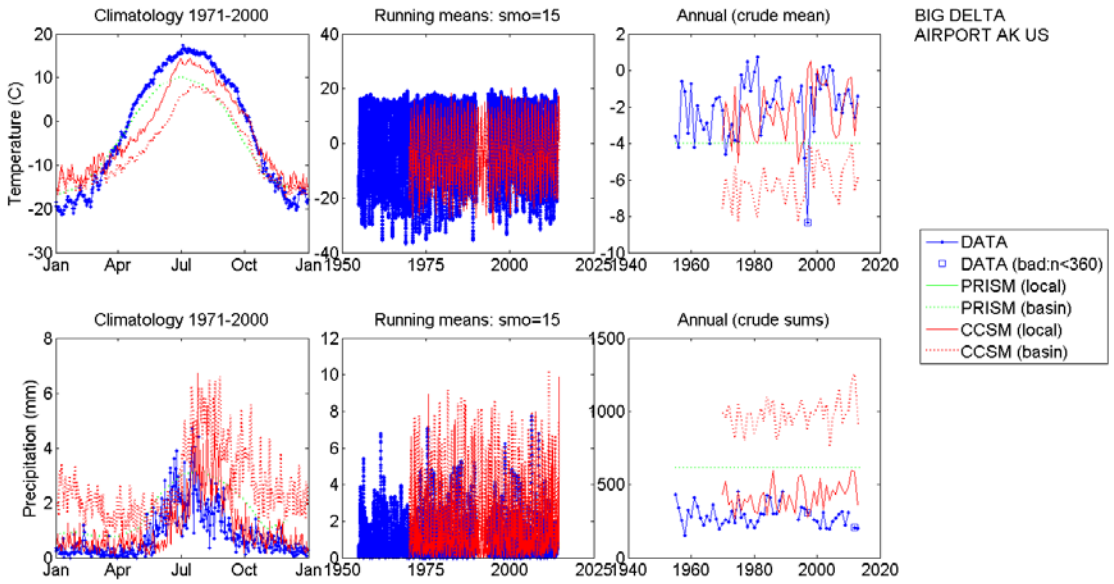


**Figure 5.5.3-2. This set of plots compares station data (station name listed in the upper right) to CCSM WRF 5km time series and PRISM climatology.**
The upper row is for temperature (degrees C) and the lower row is for precipitation (mm). The left plots show the climatology from 1971-2000. The middle plots show the time series, smoothed with a 15-day filter. The right plots show the time series of annual means for temperature and annual sums for precipitation. The lines on each plot represent different data sets: station data (blue solid line), PRISM at the nearest grid cell (green solid), PRISM averaged over the whole upper Susitna basin (green dotted), CCSM WRF at the nearest grid cell (red solid), CCSM WRF averaged over the whole upper Susitna basin (red dotted). In the right-most plots the blue squares represent years where the station had less than 360 days of good data, so the means and sums should be treated as suspect.

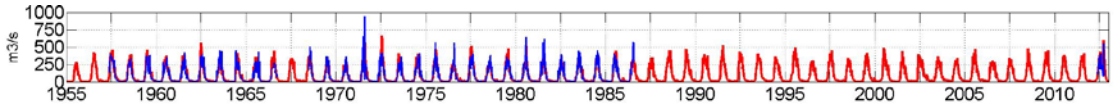


**Figure 6.1.3-1. Measured (red) and modeled (blue) daily discharge at the Susitna River near Denali gauging station for the period 1955 - 2012.**

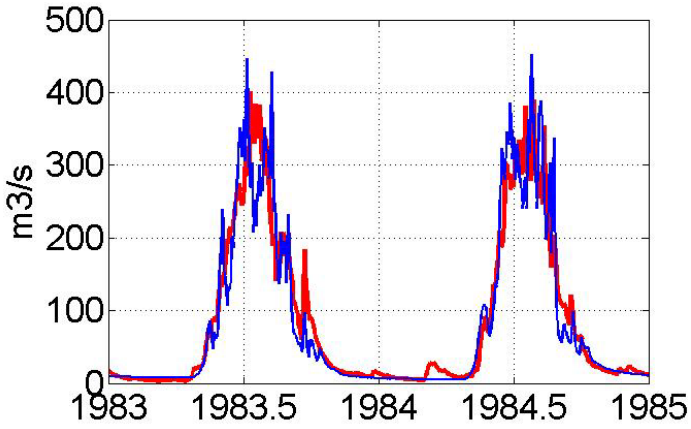


**Figure 6.1.3-2. Measured (red) and modeled (blue) daily at the Susitna River near Denali gauging station for the period 1983 – 1985.**

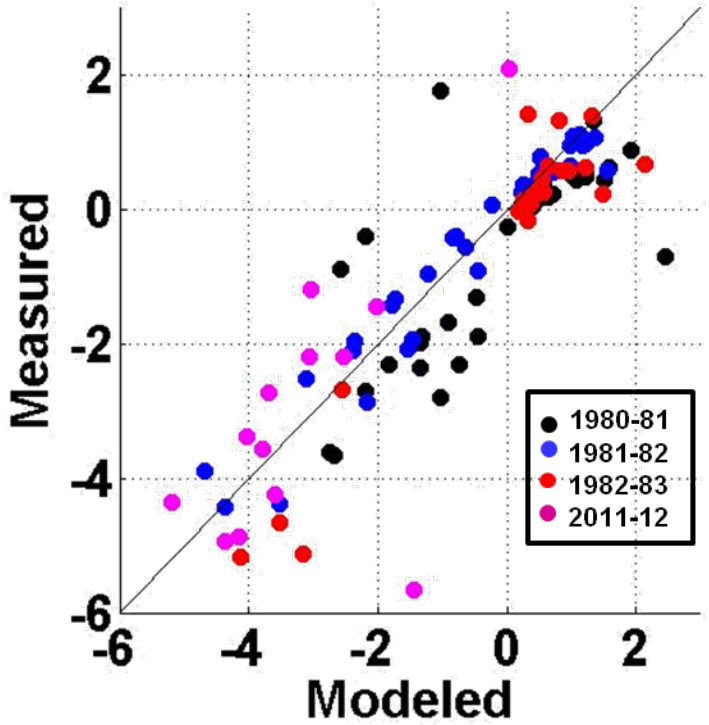


**Figure 6.1.3-3. Measured versus modeled annual mass balances (m w.e. $yr^{-1}$) for individual locations on the glaciers.**

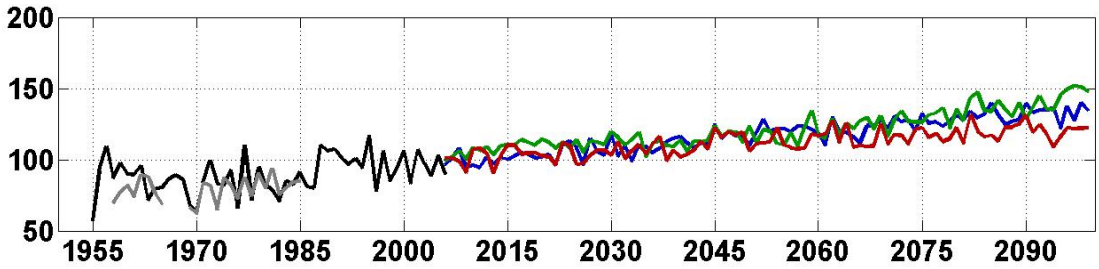


**Figure 6.1.4-1. Modeled annual discharge ($m^3$ $s^{-1}$) at Susitna River near Denali using temperature and precipitation observations for the past and the SNAP climate scenarios based on three emission scenarios (A1B: blue; A2: green; B1: red) for the period 2003-2100.**
The light grey line shows the observed discharge.

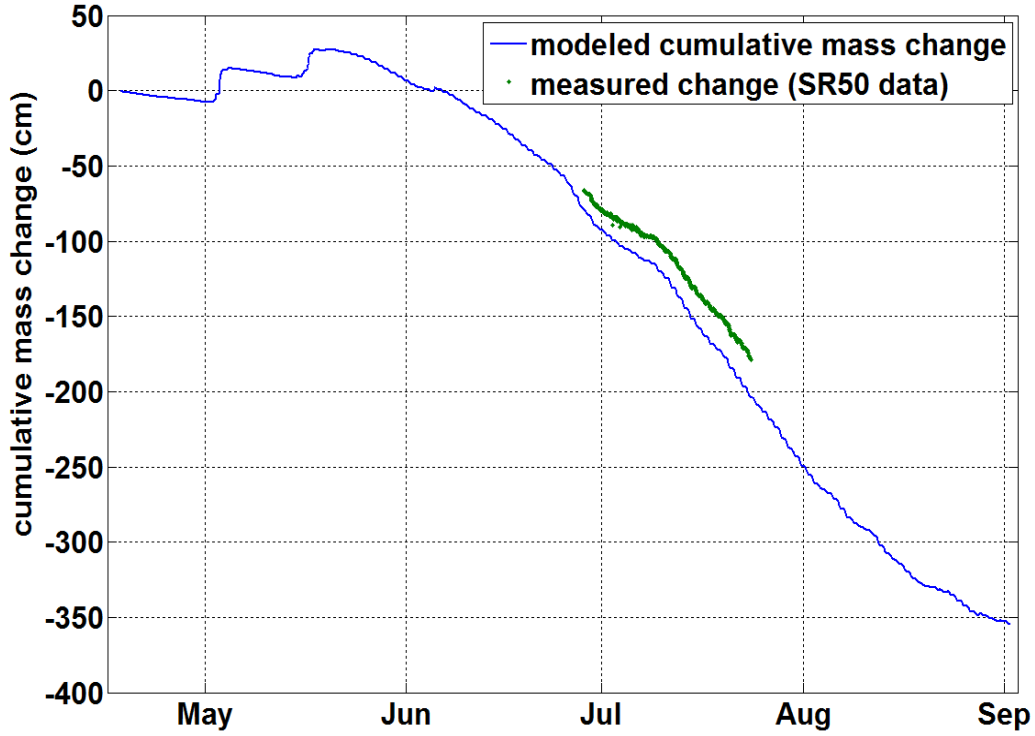


**Figure 6.2.1-1. Cumulative mass change at ESG1.**
Modeled (blue) and measured (green) cumulative daily mass change at ESG1 on West Fork Glacier during the period 15 April and 2 September 2013. Modeled values are based on an energy-balance approach. Measurements are obtained from an ultra-sonic sensor that measures the distance of the fixed the sensor height to the changing glacier surface.

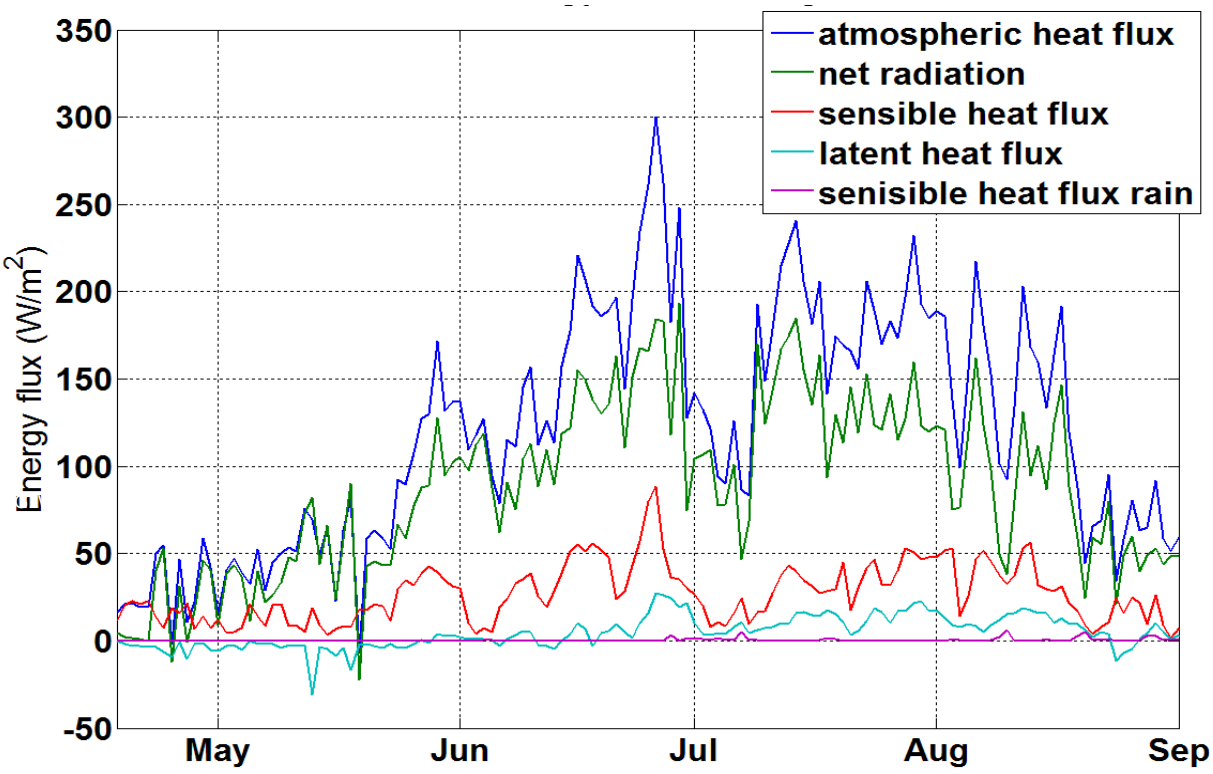


**Figure 6.2.1-2. Energy flux partitioning.**
Daily energy fluxes at the glacier surface at the on-ice weather station ESG1 on West Fork Glacier during the period 15 April and 2 September 2013. The atmospheric energy flux is the sum of all other fluxes, thus indicating how much energy is available for melt.

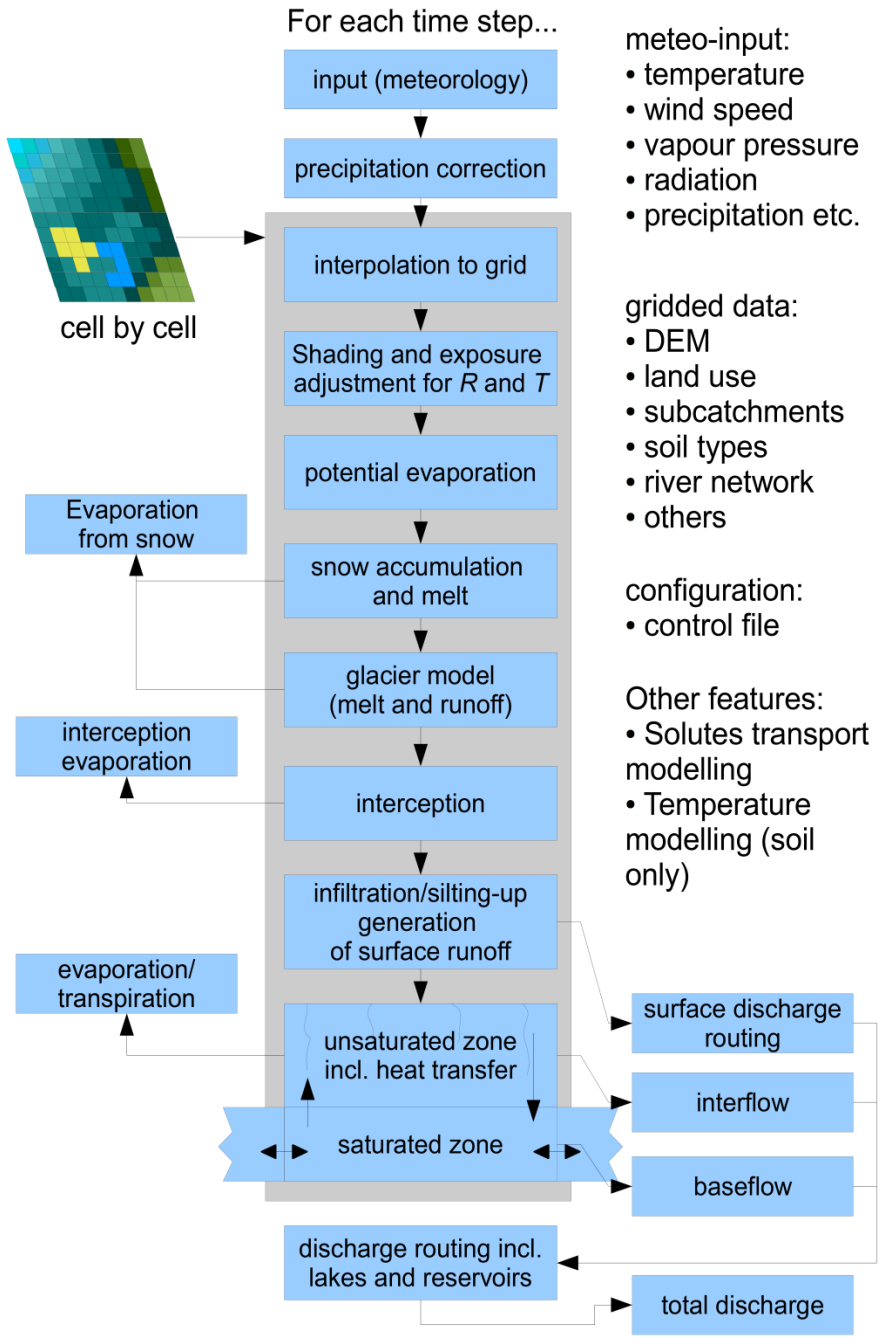


**Figure 7.1-1 WaSiM model structure.**
The modules shown on a grey background simulate the water flow per grid cell while the remaining modules are calculated on the basis of sub-catchments (Schulla, J., 2012b).

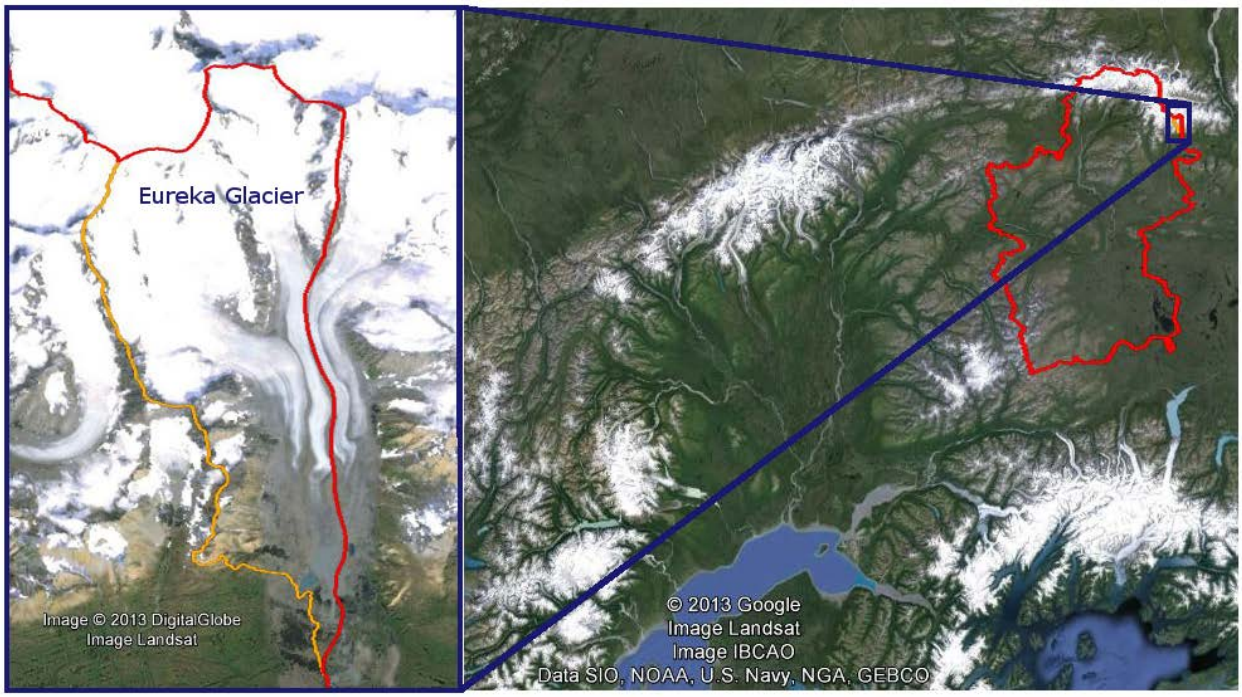


**Figure 7.1-2 Upper Susitna basin watershed divide at Eureka Glacier.**
See also F**igure 5.4-1**.

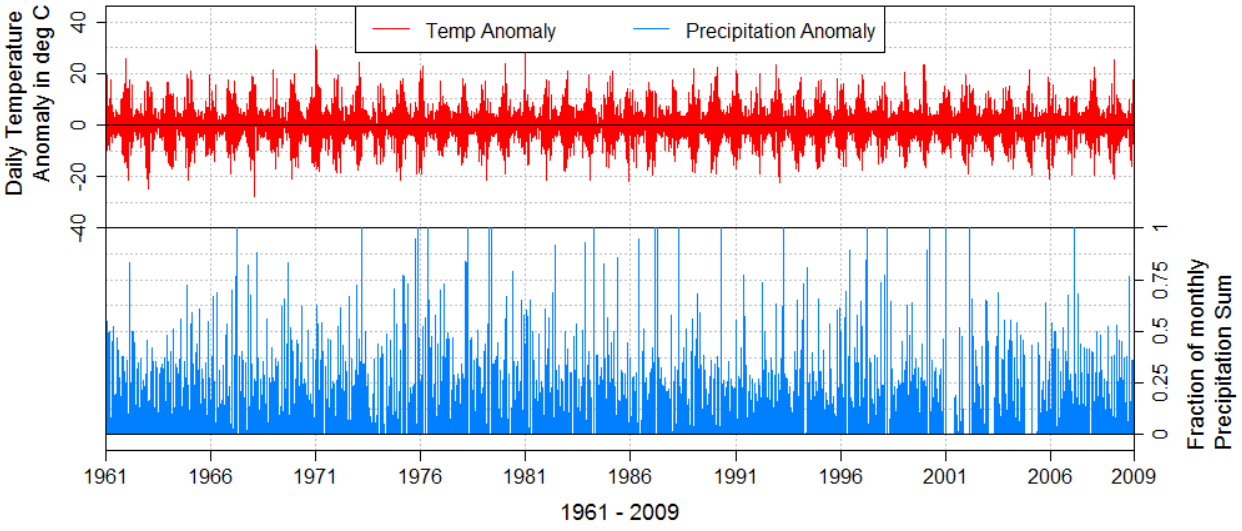


**Figure 7.3.1.2-1 Daily temperature and precipitation anomalies for Gulkana station.**

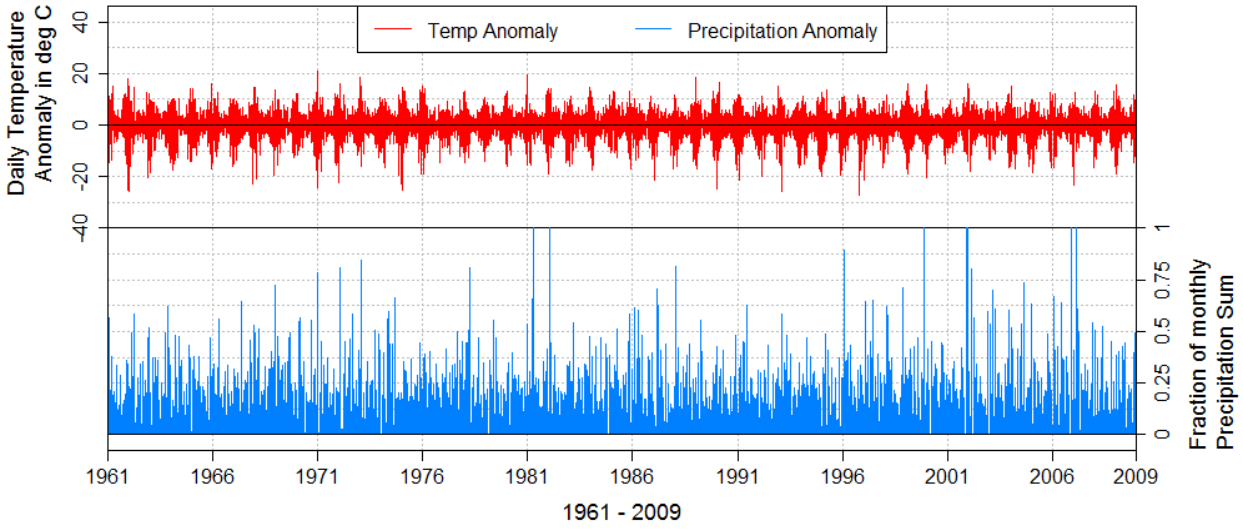


**Figure 7.3.1.2-2 Daily temperature and precipitation anomalies for Talkeetna station.**

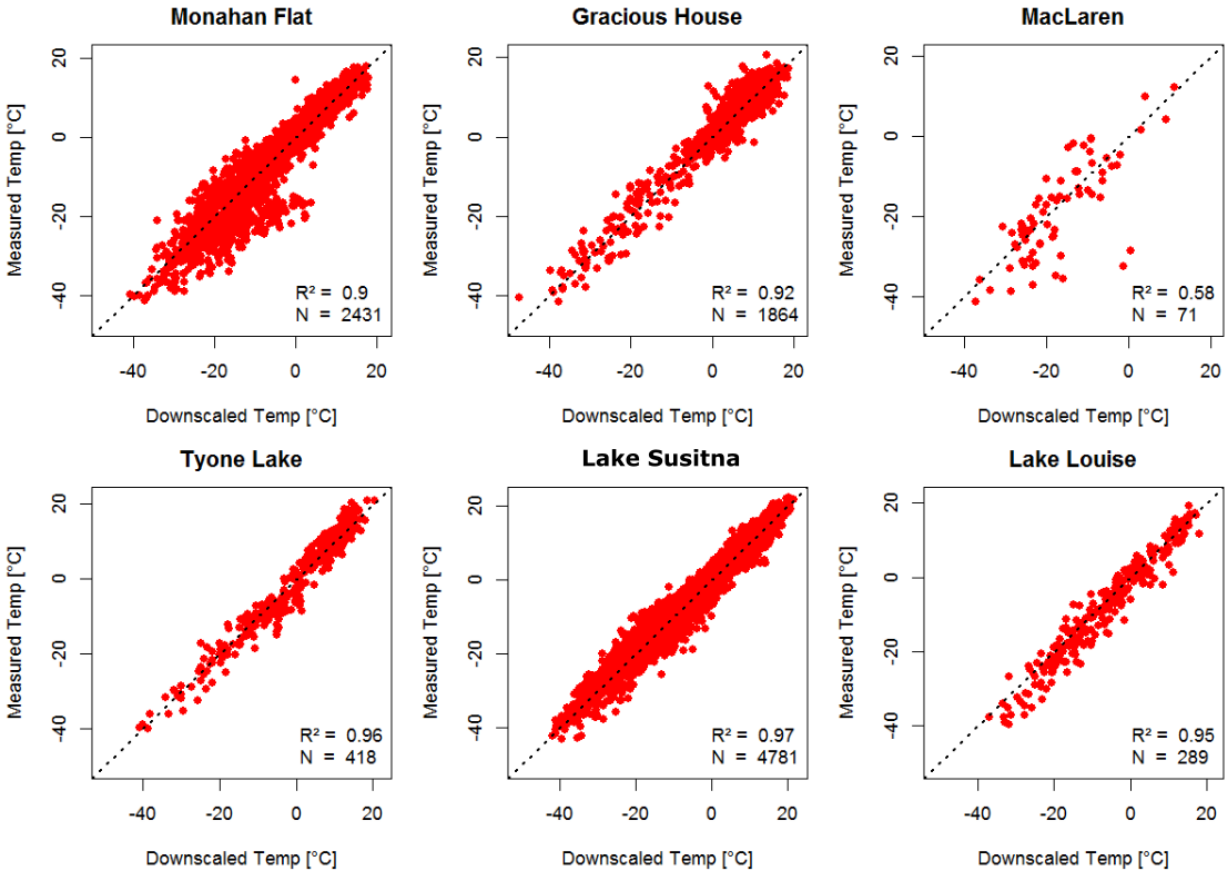


**Figure 7.3.1.2-3 Correlation of recorded and downscaled daily mean temperature at selected climate stations in the upper Susitna basin.**

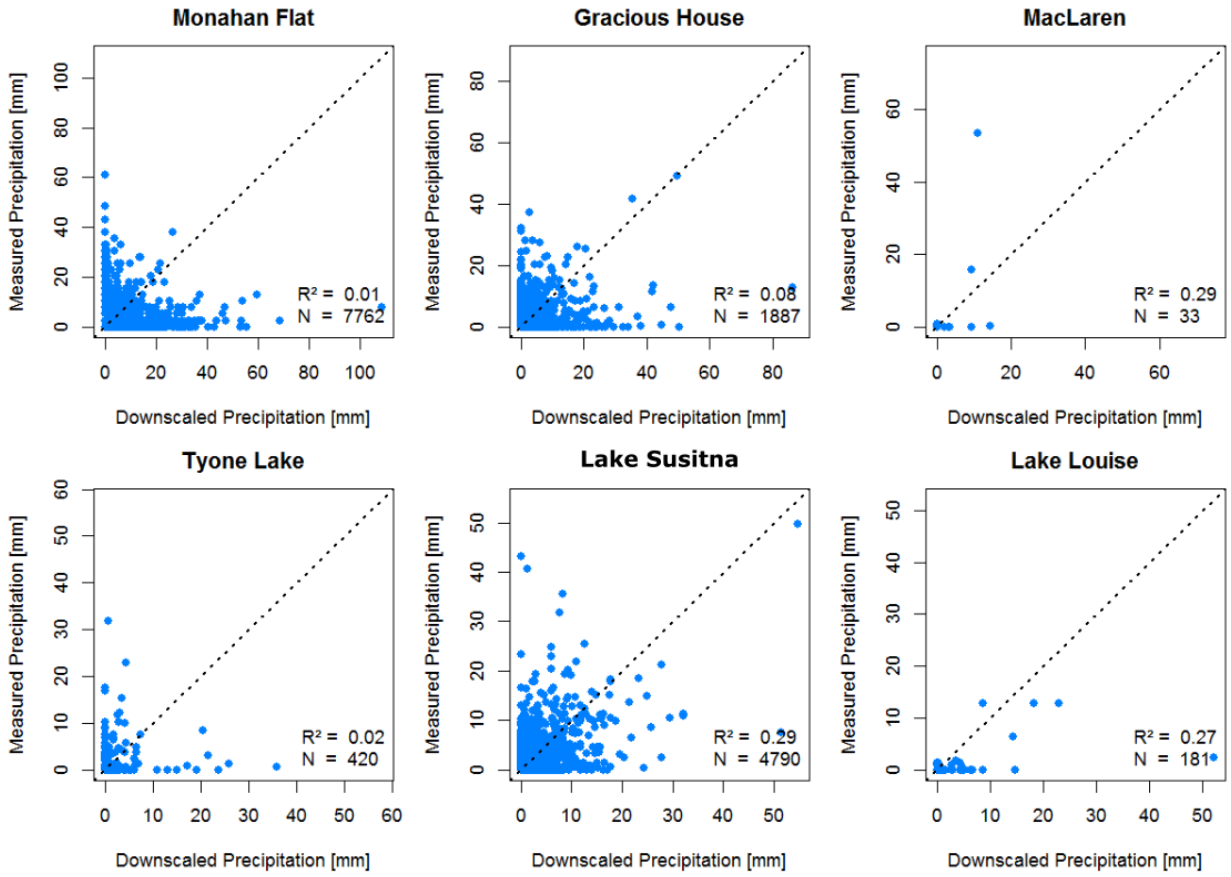


**Figure 7.3.1.2-4 Correlation of recorded and downscaled daily precipitation at selected climate stations in the upper Susitna basin.**

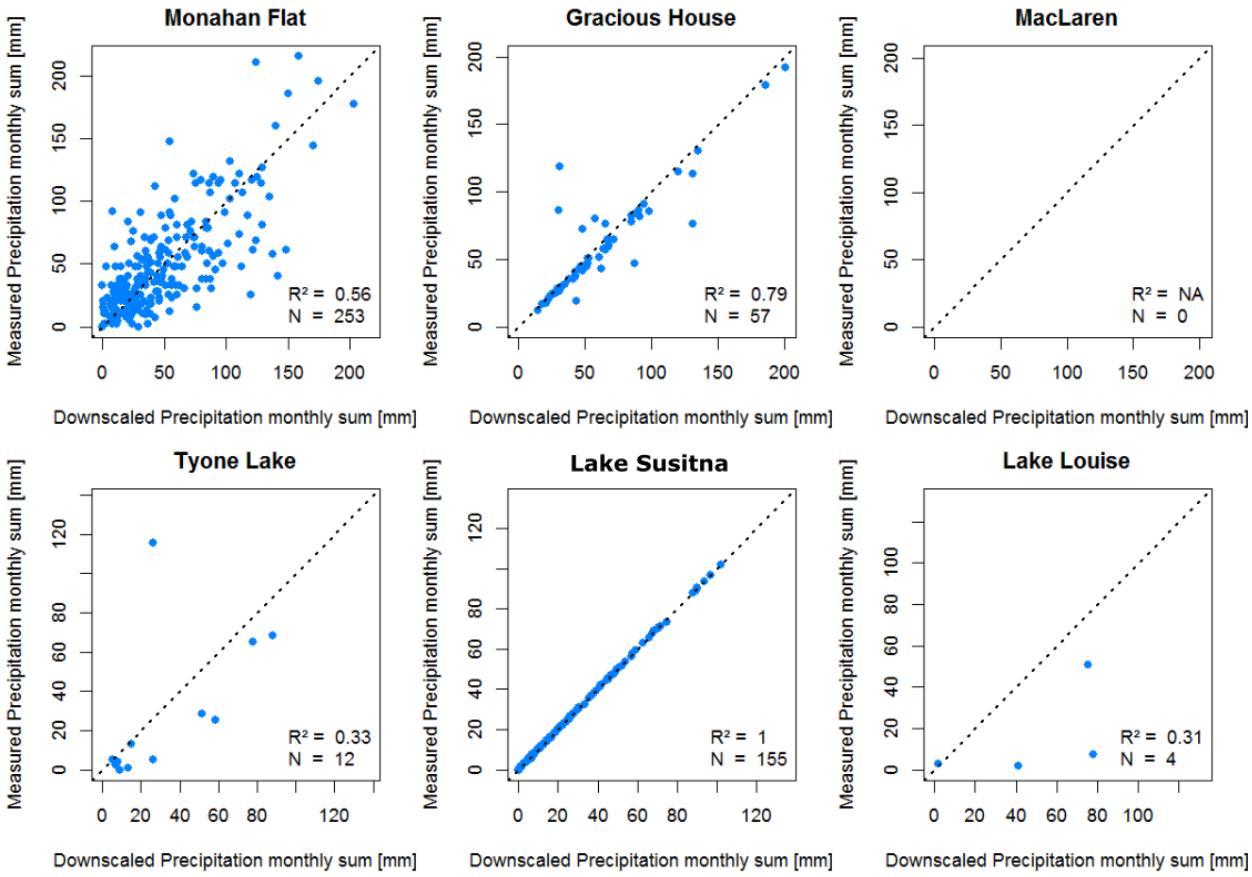


**Figure 7.3.1.2-5 Correlation of recorded and downscaled daily precipitation sums at selected climate stations in the upper Susitna basin.**

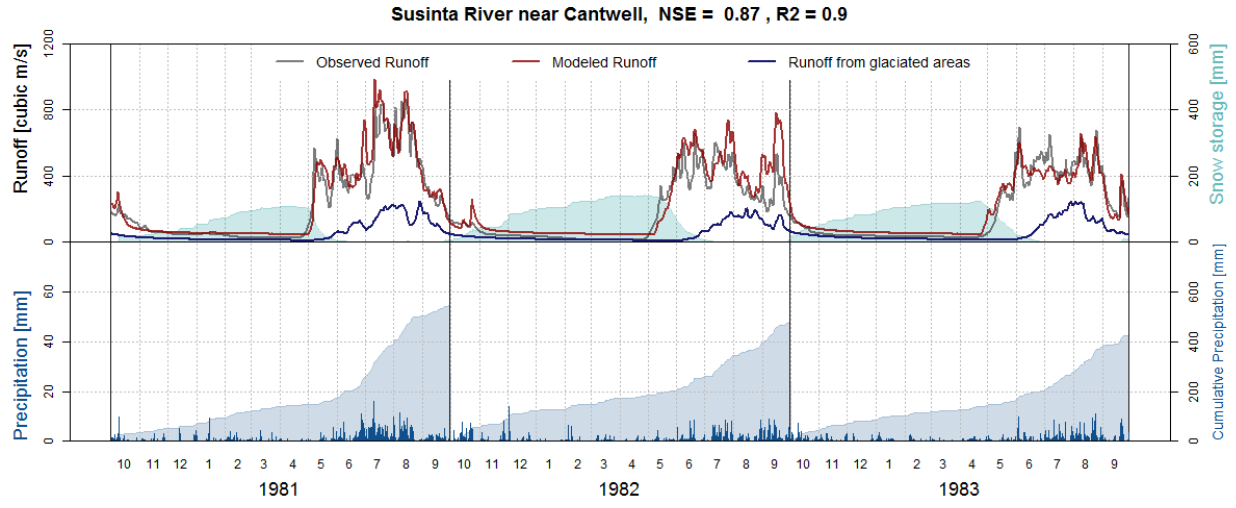

**Figure 7.3.1.4.1-1 Daily measured and modeled runoff, snow storage, and precipitation during the calibration period 1981-1983 for the Susitna River near Cantwell sub-basin in the upper Susitna basin.**
The x-axis shows each hydrologic year partitioned into months.

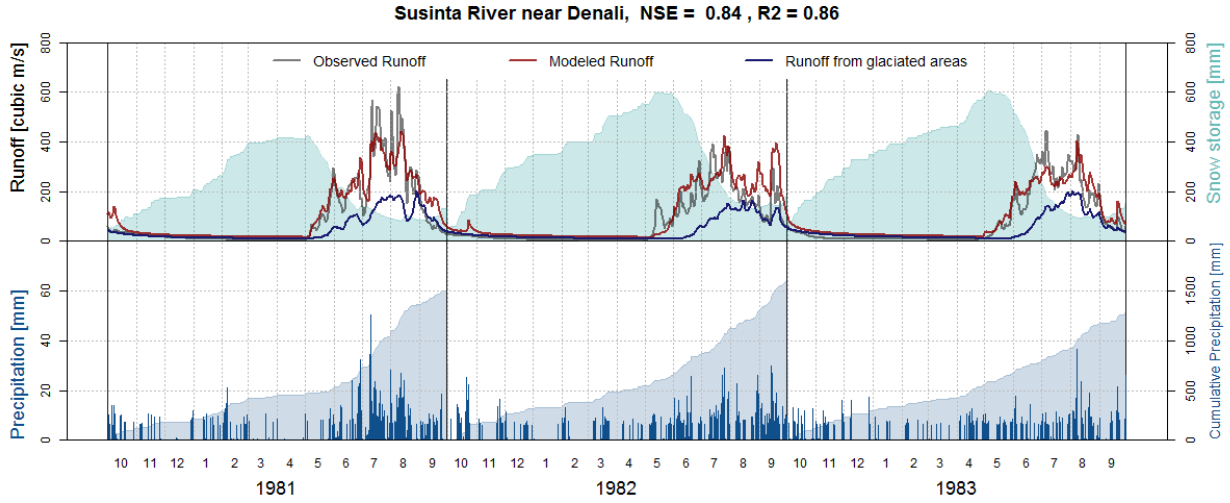


**Figure 7.3.1.4.1-2 Daily measured and modeled runoff, snow storage, and precipitation during the calibration period 1981-1983 for the Susitna River near Denali sub-basin in the upper Susitna basin.**
The x-axis shows each hydrologic year partitioned into months.

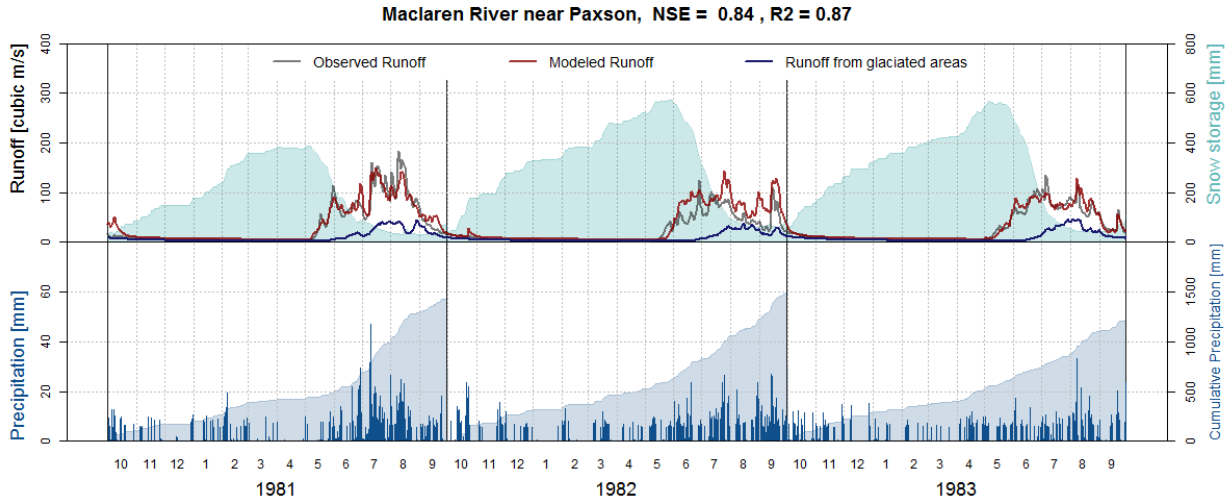


**Figure 7.3.1.4.1-3 Daily measured and modeled runoff, snow storage, and precipitation during the calibration period 1981-1983 for the MacLaren River near Paxson sub-basin in the upper Susitna basin.**
The x-axis shows each hydrologic year partitioned into months.

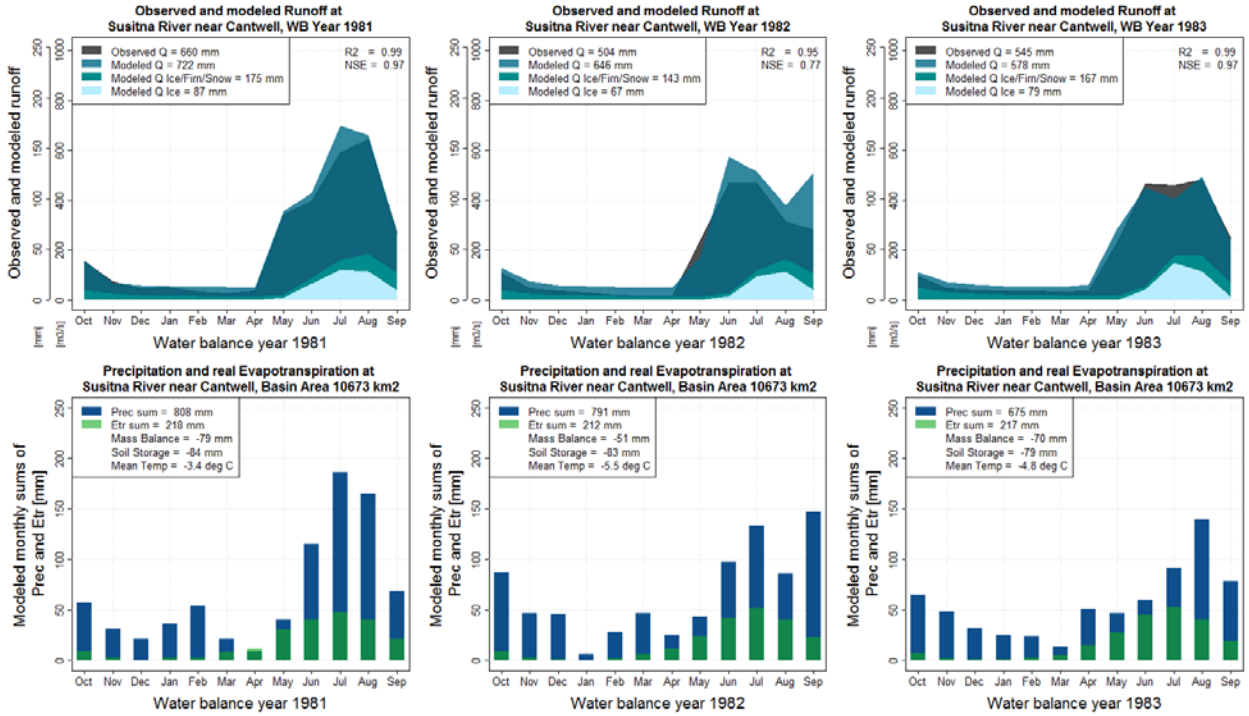


**Figure 7.3.1.4.2-1 Monthly means of measured and modeled runoff, precipitation and evapotranspiration for the calibration period 1981-1983 for the Susitna River near Cantwell sub-basin in the upper Susitna basin.**

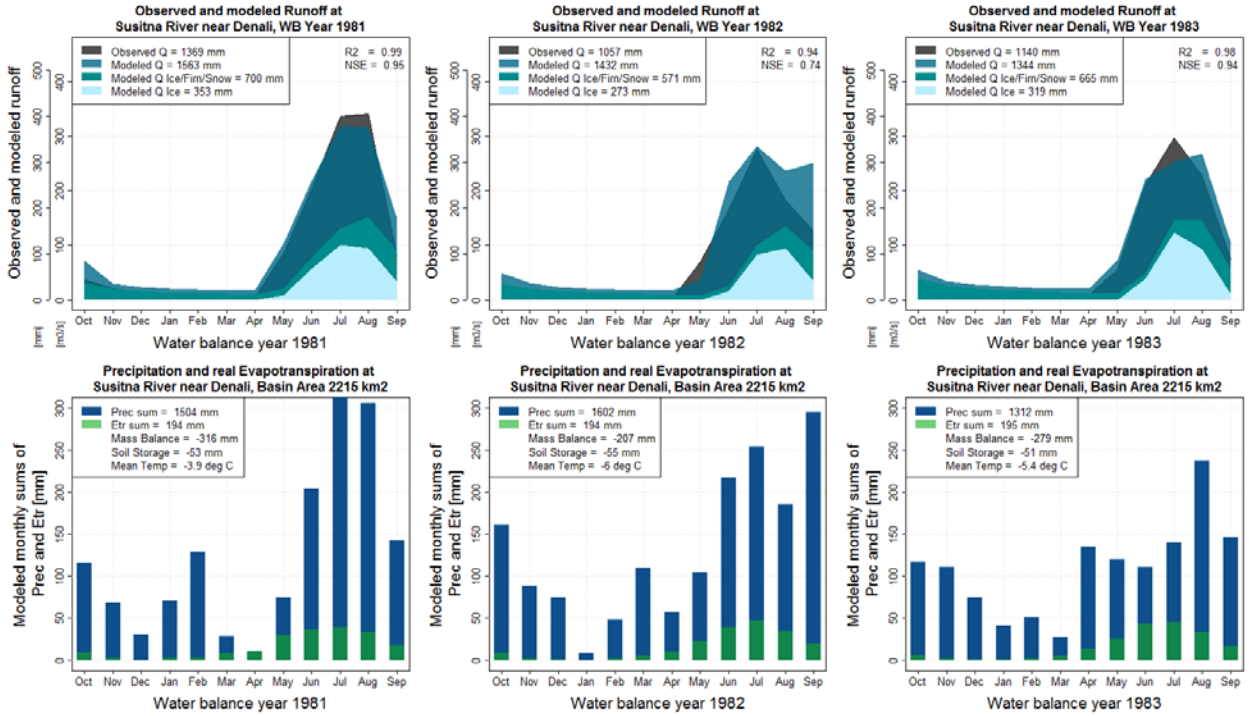

**Figure 7.3.1.4.2-2 Monthly means of measured and modeled runoff, precipitation and evapotranspiration for the calibration period 1981-1983 for the Susitna River near Denali sub-basin in the upper Susitna basin.**

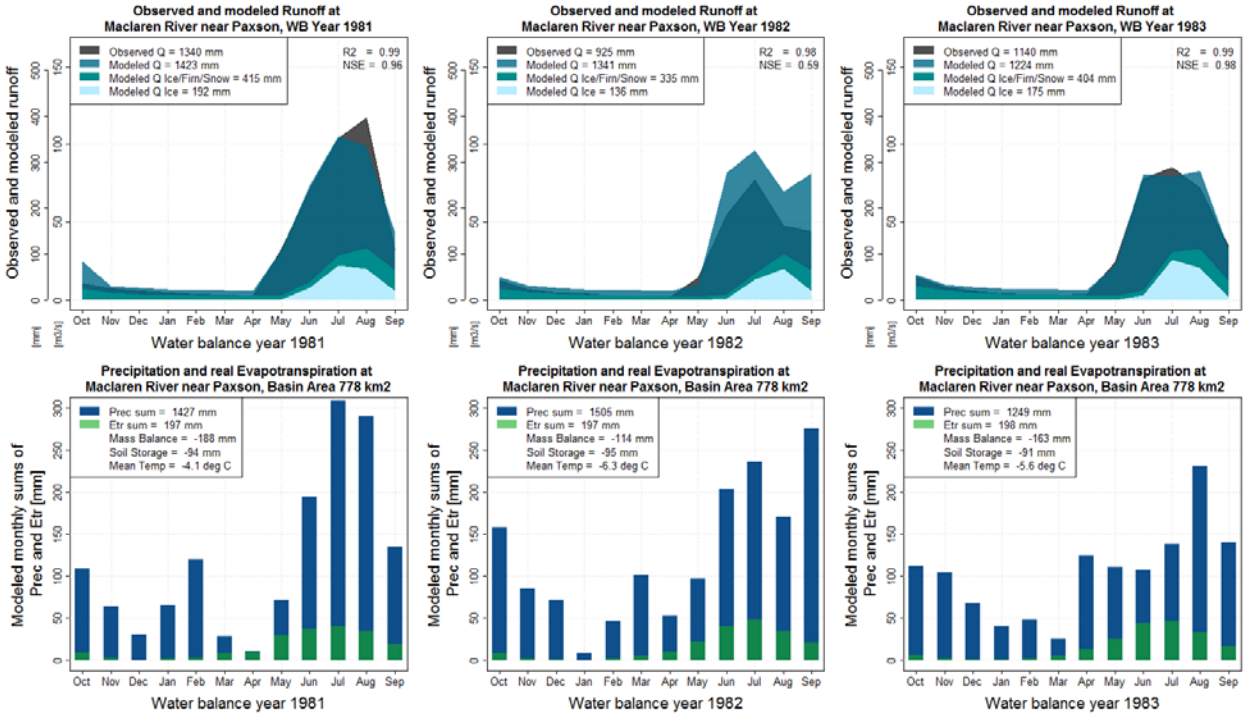


**Figure 7.3.1.4.2-3 Monthly means of measured and modeled runoff, precipitation and evapotranspiration for the calibration period 1981-1983 for the MacLaren River near Paxson sub-basin in the upper Susitna basin.**

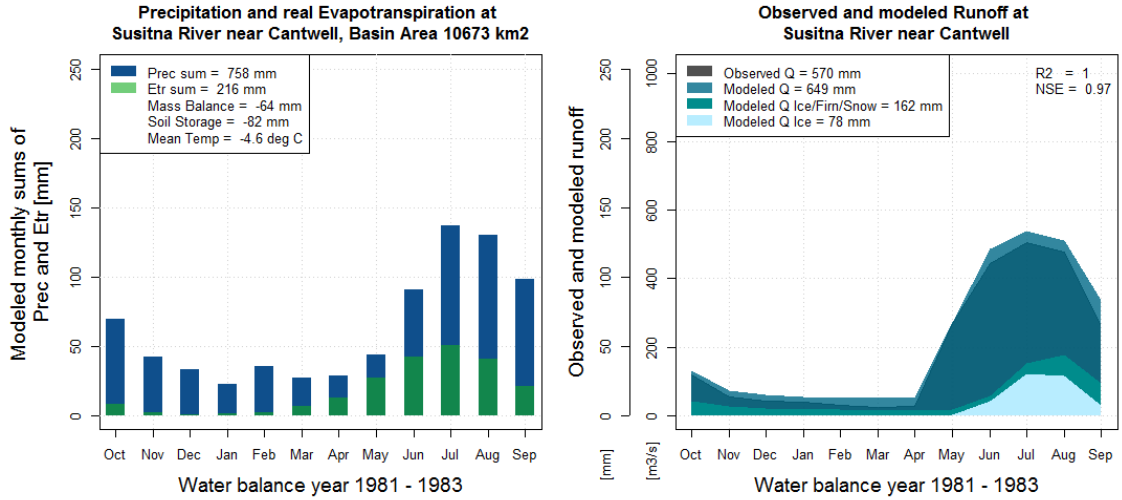


**Figure 7.3.1.4.2-4 Three-year monthly means of measured and modeled runoff, precipitation and evapotranspiration for the calibration period 1981-1983 for the Susitna River near Cantwell sub-basin in the upper Susitna basin.**

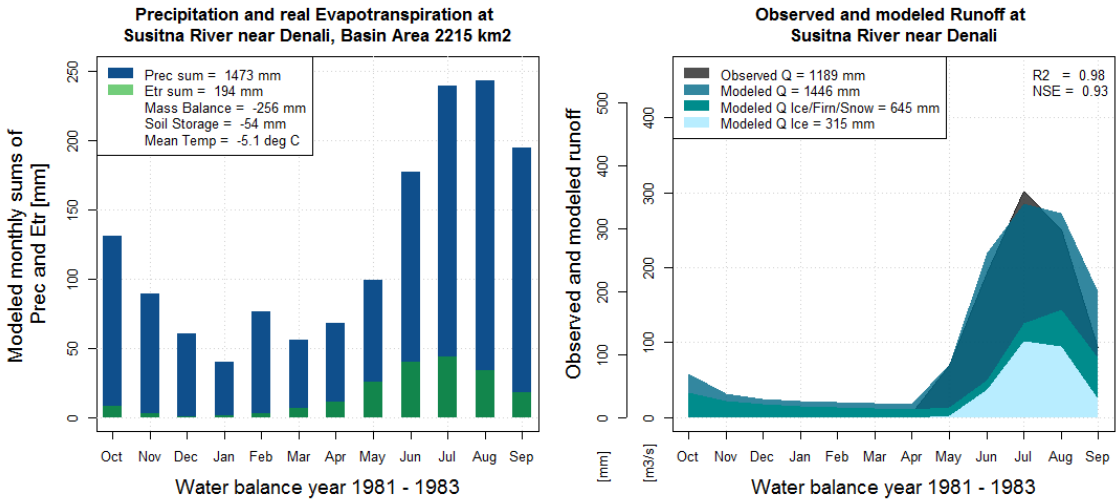


**Figure 7.3.1.4.2-5 Three-year monthly means of measured and modeled runoff, precipitation and evapotranspiration for the calibration period 1981-1983 for the Susitna River near Denali sub-basin in the upper Susitna basin.**

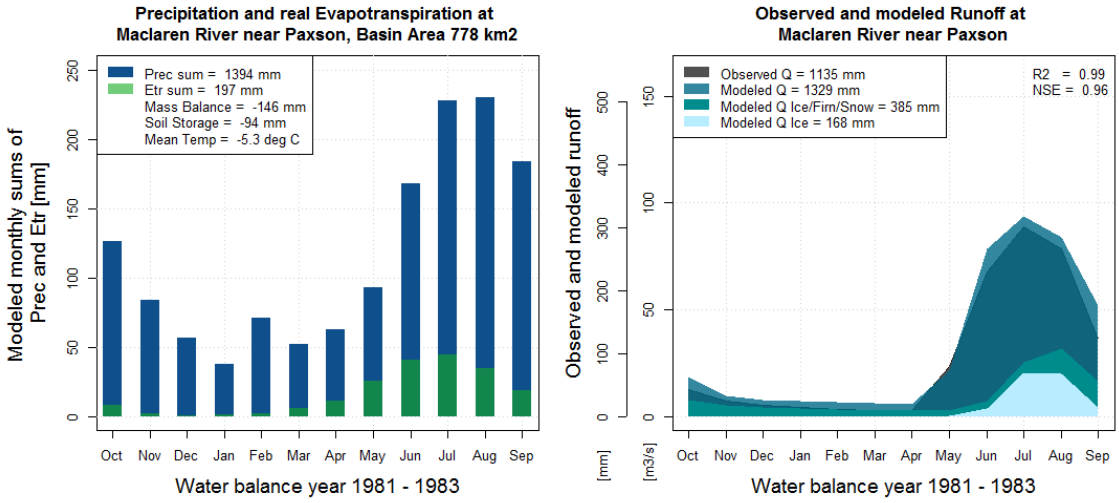


**Figure 7.3.1.4.2-6 Three-year monthly means of measured and modeled runoff, precipitation and evapotranspiration for the calibration period 1981-1983 for the MacLaren River near Paxson sub-basin in the upper Susitna basin.**

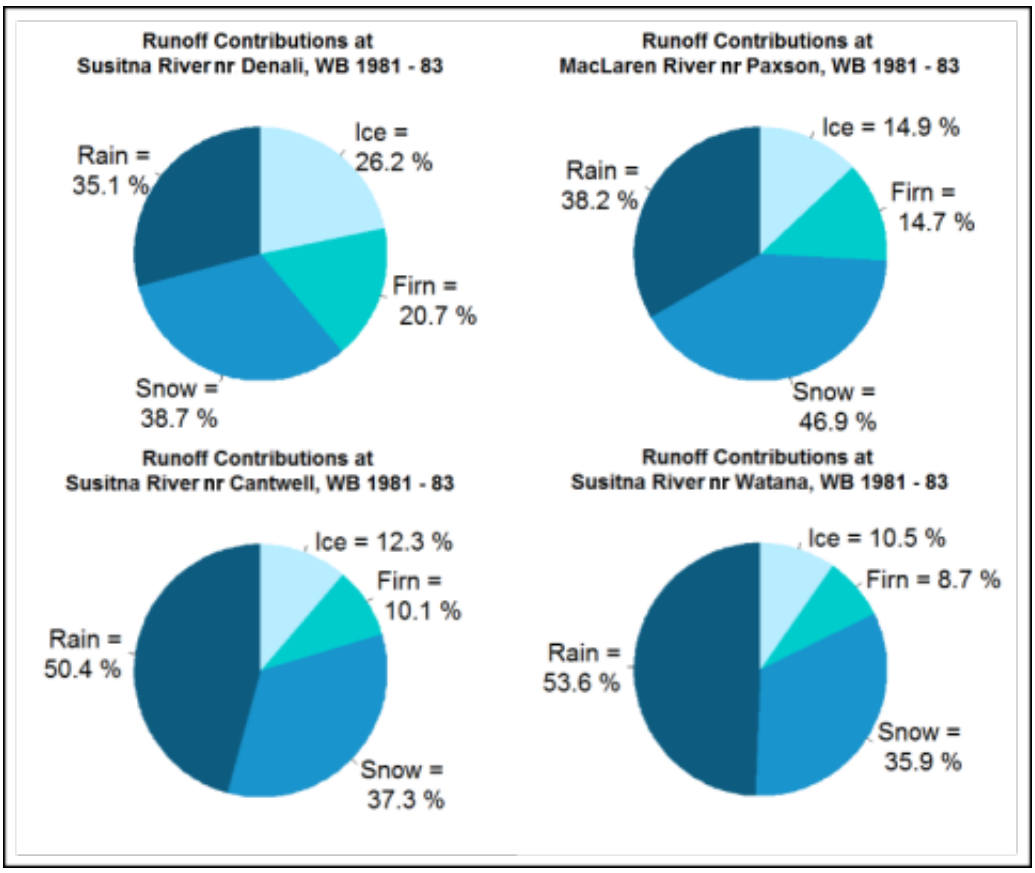


**Figure 7.3.1.4.3-1 Mean annual runoff contributions for the period 1981-1983 for each of the sub-basins in the upper Susitna basin.**

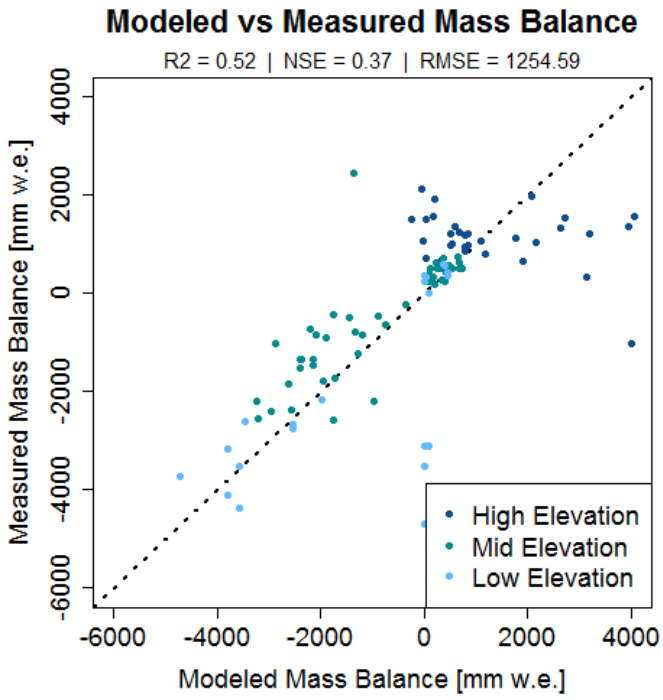


**Figure 7.3.1.4.4-1 Modeled and measured point mass balances for the period 1981-1983 in the upper Susitna basin.**

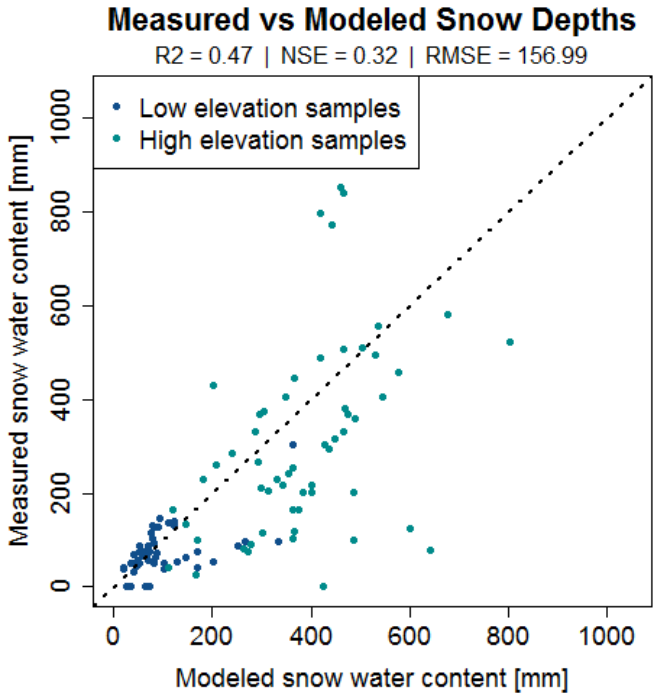


**Figure 7.3.1.4.5-1 Modeled and measured snow depths for the period 1981-1983 in the upper Susitna basin.**

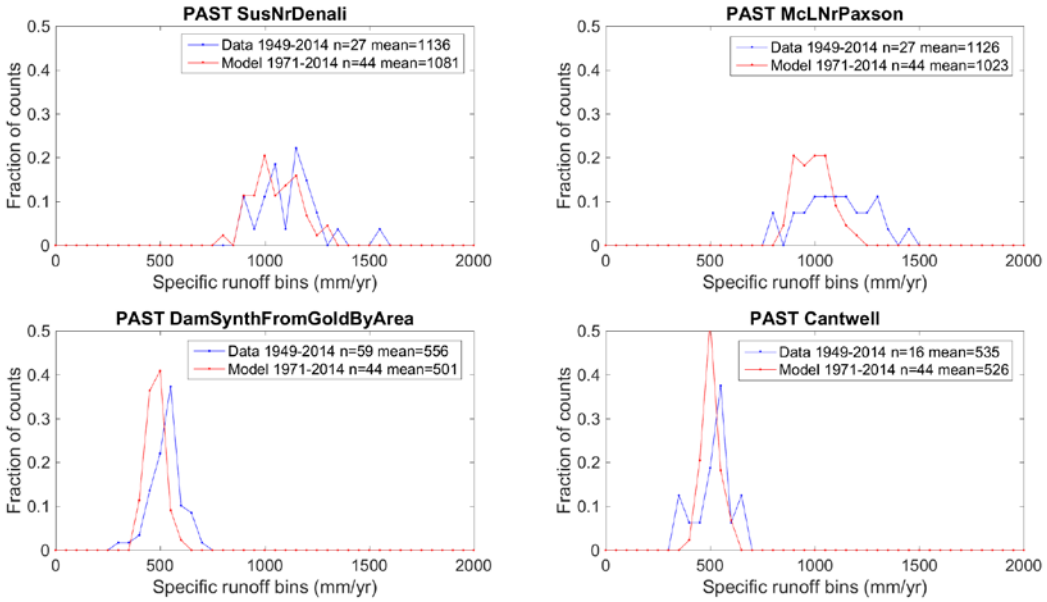


**Figure 7.3.2.2-1 Specific runoff (mm/yr) histograms for historic periods.**

This way of summarizing the data allow us to compare measured runoff data to model results. The time series of measured runoff cannot be directly compared to model results because the model is forced with climate model results, not reanalysis or local data. We minimized the offset between the two histograms by adjusting model parameters, particularly the degree day factors for snow, firn, and ice.

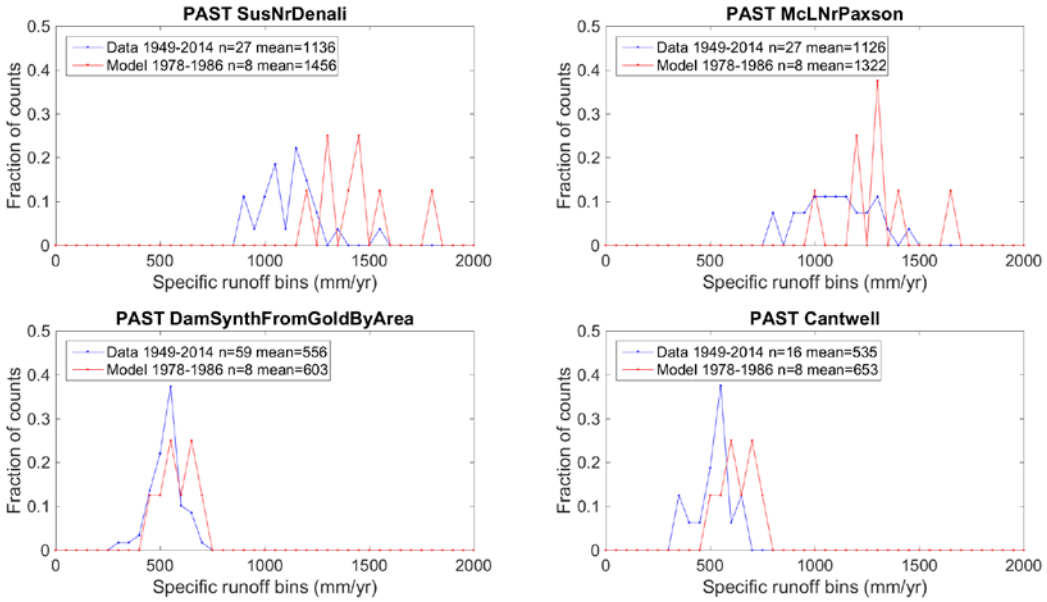


**Figure 7.3.2.2-2 Specific runoff (mm/yr) histograms for the past, where the model was forced primarily with local station data.**

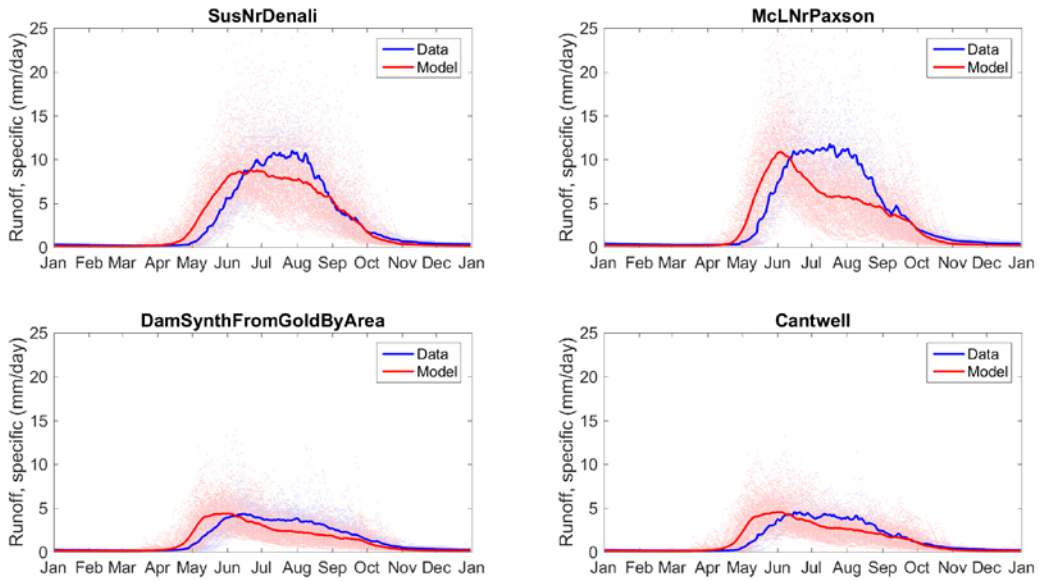


**Figure 7.3.2.2-3 Specific runoff climatology for the three gauged sub-basins in the upper Susitna basin, as well as the Dam site synthesized from Gold Creek.**

All available measured data are shown in blue. Model results (calculated for each day of the year 1-365) for 1971-2100 using the bias-corrected CCSM WRF 5 km downscaled climate forcing are shown in red. Individual years are dots, and the mean climatology is a line. Data from the higher elevation basins Susitna near Denali and MacLaren near Paxson exhibit a broad summer-long peak in runoff, while the lower basins peak earlier in the year and trail off gradually over the summer. Spring runoff in the model rises earlier than in the data, and late summer runoff is generally underestimated.

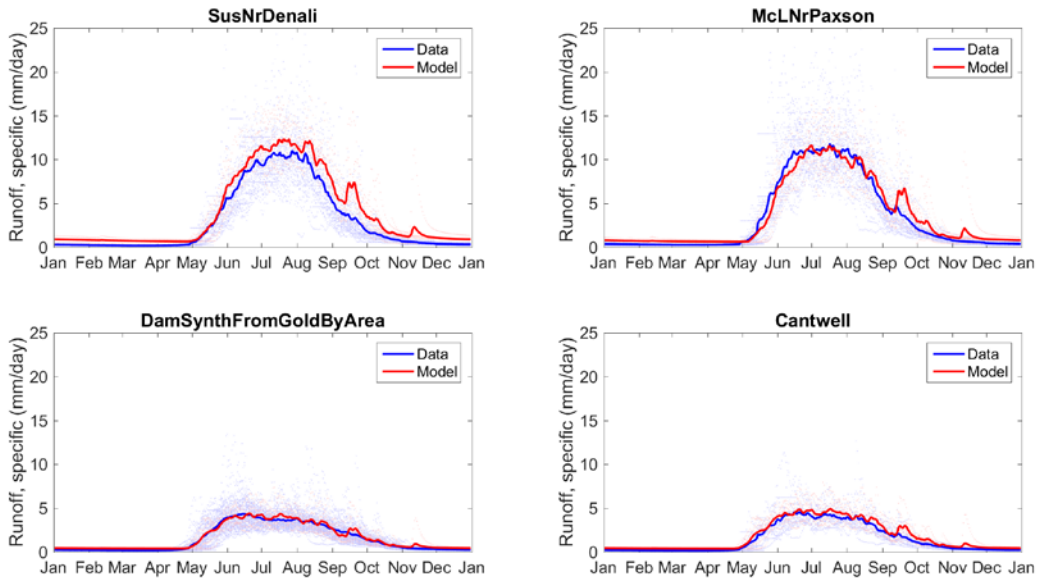


**Figure 7.3.2.2-4 Specific runoff climatology for the three gauged sub-basins in the upper Susitna basin, as well as the Dam site synthesized from Gold Creek.**

All available measured data are shown in blue. Model results (calculated for each day of the year 1-365) are shown in red for 1977-1985, where the model was forced primarily with local station data. Individual years are dots, and the mean climatology is a line. Data from the higher elevation basins Susitna near Denali and MacLaren near Paxson exhibit a broad summer-long peak in runoff, while the lower basins peak earlier in the year and trail off gradually over the summer. The magnitude and timing of the modeled runoff climatology match the data, within the range of variability. The higher day-to-day variability seen in the model results are due, at least in part, to the fact that the model is averaging a smaller number of years than the data.

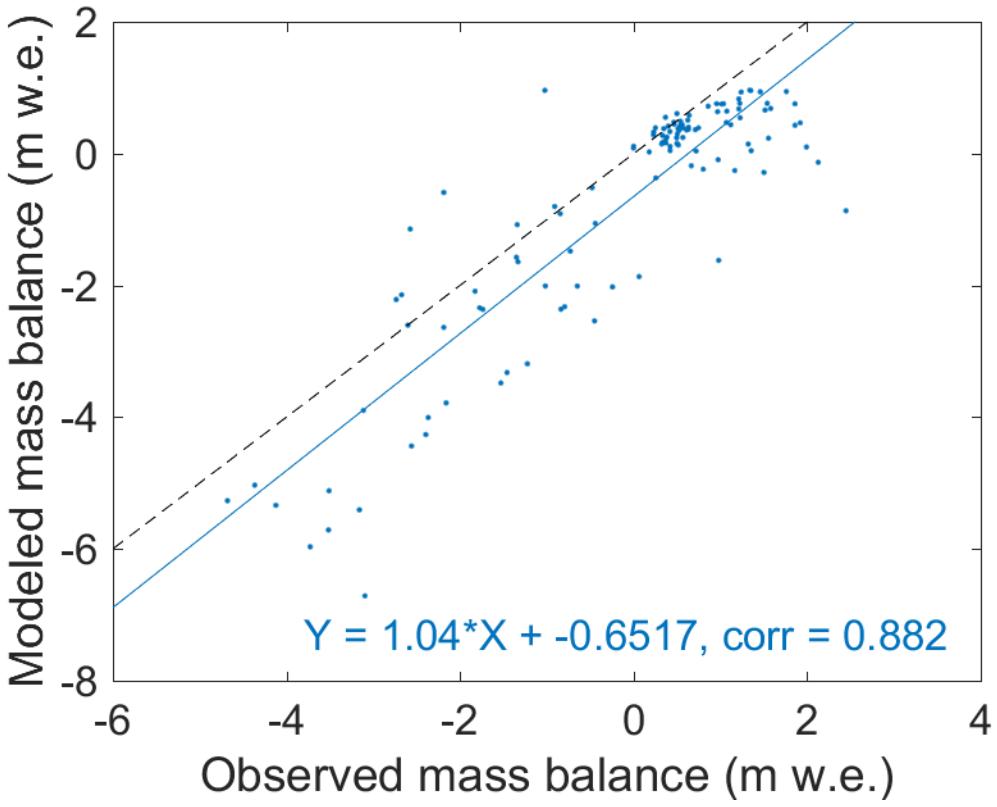


**Figure 7.3.2.2-5 Modeled vs observed mass balance for the glacier stations.**
Measurements are from 1981-1983. Model years are not meant to represent specific years in the observations, so we do not expect these relationships to be perfect. We can see that the mass balance and snow depths are generally in the right range for each station.

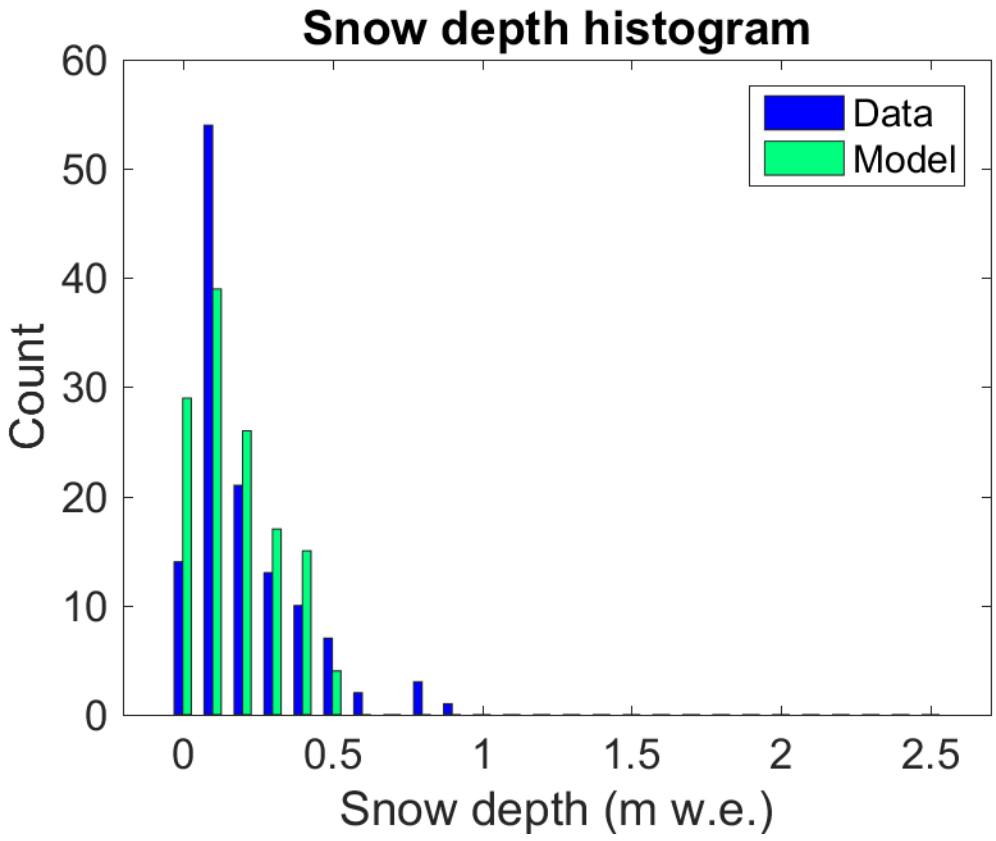


**Figure 7.3.2.2-6 Histogram of snow depth (m w.e.) shows that the data and the model are producing similar snow depths.**

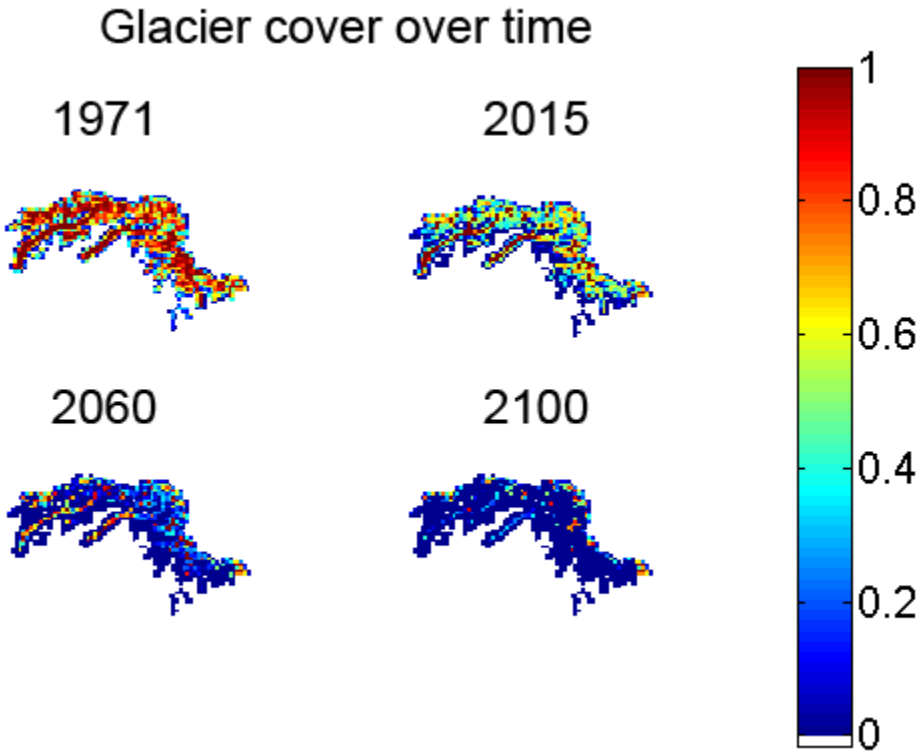


**Figure 7.4.1-1 Modeled glacier cover maps for 1971, 2015, 2060, and 2100.**
The maps are colored for all grid cells that contained glaciers at the start of the run. The colors represent the fraction of the grid cell area (1 $km^2$) that is covered by ice. The general pattern shows glacier retreat to higher elevations. Some ice remains in the lower elevation trunks of the glaciers. However, the latter effect may not be a robust result as it depends on the retreat parameterization used.

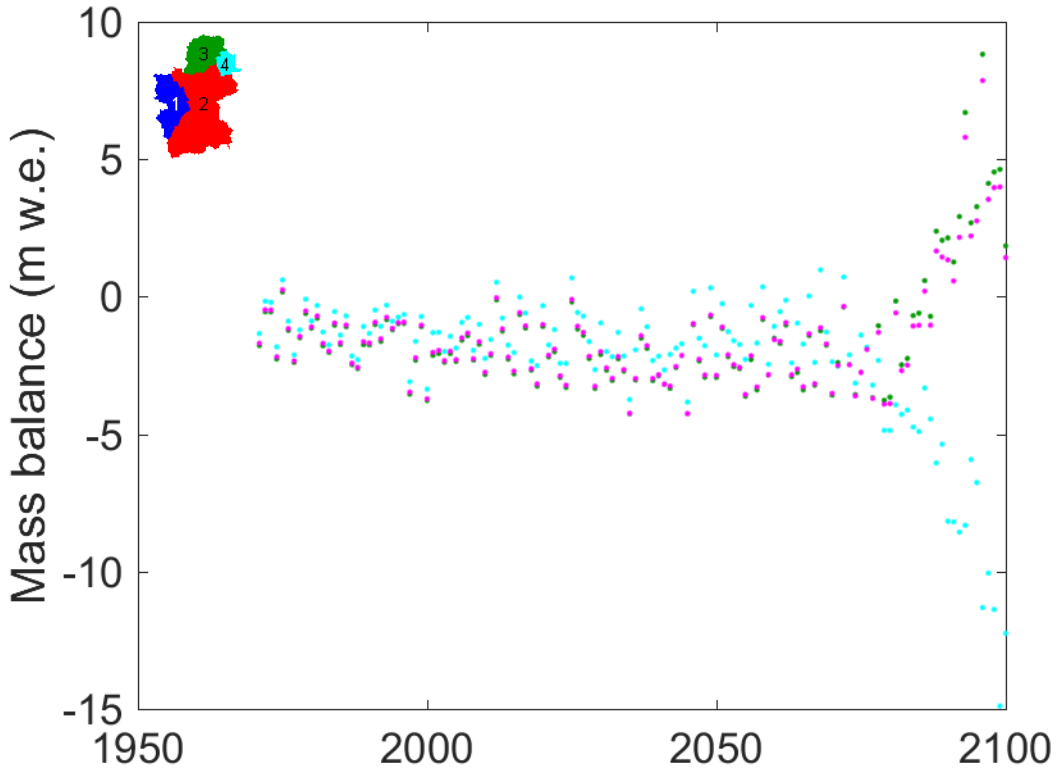


**Figure 7.4.1-2 Simulated average annual glacier-wide mass balance for sub-basins in the upper Susitna basin for the period 1970-2100.**
Basins are color-coded: magenta is for the whole basin, green is for the Denali basin, and cyan is for the Paxson basin (see sub-basin map Figure 4.1-4).

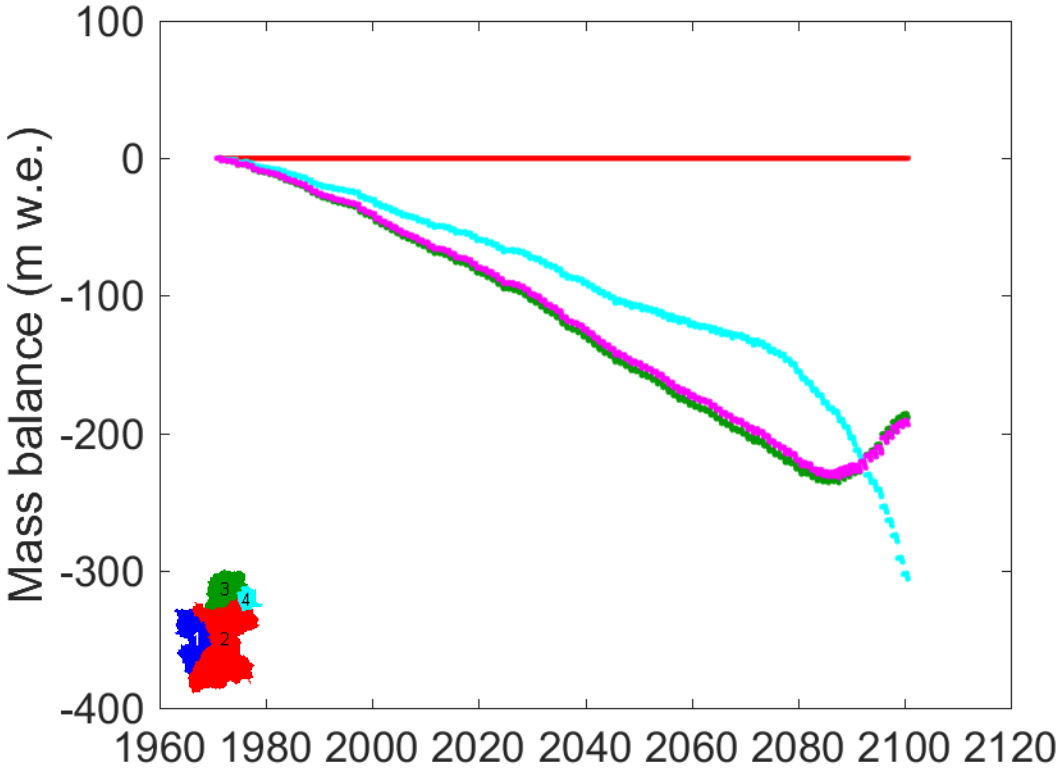


**Figure 7.4.1-3 Simulated cumulative glacier-wide mass balance for sub-basins in the upper Susitna basin for the period 1970-2100.**
Basins are color-coded: magenta is for the whole basin, blue is for the Dam basin, red is for the Cantwell basin, green is for the Denali basin, and cyan is for the Paxson basin.

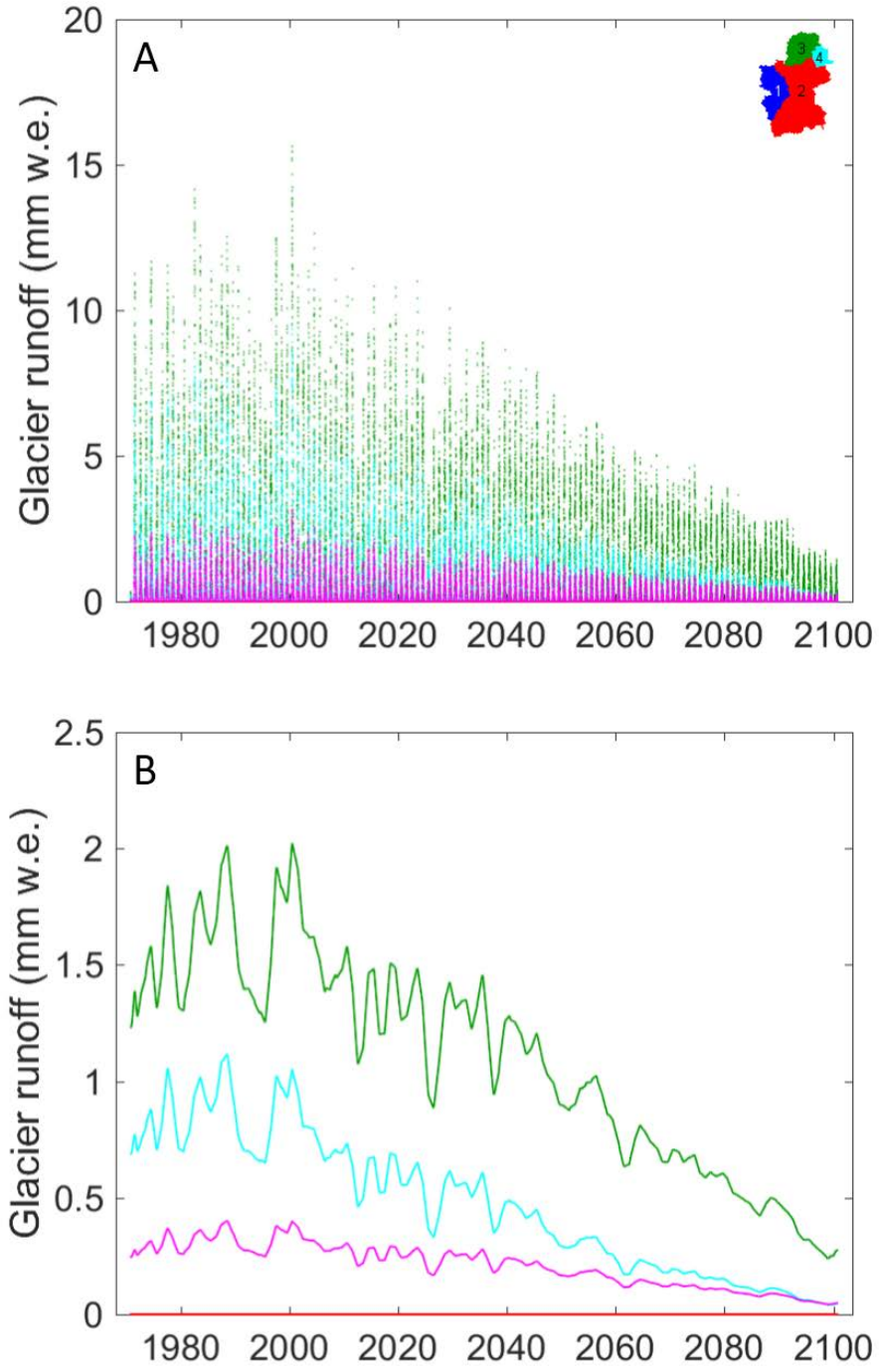


**Figure 7.4.1-4 Simulated daily runoff (mm w.e.) from glaciers for sub-basins in the upper Susitna basin for the period 1970-2100.**

Note that the entire glacier area is classified into either 'firn area' or 'ice area' so runoff estimates includes snow melt from the glaciers. Panel A contains the unsmoothed data. Panel B shows data smoothed with a triangular filter, which weights the central point highest and considers 730 points (two years) on either side. Basins are color-coded: magenta is for the whole basin, blue is for the Dam basin, red is for the Cantwell basin, green is for the Denali basin, and cyan is for the Paxson basin.

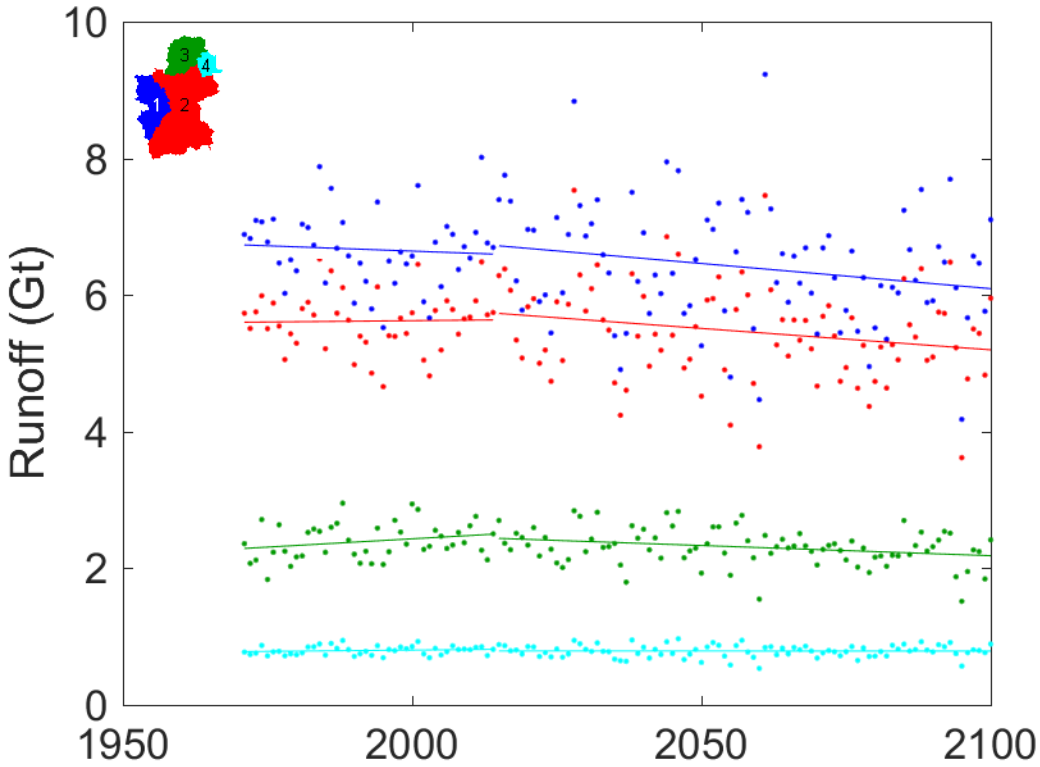


**Figure 7.4.2-1 Annual runoff (Gt) time series for the upper Susitna basin and its sub-basins.**
Fit lines are shown for each basin covering the periods 1971-2015 and 2016-2100. The Denali (green) and Paxson (cyan) sub-basins both flow into the Cantwell (red) sub-basin which in turn flows into the Dam site (blue) sub-basin. Runoff of 6 Gt/year is equivalent to 190 $m^3/s$ and 6710 cfs.

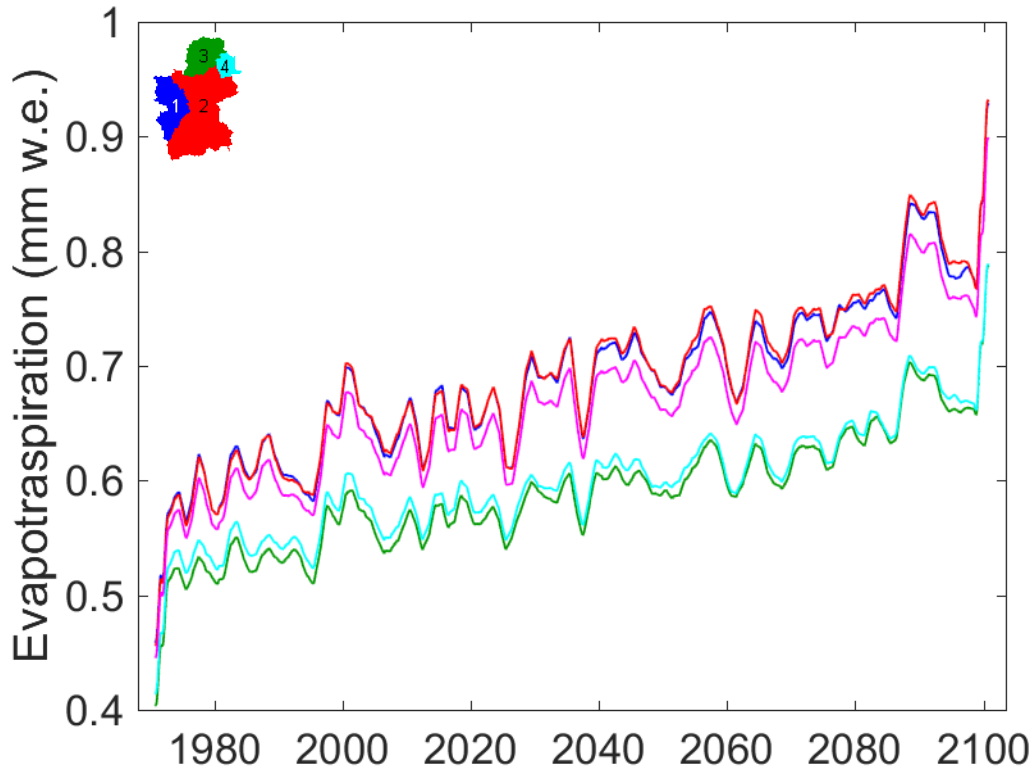


**Figure 7.4.2-2 Simulated daily evapotranspiration (mm w.e.) for sub-basins in the upper Susitna basin for the period 1970-2100.**
Data are smoothed with a triangular filter, which weights the central point highest and considers 730 points (two years) on either side. Basins are color-coded: magenta is for the whole basin, blue is for the Dam basin, red is for the Cantwell basin, green is for the Denali basin, and cyan is for the Paxson basin.

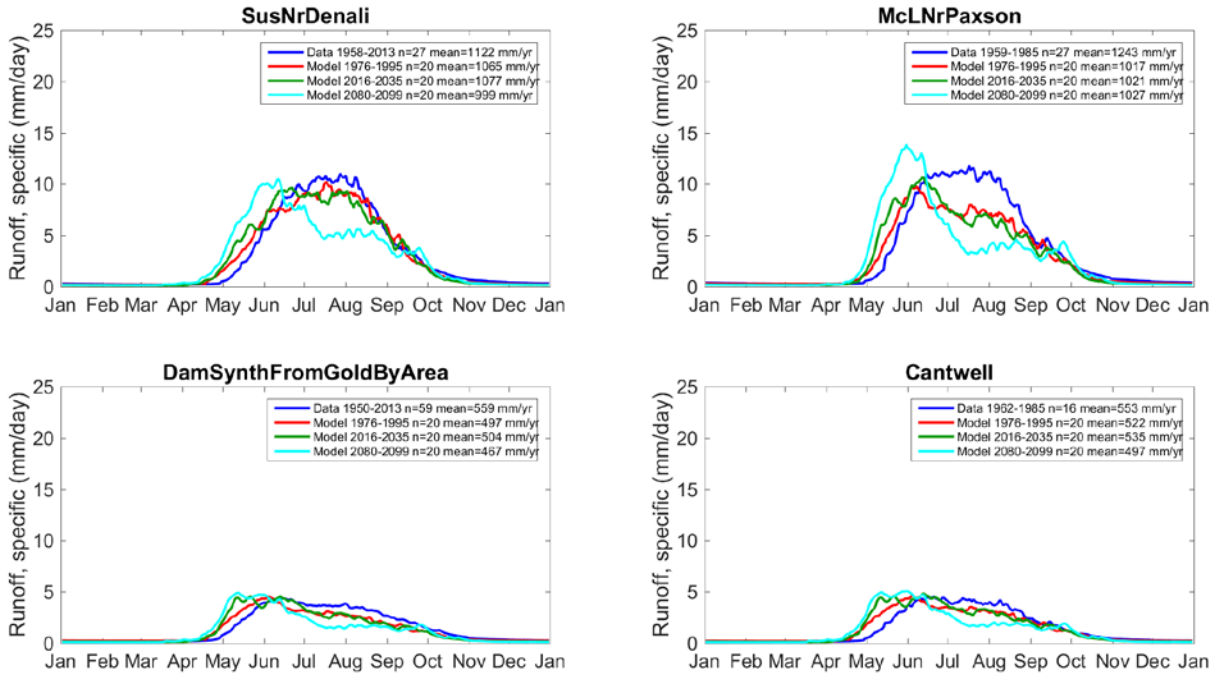


**Figure 7.4.2-3 Specific runoff climatology (calculated for each day of the year 1-365) for the three gauged sub-basins as well as the Dam site synthesized from Gold Creek.**

The climatology of all available measured data is shown in blue. Climatologies calculated from model results are shown for 1976-1995 (red), 2016-2035 (green), and 2080-2099 (cyan). Measured data from the higher elevation basins Susitna near Denali and MacLaren near Paxson exhibit a broad summer-long peak in runoff, while the lower basins peak earlier in the year and trail off gradually over the summer. Peak runoff at the proposed dam site is nearly one month earlier by the end of the century than it was for 1976-1995. By the end of the century, the spring snow melt runoff peak is up to 40% larger for the Paxson sub-basin and marginally larger for the other sub-basins. Late-summer runoff (August) for 2080-2099 at the dam site is about half of what it was for 1976-1995.

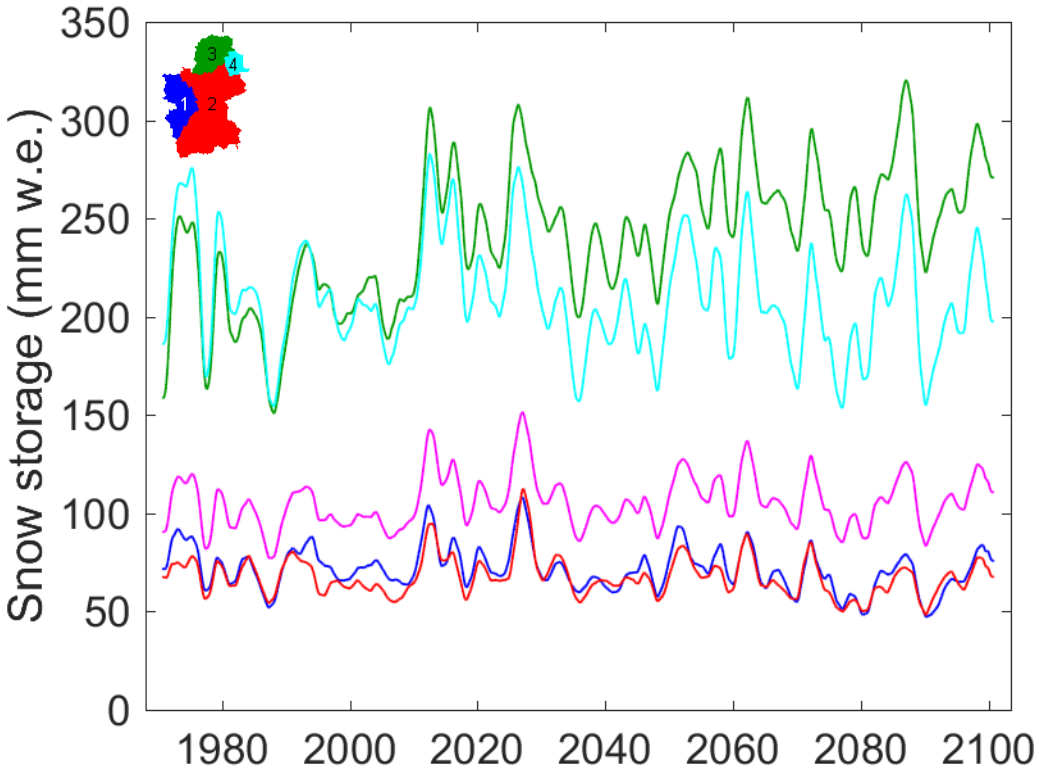


**Figure 7.4.2-4 Simulated total snow storage (mm w.e., liquid and solid fraction) for sub-basins in the upper Susitna basin for the period 1970-2100.**
Data are smoothed with a triangular filter, which weights the central point highest and considers 730 points (two years) on either side. Basins are color-coded: magenta is for the whole basin, blue is for the Dam basin, red is for the Cantwell basin, green is for the Denali basin, and cyan is for the Paxson basin.

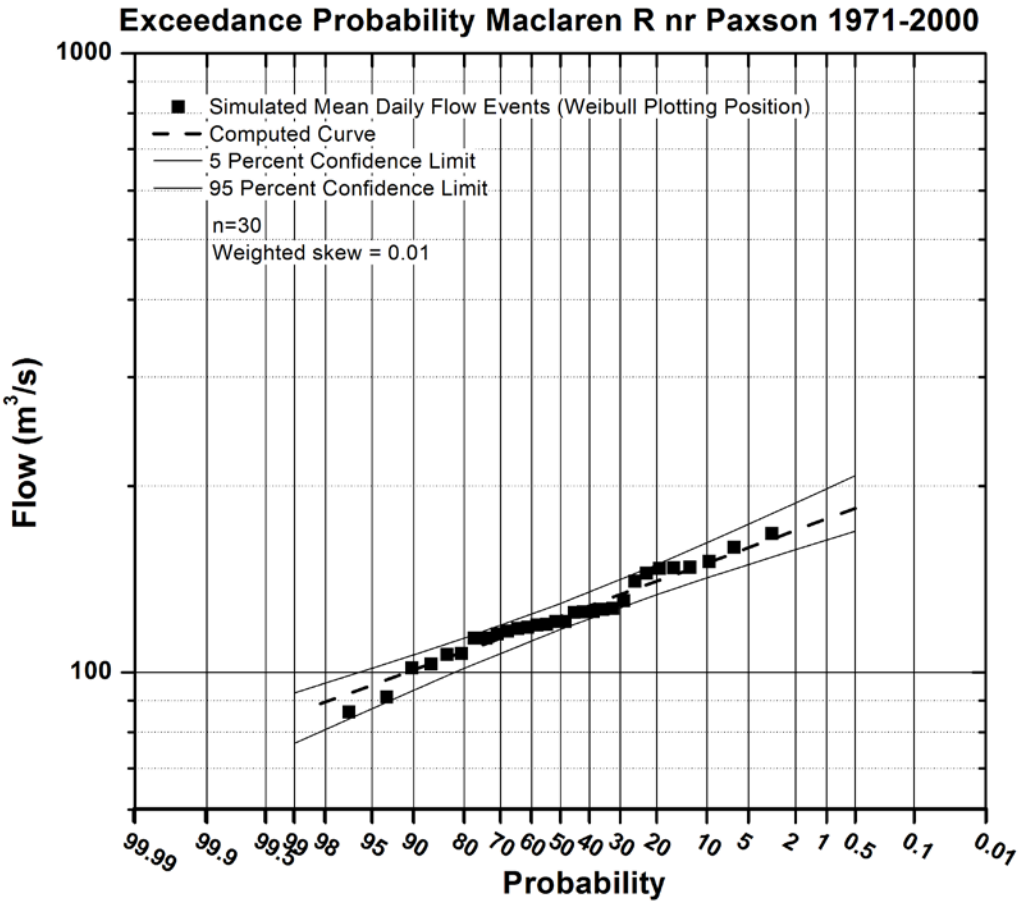


**Figure 7.4.2.1-1 Maclaren River 1971-2000. Flows are simulated mean daily annual maximum.**

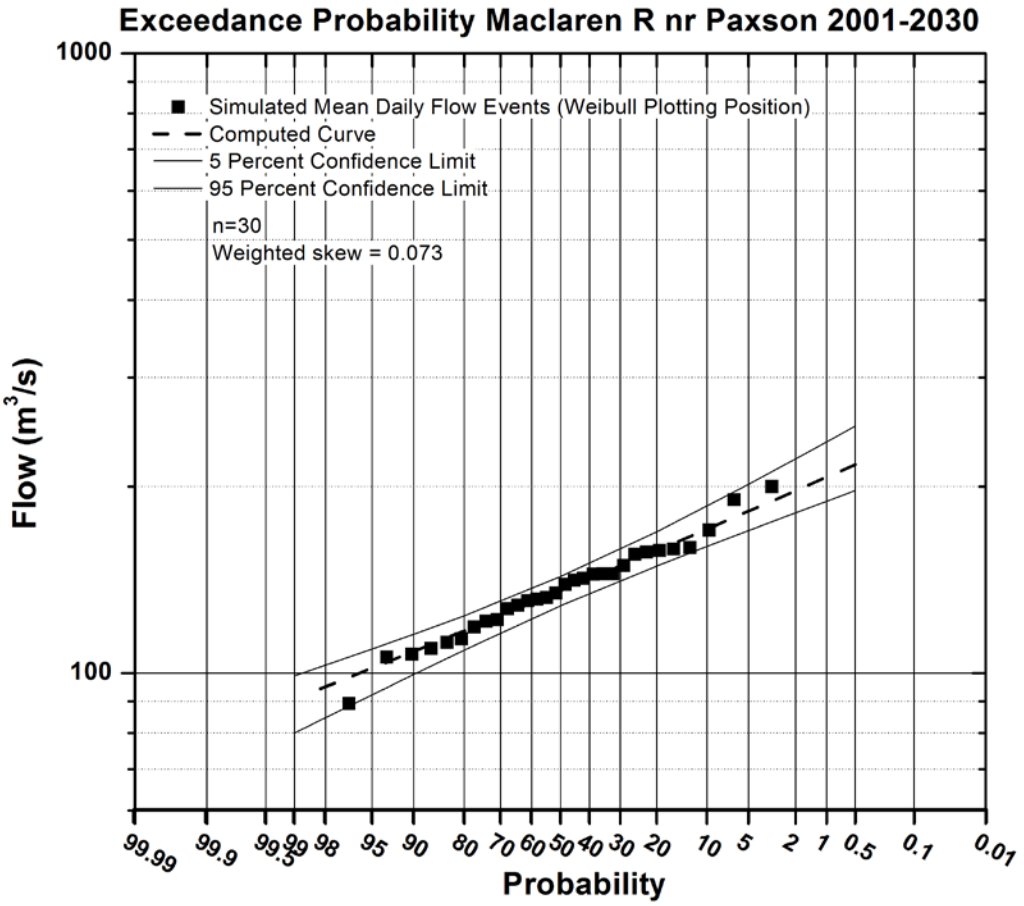


**Figure 7.4.2.1-2 Maclaren River 2001-2030. Flows are simulated mean daily annual maximum.**

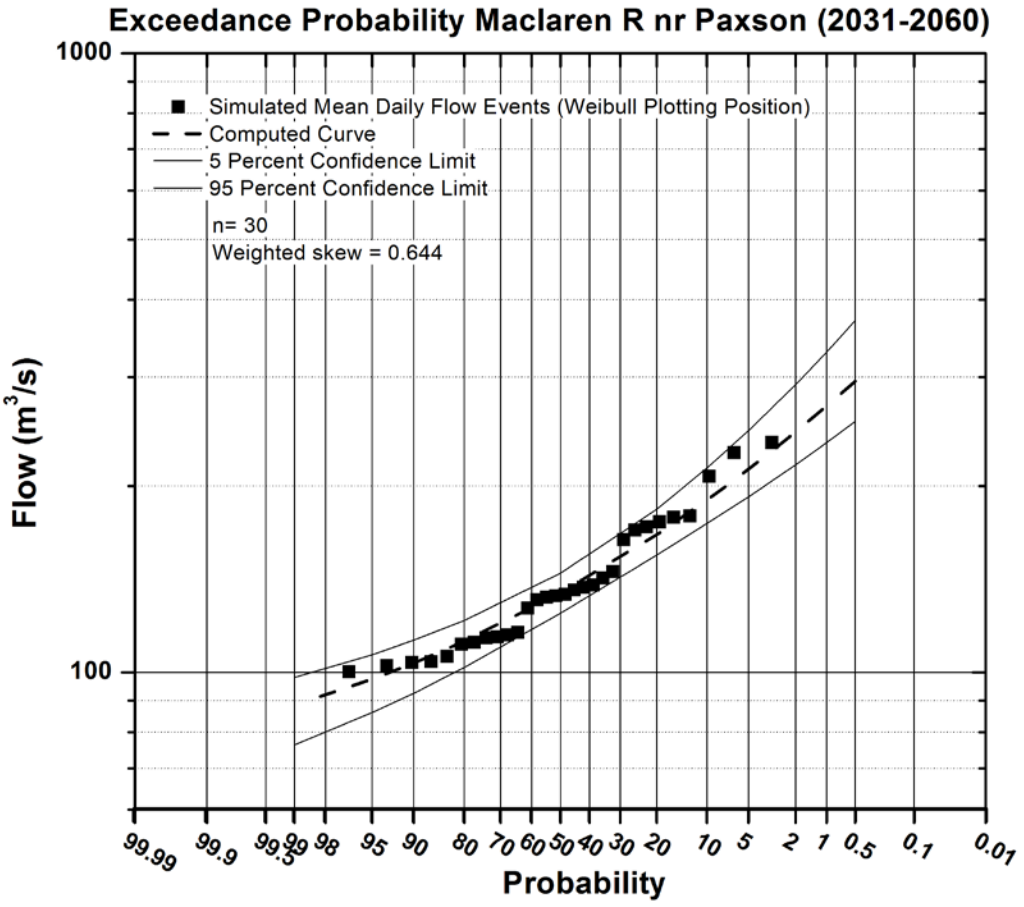


**Figure 7.4.2.1-3 Maclaren River 2031-2060. Flows are simulated mean daily annual maximum.**

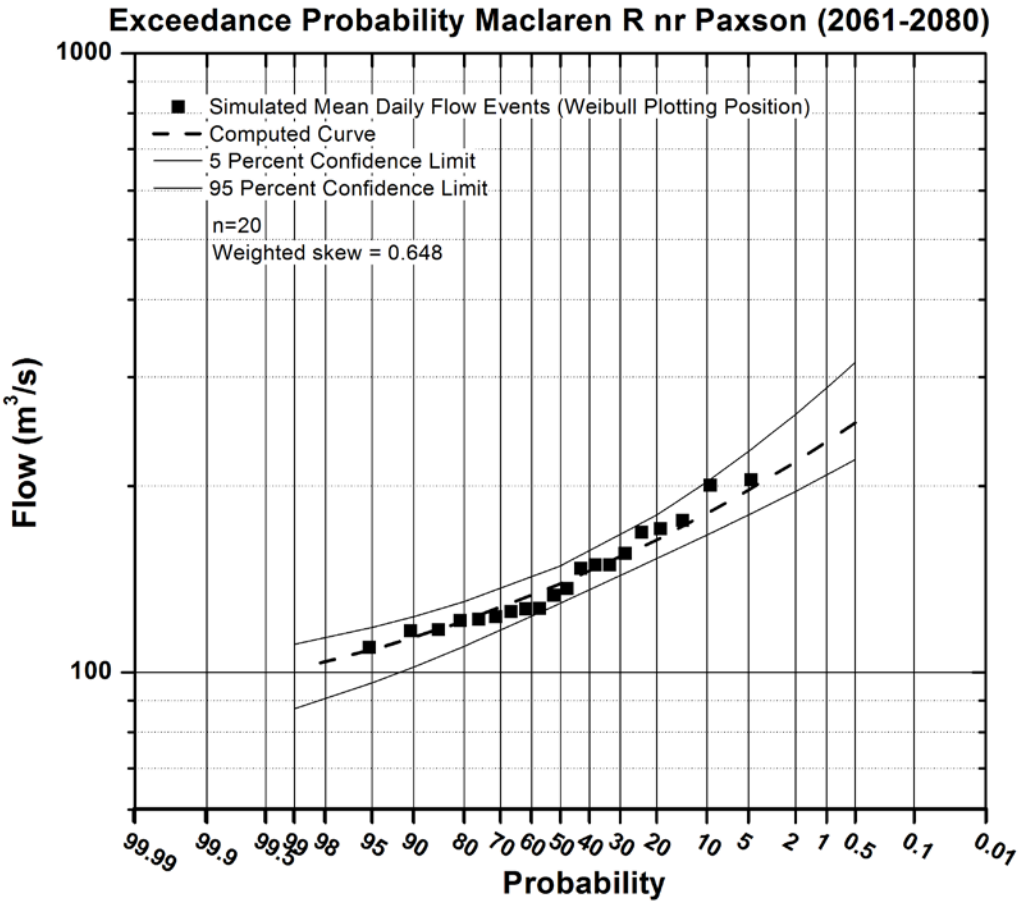


**Figure 7.4.2.1-4 Maclaren River 2061-2080. Flows are simulated mean daily annual maximum.**

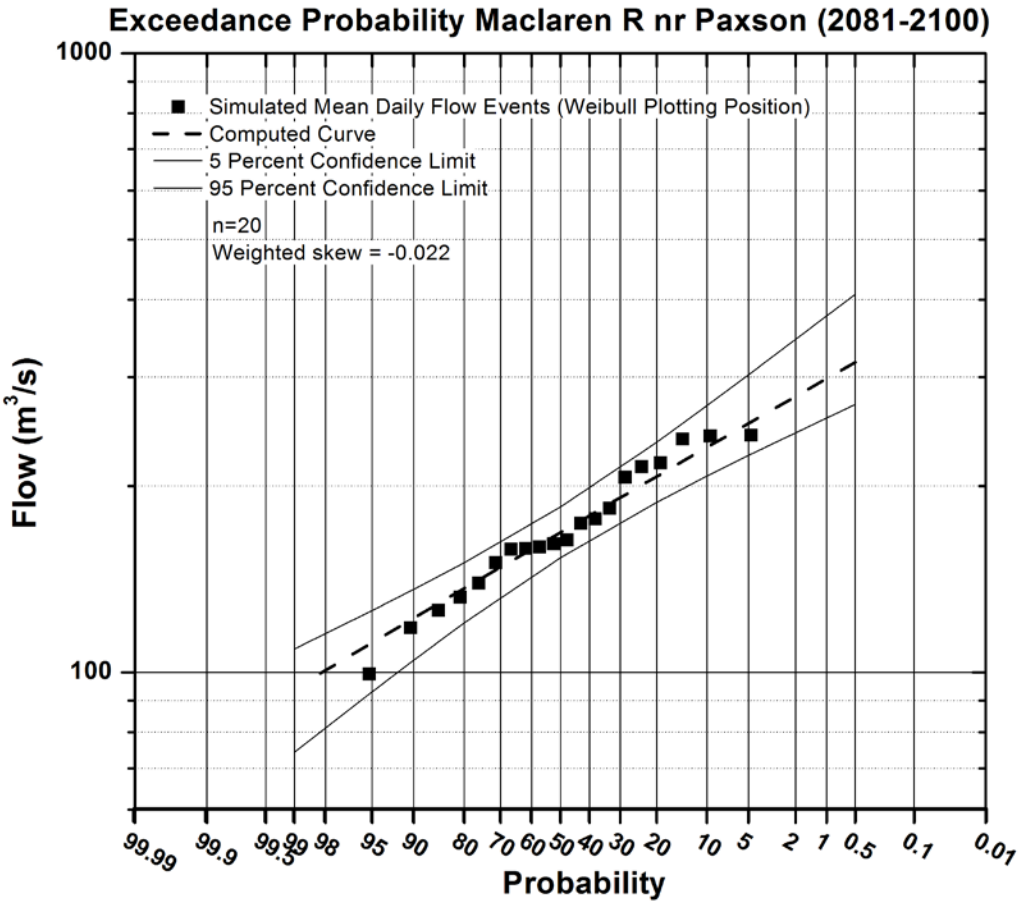


**Figure 7.4.2.1-5 Maclaren River 2081-2100. Flows are simulated mean daily annual maximum.**

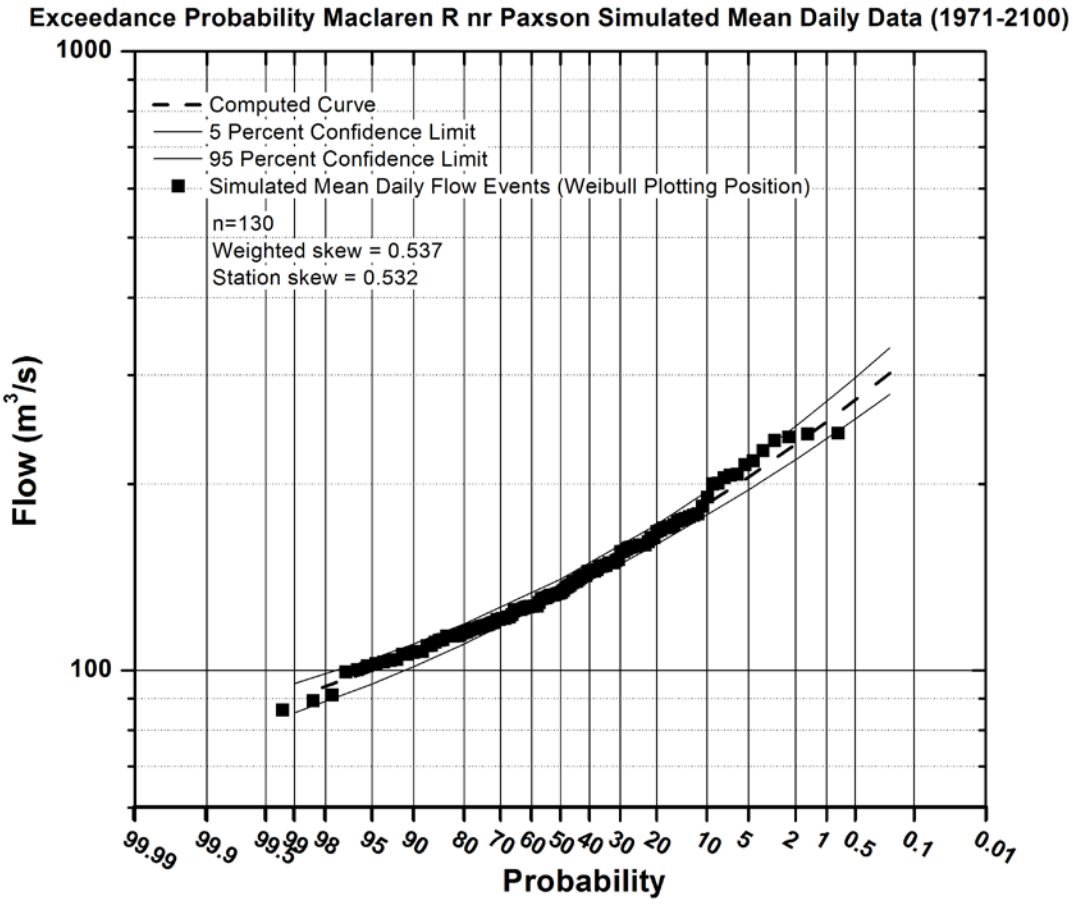


**Figure 7.4.2.1-6 Maclaren River 1971-2100. Flows are simulated mean daily annual maximum.**

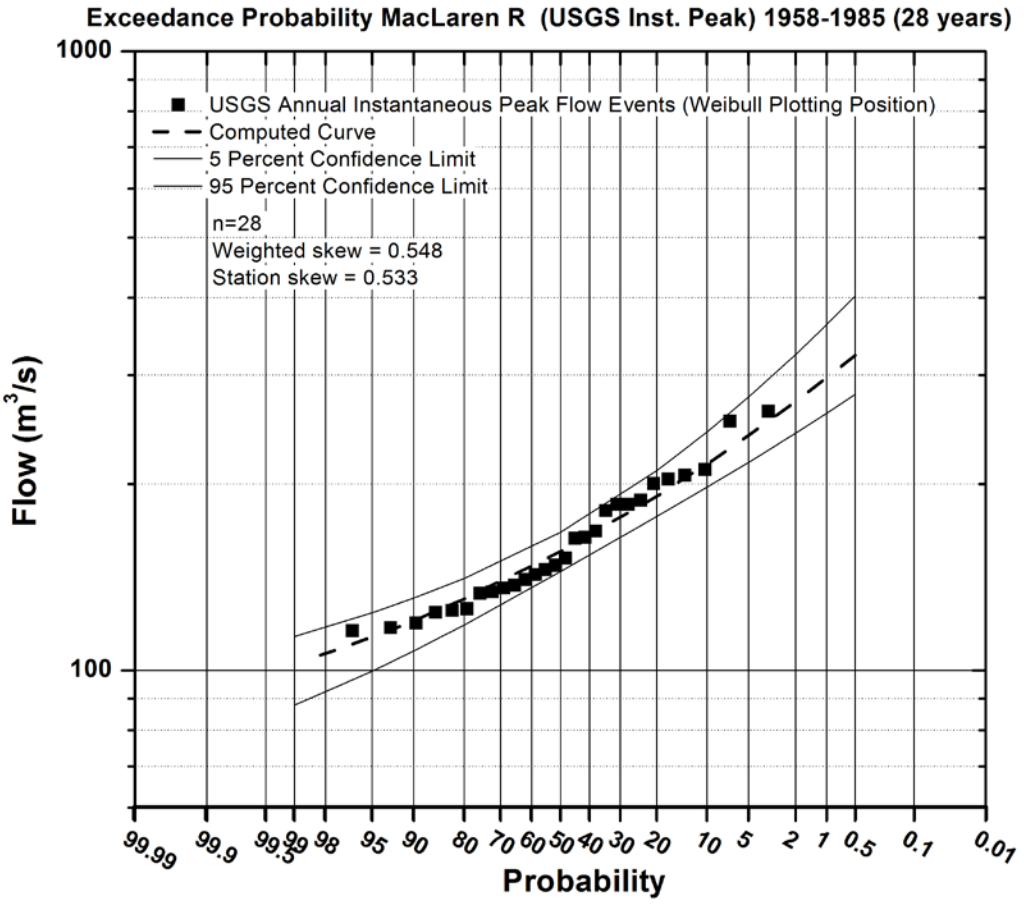


**Figure 7.4.2.1-7 Maclaren River USGS Instantaneous Peak Flows.**

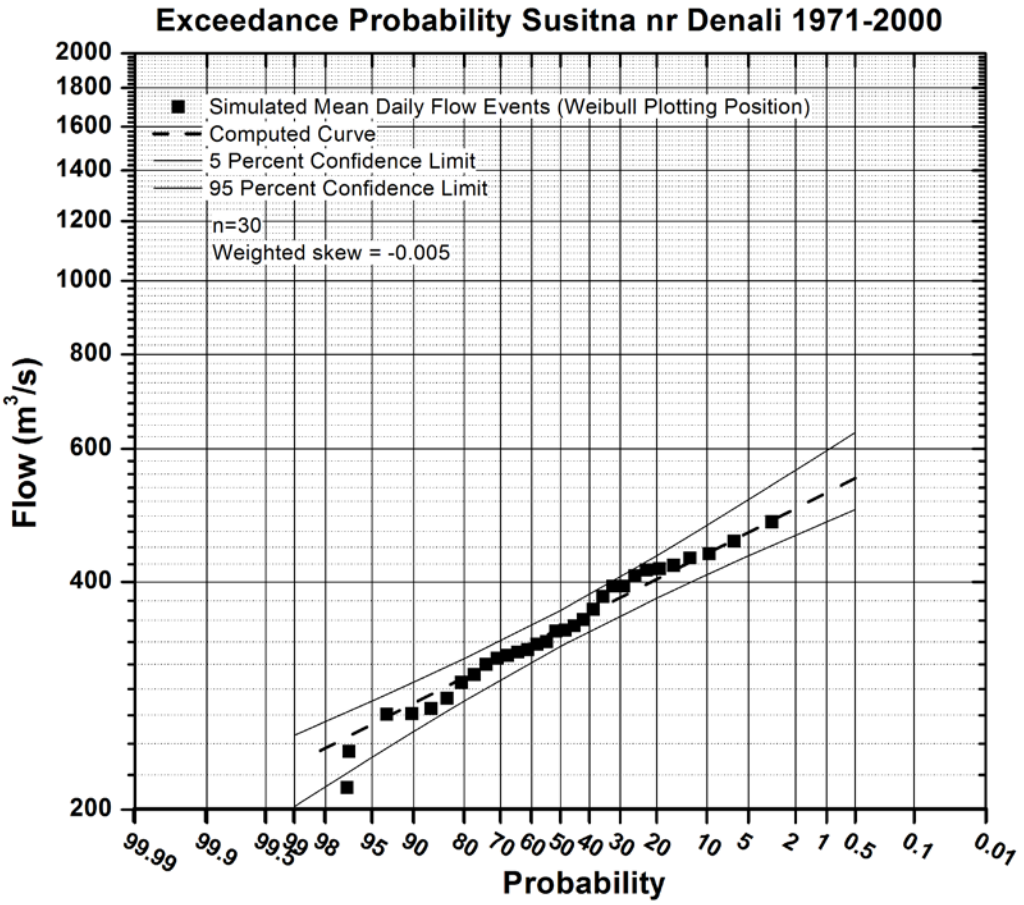


**Figure 7.4.2.1-8 Susitna River near Denali 1971-2000. Flows are simulated mean daily annual maximum.**

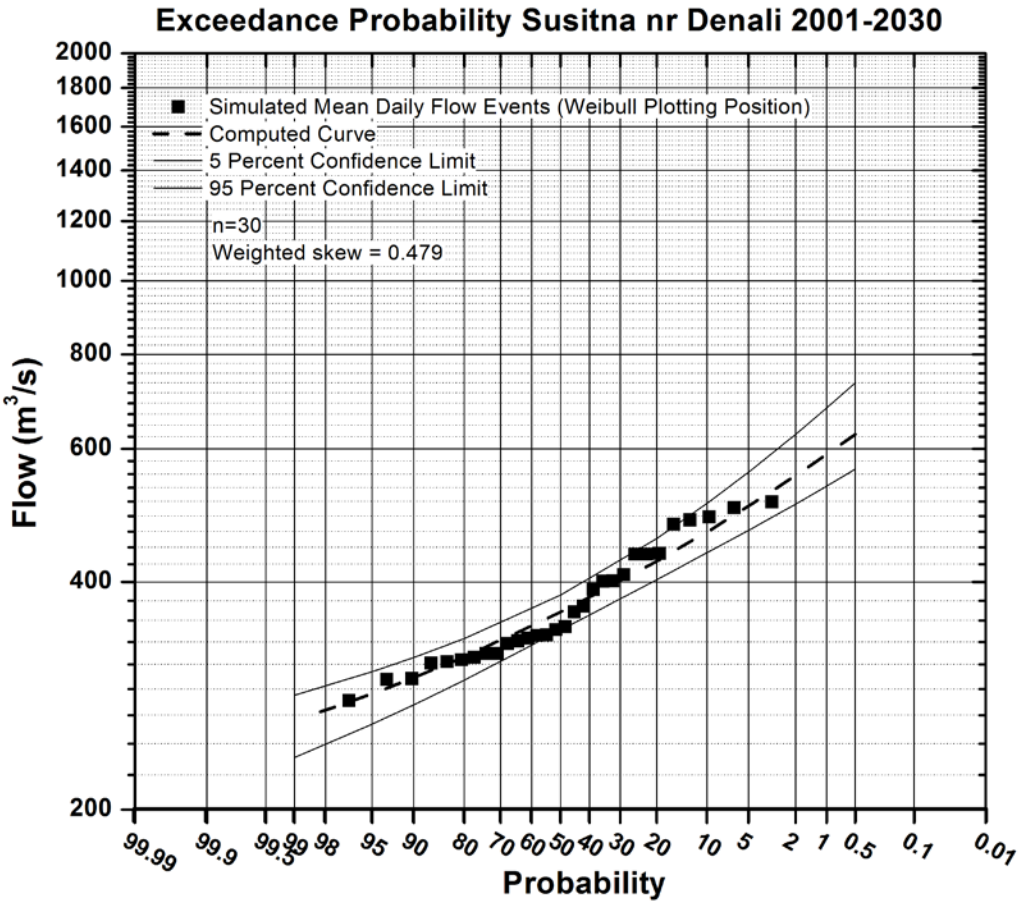


**Figure 7.4.2.1-9 Susitna River near Denali 2001-2030. Flows are simulated mean daily annual maximum.**

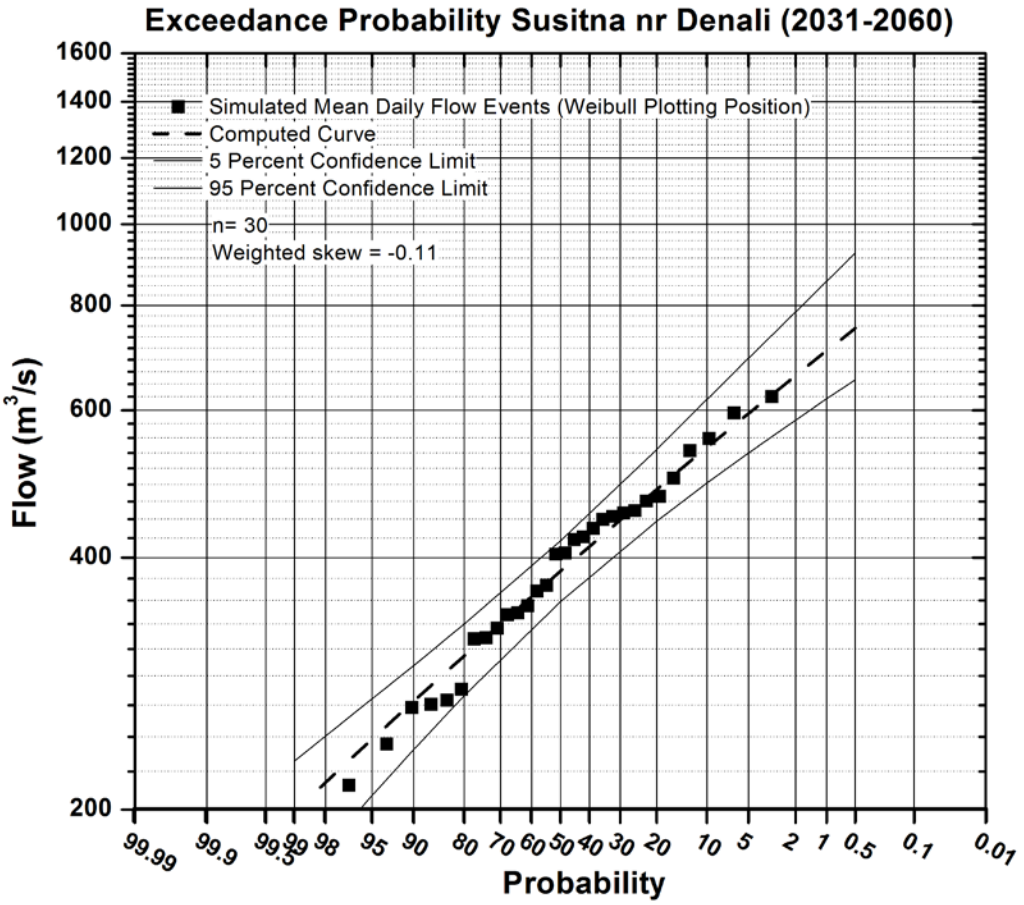


**Figure 7.4.2.1-10 Susitna River near Denali 2031-2060. Flows are simulated mean daily annual maximum.**

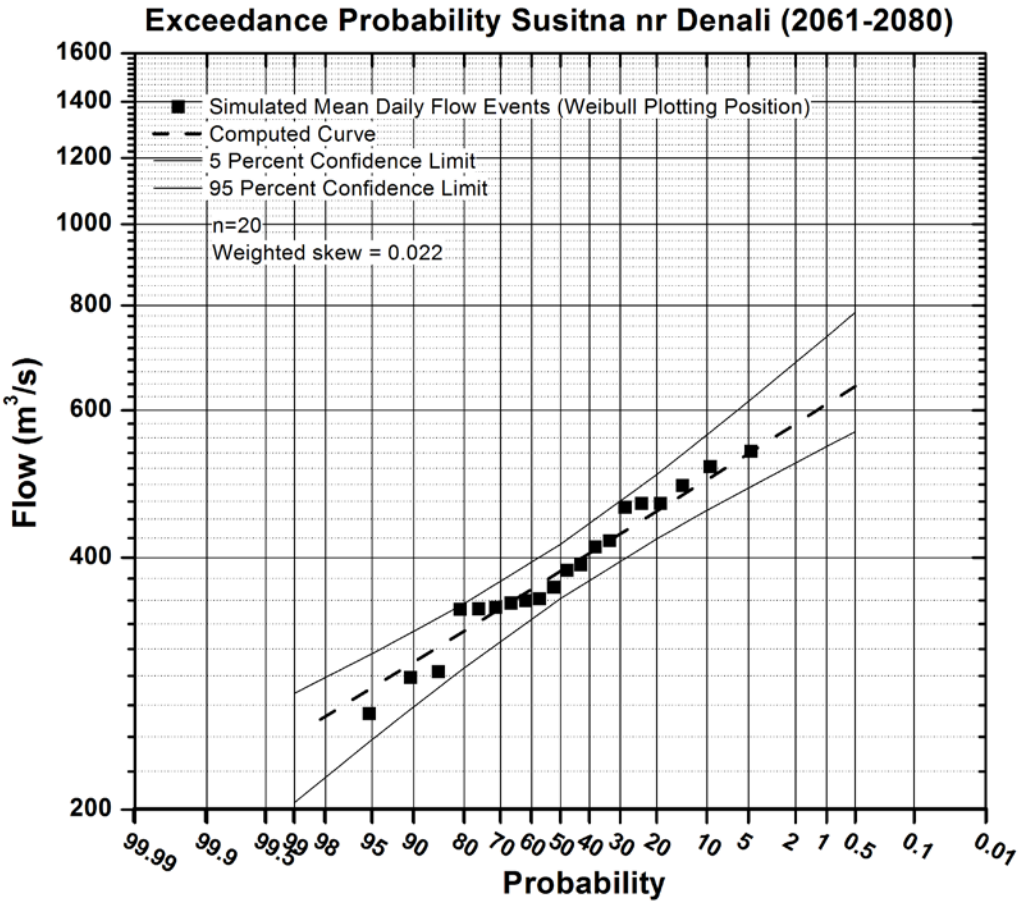


**Figure 7.4.2.1-11 Susitna River near Denali 2061-2080. Flows are simulated mean daily annual maximum.**

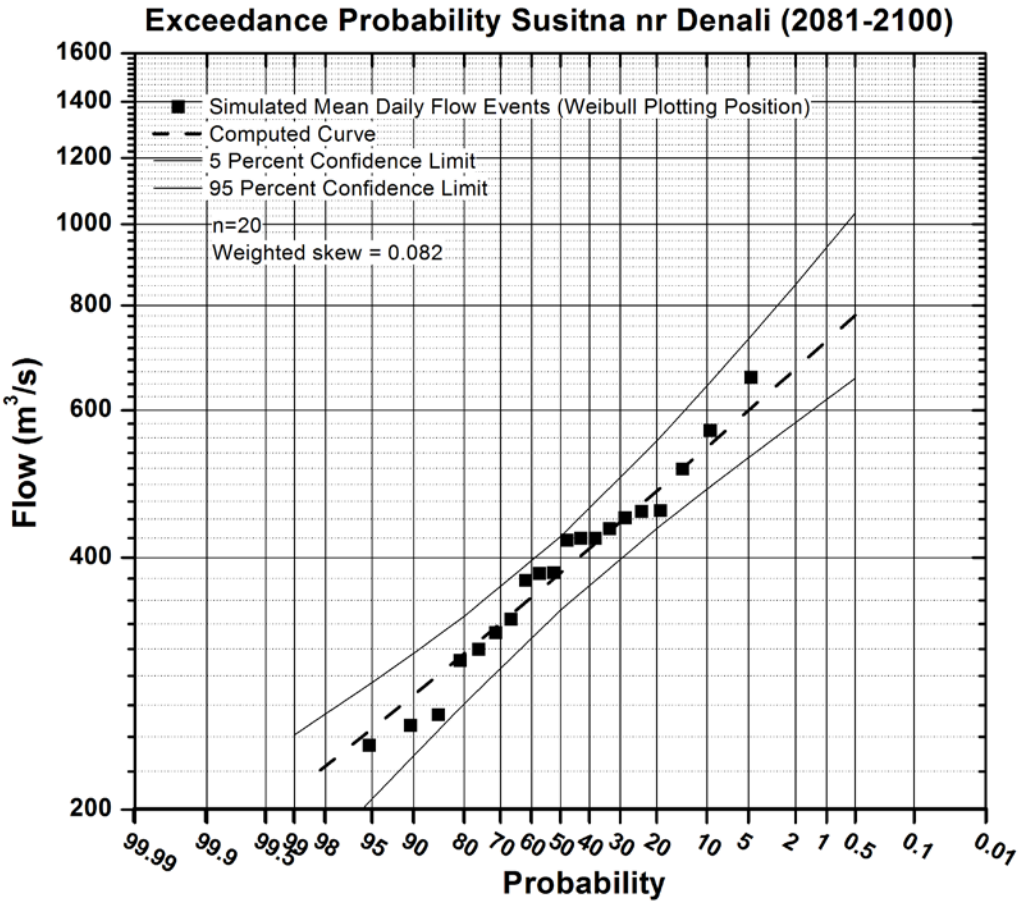


**Figure 7.4.2.1-12 Susitna River near Denali 2081-2100. Flows are simulated mean daily annual maximum.**

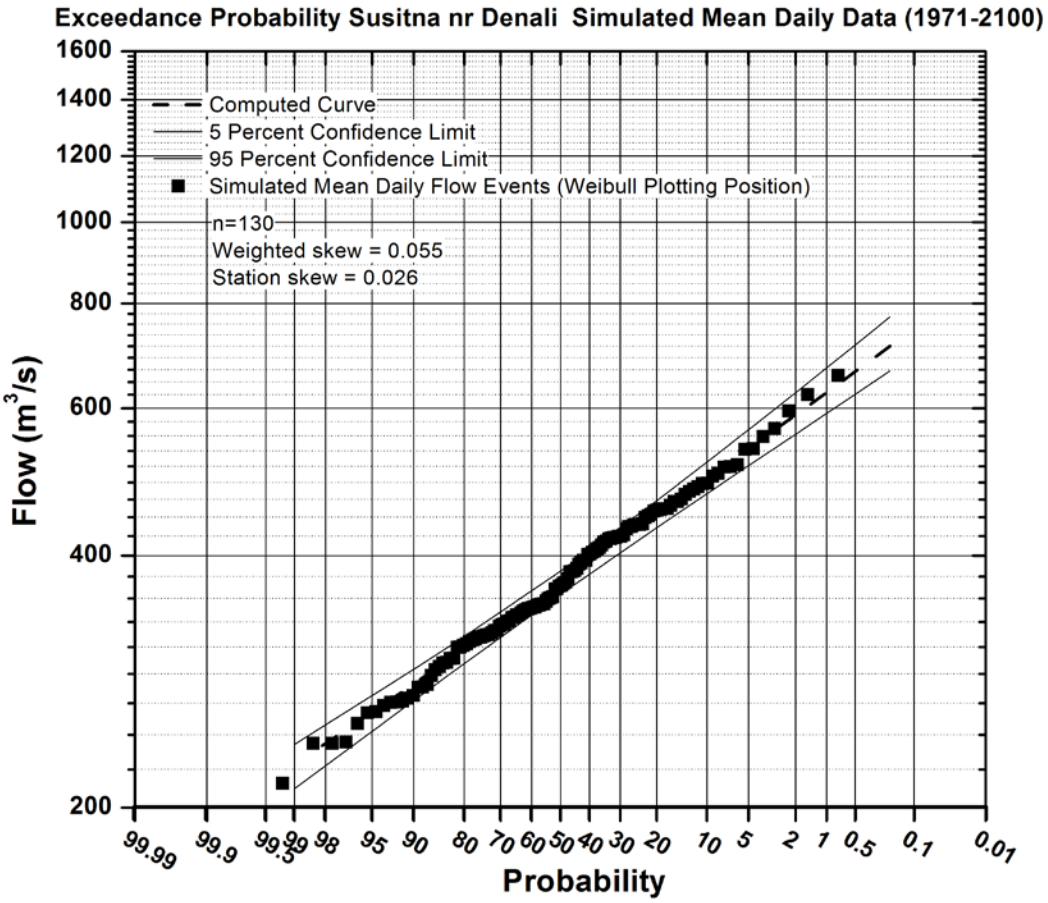


**Figure 7.4.2.1-13 Susitna River near Denali 1971-2100. Flows are simulated mean daily annual maximum.**

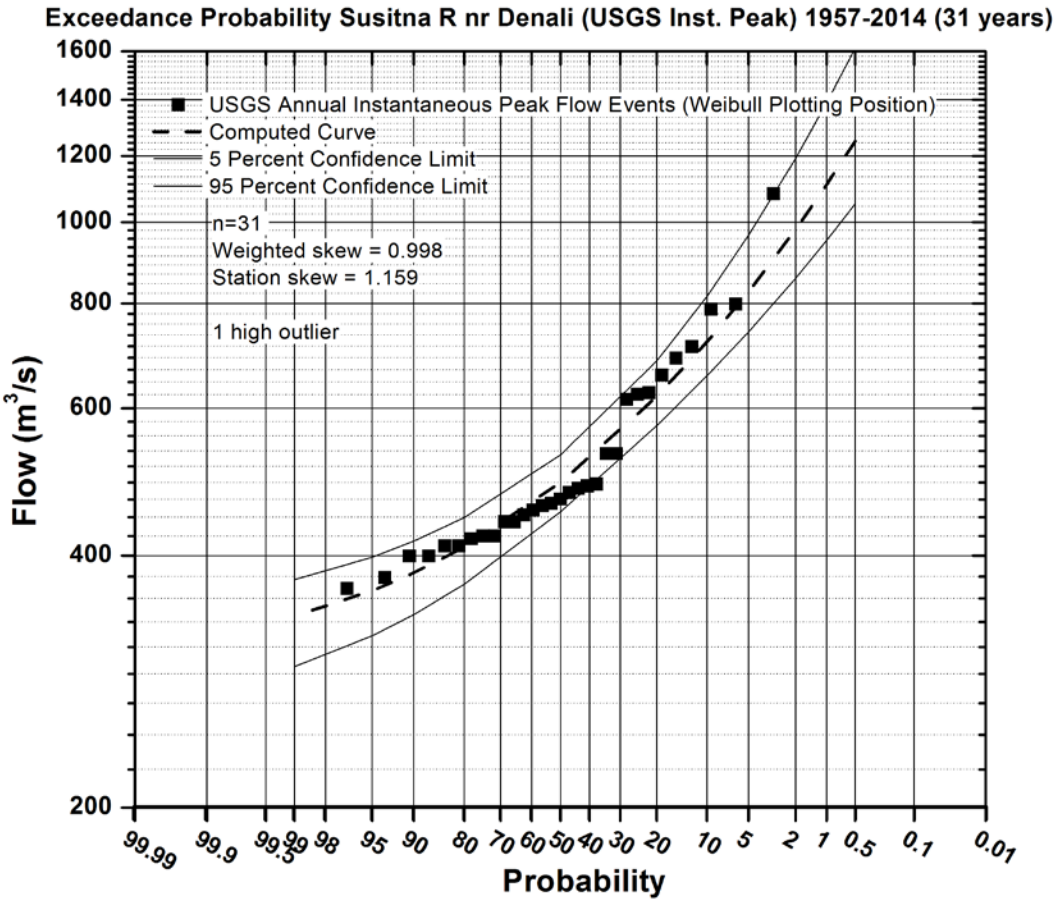


**Figure 7.4.2.1-14 Susitna River near Denali USGS Instantaneous Peak Flows.**

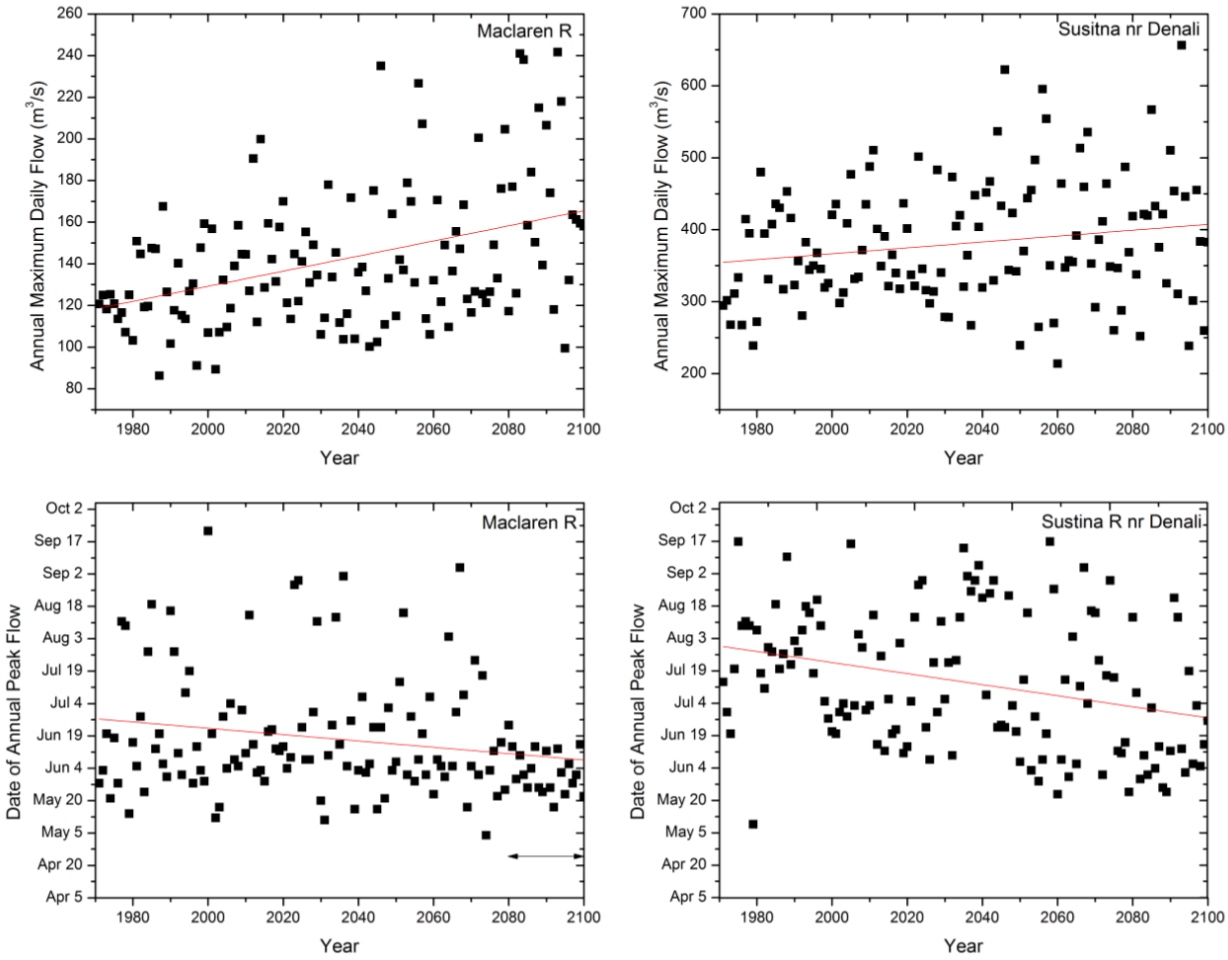


**Figure 7.4.2.1-15 Simulated annual maximum daily flows and their dates of occurrence from 1971 to 2100 for MacLaren River near Paxson and Susitna River near Denali.**

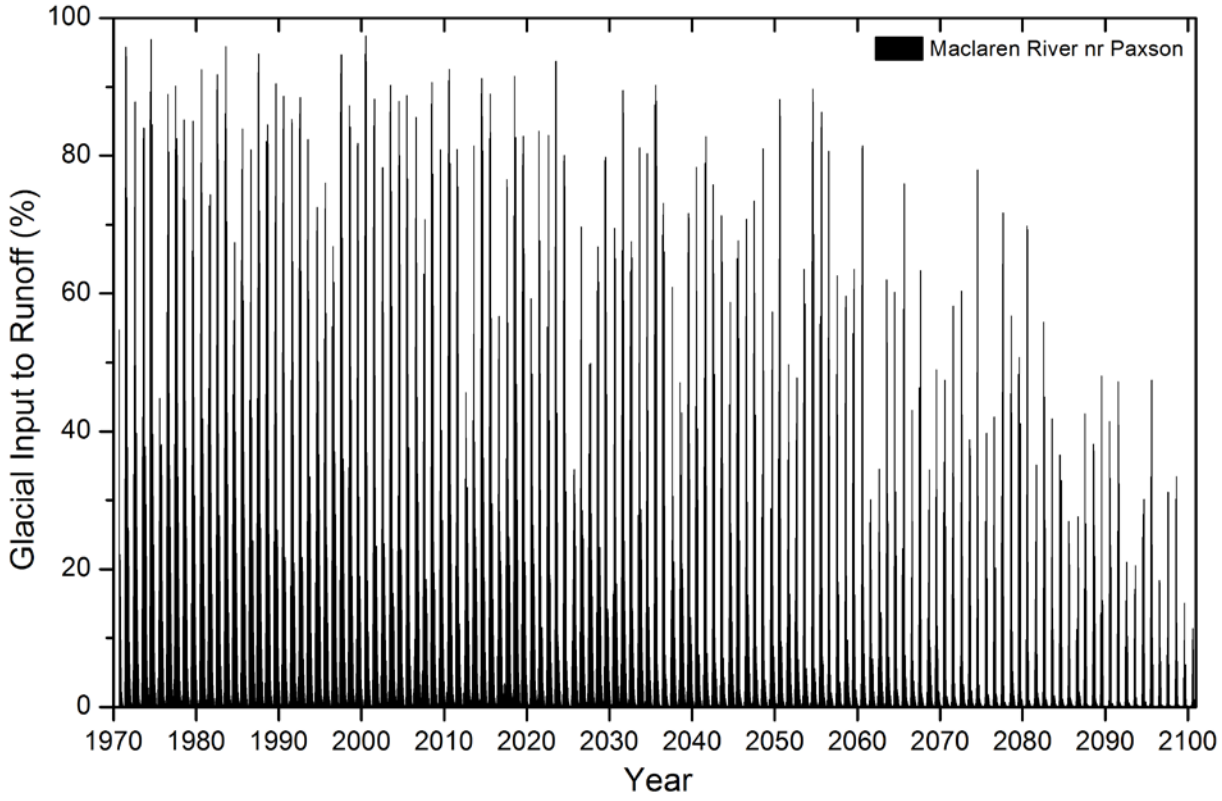


**Figure 7.4.2.1-16 The percentage of glacial input to simulated total runoff at the MacLaren River near Paxson station for the period 1971-2100.**

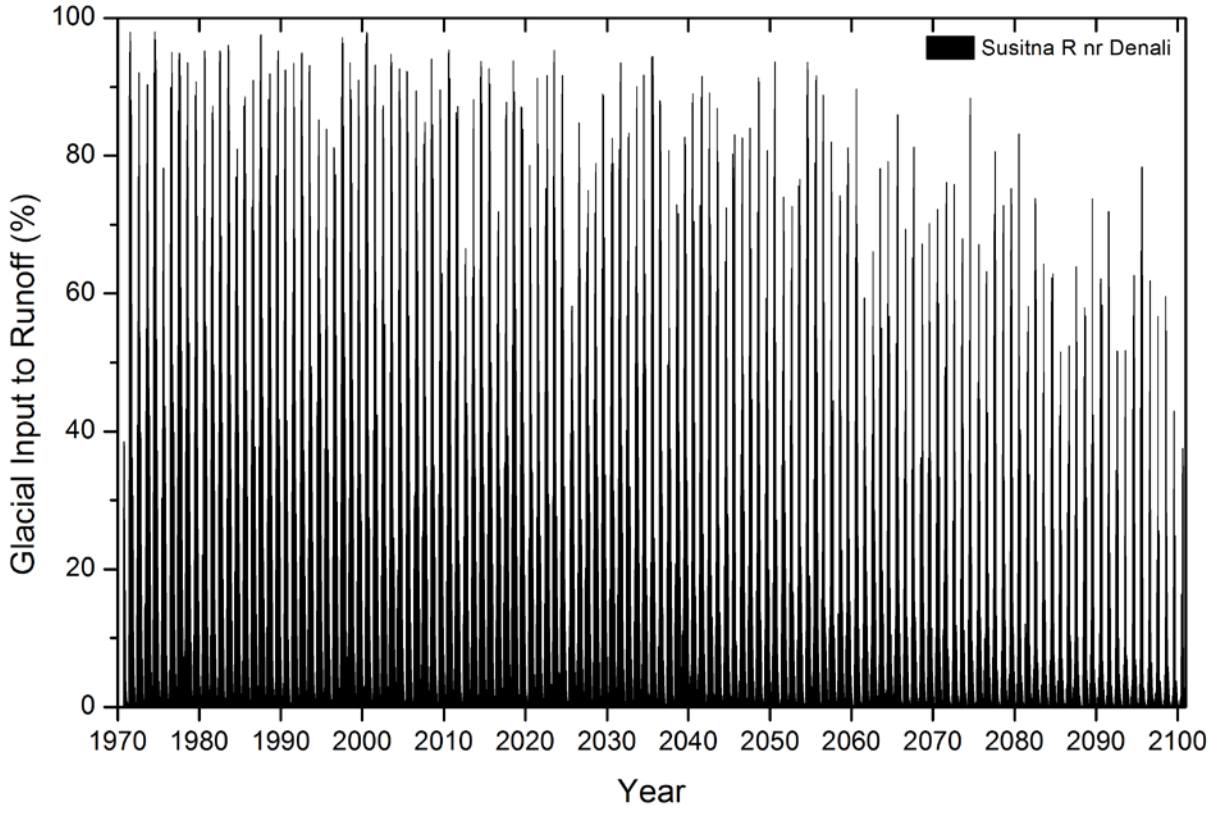


**Figure 7.4.2.1-17 The percentage of glacial input to simulated total runoff at the Susitna River near Denali station for the period 1971-2100.**